Single particle motion in active matter

Thesis by
Eric W. Burkholder

In Partial Fulfillment of the Requirements for the
degree of
Doctor of Philosophy

CALIFORNIA INSTITUTE OF TECHNOLOGY
Pasadena, California

2019
Defended July 16, 2018

Eric W. Burkholder
ORCID: 0000-0001-7420-4290

ACKNOWLEDGEMENTS

Just as active matter can only move by pushing against a substrate or embedding medium, a thesis cannot be written without a strong base of support from which to move oneself forward. First and foremost I must thank my advisor, John Brady. John is a researcher of unparalleled physical insight and mathematical abilities, and I am privileged to have had the opportunity to learn from and work with him. I am grateful for his integrity, professionalism, and the opportunities I have had—from attending a summer conference in Corsica to presenting at the Society of Rheology Meeting—with his support. I am most grateful for his respect for and encouragement of my independence as a researcher.

I would like to thank the members of my thesis committee: Zhen-Gang Wang, Richard Flagan, and Julia Kornfield. Professor Wang has been not only an ardent supporter during my time at Caltech, but perhaps the best teacher I've ever known. All of his lectures in Thermodynamics, Statistical Mechanics, and Polymer Physics are perfectly crafted and clear. At the end of class, I often felt as if I had meditated on the subject matter for the past 90 minutes. I thank Professor Kornfield for her passion and enthusiasm in her committee service, and for challenging me and teaching me to defend my work. Professor Flagan—thank you for your service, and for keeping the lofty ideas of a theorist grounded in reality.

A special note of thanks to a Brady group alumna and my undergraduate research advisor, Roseanna Zia. From her I learned the fundamentals of microhydrodynamics, microrheology, and fluid mechanics that allowed me to be successful in graduate school. Even as an undergraduate, she held me to high expectations and supported me and encouraged me to strive for great things. I thank Ron Phillips, Joel Christenson, Stephanie Dungan, Robert Guy, and Becca Thomases for their hospitality during my visits at the University of California Davis.

I am grateful to all members and visitors of the Brady group: Austin Dulaney, Camilla Kjeldbjerg, Hyeongjoo Row, Zhiwei Peng, Sho Takatori, Kevin Marshall, Ahmad Omar, Kevin Shen, Charlie Slominski, Wen Yan, Mu Wang, Mikey Phan, Marco Heinen, Stewart Mallory, Karol Makuch, Markus Gruber, Mario Sandoval, Charles Schroeder, Sara Abdelsalam, and Tyler Ross. I owe a particular debt of gratitude to Mikey for helping me learn how to use the cluster, and to Sho and Ahmad for providing me with code and countless pieces of scientific and academic

advice over the years. I would have been lost had I not been able to bombard them with questions. I would like to thank Suresh Guptha for helping me navigate the foreign world of computer clusters, and Kathy Bubash and Allison Oulette for their assistance throughout my PhD.

Thank you to my friends and family for all their love and support. Thank you Mom and Dad for listening to me rant about problems at work, validating my grievances, and being supportive of all the decisions I've made throughout my academic career. Thank you Patrick and Emily for always taking my phone calls when I was upset about something, and thank you to Ben and Devon for always being willing to go on an adventure when I needed a break from work. Thank you to all the members of my incoming class at Caltech for providing much-needed commiseration and celebration as appropriate.

To Jason LeGrand—my partner and most vehement supporter—I owe all of my successes at Caltech and in my future endeavors. Thank you for encouraging me to celebrate the small victories, keeping me grounded when faced with small problems, and giving me strength and love in times of adversity. Words can scarcely express my gratitude and appreciation. Ich liebe dich immer, mein Schatz.

ABSTRACT

"Active matter" refers to a broad class of materials in which the constituent particles or organisms are able to self-propel (swim) by some internal physicochemical mechanism. Though the origin of this self-propulsive motion is a rich area of study, we are primarily interested in the collective effects of this motion on the physical properties—and in particular, the rheology—of the active material as a whole. As such we model self-propulsive motion using the minimal active Brownian particle (ABP) model: a particle of size a, swims in a direction $\boldsymbol{q}$ with a speed U_0, and the direction of its motion changes randomly over some time scale τ_R.

On a macroscopic scale, active motion leads to unique hydrodynamic and mechanical stresses exerted by the particles on their embedding medium. These stresses arise from the microscopic force associated with particle locomotion—the swim force $\boldsymbol{F}^{swim}$. Though the idea of the swim force is widely recognized in the abstract, little attention has been given to the characterization and mechanical consequences of this force. In this work we are particularly interested the role of the swim force in the effective motion of passive constituents in active environments, and how the swim force affects long-ranged hydrodynamic interactions (HI) in active suspensions. We examine these issues through the lens of microrheology: tracking the motion of a colloidal probe particle through an active medium, and using its motions to infer the effective viscoelastic properties of the suspension.

Using generalized Taylor dispersion theory, we find an activity-driven enhancement to the diffusion of the probe in an active medium. This first-principles theory unites many experimental observations of tracer diffusion, and provides simple physical descriptions of the problem that do not rely on the specific self-propulsion mechanism of the swimmer. This same framework is then used to compute the suspension microviscosity (as measured by the drag on the probe particle), and the fluctuation-dissipation relation in an active system. We find that activity reduces the drag on the probe, but the drag is still larger than it would be in a Newtonian fluid; this stands in contrast to experimental measurements of reduced shear viscosities. We show that the microviscosity of a suspension is reduced—and may even become negative!—due to HI, and that this effect is *not* due to the fluid velocity disturbance associated with the swimmers' self-propulsion.

PUBLISHED CONTENT AND CONTRIBUTIONS

[1]E. W. Burkholder, and J. F. Brady, "Tracer diffusion in active suspensions", Phys. Rev. E - Stat. Nonlinear, Soft Matter Phys. (2017) 10.1103/PhysRevE.95.052605,
E.W.B. participated in the conception of the project, performed the calculations, analyzed the data, and participated in the writing of the manuscript.

[2]E. W. Burkholder, and J. F. Brady, "Do hydrodynamic interactions affect the swim pressure?", Soft Matter **14**, 3581–3589 (2018),
E.W.B. participated in the conception of the project, performed the calculations, analyzed the data, and participated in the writing of the manuscript.

TABLE OF CONTENTS

LIST OF ILLUSTRATIONS

Chapter 1

INTRODUCTION

"How can the events in space and time which take place within the spatial boundary of a living organism be accounted for by physics and chemistry?" Since Schrödinger's philosophizing on this subject [1], countless physicists, chemists, mathematicians—even engineers—have spent their careers in pursuit of simple physical models that describe emergent behaviors in biological systems. Schrödinger understood that the quantum and statistical interactions between the atoms and molecules which comprise all matter must be responsible for emergent phenomena in living organisms. In this dissertation, we take the same philosophical approach to the description of active suspensions—a subject of active research among soft-matter physicists today.

"Active suspensions" denote a class of materials in which collections of organisms, particles, or even molecules are capable of converting chemical energy in to mechanical work. A further distinction is made between wet active suspensions, in which the particles are immersed in a (usually continuous) suspending medium that mediates long-ranged interactions between constituents [2, 3], and dry active suspensions (e.g. vibrated granular media) in which the constituents generally do not interact through the substrate off of which they self-propel.[1] Common examples of wet active matter are collections of bacteria, suspensions of chemically reactive nanoparticles [5], and bundles of cytoskeletal filaments (e.g. actin) bound together by motor proteins [6]. Such materials are known to exhibit fascinating dynamic behavior such as spontaneous collective motion [7–13], phase-separation [4, 10, 14–23], and enhanced diffusion [24–30]. Of particular interest to us is the rheological behavior of active suspensions. Viscosity reduction [31–35] is but one observed behavior not typically found in passive suspensions of colloids.

In this work, we develop coarse-grained descriptions of the mechanics of active suspensions. To do so, we need only to think carefully about how phenomenological

[1] A common misconception regarding dry active systems is that they do not conserve momentum [4]—a conclusion which arises if one neglects the substrate or solvent in the analysis. Indeed, even if the active constituents do not interact through the substrate, the substrate is still essential to their self propulsion and thus, the mechanical equations of motion. This idea is used in later chapters of this work.

models of biological and diffusiophoretic locotmotion [36–39] can be incorporated into existing microscopic frameworks used to describe the behavior of passive colloidal suspensions [40–43]. In doing so, we need never concern ourselves with the details of how the active constituents convert chemical into mechanical energy, only the nature of the emergent motion. From these models, we make predictions about the microrheological behavior of active materials—how the microscopic interactions between active and passive constituents inform the osmotic pressure, diffusivity, and viscosity of the medium.

1.1 Locomotion, stress, and pressure

At its core, biological motion is a mechanics problem, and thus beholden to the the same fundamental laws introduced in any introductory physics course—conservation of mass and momentum. Consider a body of size a and density ρ_P moving at a speed U in a continuous medium of viscosity η and density ρ. For an incompressible medium, conservation of mass requires that the velocity field is divergence free $\boldsymbol{\nabla}\cdot\boldsymbol{u} = 0$. We consider motions at low Reynolds number $Re \equiv \rho U a/\eta$ and low Stokes number $St \equiv (\rho_P/\rho)Re$. In this regime, both the particles and fluid have no inertia, and thus all motion is force-free: Newton's second law requires that the sum of the forces (and torques) on the body be equal to zero, and the Stokes equations then require that the the suspension stress is divergence free $\boldsymbol{\nabla}\cdot\boldsymbol{\sigma} = 0$.

Taylor [44], Lighthill [36], and later Blake [37] were the first to recognize the relevance of low Reynolds number fluid mechanics, in particular the consequences of negligible inertia, to the problem of locomotion on microscopic length scales. In low Reynolds number flows all motions are instantaneous and time-reversible; thus microscopic organisms are unable to swim (with non-zero net displacement) unless they make non-reciprocal motions, such as the chiral rotations of a flagellum in *E. coli* [45, 46]. This is commonly known as Purcell's scallop theorem. Because local time-reversal symmetry *must* be broken to achieve net self-propulsion, active systems are inherently non-equilibrium and cannot be described in terms of typical thermodynamic relations.

Blake's squirmer model provides a phenomenological description of the swimming of ciliated organisms, which move through time-asymmetric modulations of their surfaces (see Fig. 1.1) [37]. Blake expresses this motion as a series of small harmonic modulations to the surface of a spherical organisms—e.g. parasites of the genus *Opalina*. One can then determine the average speed of the organism

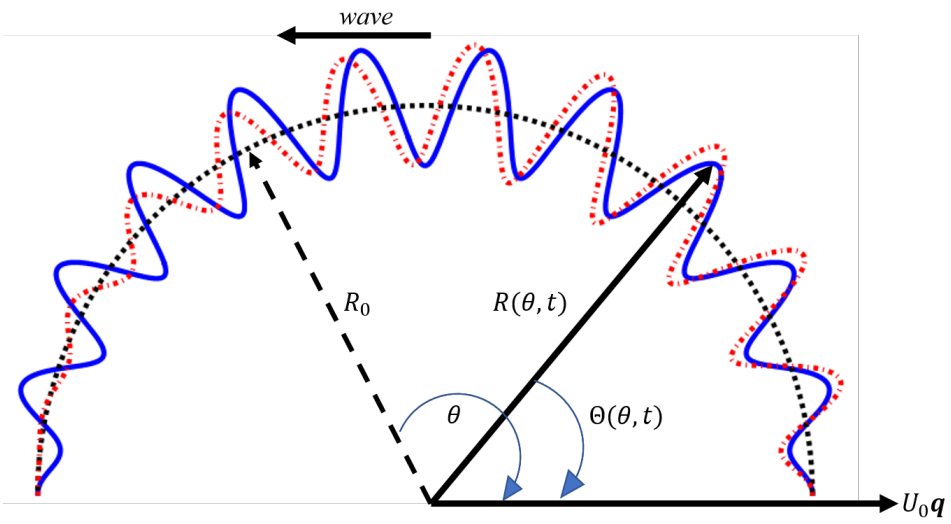

Figure 1.1: Sketch of the half-surface of a squirming organism as described by Blake's model of ciliary propulsion [37]. The black (dotted) hemispherical line is the equilibrium (stationary) surface of the organism R_0, and the stationary polar angle for the organism is θ. The blue (solid) line is a surface modulation (mode $N = 22$ in Eqn. 19 of [37]) at some initial time with amplitude $R_0/10$, and the red (dot-dashed) line is the same surface modulation at 0.8 of the beat period later. The surface wave travels to the left, which results in a net propulsion of the organism to the right.

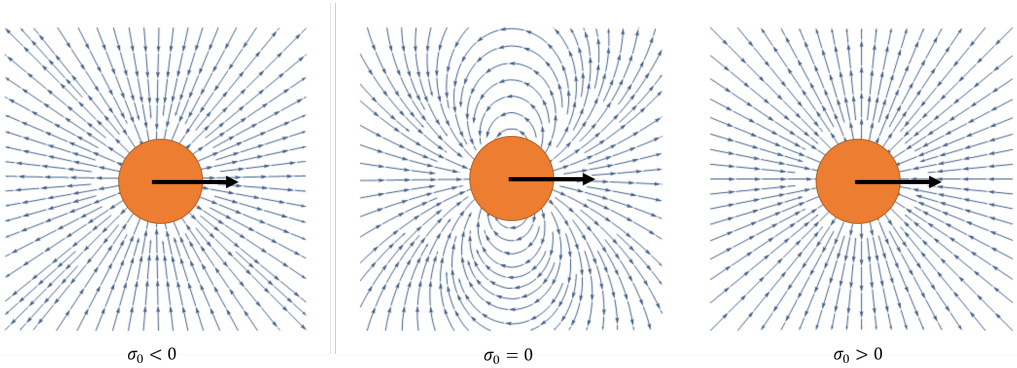

Figure 1.2: Sketch of the fluid flow fields created by a pusher (left), mover (center), and puller (right).

and the hydrodynamic stress $\boldsymbol{\sigma}^{\boldsymbol{H}}$ exerted on the fluid due to the particles self-propulsion. Because the particle motion is force-free, the swim force—the internal body force which drives the self-propulsive motion of the particles [3, 21, 47]—is precisely balanced by the fluid drag. The fluid velocity disturbance associated with self-propulsion is thus dipolar and decays as $1/r^2$ (or faster) [48]. This has been experimentally verified by particle-image velocimetry [49, 50]. This velocity field is $\boldsymbol{u}' = \boldsymbol{\sigma}^{\boldsymbol{H}} : \boldsymbol{\nabla J}$, where $\boldsymbol{J}$ is the familiar Stokeslet [40]. It is common to use

experimental measurements of the particle's self-propulsive swim force $\boldsymbol{F}^{swim}$ to predict the magnitude σ_0 of $\boldsymbol{\sigma}^{\boldsymbol{H}}$: $\sigma_0 = \pm F^{swim} a$, where a is the particle size. If $\sigma_0 > 0$, the organism is said to be a puller like *C. reinhardtii*, if $\sigma_0 < 0$ it is a pusher like *B. subtilis* or *E. coli*, and for $\sigma_0 = 0$, it is a mover, like *Volvox*. Flow fields for the various types of swimmers are sketched in Fig. 1.2. Nearly all descriptions of the rheology of active suspensions rely on the calculation of $\boldsymbol{\sigma}^{\boldsymbol{H}}$—the work of [51] and this thesis being notable exceptions. Viscosity reductions and instabilities are thus attributed to a negative active hydrodynamic stresslet.

However, there is a key feature missing from the squirmer model. As observed by Berg [46], flagellated microorganisms do not simply swim, they also tumble; tumbling is a sudden change in their swimming direction associated with unbundling of the flagella. Similarly, chemically active colloids will change their direction due to rotary Brownian motion. This observation informs the active Brownian particle (ABP) and run-and-tumble particle (RTP) models, which neglect the hydrodynamic details associated with the particles' self-propulsion, and simply ascribe a swim velocity $\boldsymbol{U}_0$ and a characteristic time for reorientations (tumbles) τ_R [38]. For ABPs, the reorientation process is continuous on scales long compared to the momentum relaxation time of the fluid whereas the reorientations of RTPs are discrete [52]. RTPs are commonly modeled as having a Poisson-distributed orientation with a mean that is usually matched to empirical measurements (for example, the average tumbling angle for *E. coli* is 68.5 degrees, with a similar variance [27]). At times long compared to τ_R, these models are equivalent; as we are primarily concerned with steady-state behaviors, we always assume a diffusive reorientation process in this work—the tumbles are not correlated at long times.

This run-and-tumble motion is described by an effective mechanical "swim" diffusivity $D^{swim} \sim \ell^2/\tau_R \sim U_0^2 \tau_R$, where the $\ell = U_0 \tau_R$ is the run-length (the distance traveled between reorientations) [21, 46]. Diffusive motion implies an unbounded (linear) growth of the mean-squared displacements of the particle at long times—a particle diffusing in an unbounded medium will tend to "run away" in space. Thus, if one wishes to consider an unbounded suspension of active particles at a constant number density n, there must be a stress in the fluid $\boldsymbol{\sigma}^{\boldsymbol{swim}} = -n\zeta \boldsymbol{D}^{\boldsymbol{swim}}$ that prevents the particles from diffusing off to infinity (ζ is the drag on a particle). Though this is a new mechanical stress unique to active systems, it should be noted that even *Brownian* particles have a similar Brownian stress associated with their thermal Stokes-Einstein-Sutherland diffusivity $\boldsymbol{\sigma}^{\boldsymbol{B}} = -n\zeta \boldsymbol{D}_{\boldsymbol{T}}$ [21, 48, 53–55]. Indeed, any

diffusive process has a corresponding stress of the same form. The swim stress scales as $F^{swim}\ell \sim (\ell/a)\sigma_0$. The run length is typically large compared to the body size, and thus this stress is much larger than the active stresslet that characterizes the swimming gait; it should be emphasized that this stress exists for all swimmers. Indeed Takatori and Brady have used this idea extensively and shown that phase-separation, and "superfluidity" can both be explained by this swim stress [51, 56].

Where there is stress, there is pressure: $\Pi = -tr(\boldsymbol{\sigma})/d$, where d is the spatial dimension; this implies the existence of a unique particle-phase pressure $\Pi^{swim} = n\zeta D^{swim}$ given that these particles diffuse. Takatori et al. showed that one can use the swim pressure to explain the phase separation of active systems [21], and even give an analytic prediction for the mechanical instability of active suspensions [56]. This concept of the swim pressure has been highly contentious[2], despite its clear physical origins [57]. Though one can always define a mechanical pressure from stress, it has been argued that this pressure is not necessarily equal to the average force the suspension exerts on confining boundaries as it dependents on the particle-boundary interactions. This mechanical pressure is thus said *not* to be a function of state, rendering attempts to use it as a description of phase behavior invalid [57]. We address this in detail in Chapter 6, but there is a key point that counters this criticism. If mass and momentum are conserved, one can show that the force per unit area on the confining boundaries *must* be equal to the pressure in the bulk of the suspension. It must simply be recognized that this conservation statement applies to the total system pressure, and not necessarily each component individually. The same is true for a box of air—we may not know how the pressure of each component gas is distributed in the container, only that the total pressure is uniform for a given volume and temperature. Even in dry active matter, the second 'component' of the active suspension is the substrate from which the constituents are able to self-propel. Thus, any container-dependent particle-wall interactions cannot cause spatial variations in the total pressure in a container, so the total pressure in active suspensions is a function of state.

[2]Most hotly debated have been attempts at thermodynamic descriptions of active matter—specifically because the breaking of local detailed balance means the system is far from equilibrium. For example, if one can define a pressure, one could analogously construct a chemical potential and free energy of the suspension based on this pressure, though no such quantities can be assumed to exist *a priori*.

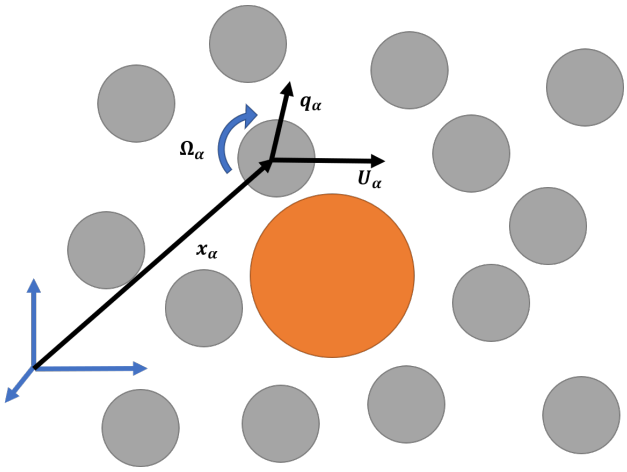

Figure 1.3: Sketch of a generic N particle colloidal suspension. Each particle α has a position $\boldsymbol{x}_\alpha$ and orientation $\boldsymbol{q}_\alpha$ in the laboratory coordinate frame. Each particle moves with a velocity $\boldsymbol{U}_\alpha$ and rotates with an angular velocity $\boldsymbol{\Omega}_\alpha$. Note that the particle orientation may not be in the direction of motion.

1.2 Suspension mechanics & microrheology

Though stresses provide a continuum-level description of active materials, we are primarily interested in the effects of acitvity on the suspension microstructure P_N—the N-particle probabability distribution for finding the suspension in a certain configuration at a given time. From P_N, one can compute the mean physical properties of the suspension, e.g. the viscometric functions and the swim stress. The microstructure for a fixed number of particles is a conserved quantity; thus the dynamics are described by a Smoluchoski equation:

$$\frac{\partial P_N}{\partial t} + \sum_{\alpha=1}^{N} \nabla_{\boldsymbol{x}_\alpha} \cdot \boldsymbol{j}_{\boldsymbol{\alpha}}^{\boldsymbol{T}} + \sum_{\alpha=1}^{N} \nabla_{R_\alpha} \cdot \boldsymbol{j}_{\boldsymbol{\alpha}}^{\boldsymbol{R}} = 0, \tag{1.1}$$

where the position $\boldsymbol{x}_\alpha$ and orientation $\boldsymbol{q}_\alpha$ of each particle α are measured in a fixed (or laboratory) reference frame, and $\nabla_{R_\alpha} = \boldsymbol{q}_{\boldsymbol{\alpha}} \times \nabla_{\boldsymbol{q}_\alpha}$ is the appropriate rotational operator for a particle α that can be characterized by a single orientation vector $\boldsymbol{q}_\alpha$. The translational flux of particle α is $\boldsymbol{j}_\alpha^T = \boldsymbol{U}_{\boldsymbol{\alpha}} P$ and its rotational flux is $\boldsymbol{j}_{\boldsymbol{\alpha}}^{\boldsymbol{R}} = \boldsymbol{\Omega}_{\boldsymbol{\alpha}} P$, where $\boldsymbol{U}_\alpha$ and $\boldsymbol{\Omega}_\alpha$ are, respectively, the velocity and angular velocity of particle α. Low Reynolds number flows are linear, and thus the velocity of each particle is linearly proportional to the forces and torques acting on all other particles in the suspension—this includes the swim force. In Chapter 6 we derive a systematic way to incorporate the self-propulsive swim force into the typical $N-$body hydrodynamics problem. This framework also provides a way to account for the particle motion

due to higher-order moments of a particle squirming set [37], and for particle reorientations due to a phenomenological, non-hydrodynamic mechanism. From this framework, one can (in principle) model all emergent behaviors in biological and active matter systems.

In real systems, organisms and active colloids do not move in isolation. Consider the interior of a cell, modeled as a colloidal suspension. The cytoplasm is a dense polydisperse suspension (volume fraction $\phi \sim 30 - 50\%$ [58, 59]) of both passive and active constituents—organelles, motor proteins, etc.—embedded in a gel-like matrix comprised of cytosol and filaments. Furthermore, this suspension is confined by a selectively-permeable, flexible membrane. While we do not claim to be—nor desire to be—modeling the interior of a cell, we do wish to address the fundamental idea that active constituents are often embedded in materials with other passive constituents. Bacteria may exchange signaling proteins, autophoretic nanoparticles may be in the presence of tracers or finite-sized fuel molecules, and motor proteins move in complex environments. The activity of certain constituents directly impacts the average motion of the passive counterparts, thus altering effective properties of the medium in which these particles are embedded. In biological systems, these mean properties are linked to important physiological indicators of disease [60]. In synthetic active matter systems—e.g. chemically reactive nanoparticles used in environmental remediation [5]—these active-passive interactions may inform crucial design parameters such as the surface patterning of the chemically active material.

The study of the microscopic motion of a particle through some medium is known as microrheology [60, 61]. Using the same framework as above to describe the motions of all particles in a suspension, one (or multiple) "probe" particle(s) is (are) selected [62], and its (their) passive (diffusive) and active (moving under the influence of a targeted external field or force) motions are tracked. Standard correlations such as mean-squared displacements and average particle velocities are then related to an effective tracer diffusivity [63] and viscosity of the medium [64, 65]. In the linear response regime, colloidal suspensions are known to obey a generalized Stokes-Einstein-Sutherland relation (GSESR) relating the drag and diffusivity—namely the product of the drag and diffusivity is always equal to the system temperature $k_B T$ [66, 67]. These suspension properties characterize the mean viscoelastic behavior of a material on length scales comparable to the tracer particles or the distance between tracer particles [62], whereas traditional *macro*rheology

measures the material properties on length scales much larger than the interparticle spacing. For many biological realizations of active materials, the microrheological response is often more relevant to understanding how particles move through their environment.

1.3 Contributions and outlooks

Few experimental [31, 68], computational [69], or theoretical studies have attempted to address problems of passive particle motion in active matter—the problem of tracer diffusion being a notable exception. The next two chapters aim to unify the numerous predictions of tracer diffusion in active suspensions with the local viscous response as measured by a tracer being dragged through the suspension by an external force. We compute the long-time self-diffusivity of a passive tracer using generalized Taylor dispersion theory [63, 70]. From the same theory, we compute the average velocity of the tracer particle as it actively moves through the suspension under the action of an external force. When the external force is weak compared to Brownian fluctuations, this should be related to the tracer diffusivity via a GSESR. However, because active matter systems do not obey detailed balance, this relation is not guaranteed *a priori* (and indeed has been shown to be violated in certain instances [68]). We show that an equivalent GSESR is obeyed in active systems when the run length of the swimmers is much smaller than the size of the tracer particle $\ell \ll R$: the product of the drag on the tracer and its self-diffusivity is equal to the system temperature, plus the kinetic energy of the active bath particles. We then investigate the nonlinear viscoelastic behavior via microrheology, and discover that highly active suspensions are nearly Newtonian, as measured in some experiments [31].

The results in Chapters 2 and 3 rely on a mean-field description of active systems that accounts for particle reorientations through average vector (polar) and tensor (nematic) order; this method is favored by Saintillan in his work on rheology in active suspensions [33, 71, 72]. In Chapter 4, we analyze the validity of this mean-field representation through comparison to exact numerical results for the 2-D microrheology problem. We show that—for problems in steady-state microrheology—representing the probability distribution in phase space as position-space concentration, polar order, and nematic order fields is sufficient for correct quantitative predictions.

Chapters 2-5 describe dry active systems, in that we neglect the hydrodynamic interactions between particles (though they are still embedded in a continuous medium).

Chapters 6-8 focus on an outstanding problem in the field of soft, active matter: the role of hydrodynamic interactions (HI). Most descriptions of HI in active systems rely on ad hoc approximations of the effects of activity on the fluid mechanics. The most common assumption is that the particle-phase stress is completely described by the active hydrodynamic stresslet [28, 33, 35, 73, 74], or a distribution of such stresslets along the length of a body [27]. They largely neglect interparticle and Brownian contributions to the rheological behavior. In Chapter 6 we systematically incorporate self-propulsion into the framework familiar to those who study colloidal suspensions. In Chapter 7, we apply this framework to a simple problem: the force on a boundary in a suspension of movers. In this approximation, any disturbances to the fluid velocity field are a result of the Brownian forces on the particles and the interactions with the wall; there is no contribution due to active stresses, just the swim force. We show that HI produce a substantial quantitative effect in the swim pressure measured at the wall, but that the pressure is qualitatively no different from that in the absence of HI.

In Chapter 8, we investigate the role of HI in the microrheology of active suspensions. Again, we neglect active stresses, as the necessary mobility functions for these are limited [3]. Here we find that HI are necessary to recover reports of decreased viscosities in active suspensions (though all previous reports refer to shear or extensional viscosity). In fact, we find that the microviscosity of the medium may become zero—or even negative!—as previously measured and predicted for the shear macroviscosity of active materials [34, 51]. In Chapter 9, we briefly investigate a mode of "fixed probe" microrheology, wherein the probe is held fixed, and an external field biases the motion of the active particles—similar (but not identical) to holding the probe fixed in a uniformly flowing suspension.

These findings open up an exciting realm of exploration in the micromechanics of biological systems. If self-propulsion makes a material effectively less viscous, how does it change the elasticity, and then what are the implications for physiological indicators of disease in cells? Perhaps increased compliance of infected cells is simply due to a viscosity reduction by bacteria that have invaded a host cell. Motility is also essential to processes associated with healthy cellular function, so what do these viscoelastic effects imply for cellular divison? These findings also give key design cues to those interested in developing 'smart' active, or autonomous materials. One can control the activity level with fuel concentration, but it is

[3] Ishikawa and co-workers have devised descriptions of the basic pair particle hydrodynamics for squirmers [75].

important to know that this in turn affects drag and changes the material viscoelastic response. Indeed, despite the glut of research activity in soft active materials, numerous phenomena have yet to be fully explored, and even more have yet to be exploited.

BIBLIOGRAPHY

[1]E. Schrödinger, "What Is Life?", Bioscience **41**, 631–634 (1991).

[2]M. C. Marchetti, J. F. Joanny, S. Ramaswamy, T. B. Liverpool, J. Prost, M. Rao, and R. A. Simha, "Hydrodynamics of soft active matter", Rev. Mod. Phys. **85**, 1143–1189 (2013).

[3]D. Saintillan, and M. J. Shelley, "Theory of Active Suspensions", in *Complex fluids biol. syst.* Edited by S. Spagnolie, (Springer, New York, 2015) Chap. 9, pp. 319–355.

[4]Y. Fily, Y. Kafri, A. P. Solon, J. Tailleur, and A. Turner, "Mechanical pressure and momentum conservation in dry active matter", ArXiv e-prints (2017).

[5]S. Ebbens, "Active colloids: Progress and challenges toward realising autonomous applications", Curr. Opin. Colloid Interface Sci. **21**, 14–23 (2016).

[6]F. G. Woodhouse, and R. E. Goldstein, "Spontaneous circulation of confined active suspensions", Phys. Rev. Lett. **109** (2012) 10.1103/PhysRevLett.109.168105.

[7]G. Subramanian, and D. L. Koch, "Critical bacterial concentration for the onset of collective swimming", J. Fluid Mech. **632**, 359 (2009).

[8]D. L. Koch, and G. Subramanian, "Collective Hydrodynamics of Swimming Microorganisms: Living Fluids", Annu. Rev. Fluid Mech. **43**, 637–659 (2011).

[9]A. Sokolov, and I. S. Aranson, "Physical properties of collective motion in suspensions of bacteria", Phys. Rev. Lett. **109**, 1–5 (2012).

[10]A. Zöttl, and H. Stark, "Hydrodynamics Determines Collective Motion and Phase Behavior of Active Colloids in Quasi-Two-Dimensional Confinement", Phys. Rev. Lett. **112**, 1–5 (2014).

[11]F. Alarcón, and I. Pagonabarraga, "Spontaneous aggregation and global polar ordering in squirmer suspensions", J. Mol. Liq. **185**, 56–61 (2013).

[12]D. Grossman, I. S. Aranson, and E. Ben-Jacob, "Emergence of agent swarm migration and vortex formation through inelastic collisions", New J. Phys. **10** (2008) 10.1088/1367-2630/10/2/023036.

[13]J. M. Yeomans, "The hydrodynamics of active systems", Riv. del Nuovo Cim. **40**, 1–31 (2017).

[14]J. Tailleur, and M. E. Cates, "Statistical mechanics of interacting run-and-tumble bacteria", Phys. Rev. Lett. **100**, 3–6 (2008).

[15]J. Stenhammar, A. Tiribocchi, R. J. Allen, D. Marenduzzo, and M. E. Cates, "Continuum theory of phase separation kinetics for active brownian particles", Phys. Rev. Lett. **111**, 1–5 (2013).

[16]T. Speck, "Collective behavior of active Brownian particles: From microscopic clustering to macroscopic phase separation", Eur. Phys. J. Spec. Top. **225**, 2287–2299 (2016).

[17]J. Bialké, H. Löwen, and T. Speck, "Microscopic theory for the phase separation of self-propelled repulsive disks", EPL **103**, 30008 (2013).

[18]M. E. Cates, D. Marenduzzo, I. Pagonabarraga, and J. Tailleur, "Arrested phase separation in reproducing bacteria creates a generic route to pattern formation", Proc. Natl. Acad. Sci. U. S. A. **107**, 11715–11720 (2010).

[19]G. S. Redner, A. Baskaran, and M. F. Hagan, "Reentrant phase behavior in active colloids with attraction", Phys. Rev. E - Stat. Nonlinear, Soft Matter Phys. **88**, 1–5 (2013).

[20]T. Vicsek, A. Czirk, E. Ben-Jacob, I. Cohen, and O. Shochet, "Novel type of phase transition in a system of self-driven particles", Phys. Rev. Lett. **75**, 1226–1229 (1995).

[21]S. C. Takatori, W. Yan, and J. F. Brady, "Swim pressure: Stress generation in active matter", Phys. Rev. Lett. **113**, 1–5 (2014).

[22]T. Brotto, J. B. Caussin, E. Lauga, and D. Bartolo, "Hydrodynamics of confined active fluids", Phys. Rev. Lett. **110**, 1–5 (2013).

[23]A. Patch, D. Yllanes, and M. C. Marchetti, "Kinetics of motility-induced phase separation and swim pressure", Phys. Rev. E - Stat. Nonlinear, Soft Matter Phys. **95**, 1–9 (2017).

[24]X.-l. Wu, and A. Libchaber, "Particle Diffusion in a Quasi-Two-Dimensional Bacterial Bath", Phys. Rev. Lett. **84**, 3017–3020 (2000).

[25]M. J. Kim, and K. S. Breuer, "Enhanced diffusion due to motile bacteria", Phys. Fluids **16**, 1–5 (2004).

[26]T. Ishikawa, J. T. Locsei, and T. J. Pedley, "Fluid particle diffusion in a semidilute suspension of model micro-organisms", Phys. Rev. E - Stat. Nonlinear, Soft Matter Phys. **82**, 1–15 (2010).

[27]T. V. Kasyap, D. L. Koch, and M. Wu, "Hydrodynamic tracer diffusion in suspensions of swimming bacteria", Phys. Fluids **26**, 081901 (2014).

[28]A. Morozov, and D. Marenduzzo, "Enhanced diffusion of tracer particles in dilute bacterial suspensions.", Soft Matter **10**, 2748–58 (2014).

[29]A. Jepson, V. a. Martinez, J. Schwarz-Linek, A. Morozov, and W. C. K. Poon, "Enhanced diffusion of nonswimmers in a three-dimensional bath of motile bacteria", Phys. Rev. E - Stat. Nonlinear, Soft Matter Phys. **88**, 3–7 (2013).

[30]A. E. Patteson, A. Gopinath, P. K. Purohit, and P. E. Arratia, "Particle diffusion in active fluids is non-monotonic in size.", Soft Matter **12**, 2365–72 (2016).

[31]A. Sokolov, and I. S. Aranson, "Reduction of viscosity in suspension of swimming bacteria", Phys. Rev. Lett. (2009) 10.1103/PhysRevLett.103.148101.

[32]Y. Hatwalne, S. Ramaswamy, M. Rao, and R. A. Simha, "Rheology of Active-Particle Suspensions", Phys. Rev. Lett. **92**, 1–4 (2004).

[33]D. Saintillan, "The Dilute Rheology of Swimming Suspensions: A Simple Kinetic Model", Exp. Mech. **50**, 1275–1281 (2010).

[34]H. M. López, J. Gachelin, C. Douarche, H. Auradou, and É. Clément, "Turning Bacteria Suspensions into Superfluids", Phys. Rev. Lett. **115**, 028301 (2015).

[35]M. Moradi, "Rheology of active suspensions with hydrodynamic interactions", 1–5 (2017).

[36]M. J. Lighthill, "On the Squirming Motion of Nearly Spherical Deformable Bodies through Liquids at Very Small Reynolds Numbers", Commun. Pure Appl. Math. **5**, 109–118 (1952).

[37]J. Bialké, "A spherical envelope approach to ciliary propulsion", J. Fluid Mech. **46**, 199 (1971).

[38]L. Schimansky-Geier, M. Mieth, H. Rosé, and H. Malchow, "Structure formation by active Brownian particles", Phys. Lett. A **207**, 140–146 (1995).

[39]J. F. Brady, "Particle motion driven by solute gradients with application to autonomous motion: continuum and colloidal perspectives", J. Fluid Mech. **667**, 216–259 (2011).

[40]S. Kim, and S. J. Karilla, *Microhydrodynamics : Principles and Selected Applications* (1991).

[41]J. K. G. Dhont, "Fundamental Equations of Motion", in *An introd. to dyn. colloids*, 1st ed. (Elsevier, 1996) Chap. 4, pp. 172–195.

[42]D. McQuarrie, "Theory of Brownian Motion", in *Stat. mech.* (2000) Chap. 20, pp. 452–260.

[43]É. Guazzelli, and J. F. Morris, *A physical introduction to suspension dynamics* (2011), pp. 1–229.

[44]G. Taylor, "Analysis of the Swimming of Microscopic Organisms", Proc. R. Soc. A Math. Phys. Eng. Sci. **209**, 447–461 (1951).

[45]E. Purcell, *Life at low Reynolds number*, 1977.

[46]H. C. Berg, and R. A. Anderson, "Bacteria swim by rotating their flagellar filaments", Nature **245**, 380–382 (1973).

[47]W. Yan, and J. F. Brady, "The swim force as a body force", Soft Matter **11**, 6235–6244 (2015).

[48]G. K. Batchelor, "The stress system in a suspension of force-free particles", J. Fluid Mech. **41**, 545 (1970).

[49]K. Drescher, R. E. Goldstein, N. Michel, M. Polin, and I. Tuval, "Direct measurement of the flow field around swimming microorganisms", Phys. Rev. Lett. **105**, 1–4 (2010).

[50]K. Drescher, J. Dunkel, L. H. Cisneros, S. Ganguly, and R. E. Goldstein, "Fluid dynamics and noise in bacterial cell – cell and cell – surface scattering", Proc. Natl. Acad. Sci. U. S. A. **108**, 10940–10945 (2011).

[51]S. C. Takatori, and J. F. Brady, "Superfluid Behavior of Active Suspensions from Diffusive Stretching", Phys. Rev. Lett. **118**, 018003 (2017).

[52]A. P. Solon, M. E. Cates, and J. Tailleur, "Active brownian particles and run-and-tumble particles: A comparative study", Eur. Phys. J. Spec. Top. **224**, 1231–1262 (2015).

[53]A. Einstein, "Neue Bestimmung der Moleküldimensionen", Ann. Phys., 1–5 (1906).

[54]M. von Smoluchowski, "Zur kinetischen Theorie der Brownschen Molekularbewegung und der Suspensionen", Ann. Phys. **326**, 756–780 (1906).

[55]W. Sutherland, "A dynamical theory of diffusion for non-electrolytes and the molecular mass of albumin", Philos. Mag. Ser. 6 **9**, 781–785 (1905).

[56]S. C. Takatori, and J. F. Brady, "A theory for the phase behavior of mixtures of active particles", Soft Matter **11**, 7920–7931 (2015).

[57]A. P. Solon, Y. Fily, A. Baskaran, M. E. Cates, Y. Kafri, M. Kardar, and J. Tailleur, "Pressure is not a state function for generic active fluids", Nat. Phys. **11**, 673–678 (2015).

[58]R. P. Sear, "The cytoplasm of living cells: A functional mixture of thousands of components", J. Phys. Condens. Matter **17**, 3587–3595 (2005).

[59]J. Spitzer, and B. Poolman, "How crowded is the prokaryotic cytoplasm?", FEBS Lett. **587**, 2094–2098 (2013).

[60]D. Wirtz, "Particle-tracking microrheology of living cells: principles and applications.", Annu. Rev. Biophys. **38**, 301–326 (2009).

[61]T. M. Squires, and T. G. Mason, "Fluid Mechanics of Microrheology", Annu. Rev. Fluid Mech. **42**, 413–438 (2010).

[62]J. C. Crocker, and B. D. Hoffman, *Multiple-Particle Tracking and Two-Point Microrheology in Cells*, 2007.

[63]R. N. Zia, and J. F. Brady, "Single-particle motion in colloids: force-induced diffusion", J. Fluid Mech. **658**, 188–210 (2010).

[64]T. M. Squires, and J. F. Brady, "A simple paradigm for active and nonlinear microrheology", Phys. Fluids **17**, 1–21 (2005).

[65]A. S. Khair, and J. F. Brady, "Single particle motion in colloidal dispersions: a simple model for active and nonlinear microrheology", J. Fluid Mech. **557**, 73 (2006).

[66]T. G. Mason, and D. A. Weitz, "Optical measurements of frequency-dependent linear viscoelastic moduli of complex fluids", Phys. Rev. Lett. **74**, 1250–1253 (1995).

[67]T. G. Mason, K. Ganesan, J. H. Van Zanten, D. Wirtz, and S. C. Kuo, "Particle tracking microrheology of complex fluids", Phys. Rev. Lett. **79**, 3282–3285 (1997).

[68]D. T. N. Chen, A. W. Lau, L. A. Hough, M. F. Islam, M. Goulian, T. C. Lubensky, and A. G. Yodh, "Fluctuations and rheology in active bacterial suspensions", Phys. Rev. Lett. **99**, 1–4 (2007).

[69]C. Reichhardt, and C. J. O. Reichhardt, "Active microrheology in active matter systems: Mobility, intermittency, and avalanches", Phys. Rev. E - Stat. Nonlinear, Soft Matter Phys. **91**, 1–7 (2015).

[70]I. Frankel, and H. Brenner, "Taylor diserpsion of orientable Brownian particles in unbounded homogeneous shear flows", J. Fluid Mech. **355**, 129–156 (1993).

[71]D. Saintillan, and M. J. Shelley, "Active suspensions and their nonlinear models", Comptes Rendus Phys. **14**, 497–517 (2013).

[72]R. Alonso-Matilla, B. Ezhilan, and D. Saintillan, "Microfluidic rheology of active particle suspensions: Kinetic theory", Biomicrofluidics **10** (2016).

[73]S. Nambiar, P. R. Nott, and G. Subramanian, "Stress relaxation in a dilute bacterial suspension", J. Fluid Mech. **812**, 41–64 (2017).

[74]T. M. Bechtel, and A. S. Khair, "Linear viscoelasticity of a dilute active suspension", Rheol. Acta **56**, 149–160 (2017).

[75]T. Ishikawa, M. P. Simmonds, and T. J. Pedley, *Hydrodynamic interaction of two swimming model micro-organisms*, Vol. 568 (2006), p. 119.

Chapter 2

TRACER DIFFUSION

[1]E. W. Burkholder, and J. F. Brady, "Tracer diffusion in active suspensions", Phys. Rev. E - Stat. Nonlinear, Soft Matter Phys. (2017) 10.1103/PhysRevE.95.052605,

Diffusive and rheological properties of active suspensions are important for understanding many biological systems and processes, such as transport within cells. Active Brownian particles (ABPs), which move with a self-propulsive velocity $\boldsymbol{U}_0$ and randomly reorient with a characteristic time scale τ_R, provide a minimal model for active suspensions; even the precise mechanism of their autonomous motion need not be specified. The motion of these active particles, or "swimmers," affects not only material properties (e.g. viscosity), but also the motion of passive constituents, such as nutrients or signaling proteins that may be important for cell survival.

In a passive suspension where particles lack the ability to self-propel, it is well known that "collisions" between a probe and the bath particles sterically hinder the long-time diffusive motion of a probe; the effective long-time diffusivity is less than the isolated Stokes-Einstein-Sutherland (SES) value [1, 2]. By contrast, experiments have confirmed that colloidal tracers (both Brownian and non-Brownian) in active bacterial suspensions undergo enhanced diffusive motion at long times due to bath activity. This is observed not only in liquid cultures, but also in porous media and on agar surfaces [3–5]. As a result, recent theoretical and experimental investigations have been motivated to understand the character of this enhanced diffusive motion and to provide models that describe this behavior [6–15]. For example, Kasyap et al. [10] developed a mean-field hydrodynamic theory to describe the effects of binary interactions between point tracers and ellipsoidal bacterial swimmers. This theory predicts a net enhancement of tracer diffusivity arising from the fluid flow induced by the swimming bacteria, which was shown to be a non-monotonic function of a Péclet number relating the strength of bacterial advection to the Brownian motion of the tracer. Experiments have also observed a non-monotonicity in Péclet number when varying the size of the tracer particle [16]. Other theory and experiments propose that the enhancement to the diffusivity is linear in the "active flux" due to the swimmers' autonomous motion [6–9], and that, in close-contact, entrainment

of tracers in the swimmers' flow field is primarily responsible for this enhancement [13, 14].

Here we show that these same qualitative features are recovered without considering hydrodynamic interactions (HI)—the enhanced diffusivity of passive particles may be understood as a result of the activity of the bath particles and excluded volume interactions alone. This does not mean the HI are not important, only that their effect is quantitative, not qualitative. We use a Smoluchowski-level analysis to model the active suspension and compute the long-time diffusivity of a passive probe using generalized Taylor dispersion theory and expansions in orientational tensor harmonics [2, 17, 18]. The derivation and complete expressions for the active diffusivity of the probe are given in the appendix; here we focus on limiting behaviors. Additionally, we show that these excluded volume interactions have important implications for experimental measurements of activity-enhanced diffusion: steric hindrance to passive diffusion is in competition with active enhancement and both effects must be considered when designing and analyzing experiments.

2.1 Mechanical model

Consider a passive Brownian particle of size R moving through a bath composed of a Newtonian solvent of viscosity η, and a dispersion of ABPs of size a, swim speed U_0, and reorientation time τ_R. This reorientation time may be the Brownian reorientation time, or a characteristic tumbling time of a swimmer. The origin of fluctuations in swimmer orientation is unimportant; at long times ($t \gg \tau_R$), it may be effectively modeled by a diffusive process. In the absence of the probe, the swimmers undergo both a thermal and an active random-walk, where the thermal walk is characterized by the SES diffusivity D_T, and the random walk due to their self-propulsion is characterized by a swim diffusivity $D^{swim} = U_0^2\tau_R/6$. We define the mechanical activity of the bath as the Stokes drag times the swim diffusivity: $k_sT_s = \zeta_s D^{swim}$, just as $k_BT = \zeta_s D_T$ [19]. The volume fraction of swimmers is $\phi = 4\pi a^3 n^\infty/3$, where n^∞ is the uniform number density of swimmers far from the probe. The probe has a thermal diffusivity $D_P = k_BT/\zeta_P$, and the probe-swimmer pair has a relative thermal diffusivity $D^{rel} = D_T + D_P$. The competition between swimming and Brownian motion is governed by the swim Péclet number: $Pe_s = U_0R_c/D^{rel} = U_0R/D_T = U_0a/D_P$, and $R_c = R + a$ is the center-to-center separation distance of the probe and swimmer upon contact.

It should be noted that the radii R and a are the thermodynamic particle radii, and

reflect the distance from the particle centers where their no-flux surfaces lie. This excluded annulus model is commonly used in colloidal suspensions to easily tune the strength of hydrodynamic interactions [2, 20–22]. We neglect hydrodynamic interactions in this chapter, which means that the 'contact' distance R_c may actually be many times the true body sizes (where the no-slip condition in the fluid applies). In this sense, R_c is truly the appropriate length scale, and reflective of the interparticle spacing in the fluid. In later chapters, we discuss this model in greater detail.

In the absence of activity, the (passive) bath particles hinder the probe's motion due to steric interactions [1]. For dilute suspensions the active contribution to the diffusivity is $\langle \boldsymbol{D}^{\boldsymbol{act}} \rangle \equiv \langle \boldsymbol{D} \rangle - D_P \boldsymbol{I}(1 - \phi^{ex})$, where $\langle \boldsymbol{D} \rangle$ is the effective long-time self-diffusivity of the probe and $\phi^{ex} \equiv \phi(R_c/a)^2/2$ measures the number of swimmers colliding with the probe (which can be much larger than the actual volume fraction ϕ for large probes). The diffusivity of a probe in a suspension of inactive swimmers is $D_P \boldsymbol{I}(1 - \phi^{ex})$. When the probe and ABP are the same size, $\phi^{ex} = 2\phi$, and the steric reduction is $1 - 2\phi$, a well-known result in the absence of HI. (With full HI, the reduction is $1 - 2.1\phi$ [1].) Both the effective and active diffusivities are isotropic.

We can predict D^{act} with simple scaling arguments. The kinematic definition of the diffusivity is $D^{act} = N(U')^2\tau$, where U' is the magnitude of the probe's velocity fluctuations due to collisions with the swimmers, τ is the time scale over which these fluctuations become decorrelated, and N is the number of swimmers colliding with the probe. Upon collision a swimmer pushes the probe with its propulsive swim force $\boldsymbol{F}^{swim} = \zeta_s \boldsymbol{U}_0$, while the solvent resists this motion via the probe's Stokes drag. Thus, the magnitude of velocity fluctuations is $U' \sim \zeta_s U_0/\zeta_P$. (When the probe is small compared to the swimmers, the velocity fluctuations scale with the swim speed, $U' \sim U_0$.) On average the probe will experience $N \sim n^\infty R_c^3$ collisions, where R_c^3 is the volume occupied by a swimmer-probe pair. Therefore,

$$\begin{aligned} D^{act} \quad &\sim \quad n^\infty R_c^3 \left(\frac{\zeta_s}{\zeta_P}\right)^2 U_0^2 \, \tau, \quad R \gtrsim a, \\ &\qquad n^\infty R_c^3 \, U_0^2 \, \tau, \quad R \ll a \, . \end{aligned} \tag{2.1}$$

The time scale τ differs depending on the dominant physical process governing the decorrelation and can take one of three values: (1) the diffusive time $\tau_D = R_c^2/D^{rel}$, (2) the advective time $\tau_{adv} = R_c/U_0$, and (3) the reorientation time τ_R.

2.2 Active Diffusivity

(1) When the decorrelation time $\tau = \tau_D \equiv R_c^2/D^{rel}$, the probe's fluctuations are induced by the swimming bath particles, but the fluctuations are sufficiently weak ($Pe_s \ll 1$) that they decay on the time scale of Brownian diffusion. The scaling argument predicts $D^{act} \sim D_P Pe_s^2 \phi^{ex}$, and the detailed calculations give

$$D^{act} = \frac{29}{54} D_P Pe_s^2 \phi^{ex}, \tag{2.2}$$

as one would expect for Taylor dispersion: the linear response diffusivity scales as Pe_s^2 (or U_0^2). Kasyap et al. [10] found that the hydrodynamically-driven diffusivity of a point tracer scales as $Pe_s^{3/2}\sqrt{U_0\tau_R/a}$ when swimming is weak, which is also quadratic in U_0. We predict that $D^{act} \sim Pe_s^2$ for all a/R, but curiously we find no explicit dependence on τ_R, although such a dependence is evident in Fig. 2.1; we address this in (3) below.

(2) When swimming is strong compared to Brownian motion, the appropriate time scale is $\tau = \tau_{adv} = R_c/U_0$. The swimmers are bombarding the probe so rapidly that the resulting fluctuations become decorrelated on the time it takes for a swimmers to traverse the distance R_c. The scaling analysis (2.1) predicts $D^{act} \sim D_P Pe_s \phi^{ex} \sim U_0 a \phi^{ex}$, and the detailed Smoluchowski approach gives:

$$D^{act} = \frac{1}{3\sqrt{3}} U_0 a \left(\frac{2 + \sqrt{2\tau_D/\tau_R}}{1 + \sqrt{2\tau_D/\tau_R}} \right) \phi^{ex}. \tag{2.3}$$

The probe's diffusivity is now linear in the swim speed U_0 (or linear in Pe_s), as expected from Taylor dispersion theory. Kasyap et al. [10] find that $D^{act} \sim n^\infty a^3 U_0 a$ (because the tracers have no size in their analysis the only geometric length scale is the swimmer size a), but their result is independent of τ_R. The transition from diffusive to advective behavior is shown in Fig. 2.1.

In this limit the run length of a swimmer, $\ell \equiv U_0\tau_R$, is large compared to the pair size R_c, and a swimmer collides with the probe before it is able to traverse its full run length. The swimmer pushes the probe with force $\zeta_s U_0$, but is only able to move it a distance of $O(a)$ on average. One might think that the swimmer should be able to push the probe the contact length R_c, but the no-flux boundary condition allows the swimmer to slide along the probe's surface, and thus the average distance of a push is only $O(a)$. (Only a perfect head-on collision would push the probe the full run length, but the probability measure for this is zero.) Just as in the diffusion-controlled regime, the result is insensitive to the swimmer-probe size ratio a/R. It

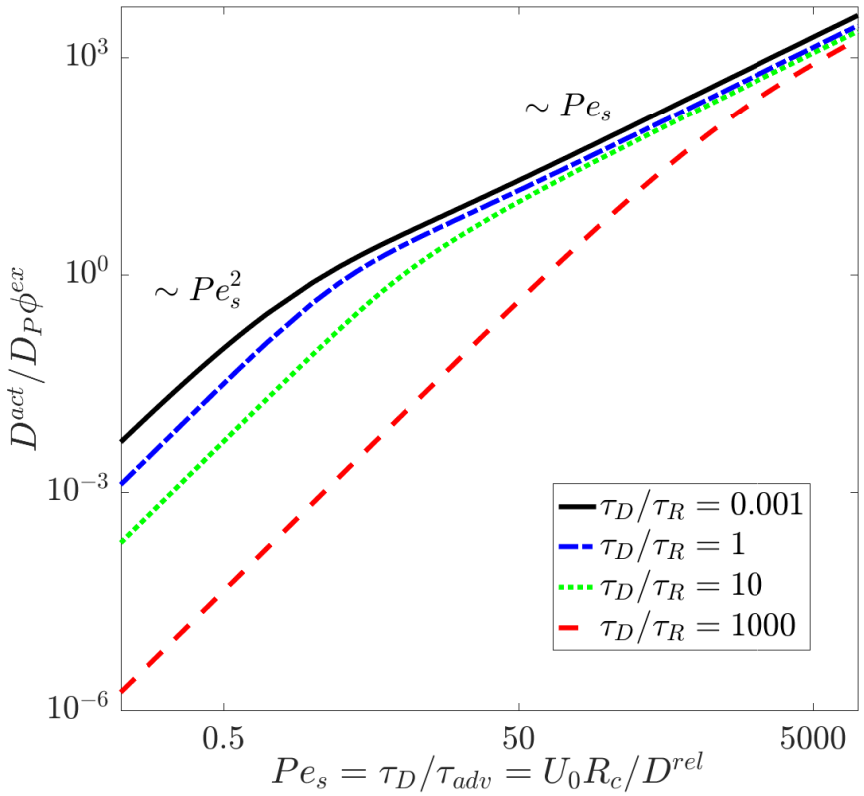

Figure 2.1: Active diffusivity of the probe as a function of the ratio of the pair-diffusion time to the advection time $Pe_s = \tau_D/\tau_{adv} = U_0 R_c/D^{rel}$, where U_0 is the swim speed, R_c is the center-to-center separation distance of the probe and swimmer upon contact, and D^{rel} is the relative thermal diffusivity of the probe-swimmer pair. The ratio τ_D/τ_R indicates the strength of Brownian motion relative to the reorienations of the swimmers. The active diffusivity is non-dimensionalized by the probe's SES diffusivity D_P times the active volume fraction $\phi^{ex} = (4\pi/3)n^{\infty}R_c^2 a/2$, where a is the swimmer size and n^{∞} is the number density of swimmers.

manifests only in ϕ^{ex}, which simply becomes ϕ for point tracers. Finally, we note that the ratio of the other two time scales τ_D/τ_R has no bearing on the scaling of the diffusivity in this limit—it can only change the result by a factor of two.

However, τ_D/τ_R significantly affects the behavior in the diffusion-dominated regime and the location of the transition from the diffusive to advective behavior. When $\tau_D/\tau_R \ll 1$, reorientations are slow and the transition occurs for $Pe_s \sim O(1)$ as one would expect. However, as reorientations become faster (τ_D/τ_R increases), the transition occurs at much higher values of Pe_s (see Fig. 2.1). In the athermal limit of no translational diffusion ($\tau_D \to \infty$), the transition to strong swimming is governed by the reorienation Péclet number $Pe_R \equiv \tau_{adv}/\tau_R = R_c/\ell \sim O(1)$ rather than the

swim Péclet number Pe_s.

(3) When Brownian motion is weak compared to the swimmers' reorientations, the decorrelation time is set by the reorientation time: $\tau = \tau_R$. The scaling arguments predict $D^{act} \sim (k_s T_s/\zeta_P)\phi^{ex}$, or $D^{act} \sim D^{swim}\phi$ for small probes. The result of the Smoluchowski analysis is in agreement:

$$D^{act} = \left(\frac{k_s T_s}{\zeta_P}\right)\frac{R}{R_c}\phi^{ex}\,. \tag{2.4}$$

Note that there is no dependence on $k_B T$.

Suppose that the swimmers and probe are large enough so that Brownian motion is not important, but the swimmers' reorientation time is relatively fast. The probe receives many small active kicks of size $k_s T_s$ from the swimmers, which are dissipated by the Stokes drag ζ_P. Thus, the diffusivity looks like what one would expect from a stochastic "Brownian" process, where the energy is $k_s T_s$ rather than $k_B T$. In the limit when the probe is very small, $(k_s T_s/\zeta_P)(R/R_c) \to U_0^2\tau_R/6$, $\phi^{ex} \to \phi$, and the active diffusivity is simply the swim diffusivity times the volume fraction of swimmers: $D^{act} = D^{swim}\phi$. As a swimmer hops in one direction and equal volume for solvent is displaced in the opposite direction.

Because the probe receives many small kicks from the swimmers, its motion is governed by a Langevin equation $0 = -\zeta_P \boldsymbol{U} + \boldsymbol{F}^{swim}$, where $\boldsymbol{U}$ is the probe velocity and the swimmers exert a fluctuating force with zero mean $\langle \boldsymbol{F}^{swim}\rangle = \boldsymbol{0}$ and autocorrelation $\langle \boldsymbol{F}^{swim}(t)\boldsymbol{F}^{swim}(t')\rangle = 2k_s T_s \zeta_P \boldsymbol{I}\delta(t-t')$ for times long compared to τ_R. The mean-squared displacement follows as $\langle(\Delta\boldsymbol{x}(t))^2\rangle = 2(k_s T_s/\zeta_P)t\boldsymbol{I}$ for the diffusivity of a particle immersed in such an active medium.

In this "continuum limit" the probe acts as a thermometer that measures the swimmers' activity $k_s T_s$. When $\ell/R_c \to 0$, active suspensions have a well-defined 'temperature' through their activity $k_s T_s$ [23] because the motion looks like a stochastic Brownian process. When $\ell/R_c \gg 1$, as is the case in the strong swimming regime, the definition of temperature breaks down because the swimmers no longer move the probe a distance ℓ, they only push it a distance a between reorientations. Thus, the swimmers do not "share" their activity fully with the probe; the appropriate shared quantity in this limit is Pe_R.

Figure 2.2 shows D^{act} as a function of τ_D/τ_R for various values of $D^{swim}/D^{rel} = (\tau_D/\tau_R)/\tau_{adv}^2 \sim k_s T_s/k_B T$. For $\tau_D/\tau_R \to \infty$ we recover the continuum-like scaling for any value of $k_s T_s/k_B T$. Though intuition might say that the diffusivity should

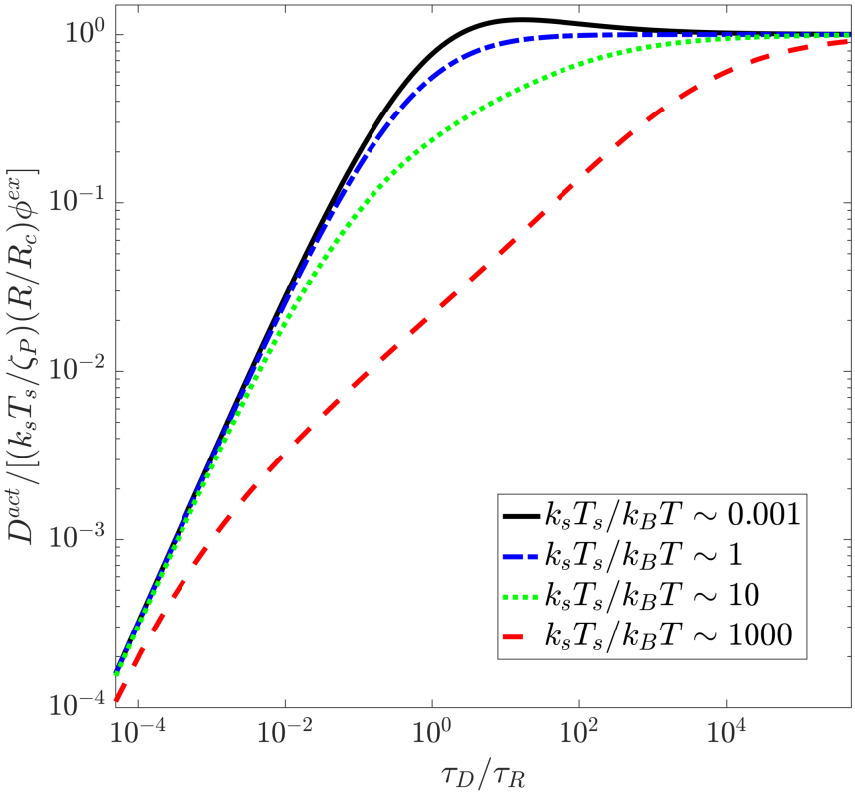

Figure 2.2: Active diffusivity of the probe non-dimensionalized by $(k_sT_s/\zeta_P)(R/R_c)\phi^{ex}$ as a function of the ratio of the diffusion time to the swimmer reorientation time $\tau_D/\tau_R = R_c^2/\tau_R D^{rel}$ for various values of the mechanical to thermal energy, k_sT_s/k_BT, where $k_sT_s = \zeta_s U_0^2 \tau_R/6$.

be dominated by thermal kicks when $k_sT_s \ll k_BT$, it is important to remember that it is the solvent, not the bath particles, that give the probe thermal kicks. The swimmers can only give kicks of size k_sT_s. The finite size of the swimmers replaces a volume of solvent, thus reducing the number of thermal kicks the probe receives. The $O(\phi^{ex})$ change in the probe diffusivity is actually *negative* when $k_sT_s < k_BT$ (see the inset of Fig. 2.3): steric hinderance exceeds active enhancement.

An interesting feature predicted by the detailed theory is a nonmontonic dependence of D^{act} on both τ_D/τ_R and Pe_s, as seen in Figs 2.2 and 2.3, respectively. As Pe_s increases, thermal diffusion slows and swimming becomes more important, so we transition from a diffusive to advective behavior. This transition does not occur monotonically with Pe_s because $Pe_R = \tau_{adv}/\tau_R$ also influences the dynamics. Imagine a scenario where τ_D and τ_R are fixed and $R \gg a$, but we adjust the swimmers' speed (perhaps by altering the amount of available fuel). When the

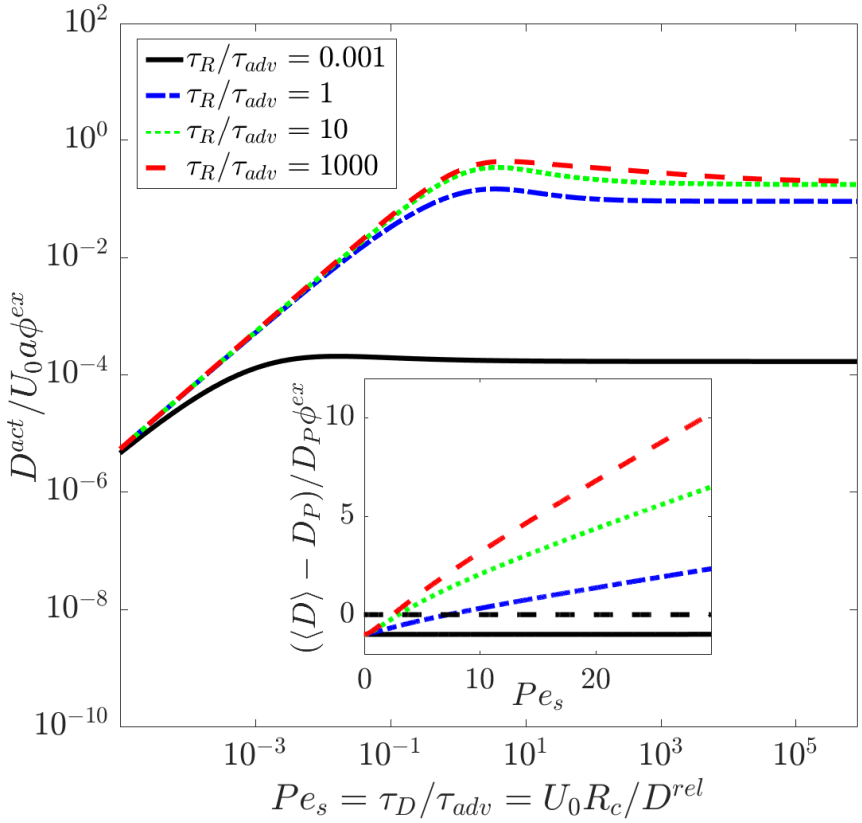

Figure 2.3: Active diffusivity of the probe non-dimensionalized by $U_0 a$ as a function of $Pe_s = \tau_D/\tau_{adv} = U_0 R_c/D^{rel}$. The ratio $\tau_R/\tau_{adv} = U_0\tau_R/R_c = \ell/R_c$ reflects the speed of reorientation relative to advection. The inset shows the total $O(\phi^{ex})$ change in the probe's diffusivity, non-dimensionalized by $D_P\phi^{ex}$, where D_P is the bare diffusivity of the probe.

swimmers move slowly, Brownian motion dominates: $\overline{D^{act}} \equiv D^{act}/(U_0 a\phi^{ex}) \sim Pe_s$. When the swim speed is large, advection dominates and $\overline{D^{act}}$ is constant. When $\tau_D \sim \tau_{adv}$, neither wins out and the reorientations are allowed to influence the dynamics. Finite Brownian motion keeps the swimmers close to the probe after a collision, and slow reorientation allows the swimmer to collide with the probe again rather than run off, thus the diffusivity is slightly higher than the advective scaling. When reorientations are too fast, this peak disappears. This is corroborated by Fig. 2.2, which reveals that D^{act} is only non-monotonic when $k_s T_s < k_B T$. The nonmontonicity still occurs when $\tau_D \sim \tau_R$, but Brownian motion is only strong enough to compete with activity if the thermal energy of the solvent exceeds the activity of the bath.

Kasyap et al. [10] find the same phenomenon in their treatment. When the diffusion is hydrodynamic in origin and advection dominates, the tracer follows a straight

trajectory along fluid streamlines. Weak Brownian motion allows the tracer to sample more trajectories, and the odd symmetry of the bacterium's dipolar flow field results in an increased correlation in probe motion. When Brownian motion is strong, the probe's motion decorrelates and the diffusivity decreases. Thus the diffusivity decreases non-monotonically with increasing Brownian motion (i.e. as one moves from right to left in Fig. 2.3). Patteson et al. [16] see something similar in experiments by varying the probe size, which is equivalent to varying Pe_s when all other parameters are fixed. They scale D^{act} by $n^{\infty}L^3U_0L$, where L is the total bacterium length. They find that this scaled diffusivity first increases with probe size as approximately R^2 and then decreases to a plateau. Our scaling analysis predicts that $\overline{D^{act}}$ is linear in probe size when diffusion dominates, and indepedent of probe size when advection dominates. In between, when the appropriate time scale is τ_R, $\overline{D^{act}}$ scales as $1/R$, thus capturing the non-monotonicity. The peak in $\overline{D^{act}}$ is predicted around $Pe_s \sim 5$ in our study and in [10], but is found experimentally around $Pe_s \sim O(10^3)$; the source of such a large discrepancy is not known. Lastly, we note that the inset of Fig. 2.3 shows that this non-monotonicity is obscured by the steric hindrance, reinforcing the importance of considering excluded-volume interactions in active suspensions.

Another common model, used by Miño et al. [7] to describe enhanced diffusion of tracers in bacterial suspensions, says that the active enhancement is proportional to the advective flux of the active particles: $\langle D \rangle = D_P + \beta J_a$, where $J_a = n^{\infty}U_0$ in our notation, similar to what we find for strong swimming. Lin et al. [11] predict that β scales as the body size to the fourth power for squirmers, but subsequent theoretical derivations indicate that $\beta^{1/4}$ also depends on the swimmer's hydrodynamic dipole moment, particle size, system geometry, swimming efficiency, etc. As in [10], these studies do not take the swimmers to be thermally active. Additionally, they argue that the size of the tracer particle does not affect β [7], and thus excluded-volume effects are generally neglected. This is valid when the tracer particles are always far enough away from the bacteria that the size effects in the Faxén expression for their velocity are negligible, which is consistent with theoretical models that assume the bacteria to be simple hydrodynamic dipoles (which is only true in the far field [24, 25]). In simulations by Ishikawa et al. [15], it was observed that point tracers diffuse more freely than tracers of finite size in suspensions of squirmers. They also argue that the effect is small, and thus do not quantify the effect systematically as a function of tracer size.

For this β model, our Smoluchowski theory predicts

$$\beta = \frac{2\pi}{9\sqrt{3}} R_c^2 a^2 \Big(\frac{2 + \sqrt{2\tau_D/\tau_R}}{1 + \sqrt{2\tau_D/\tau_R}} \Big). \tag{2.5}$$

The ability of the swimmer to randomly reorient is not required for this enhancement to the diffusivity, as argued in [8]. In contrast to some of these experimental studies, our result depends on the size of the tracer particle. In the system of Jepson et al. [6] the tracers are non-motile *E. Coli* in a suspension of motile *E. Coli* with equivalent spherical dimension $a = 1.4\mu m$. From their experimental parameters, we predict $\beta = 3.22a^4 - 6.45a^4$. To match the experimentally found value of $\beta = 7.1\mu m^4$, our theory predicts that the *E. Coli* would have an equivalent spherical dimension of $a = 1.02 - 1.22\mu m$.

As previously proposed, this advective flux model ignores the steric hinderance of the passive suspension, which should accounted for by

$$\langle D \rangle = D_P(1 - \phi^{ex}) + \beta J_a \, . \tag{2.6}$$

The steric hinderance is especially important when swimming is weak (Fig. 2.3). Experimentally, one should measure the bare diffusivity of a tracer, and then the change in diffusivity among non-motile swimmers to recover the effective particle size R_c from Batchelor's theory [1]. Knowing R_c, the average swim speed, reorientation time, and the bare particle diffusivities, one can calculate the active diffusivity from our theory, and then compare to experimental measurements.

We presented a micromechanical model for the effective diffusivity of a passive particle embedded in a suspension of ABPs. Using a generalized Taylor dispersion approach, and employing an expansion in orientational tensor harmonics, we found an exact analytical expression for the effective diffusivity of a Brownian probe for arbitrary particle sizes, swimmer activity, and time scales. Our theory agrees qualitatively with previous experimental and theoretical investigations of enhanced diffusion in active suspensions, and is able to explore regimes of parameter space not typically considered in most experiments. It highlights several key features of diffusion in active suspensions: (1) the diffusion of a tracer is nonomontonic in a Péclet number comparing swimming to thermal diffusion, (2) steric hindrance of tracer motion is in competition with the enhancement due to bath activity, and (3), when fluctuations of the tracer's motion decorrelate on the same time scale as swimmers' reorientations, the bath mimics a homogeneous solvent with energy $k_s T_s$.

Appendix

A: Average probe motion

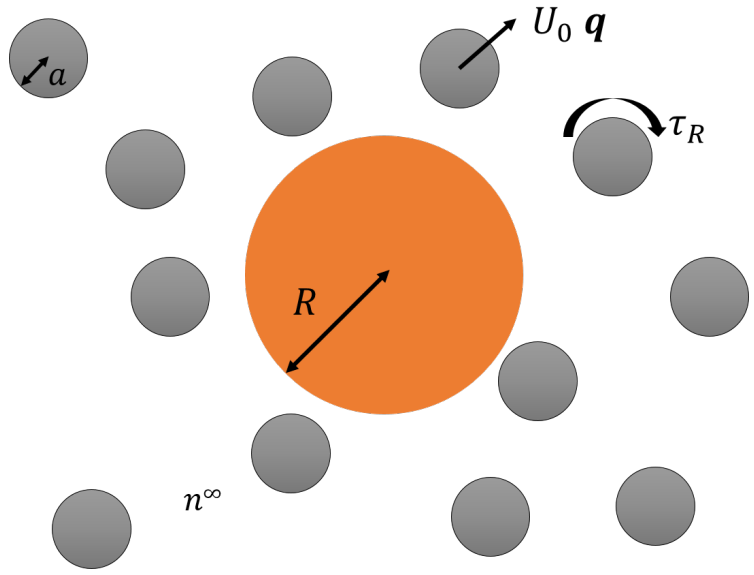

Figure 2.4: Depiction of the model system. There is a Brownian probe of size R immersed in a dispersion of ABPs with size a at number density n^∞. The ABPs swim in a direction $\boldsymbol{q}$ with speed U_0, and reorient with a characteristic time τ_R.

The dynamics of the suspension are described by a Smoluchowski equation for $P_N(\{\boldsymbol{x_\alpha}\},\{\boldsymbol{q_\alpha}\},t)$, the N-particle conditional probability of finding particle α at position $\boldsymbol{x_\alpha}$, with orientation $\boldsymbol{q_\alpha}$ at time t. The braces indicate a dependence on the position and orientation of each particle in the suspension. When the suspension is sufficiently dilute, only the pair-wise interactions between the probe and a single swimmer matter, and one may write a Smoluchowski equation for the joint probability distribution, $P_2(\boldsymbol{z},\boldsymbol{r},\boldsymbol{q};t)$, where $\boldsymbol{z}$ is the position of the probe, $\boldsymbol{r}$ is the position of the swimmer relative to the probe, and $\boldsymbol{q}$ is the orientation of the swimmer relative to the probe (see figure 2.4):

$$\frac{\partial P_2(\boldsymbol{z},\boldsymbol{r},\boldsymbol{q};t)}{\partial t} + \nabla_z \cdot \boldsymbol{j}_1^T + \nabla_r \cdot (\boldsymbol{j}_2^T - \boldsymbol{j}_1^T) + \nabla_R \cdot \boldsymbol{j}_2^R = 0, \tag{2.7}$$

where

$$\boldsymbol{j}_1^T = -D_P \nabla_z P_2 + D_P \nabla_r P_2 \tag{2.8}$$

$$\boldsymbol{j}_2^T = U_0 \boldsymbol{q} P_2 - D_T \nabla_r P_2 \tag{2.9}$$

$$\boldsymbol{j}_2^R = -\tau_R^{-1} \nabla_R P_2, \tag{2.10}$$

and $\nabla_R = \boldsymbol{q} \times \nabla_{\boldsymbol{q}}$ is the rotational operator. Again, we have neglected HI in this chapter.

When computing the effective diffusivity of the probe, we must track the average single-particle motion due to collisions with bath particles. To accomplish this, one averages the pair-level equation over all possible positions and orientations of the swimmer relative to the probe. This yields an equation for $P_1(\boldsymbol{z};t)$, the probe's single particle probability distribution:

$$\frac{\partial P_1}{\partial t} + \nabla_z \cdot \langle \boldsymbol{j}_1^T \rangle = 0, \tag{2.11}$$

where we have made use of the divergence theorem and the condition that there is no relative translational flux at contact or infinity. The angle brackets denote an ensemble average over all possible relative configurations of the swimmer relative to the probe—over $d\boldsymbol{r}d\boldsymbol{q}$. It is easier to work in Fourier space, and as such we take a Fourier transform with respect to the coordinate $\boldsymbol{z}$ to give

$$\frac{\partial \hat{P}_1}{\partial t} + i\boldsymbol{k} \cdot \langle \hat{\boldsymbol{j}}_1^{\boldsymbol{T}} \rangle = 0, \tag{2.12}$$

where the hats denote the Fourier transform of their corresponding quantities in physical space, and $\boldsymbol{k}$ is the Fourier wave vector which has the interpretation of the inverse wavelength for the probe's fluctuations. The ensemble averaged flux of the probe in Fourier space is

$$\langle \hat{\boldsymbol{j}}_1^{\boldsymbol{T}} \rangle = -i\boldsymbol{k}D_P\hat{P}_1 - D_P \int\int \nabla_r \hat{P}_2 d\boldsymbol{r}d\boldsymbol{q}. \tag{2.13}$$

The last term in the above expression shows that the collisional effects on probe motion are governed by the average gradient in the pair-level probability distribution. To determine the distribution of the bath particles relative to the probe, it is useful to define a structure function, $g(\boldsymbol{k},\boldsymbol{r},\boldsymbol{q};t)$ such that

$$\hat{P}_2(\boldsymbol{k},\boldsymbol{r},\boldsymbol{q};t) = g(\boldsymbol{k},\boldsymbol{r},\boldsymbol{q};t)\hat{P}_1(\boldsymbol{k};t). \tag{2.14}$$

To find the long-time diffusivity of the probe, we take a small-wave vector expansion of the structure function

$$g = g_0(\boldsymbol{r},\boldsymbol{q};t) + i\boldsymbol{k}\cdot\boldsymbol{d}(\boldsymbol{r},\boldsymbol{q};t) + O(k^2), \tag{2.15}$$

where $\boldsymbol{d} = (\nabla_{\boldsymbol{k}} g)_{\boldsymbol{k}=0}$ is the fluctuation field.

The average flux of the probe is

$$\begin{aligned}\langle \hat{\boldsymbol{j}}_1^{\boldsymbol{T}} \rangle = \hat{P}_1\Big(&D_P \int\int \nabla_r g_0(\boldsymbol{r},\boldsymbol{q};t) d\boldsymbol{r}d\boldsymbol{q} \\ &-D_P i\boldsymbol{k}\cdot\Big[\boldsymbol{I} - \int\int \nabla_r \boldsymbol{d}(\boldsymbol{r},\boldsymbol{q};t) d\boldsymbol{r}d\boldsymbol{q}\Big]\Big).\end{aligned} \tag{2.16}$$

The first bracketed term gives the average probe speed as it moves through the suspension:

$$\langle \boldsymbol{U}^{\boldsymbol{probe}} \rangle = \int_{r=R_c} \int \boldsymbol{n} g_0(\boldsymbol{r}, \boldsymbol{q}; t) d\boldsymbol{q} dS. \tag{2.17}$$

The $O(\boldsymbol{k})$ bracketed term represents the probe dispersion, and defines the effective diffusivity:

$$\langle \boldsymbol{D} \rangle = D_P \Big[\boldsymbol{I} - \int_{r=R_c} \int \boldsymbol{n}\, \boldsymbol{d}(\boldsymbol{r}, \boldsymbol{q}; t) d\boldsymbol{q} dS \Big], \tag{2.18}$$

which follows from eqn 2.16 by the divergence theorem. Because we are considering steric effects, the surface integral is computed over the exclusion region around the probe-swimmer contact distance: $r = R_c$.

B: Microstructure governing equations

To determine the structure functions, we write the pair-level Smoluchowski equation in Fourier space:

$$\frac{\partial \hat{P}_2}{\partial t} + i\boldsymbol{k} \cdot \hat{\boldsymbol{j}}_1^T + \nabla_r \cdot (\hat{\boldsymbol{j}}_2^T - \hat{\boldsymbol{j}}_1^T) + \nabla_R \cdot \hat{\boldsymbol{j}}_2^R = 0, \tag{2.19}$$

which can be simplified using the definition of g:

$$\begin{aligned} \frac{\partial g}{\partial t} \hat{P}_1 + g \frac{\partial \hat{P}_1}{\partial t} + i\boldsymbol{k} \cdot [-i\boldsymbol{k} D_P + \int \nabla_r g d\boldsymbol{r}] \hat{P}_1 + \nabla_r \cdot [U_0 \boldsymbol{q} g - D^{rel} \nabla_r g] \hat{P}_1 \\ + i\boldsymbol{k} \cdot \nabla_r g \hat{P}_1 - \tau_R^{-1} \nabla_R^2 g \hat{P}_1 = 0. \end{aligned} \tag{2.20}$$

Making use of the governing equation for $\hat{P}_1$ and taking the system to be at steady state, the Smoluchowski equation reduces to

$$\nabla_r \cdot [U_0 \boldsymbol{q} g - D^{rel} \nabla_r g] + 2 D_P i\boldsymbol{k} \cdot \nabla_r g - \tau_R^{-1} \nabla_R^2 g = 0, \tag{2.21}$$

with boundary conditions of no-flux at particle contact and uniform probability distribution at infinity:

$$\boldsymbol{n} \cdot [U_0 \boldsymbol{q} g - D^{rel} \nabla_r g + D_P i\boldsymbol{k} g] = 0, \quad r = R_c, \tag{2.22}$$

$$g \sim n^{\infty}, \quad r \to \infty. \tag{2.23}$$

We expand the function g_0 and the fluctuation field $\boldsymbol{d}$ in terms of orientational tensor harmonics,

$$g_0(\boldsymbol{r}, \boldsymbol{q}; t) = G^{(0)}(\boldsymbol{r}; t) + \boldsymbol{q} \cdot \boldsymbol{G}^{(\mathbf{1})}(\boldsymbol{r}; t) + \Big(\boldsymbol{qq} - \tfrac{1}{3} \boldsymbol{I} \Big) : \boldsymbol{G}^{(\mathbf{2})}(\boldsymbol{r}; t) + \ldots \tag{2.24}$$

$$\boldsymbol{d}(\boldsymbol{r},\boldsymbol{q};t) = \boldsymbol{d^{(0)}}(\boldsymbol{r};t) + \boldsymbol{q}\cdot\boldsymbol{d^{(1)}}(\boldsymbol{r};t) + \left(\boldsymbol{qq} - \tfrac{1}{3}\boldsymbol{I}\right) : \boldsymbol{d^{(2)}}(\boldsymbol{r};t) + \ldots \quad (2.25)$$

and make the closures $\boldsymbol{G^{(2)}} = 0, \boldsymbol{d^{(2)}} = 0$. We take the zeroth and first orientational moments of equation 2.21, scale the coordinate $\boldsymbol{r}$ by R_c, and divide through by $n^{\infty}R_c^2/D^{rel}$ to obtain four coupled PDEs:

$$\nabla\cdot[Pe_s\boldsymbol{G}^{(1)} - \nabla G^{(0)}] = 0, \quad (2.26)$$

$$\boldsymbol{n}\cdot[Pe_s\boldsymbol{G}^{(1)} - \nabla G^{(0)}] = 0, \quad r = 1, \quad (2.27)$$

$$G^{(0)} \sim 1, \quad r\to\infty, \quad (2.28)$$

$$\nabla\cdot[\frac{Pe_s}{3}\boldsymbol{I}G^{(0)} - \nabla\boldsymbol{G}^{(1)}] + \gamma^2\boldsymbol{G}^{(1)} = 0, \quad (2.29)$$

$$\boldsymbol{n}\cdot[\frac{Pe_s}{3}\boldsymbol{I}G^{(0)} - \nabla\boldsymbol{G}^{(1)}] = 0, \quad r = 1, \quad (2.30)$$

$$\boldsymbol{G}^{(1)} \sim \boldsymbol{0}, \quad r\to\infty, \quad (2.31)$$

$$\nabla\cdot[Pe_s\boldsymbol{d}^{(1)} - \nabla\boldsymbol{d}^{(0)} - \epsilon\boldsymbol{I}G^{(0)}] = 0, \quad (2.32)$$

$$\boldsymbol{n}\cdot[Pe_s\boldsymbol{d}^{(1)} - \nabla\boldsymbol{d}^{(0)} - \frac{\epsilon}{2}\boldsymbol{I}G^{(0)}] = 0, \quad r = 1, \quad (2.33)$$

$$\boldsymbol{d}^{(0)} \sim \boldsymbol{0}, \quad r\to\infty, \quad (2.34)$$

$$\nabla\cdot[\frac{Pe_s}{3}\boldsymbol{I}\boldsymbol{d}^{(0)} - \nabla\boldsymbol{d}^{(1)} - \epsilon\boldsymbol{I}\boldsymbol{G^{(1)}}] + \gamma^2\boldsymbol{d}^{(1)} = 0, \quad (2.35)$$

$$\boldsymbol{n}\cdot[\frac{Pe_s}{3}\boldsymbol{I}\boldsymbol{d}^{(0)} - \nabla\boldsymbol{d}^{(1)} - \frac{\epsilon}{2}\boldsymbol{I}\boldsymbol{G^{(1)}}] = 0, r = 1, \quad (2.36)$$

$$\boldsymbol{d}^{(1)} \sim \boldsymbol{0}, \quad r\to\infty, \quad (2.37)$$

where $\epsilon = 2a/R_c$. The natural dimensionless groups that arise in scaling the equations are the swim Péclet number $Pe_s = U_0R_c/D^{rel}$ and the rotational parameter $\gamma^2 = 2\tau_D/\tau_R$. The effective diffusivity will be determined entirely by $\boldsymbol{d}^{(0)}$.

C: Screened harmonic solution

Equations 2.26 and 2.29 may be decoupled by taking the divergence of 2.29:

$$\nabla^2(\nabla\cdot\boldsymbol{G^{(1)}}) - \lambda^2(\nabla\cdot\boldsymbol{G^{(1)}}) = 0, \quad (2.38)$$

where $\lambda^2 = Pe_s^2/3 + \gamma^2$. This is a Helmholtz equation for the divergence of $\boldsymbol{G}^{(1)}$, so we can expand it in gradients of the fundamental solution:

$$\nabla\cdot\boldsymbol{G^{(1)}} = C_0\frac{e^{-\lambda r}}{r} + \boldsymbol{B_0}\cdot\nabla\left(\frac{e^{-\lambda r}}{r}\right) + \boldsymbol{A_0} : \nabla\nabla\left(\frac{e^{-\lambda r}}{r}\right) + \ldots, \quad (2.39)$$

where the constants $\boldsymbol{A}_0, \boldsymbol{B}_0, C_0, ...$ are determined from the boundary conditions. Because there is no tensorial order at the boundaries $\nabla \cdot \boldsymbol{G^{(1)}} = C_0 e^{-\lambda r}/r$ only. We then substitute into equation 2.26 and obtain a Poisson's equation for the function $G^{(0)}$:

$$\nabla^2 G^{(0)} = C_0 Pe_s \frac{e^{-\lambda r}}{r}, \tag{2.40}$$

which has the solution

$$G^{(0)} = C_1 + \frac{C_2}{r} + \frac{C_0 Pe_s}{\lambda^2}\frac{e^{-\lambda r}}{r}. \tag{2.41}$$

This can be substituted into the governing equation for $\boldsymbol{G}^{(1)}$:

$$\nabla^2 \boldsymbol{G}^{(1)} - \gamma^2 \boldsymbol{G}^{(1)} = \frac{Pe_s}{3}\nabla G^{(0)}, \tag{2.42}$$

which has the solution

$$\boldsymbol{G}^{(1)} = -\frac{1}{\lambda^2}\nabla\left(C_0 \frac{e^{-\lambda r}}{r}\right) + C_2 \frac{Pe_s}{3\gamma^2}\frac{\boldsymbol{n}}{r^2}. \tag{2.43}$$

The boundary condition at infinity requires $C_1 = 1$ and the contact conditions require $C_2 = 0$. Thus,

$$G^{(0)} = 1 + \frac{Pe_s^2/3}{2(\lambda+1)+\gamma^2}\frac{e^{-\lambda(r-1)}}{r}, \tag{2.44}$$

which is the same as the concentration profile of ABPs outside a sphere. From here, one can then solve the equations for the fluctuation field by the same method.

The fluctuation field $\boldsymbol{d^{(0)}}$ in terms of two undetermined coefficients is

$$\begin{aligned}\boldsymbol{d}^{(0)} \quad &= \epsilon \boldsymbol{n}\Bigg(\frac{B}{r^2} - \frac{Pe_s^4/9\lambda^4}{2(\lambda+1)+\gamma^2}e^{-\lambda(r-1)}\left(\frac{\lambda}{r}+\frac{1}{r^2}\right) - A\frac{Pe_s}{\lambda^2}e^{-\lambda(r-1)}\left(\frac{\lambda}{r}+\frac{1}{r^2}\right) \\ &\quad -\frac{Pe_s^2/3\lambda^2}{2(\lambda+1)+\gamma^2}\left(\frac{1}{3}\frac{Pe_s^2}{\lambda^2}+1\right)e^{-\lambda(r-1)}\left(\frac{3}{4\lambda^2}\frac{1}{r^2}+\frac{3}{4\lambda}\frac{1}{r}+\frac{1}{2}\right)\Bigg),\end{aligned} \tag{2.45}$$

where the coefficients A and B are coupled to the field $\boldsymbol{d^{(1)}}$, which can be constructed with screened multipoles and linearity arguments:

$$
\begin{aligned}
\boldsymbol{d}^{(1)} \;=\; \epsilon\Bigg(& Ce^{-\gamma(r-1)}\Big\{\frac{\boldsymbol{I}}{r}-\frac{1}{\gamma^2}\Big[\Big(3\frac{\boldsymbol{nn}}{r^3}-\frac{\boldsymbol{I}}{r^3}\Big)+\gamma\Big(3\frac{\boldsymbol{nn}}{r^2}-\frac{\boldsymbol{I}}{r^2}\Big)+\gamma^2\frac{\boldsymbol{nn}}{r}\Big]\Big\} \\
& -\frac{1}{\lambda^2-\gamma^2}\frac{\frac{1}{3}Pe_s}{2(\lambda+1)+\gamma^2}e^{-\lambda(r-1)}\Big[\Big(3\frac{\boldsymbol{nn}}{r^3}-\frac{\boldsymbol{I}}{r^3}\Big)+\lambda\Big(3\frac{\boldsymbol{nn}}{r^2}-\frac{\boldsymbol{I}}{r^2}\Big)+\lambda^2\frac{\boldsymbol{nn}}{r}\Big] \\
& -\frac{\frac{1}{3}Pe_s/\lambda^2}{2(\lambda+1)+\gamma^2}e^{-\lambda(r-1)}\Big[\Big(3\frac{\boldsymbol{nn}}{r^3}-\frac{\boldsymbol{I}}{r^3}\Big)+\lambda\Big(3\frac{\boldsymbol{nn}}{r^2}-\frac{\boldsymbol{I}}{r^2}\Big)+\lambda^2\frac{\boldsymbol{nn}}{r}\Big] \\
& +\frac{1}{\lambda^2}Ae^{-\lambda(r-1)}\Big[\Big(3\frac{\boldsymbol{nn}}{r^3}-\frac{\boldsymbol{I}}{r^3}\Big)+\lambda\Big(3\frac{\boldsymbol{nn}}{r^2}-\frac{\boldsymbol{I}}{r^2}\Big)+\lambda^2\frac{\boldsymbol{nn}}{r}\Big]+B\frac{1}{3}\frac{Pe_s}{\gamma^2}\Big(3\frac{\boldsymbol{nn}}{r^3}-\frac{\boldsymbol{I}}{r^3}\Big) \\
& +\frac{(2\lambda^2-\gamma^2)^2}{Pe_s\lambda^4[2(\lambda+1)+\gamma^2]}e^{-\lambda(r-1)}\Big[\Big(3\frac{\boldsymbol{nn}}{r^3}-\frac{\boldsymbol{I}}{r^3}\Big)+\lambda\Big(3\frac{\boldsymbol{nn}}{r^2}-\frac{\boldsymbol{I}}{r^2}\Big)+\lambda^2\frac{\boldsymbol{nn}}{r}\Big] \\
& +\frac{Pe_s(2\lambda^2-\gamma^2)/3\lambda^2}{2(\lambda+1)+\gamma^2}e^{-\lambda(r-1)}\Big[\frac{3}{4\lambda^2}(\lambda r+1)\Big(\frac{\boldsymbol{I}}{r^3}-3\frac{\boldsymbol{nn}}{r^3}\Big)+\frac{1}{2}\Big(\frac{\boldsymbol{I}}{r}-\frac{\boldsymbol{nn}}{r}\Big)- \\
& \lambda\boldsymbol{nn}\Big(\frac{3}{4\lambda^2 r}+\frac{1}{2}\Big)\Big]\Bigg). \qquad (2.46)
\end{aligned}
$$

The coeffcients A, B, and C are determined by the no-flux boundary condition at $r = 1$. We have a linear system of three equations that may be solved to find algebraic expressions for $\boldsymbol{d}^{(\mathbf{0})}$:

$$
2B\Big(1+\frac{Pe_s^2}{3\gamma^2}\Big)-2CPe_s\Big(\frac{1+\gamma}{\gamma^2}\Big)=\frac{1}{2}\Big(1+C_0\frac{Pe_s}{\lambda^2}\Big)-C_0Pe_s\frac{(2+2\lambda+\lambda^2)}{\lambda^4} \qquad (2.47)
$$

$$
\begin{aligned}
& B\frac{Pe_s}{\gamma^2}-C\Big(2+\frac{3}{\gamma^2}+\frac{3}{\gamma}+\gamma\Big)+\frac{C_0}{\lambda^4}(2\lambda^2-\gamma^2)\Big(\frac{1}{2}+\frac{9}{4\lambda^2}+\frac{3}{2\lambda}+\frac{\lambda}{2}+\frac{3(1+\lambda)}{4\lambda}\Big) \\
& \quad =(3+3\lambda+\lambda^2)\Big(\frac{C_0}{\lambda^4}-\frac{A}{\lambda^2}+\frac{C_0}{\lambda^2(\lambda^2-\gamma^2)}-\frac{C_0(2\lambda^2-\gamma^2)^2}{\lambda^6(\lambda^2-\gamma^2)}\Big) \qquad (2.48)
\end{aligned}
$$

$$
\begin{aligned}
& -3B\frac{Pe_s}{\gamma^2}+C\Big(4+\frac{9}{\gamma^2}+\frac{9}{\gamma}+\gamma\Big)-\frac{C_0}{\lambda^4}(2\lambda^2-\gamma^2)\Big(\frac{5}{4}+\frac{27}{4\lambda^2}+\frac{9}{2\lambda}+\frac{5\lambda}{4}+\frac{\lambda^2}{2}+\frac{9(1+\lambda)}{4\lambda}\Big) \\
& \quad -(9+9\lambda+4\lambda^2+\lambda^3)\Big(-\frac{C_0}{\lambda^4}+\frac{A}{\lambda^2}-\frac{C_0}{\lambda^2(\lambda^2-\gamma^2)}+\frac{C_0(2\lambda^2-\gamma^2)^2}{\lambda^6(\lambda^2-\gamma^2)}\Big)-\frac{C_0(1+\lambda)}{2\lambda^2} \\
& \quad =\frac{Pe_s}{3}\Big[\frac{C_0Pe_s^3(1+\lambda)}{3\lambda^6}+\frac{APe_s(1+\lambda)}{\lambda^2}-B+\frac{C_0(2\lambda^2-\gamma^2)}{\lambda^4}\Big(\frac{1}{2}+\frac{3(1+\lambda}{4\lambda^2}\Big)\Big]. \qquad (2.49)
\end{aligned}
$$

We solved this system of equations in Mathematica to create the figures in this article. They may be solved by hand as well, but the expressions are long and it is difficult to elucidate important physics from the full expressions.

The effective diffusivity is given by

$$\langle \boldsymbol{D} \rangle = D_P \left[\boldsymbol{I} - n^{\infty} \int_{r=R_c} \boldsymbol{n}\, \boldsymbol{d}^{(\mathbf{0})} dS \right], \tag{2.50}$$

which, in terms of the undetermined coefficients, is

$$\begin{aligned} \langle \boldsymbol{D} \rangle \;=\; & D_P \boldsymbol{I} \Bigg[1 - \frac{4\pi}{3} \epsilon n^{\infty} R_c^3 \Bigg(B - \frac{Pe_s^4/9\lambda^4}{2(\lambda+1)+\gamma^2}(\lambda+1) - A \frac{Pe_s}{\lambda^2} e^{-\lambda(r-1)}(\lambda+1) \\ & - \frac{Pe_s^2/3\lambda^2}{2(\lambda+1)+\gamma^2} \Big(\frac{1}{3}\frac{Pe_s^2}{\lambda^2} + 1 \Big) \Big(\frac{3}{4\lambda^2} + \frac{3}{4\lambda} + \frac{1}{2} \Big) \Bigg) \Bigg]. \end{aligned} \tag{2.51}$$

When the bath particles are inactive, $Pe_s = 0, A = 0, B = 1/4$ and we recover the classic result: $\langle \boldsymbol{D} \rangle = D_P \boldsymbol{I} \Big(1 - \frac{1}{2} \Big(\frac{R_c}{a} \Big)^2 \phi \Big)$.

BIBLIOGRAPHY

[1]G. K. Batchelor, "Brownian diffusion of particles with hydrodynamic interaction", J. Fluid Mech. **74**, 1 (1976).

[2]R. N. Zia, and J. F. Brady, "Single-particle motion in colloids: force-induced diffusion", J. Fluid Mech. **658**, 188–210 (2010).

[3]M. J. Kim, and K. S. Breuer, "Enhanced diffusion due to motile bacteria", Phys. Fluids **16**, 1–5 (2004).

[4]X.-l. Wu, and A. Libchaber, "Particle Diffusion in a Quasi-Two-Dimensional Bacterial Bath", Phys. Rev. Lett. **84**, 3017–3020 (2000).

[5]Y. Wu, B. G. Hosu, and H. C. Berg, "Microbubbles reveal chiral fluid flows in bacterial swarms.", Proc. Natl. Acad. Sci. U. S. A. **108**, 4147–4151 (2011).

[6]A. Jepson, V. a. Martinez, J. Schwarz-Linek, A. Morozov, and W. C. K. Poon, "Enhanced diffusion of nonswimmers in a three-dimensional bath of motile bacteria", Phys. Rev. E - Stat. Nonlinear, Soft Matter Phys. **88**, 3–7 (2013).

[7]G. Miño, T. E. Mallouk, T. Darnige, M. Hoyos, J. Dauchet, J. Dunstan, R. Soto, Y. Wang, A. Rousselet, and É. Clément, "Enhanced diffusion due to active swimmers at a solid surface", Phys. Rev. Lett. **106**, 1–4 (2011).

[8]G. Miño, J. Dunstan, A. Rousselet, É. Clément, and R. Soto, "Induced Diffusion of Tracers in a Bacterial Suspension: Theory and Experiments", J. Fluid Mech. **729**, 20 (2013).

[9]A. Morozov, and D. Marenduzzo, "Enhanced diffusion of tracer particles in dilute bacterial suspensions.", Soft Matter **10**, 2748–58 (2014).

[10]T. V. Kasyap, D. L. Koch, and M. Wu, "Hydrodynamic tracer diffusion in suspensions of swimming bacteria", Phys. Fluids **26**, 081901 (2014).

[11]Z. Lin, J.-L. Thiffeault, and S. Childress, "Stirring by squirmers", J. Fluid Mech. **669**, 167–177 (2011).

[12]J.-L. Thiffeault, and S. Childress, "Stirring by swimming bodies", Phys. Lett. Sect. A Gen. At. Solid State Phys. **374**, 3487–3490 (2010).

[13]D. O. Pushkin, and J. M. Yeomans, "Fluid mixing by curved trajectories of microswimmers", Phys. Rev. Lett. **111**, 1–5 (2013).

[14]R. Jeanneret, D. O. Pushkin, V. Kantsler, and M. Polin, "Entrainment dominates the interaction of microalgae with micron-sized objects", Nat. Commun. **7**, 12518 (2016).

[15]T. Ishikawa, J. T. Locsei, and T. J. Pedley, "Fluid particle diffusion in a semidilute suspension of model micro-organisms", Phys. Rev. E - Stat. Nonlinear, Soft Matter Phys. **82**, 1–15 (2010).

[16]A. E. Patteson, A. Gopinath, P. K. Purohit, and P. E. Arratia, "Particle diffusion in active fluids is non-monotonic in size.", Soft Matter **12**, 2365–72 (2016).

[17]W. Yan, and J. F. Brady, "The force on a body in active matter", J. Fluid Mech. **6**, 1–11 (2015).

[18]D. Saintillan, and M. J. Shelley, "Theory of Active Suspensions", in *Complex fluids biol. syst.* Edited by S. Spagnolie, (Springer, New York, 2015) Chap. 9, pp. 319–355.

[19]S. C. Takatori, W. Yan, and J. F. Brady, "Swim pressure: Stress generation in active matter", Phys. Rev. Lett. **113**, 1–5 (2014).

[20]W. B. Russel, "The Huggins coefficient as a means for characterizing suspended particles", J. Chem. Soc. Faraday Trans. 2 Mol. Chem. Phys. **80**, 31 (1984).

[21]T. M. Squires, and J. F. Brady, "A simple paradigm for active and nonlinear microrheology", Phys. Fluids **17**, 1–21 (2005).

[22]N. J. Hoh, and R. N. Zia, "The impact of probe size on measurements of diffusion in active microrheology", Lab Chip **16**, 3114–3129 (2016).

[23]S. C. Takatori, and J. F. Brady, "A theory for the phase behavior of mixtures of active particles", Soft Matter **11**, 7920–7931 (2015).

[24]K. Drescher, R. E. Goldstein, N. Michel, M. Polin, and I. Tuval, "Direct measurement of the flow field around swimming microorganisms", Phys. Rev. Lett. **105**, 1–4 (2010).

[25]K. Drescher, J. Dunkel, L. H. Cisneros, S. Ganguly, and R. E. Goldstein, "Fluid dynamics and noise in bacterial cell – cell and cell – surface scattering", Proc. Natl. Acad. Sci. U. S. A. **108**, 10940–10945 (2011).

Chapter 3

FLUCTUATION-DISSIPATION IN ACTIVE MATTER

The fluctuation-dissipation theorem (FDT) "states a general relationship between the response of a given system to an external disturbance and the internal fluctuation of the system in the absence of the disturbance" [1]. This is true across a variety of systems, whether the fluctuations be thermal (classical), e.g. Johnson-Nyquist noise in a resistor, or quantized such as the fluctuations of an electric field in a vacuum [2]. The key assumptions of the FDT are that the system is in equilibrium in the absence of the disturbance—the probability distribution of states is Boltzmann-distributed with respect to the Hamiltonian of the system—and that the external disturbance is sufficiently weak that the tenets of linear response theory apply.

One of the most well-known manifestations of the FDT is the Brownian motion of a tracer particle suspended in a fluid. At thermal equilibrium, the motion of the tracer particle fluctuates due to collisions with the molecules that compose the solvent, giving rise to Brownian motion. The average velocity and displacement of the particle are zero because the fluctuations are random. The tracer motion is characterized by the mean-squared displacement (MSD) of the particle, which grows over time; the time derivative of the MSD is known as the self-diffusivity $\langle \boldsymbol{D} \rangle$ of the tracer particle. If one applies a weak external force $\boldsymbol{F}^{ext}$ to the tracer particle and drags it through the fluid, the velocity of the particle $\boldsymbol{U}$ will be linear in the applied force: $\boldsymbol{U} = \langle \boldsymbol{M}^{\boldsymbol{UF}} \rangle \cdot \boldsymbol{F}^{\boldsymbol{ext}}$, where $\langle \boldsymbol{M}^{\boldsymbol{UF}} \rangle$ is the hydrodynamic mobility of the particle—the inverse of the drag on the particle. The FDT manifests in the Stokes-Einstein-Sutherland relation (SESR) $\langle \boldsymbol{D} \rangle = k_B T \langle \boldsymbol{M}^{\boldsymbol{UF}} \rangle$, where k_B is Boltzmann's constant and T is the temperature of the system. (We will refer to the quantity $k_B T$ as the temperature in this chapter, as k_B and T will never appear independently of one another.) Alternatively expressed, the product of the self-diffusivity (fluctuation) and drag (dissipation) is precisely equal to the system temperature $\langle \boldsymbol{D} \rangle \cdot \langle \boldsymbol{M}^{\boldsymbol{UF}} \rangle^{-1} = k_B T \boldsymbol{I}$ (where $\boldsymbol{I}$ is the isotropic tensor).

This theorem does not require us to say anything about the probe particle or the medium through which it moves—the relationship between the drag and the self-diffusivity is specified only by the temperature of the system. Indeed, if we instead considered the motion of a tracer particle in a suspension of other particles (see

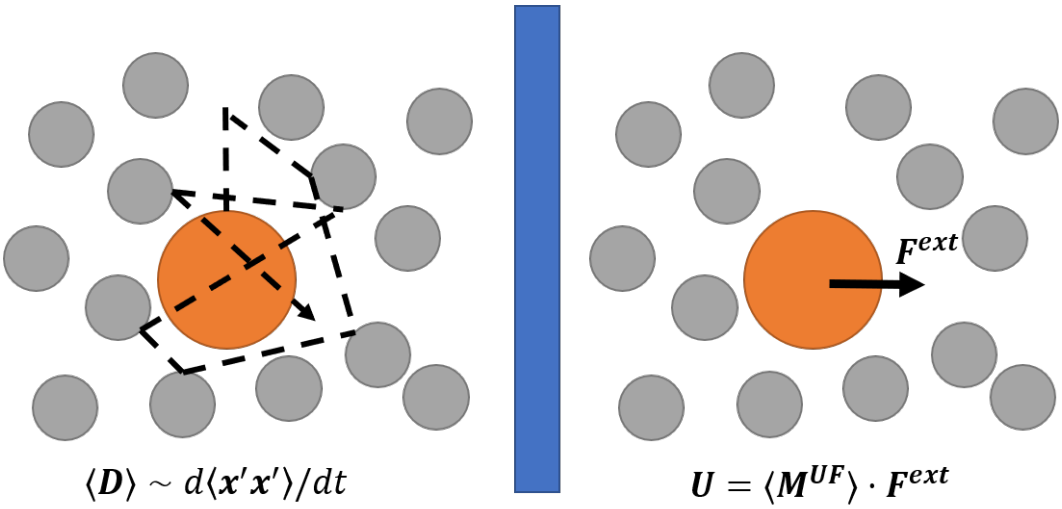

$$\langle D \rangle \cdot \langle M^{UF} \rangle^{-1} = k_B T I$$

Figure 3.1: Sketch of the fluctuation-dissipation theorem (FDT) in a colloidal suspension. LEFT: A tracer particle diffuses in a suspension of bath particles due to random Brownian motion. The time derivative of the mean squared-displacements due to Brownian motion $\langle x'x' \rangle$ is proportional to the self-diffusivity of the particle $\langle D \rangle$. RIGHT: The same tracer particle moves through the same suspension under the action of an external force F^{ext}. The speed of this particle is linear in the external force, with the constant of proportionality being the average mobility $\langle M^{UF} \rangle$. The FDT states that these two problems are fundamentally related by $\langle D \rangle \cdot \langle M^{UF} \rangle^{-1} = k_B T I$, where $k_B T$ is the temperature of the system and is independent of all other suspension properties (composition, interparticle interactions, etc.).

Fig. 3.1) this relation would be true regardless of any interactions between the particles, the concentrations of other species, or the spatial distribution of the particles (the microstructure). While both $\langle D \rangle$ and $\langle M^{UF} \rangle^{-1}$ are dependent on certain suspension properties, their product is always equal to the temperature of the system and nothing else. This is true on all time scales long compared to the momentum relaxation time of the particle, when probe motion is diffusive [3]. Thus for systems that obey the FDT one can do a single experiment—tracking the displacements of the tracer particle to compute $\langle D \rangle$ or applying a weak external force to the tracer and measuring its average speed to infer $\langle M^{UF} \rangle$—to characterize both the internal fluctuations of the system and the response to an external stimulus at a given temperature.

Active systems have recently generated substantial interest among soft-matter and statistical physicists. The constituents of these systems are able to self-propel through some physicochemical mechanism, which generates internal stresses that

drive the system out of equilibrium without the influence of external forces [4, 5]. One cannot assume *a priori* that the FDT may be applied because the steady-state internal fluctuations are not an equilibrium process. Indeed it is not even clear how one might define the chemical potential, free energy, or temperature for active systems—a challenge which has fueled a spirited debate in the literature [6–8]. Any attempts have concluded that an effective temperature depends not only on the particle activity, but also on suspension properties such as concentration and composition. Despite this complication, experimental and theoretical predictions of enhanced tracer diffusion [9–17] and reduced shear viscosity and microviscosity in active systems [18–23] are at least *qualitatively* consistent with the FDT.

As a minimal model of active systems, consider an active Brownian particle (ABP) of size a which swims at some constant speed U_0 in a direction $\boldsymbol{q}$ that changes randomly over a time scale τ_R. At times long compared to τ_R, the ABP diffuses with a long-time "active" self-diffusivity $D^{act} = D_T + D^{swim}$, where D_T is its thermal Stokes-Einstein-Sutherland (SES) diffusivity and the purely mechanical, isotropic "swim" diffusivity is $D^{swim} = U_0^2\tau_R/6$ (in 3-D). The drag on an ABP in a Newtonian solvent is given by its usual translational (Stokes) drag ζ_s. In the spirit of the SESR and FDT, we can write $\zeta_s D^{act} = k_BT + k_sT_s$, where $k_sT_s \equiv \zeta_s D^{swim}$ defines the activity of the particle. For a single active particle we thus have a generalized SESR that states that the product of the drag and the active self-diffusivity is equal to the thermal energy of the solvent, plus the kinetic energy of the swimmer. Note that we have not specified anything about the swimming mechanism, only that the particle undergoes an active random walk.

This simple single-particle result shows promising similarity with classical manifestations of the FDT, but is limited in scope. It only shows that if one uses an active particle as a tracer in a solvent, the SESR is modified by the addition of "internal" active fluctuations of the tracer itself. But what if one were to instead place a passive tracer particle in a fluid that also contained a dispersion of active particles? Is the relation between the fluctuations of the tracer particle and the drag as it moves through the suspension still linear in k_BT and k_sT_s? Does the fluctuation-dissipation relation depend on the activity only, or also on the volume fraction, etc., of the swimmers? Both the active or long-time self-diffusivity (LTSD) of a tracer in an active bath, as well as the "temperature" of an active bath have been shown to depend on properties of the system such as particle size, swimmer fraction, swimming mechanism, etc. [6, 7, 9, 10, 12, 14, 16, 24–27]. There are few measurements of the self-drag on a

tracer in an active suspension [22, 24, 28, 29]. Both the drag and the diffusivity are needed to characterize the fluctuation-dissipation relation in an active suspension.

In this chapter, we use generalized Taylor dispersion theory to make a direct connection between fluctuation and dissipation, deriving expressions for the average velocity (and thus, drag) and LTSD of a tracer (probe) particle in a generic colloidal suspension. The complete derivations regardless of suspension concentration, bath particle activity, or any other non-equilibrium effects (e.g. external shear flow) are given in appendices A and B. To illustrate the behavior we consider a dilute suspension, where only the pair-wise interactions between the tracer particle (1), and a single bath particle (2) are considered—this is depicted in Fig. 3.2. (The condition for diluteness is that the volume fraction ϕ based on the bath particle size is small $\phi \ll 1$.) In the absence of external forces, the average diffusivity $\langle \boldsymbol{D} \rangle$ of the probe in this dilute suspension is

$$\langle \boldsymbol{D} \rangle = \int \boldsymbol{D_{11}} \hat{P}^{(0,0)}_{1/1} d\boldsymbol{r} - \int \boldsymbol{U}^{(\boldsymbol{0})}_{\boldsymbol{1}} \hat{\boldsymbol{d}}^{(\boldsymbol{k})} d\boldsymbol{r} + \int (\boldsymbol{D_{12}} - \boldsymbol{D_{11}}) \cdot \nabla_r \hat{\boldsymbol{d}}^{(\boldsymbol{k})} \, d\boldsymbol{r}, \quad (3.1)$$

and the average mobility (inverse of the drag) in response to a weak external force is

$$\langle \boldsymbol{M^{UF}} \rangle = \int \boldsymbol{M^{UF}_{11}} \hat{P}^{(0,0)}_{1/1} d\boldsymbol{r} - \int \boldsymbol{U}^{(\boldsymbol{0})}_{\boldsymbol{1}} \hat{\boldsymbol{d}}^{(\boldsymbol{F})} d\boldsymbol{r} + \int (\boldsymbol{D_{12}} - \boldsymbol{D_{11}}) \cdot \nabla_r \hat{\boldsymbol{d}}^{(\boldsymbol{F})} \, d\boldsymbol{r}. \quad (3.2)$$

The probability of finding the bath particle at some position $\boldsymbol{r}$ relative to the probe in the absence of any forcing is described by $\hat{P}^{(0,0)}_{1/1}$. The diffusivity tensors $\boldsymbol{D_{11}} = k_B T \boldsymbol{M^{UF}_{11}}$, and $\boldsymbol{D_{12}} = k_B T \boldsymbol{M^{UF}_{12}}$ are based on the hydrodynamic self- and pair-mobility of the probe particle, respectively [30]. The velocity of the probe particle due to activity, interparticle forces, external shear, etc. is $\boldsymbol{U}^{(0)}_{1}$; this velocity excludes only the velocity due to the external force $\boldsymbol{M^{UF}_{11}} \cdot \boldsymbol{F^{ext}}$ and Brownian motion. The long-wavelength fluctuations in the probe's position due to Brownian forces in the solvent are described by $\hat{\boldsymbol{d}}^{(\boldsymbol{k})}$, and its fluctuations due to the action of the external force are given by $\hat{\boldsymbol{d}}^{(\boldsymbol{F})}$.

Equations 3.1 and 3.2 show that the diffusivity and mobility are formally identical (modulo a factor of $k_B T$) under the lens of generalized Taylor dispersion theory. For the FDT to hold, we only require that $\hat{\boldsymbol{d}}^{(\boldsymbol{k})} = k_B T \hat{\boldsymbol{d}}^{(\boldsymbol{F})}$. The dispersion due to the fluctuating Brownian force $-i\boldsymbol{k} k_B T$ must be mechanically identical to that from the external force $\boldsymbol{F^{ext}}$; this is the mechanical underpinning of the FDT for systems in equilibrium.

Fluctuations arising from the thermal forces in the solvent are described by

$$\frac{\partial \hat{\boldsymbol{d}}^{(\boldsymbol{k})}}{\partial t} + \nabla_r \cdot \left([\boldsymbol{U}_{\mathbf{2}}^{(\mathbf{0})} - \boldsymbol{U}_{\mathbf{1}}^{(\mathbf{0})}] \hat{\boldsymbol{d}}^{(\boldsymbol{k})} - \boldsymbol{D}^{\boldsymbol{rel}} \cdot \nabla_{r_\beta} \hat{\boldsymbol{d}}^{(\boldsymbol{k})} \right) = \hat{P}^{(0,0)}_{1/1} (\langle \boldsymbol{U}^{\boldsymbol{probe}} \rangle - \boldsymbol{U}_{\mathbf{1}}^{(\mathbf{0})})$$
$$+2(\boldsymbol{D}_{\mathbf{12}} - \boldsymbol{D}_{\mathbf{11}}) \cdot \nabla_r \hat{P}^{(0,0)}_{1/1} + \hat{P}^{(0,0)}_{1/1} \nabla_r \cdot (\boldsymbol{D}_{\mathbf{12}} - \boldsymbol{D}_{\mathbf{11}}), \tag{3.3}$$

while the fluctuations arising from the external force are described by

$$\frac{\partial \hat{\boldsymbol{d}}^{(F)}}{\partial t} + \nabla_r \cdot \left([\boldsymbol{U}_{\mathbf{2}}^{(\mathbf{0})} - \boldsymbol{U}_{\mathbf{1}}^{(\mathbf{0})}] \hat{\boldsymbol{d}}^{(F)} - \boldsymbol{D}^{\boldsymbol{rel}} \cdot \nabla_r \hat{\boldsymbol{d}}^{(F)} \right)$$
$$= \nabla_r \cdot [(\boldsymbol{M}^{\boldsymbol{UF}}_{\mathbf{12}} - \boldsymbol{M}^{\boldsymbol{UF}}_{\mathbf{11}}) \hat{P}^{(0,0)}_{1/1}]. \tag{3.4}$$

The relative thermal diffusivity is $\boldsymbol{D}^{\boldsymbol{rel}} = \boldsymbol{D}_{\mathbf{11}} + \boldsymbol{D}_{\mathbf{22}} - \boldsymbol{D}_{\mathbf{21}} - \boldsymbol{D}_{\mathbf{12}}$. The two fluctuations are the same only in the case that the local probe velocity in the absence of the external force

$$\boldsymbol{U}^{\boldsymbol{probe}} = \boldsymbol{U}_{\mathbf{1}}^{(\mathbf{0})} - (\boldsymbol{D}_{\mathbf{12}} - \boldsymbol{D}_{\mathbf{11}}) \cdot \nabla_r \ln \hat{P}^{(0,0)}_{1/1}, \tag{3.5}$$

is equal to its suspension average over $\hat{P}^{(0,0)}_{1/1}$:

$$\langle \boldsymbol{U}^{\boldsymbol{probe}} \rangle = \int \boldsymbol{U}_{\mathbf{1}}^{(\mathbf{0})} \hat{P}^{(0,0)}_{1/1} d\boldsymbol{r} - \int (\boldsymbol{D}_{\mathbf{12}} - \boldsymbol{D}_{\mathbf{11}}) \cdot \nabla_r \hat{P}^{(0,0)}_{1/1} \, d\boldsymbol{r}. \tag{3.6}$$

In general the detailed and average probe velocities are not the same. They are the same and the FDT is satisfied if $\boldsymbol{U}^{\boldsymbol{probe}}$ and $\hat{P}^{(0,0)}_{1/1}$ are spatially uniform, or if $\boldsymbol{U}^{\boldsymbol{probe}} = 0$ as is the case in [31].

In the next section, we show that this condition is not met for a dilute active suspension—the product $\langle \boldsymbol{D} \rangle \cdot \langle \boldsymbol{M}^{\boldsymbol{UF}} \rangle^{-1}$ thus depends on the geometry and activity of the suspension. However, in certain limits, we can recover the same fluctuation-dissipation relation as found for a single active particle moving in a Newtonian fluid.

3.1 Model system

Consider the motion of a tracer particle of size R with Stokes-Einstein-Sutherland (SES) diffusivity D_P in an active suspension. In addition to Brownian fluctuations from the solvent, the tracer moves under the action of a constant external force $\boldsymbol{F}^{\boldsymbol{ext}}$. The suspension is composed of ABPs with size a, (constant) swim speed U_0, SES diffusivity D_T, and a characteristic reorientation time τ_R in a Newtonian solvent of viscosity η_s. We neglect hydrodynamic interactions (HI), assume the

suspension to be sufficiently dilute ($\phi = 4\pi n^\infty a^3/3 \ll 1$ in three dimensions or $\phi_A = 4\pi a^2 n_A^\infty \ll 1$ in two-dimensions, where n^∞ is the constant volumetric number density of swimmers and n_A^∞ is the constant areal number density of swimmers) that we only need to consider pair-wise particle interactions. The dynamics of this system are described by the following Smoluchowski equation:

$$\frac{\partial P_2}{\partial t} + \nabla_z \cdot \boldsymbol{j}_{\boldsymbol{P}}^T + \nabla_r \cdot (\boldsymbol{j}_{\boldsymbol{s}}^{\boldsymbol{T}} - \boldsymbol{j}_{\boldsymbol{P}}^{\boldsymbol{T}}) + \nabla_R \cdot \boldsymbol{j}_{\boldsymbol{s}}^{\boldsymbol{R}} = 0, \tag{3.7}$$

where $\nabla_R = \boldsymbol{q} \times \nabla_{\boldsymbol{q}}$ is the orientation-space gradient operator for an axisymmetric particle. This is a conservation statement for the probability P_2 of finding a swimmer with position $\boldsymbol{r}$ and orientation $\boldsymbol{q}$ relative to a probe at position $\boldsymbol{z}$ (we neglect orientational degrees of freedom for the probe). The translational flux of the probe is $\boldsymbol{j}_{\boldsymbol{P}}^{\boldsymbol{T}} = \boldsymbol{M}^{\boldsymbol{UF}} \cdot \boldsymbol{F}^{\boldsymbol{ext}} P_2 - D_P \nabla_z P_2 + D_P \nabla_r P_2$; $\boldsymbol{M}^{\boldsymbol{UF}} = \boldsymbol{I}/\zeta_P$ is the bare probe mobility in the absence of HI and ζ_P is its (Stokes) drag coefficient. The translational flux of the swimmer is $\boldsymbol{j}_{\boldsymbol{s}}^{\boldsymbol{T}} = U_0 \boldsymbol{q} P_2 - D_T \nabla_r P_2$ and its rotational flux is $\boldsymbol{j}_{\boldsymbol{s}}^{\boldsymbol{R}} = -\tau_R^{-1} \nabla_R P_2$.

The average motion of the probe is governed by the single-particle equation

$$\frac{\partial \hat{P}_1}{\partial t} + i\boldsymbol{k} \cdot \langle \hat{\boldsymbol{j}}_{\boldsymbol{P}}^{\boldsymbol{T}} \rangle = 0, \tag{3.8}$$

where the angle brackets represent an average over the swimmer configurations—over $d\boldsymbol{r}d\boldsymbol{q}$—and we have taken a Fourier transform with respect to $\boldsymbol{z}$. The average flux of the probe is

$$\langle \hat{\boldsymbol{j}}_{\boldsymbol{P}}^{\boldsymbol{T}} \rangle = \hat{P}_1 \left[\boldsymbol{M}^{\boldsymbol{UF}} \cdot \boldsymbol{F}^{\boldsymbol{ext}} - i\boldsymbol{k} D_P + D_P \int \int \nabla_r \hat{P}_{1/1} d\boldsymbol{r} d\boldsymbol{q} \right], \tag{3.9}$$

where we have defined $\hat{P}_2(\boldsymbol{k}, \boldsymbol{r}, \boldsymbol{q}, t) = \hat{P}_{1/1}(\boldsymbol{k}, \boldsymbol{r}, \boldsymbol{q}, t) \hat{P}_1(\boldsymbol{k}, t)$. The long-time self-diffusivity of the probe is given by the long-wavelength (small $\boldsymbol{k}$) fluctuations in $\hat{P}_{1/1}$ so we write $\hat{P}_{1/1} = \hat{P}_{1/1}^{(0)} + i\boldsymbol{k} \cdot \hat{\boldsymbol{d}}^{(\boldsymbol{k})} + O(k^2)$ as in previous works [27, 31, 32]. Expanding the average probe flux with respect to $\boldsymbol{k}$ ($\langle \hat{\boldsymbol{j}}_{\boldsymbol{P}}^{\boldsymbol{T}} \rangle = \hat{P}_1 [\langle \boldsymbol{U}^{\boldsymbol{probe}} \rangle - i\boldsymbol{k} \cdot \langle \boldsymbol{D} \rangle + ...]$) defines the average velocity and long-time self-diffusivity (LTSD):

$$\langle \boldsymbol{U}^{\boldsymbol{probe}} \rangle \equiv \boldsymbol{M}^{\boldsymbol{UF}} \cdot \boldsymbol{F}^{\boldsymbol{ext}} + D_P \int \nabla_r \hat{P}_{1/1}^{(0)} \, d\boldsymbol{r} d\boldsymbol{q}, \tag{3.10}$$

$$\langle \boldsymbol{D} \rangle \equiv D_P \left[\boldsymbol{I} - \int \nabla_r \hat{\boldsymbol{d}}^{(\boldsymbol{k})} \, d\boldsymbol{r} d\boldsymbol{q} \right]. \tag{3.11}$$

When the external force is weak compared to Brownian motion, we can also expand the microstructure with respect to $\boldsymbol{F^{ext}}$: $\hat{P}^{(0)}_{1/1} = \hat{P}^{(0,0)}_{1/1} - \boldsymbol{F^{ext}} \cdot \hat{\boldsymbol{d}}^{(F)} + O(F^{ext})^2$. The average speed of the probe is now

$$\langle \boldsymbol{U^{probe}} \rangle = \underbrace{D_P \int \nabla_r \hat{P}^{(0,0)}_{1/1} \, d\boldsymbol{r} d\boldsymbol{q}}_{\langle \boldsymbol{U^{drift}} \rangle} + \boldsymbol{F^{ext}} \cdot \underbrace{\left[\boldsymbol{M^{UF}} - D_P \int \nabla_r \hat{\boldsymbol{d}}^{(F)} \, d\boldsymbol{r} d\boldsymbol{q} \right]}_{\langle \boldsymbol{M^{UF}} \rangle} . \quad (3.12)$$

The first term in the above equation is the probe's drift velocity—the average velocity resulting non-zero suspension-averaged forces acting on the probe (other than the external force). The expression for $\langle \boldsymbol{M^{UF}} \rangle$ is formally identical to that for $\langle \boldsymbol{D} \rangle$ (3.11)—the LTSD of the probe is the same as its mobility under the action of a small external force (modulo a factor of $k_B T$). Though the formal relations are the same, the mobility of the particle is not necessarily identical to its self-diffusivity unless $\hat{\boldsymbol{d}}^{(\boldsymbol{k})} = k_B T \hat{\boldsymbol{d}}^{(F)}$.

In the introduction (and more generally in Appendix B) it is shown that the two fluctuation fields are not governed by the same equations for a generic suspension not in equilibrium. For the model suspension under consideration here, the FDT is not satisfied unless $\nabla_r \ln \hat{P}^{(0,0)}_{1/1} = 0$, which is known not to be true because swimmers accumulate at the surface of the probe (see Eqn. 2.44) [33, 34]. For a single ABP, the FDT is not satisfied; however, the product of the active diffusivity and the drag $\zeta_s D^{act}$ is linear in the temperature $k_B T$ and the activity $k_s T_s$. An analogous statement for the passive tracer in an active suspension would be $\langle \boldsymbol{M^{UF}} \rangle^{-1} \cdot \langle \boldsymbol{D} \rangle = k_B T + E^{act}$; a strong statement of fluctuation-dissipation could be made if E^{act} depends only on the activity of the bath particles $k_s T_s$. E^{act} is determined by the fluctuation field $\boldsymbol{d'} \equiv \hat{\boldsymbol{d}}^{(\boldsymbol{k})} - k_B T \hat{\boldsymbol{d}}^{(F)}$, which measures departures from the FDT due to non-equilibrium processes. To determine the GSESR for active suspensions, we can thus solve for $\langle \boldsymbol{D} \rangle$ [27] and then $\langle \boldsymbol{M^{UF}} \rangle$ (or E^{act}) separately. We solve the problem for the average mobility (or average drag) as it is precisely the fixed-force microrheology problem for a probe in an active bath, and thus has applications beyond the present discussion.

We solve the Smoluchowski equation (3.7) using the familiar method popularized by Saintillan and Shelley [35] and expand the pair-distribution function in terms of

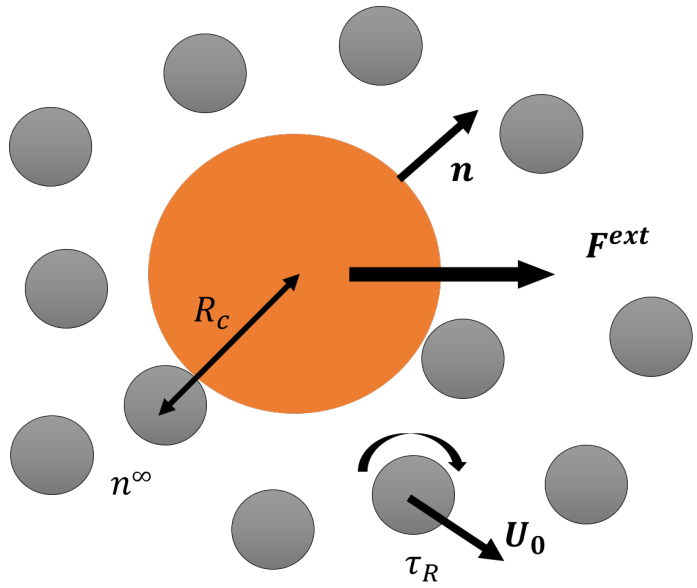

Figure 3.2: Schematic of the model system: a Brownian probe particle of size R immersed in a suspension of $ABPs$ with size a at number density n^{∞}—the center-to-center separation distance upon a collision is denoted by $R_c = R + a$. The ABPs swim in a direction $\boldsymbol{q}$ at speed U_0; $\boldsymbol{q}$ changes randomly on a time scale characterized by τ_R. The probe translates under the action of a constant external force $\boldsymbol{F^{ext}}$.

orthogonal tensor harmonics in $\boldsymbol{q}$

$$\hat{P}^{(0,0)}_{1/1}(\boldsymbol{r},\boldsymbol{q};t) = n_0(\boldsymbol{r};t) + \boldsymbol{q}\cdot\boldsymbol{m_0}(\boldsymbol{r};t) + (\boldsymbol{qq}-\boldsymbol{I}/d):\boldsymbol{Q_0}(\boldsymbol{r};t) + (\boldsymbol{qqq}-\boldsymbol{\alpha}\cdot\boldsymbol{q}/(d+2))\odot\boldsymbol{B_0} + \ldots \tag{3.13}$$

$$\hat{\boldsymbol{u}}\cdot\hat{\boldsymbol{d}}^{(F)}(\boldsymbol{r},\boldsymbol{q};t) = n'(\boldsymbol{r};t) + \boldsymbol{q}\cdot\boldsymbol{m'}(\boldsymbol{r};t) + (\boldsymbol{qq}-\boldsymbol{I}/d):\boldsymbol{Q'}(\boldsymbol{r};t) + (\boldsymbol{qqq}-\boldsymbol{\alpha}\cdot\boldsymbol{q}/(d+2))\odot\boldsymbol{B'} + \ldots, \tag{3.14}$$

where d is the spatial dimension ($d = 2, 3$ in this article), $\boldsymbol{I}$ is the identity tensor, and $\boldsymbol{\alpha}$ is the fourth-order isotropic tensor. The unit vector in the direction of the external force is $\hat{\boldsymbol{u}}$. The zeroth moment n is the concentration field, $\boldsymbol{m}$ is the polar order, $\boldsymbol{Q}$ is the nematic order, and so on [35, 36]. In the absence of external forces, the closure $\boldsymbol{Q_0 = 0}$ results in qualitative and often good quantitative agreement between calculations of the particle-phase pressure using theory and Brownian dynamics simulations—the closure $\boldsymbol{B_0} = 0$ provided nearly exact quantitative agreement between theory and simulation [33]. We examine both closures in this problem, and provide a comparison to the exact solution (for $d = 2$) for various closures in Chapter 4.

The governing equations for n_0, $\boldsymbol{m_0}$ and $\boldsymbol{Q_0}$ may be found in the appendix of [33]. Applying the moments-averaging procedure to the governing equation and boundary

conditions for $\hat{\boldsymbol{u}} \cdot \hat{\boldsymbol{d}}^{(F)}$ yields a system of coupled PDEs governing the steady-state perturbed microstructure:

$$\nabla_r \cdot [U_0 \boldsymbol{m'} - D^{rel} \nabla n'] = \boldsymbol{M^{UF}} \cdot \boldsymbol{F^{ext}} \cdot \nabla n_0 \tag{3.15}$$

$$\nabla_r \cdot [U_0 (\boldsymbol{I} n'/d + \boldsymbol{Q'}) - D^{rel} \nabla \boldsymbol{m'}] + (d-1) D_R \boldsymbol{m'} = \boldsymbol{M^{UF}} \cdot \boldsymbol{F^{ext}} \cdot \nabla \boldsymbol{m_0}, \tag{3.16}$$

$$\nabla_r \cdot [U_0 (\boldsymbol{\alpha} \cdot \boldsymbol{m'}/(d+2) - \boldsymbol{I m'}/d) - D^{rel} \nabla \boldsymbol{Q'}] + 2d D_R \boldsymbol{Q'} = \boldsymbol{M^{UF}} \cdot \boldsymbol{F^{ext}} \cdot \nabla \boldsymbol{Q_0}, \tag{3.17}$$

where we have neglected terms of $O(i\boldsymbol{k})$, as they are not necessary to determine the average probe speed. The relative translational diffusivity is the sum of the bare probe and swimmer SES diffusivities $D^{rel} = D_P + D_T$. Note that these governing equations are valid even when the external force is not weak—i.e. when the expansion $\hat{P}^{(0)}_{1/1} = \hat{P}^{(0,0)}_{1/1} - \boldsymbol{F^{ext}} \cdot \hat{\boldsymbol{d}}^{(F)} + O(F^{ext})^2$ is no longer valid—and can thus be applied to the nonlinear microrheology problem (Chapter 5).

At particle contact $r = R_c \equiv R + a$ there can be no translational flux:

$$\boldsymbol{n} \cdot [U_0 \boldsymbol{m'} - D^{rel} \nabla n'] = \boldsymbol{n} \cdot \boldsymbol{M^{UF}} \cdot \boldsymbol{F^{ext}} n_0, \; r = R_c, \tag{3.18}$$

$$\boldsymbol{n} \cdot [U_0 (\boldsymbol{I} n'/d + \boldsymbol{Q'}) - D^{rel} \nabla \boldsymbol{m'}] = \boldsymbol{n} \cdot \boldsymbol{M^{UF}} \cdot \boldsymbol{F^{ext}} \boldsymbol{m_0}, \; r = R_c, \tag{3.19}$$

$$\boldsymbol{n} \cdot [U_0 (\boldsymbol{\alpha} \cdot \boldsymbol{m'}/(d+2) - \boldsymbol{I m'}/d) - D^{rel} \nabla \boldsymbol{Q'}] = \boldsymbol{n} \cdot \boldsymbol{M^{UF}} \cdot \boldsymbol{F^{ext}} \boldsymbol{Q_0}, \; r = R_c, \tag{3.20}$$

where $\boldsymbol{n}$ is the outward-pointing unit normal of the probe. In the far-field there is no long-ranged order $\hat{P}^{(0)}_{1/1} = n^{\infty}/4\pi$ as $r \to \infty$ and thus the fluctuations are zero:

$$n', \boldsymbol{m'}, \boldsymbol{Q'} \sim 0, \; r \to \infty. \tag{3.21}$$

One may solve this system analytically when $\boldsymbol{Q'} = 0$ (see Appendix C). For $\boldsymbol{Q'} \neq 0$ the solution must be obtained numerically, which we do using a second-order finite difference scheme [37].

3.2 Probe speed and self-drag

In the linear-response regime the probe velocity is linear in the applied external force:

$$\langle \boldsymbol{U^{probe}} \rangle = \langle \boldsymbol{U^{drift}} \rangle + \boldsymbol{F^{ext}} \cdot \left[\boldsymbol{M^{UF}} - D_P \int \nabla_r \hat{\boldsymbol{d}}^{(F)} \, d\boldsymbol{r} d\boldsymbol{q} \right]. \tag{3.22}$$

Due to the symmetry of this problem, $\langle \boldsymbol{U^{drift}} \rangle$ is zero and the probe mobility is isotropic: $\langle \boldsymbol{M^{UF}} \rangle = \boldsymbol{I} \langle \mu \rangle$, where $\langle \mu \rangle$ is the mobility coefficient. In general

the mobility problem (the velocity of a particle due to an applied force) and the resistance problem (the force on a particle moving at a particular speed) are different. For the simple case of the probe particle (1) and a single swimmer (2), the probe's hydrodynamic self-mobility is

$$\boldsymbol{M}_{\mathbf{11}}^{\boldsymbol{UF}} = [\boldsymbol{R}_{\mathbf{11}}^{\boldsymbol{FU}} - \boldsymbol{R}_{\mathbf{12}}^{\boldsymbol{FU}} \cdot (\boldsymbol{R}_{\mathbf{22}}^{\boldsymbol{FU}})^{-1} \cdot \boldsymbol{R}_{\mathbf{21}}^{\boldsymbol{FU}}]^{-1} \neq (\boldsymbol{R}_{\mathbf{11}}^{\boldsymbol{FU}})^{-1}, \tag{3.23}$$

where the linear relation between the velocity of particle α and the force on particle β is $\boldsymbol{M}_{\boldsymbol{\alpha\beta}}^{\boldsymbol{UF}}$ and the relation between the force on partcile α due to the motion of particle β is $\boldsymbol{R}_{\boldsymbol{\alpha\beta}}^{\boldsymbol{FU}}$. The self-drag of the probe $\boldsymbol{R}_{11}^{\boldsymbol{FU}}$ is not equal to the inverse of its self-mobility $\boldsymbol{M}_{\mathbf{11}}^{\boldsymbol{UF}}$ in general [30], rather it depends on the hydrodynamic interactions between all the other particles in the suspension. Even if the average hydrodynamic mobility and resistance are isotropic, $\langle \boldsymbol{M}_{\mathbf{11}}^{\boldsymbol{UF}} \rangle = \langle \mu^{HI} \rangle \boldsymbol{I}$ and $\langle \boldsymbol{R}_{\mathbf{11}}^{\boldsymbol{FU}} \rangle = \langle \zeta^{HI} \rangle \boldsymbol{I}$, the mobility and drag are not necessarily inverses $\langle \mu^{HI} \rangle \neq 1/\langle \zeta^{HI} \rangle$. In the special case under consideration—where we neglect fluid velocity disturbances of the particles—the probe's hydrodynamic self-drag is just the Stokes drag ζ_P and the hydrodynamic self-drag and self-mobility are inverses. This allows us to easily move from the mobility formulation of generalized Taylor dispersion theory to the resistance formulation implicit in discussing the drag on the probe.

In addition to the hydrodynamic contribution to the mobility (and drag), there is the interparticle piece represented by the integral in Eqn. 3.22. This includes the entropic restoring force in the bath, and would also account for Brownian drift in the presence of hydrodynamic interactions (there is no such contribution in the simple scenario we consider here). The total drag on the probe—the Stokes drag plus the additional drag due to interparticle interactions—is given by

$$\langle \zeta \rangle = \zeta_P \left[1 + \frac{k_B T}{F^{ext}} \int_{R_c} \hat{\boldsymbol{u}} \cdot \boldsymbol{n}\, n' dS \right], \tag{3.24}$$

which we have expressed as an integral of the concentration fluctuation n' over the contact surface R_c. Note that the interparticle piece depends only on interactions at the no-flux boundary, whereas the hydrodynamic (and Brownian) piece will in general depend on the entire configuration of the suspension. Conventionally, the self-drag $\langle \zeta \rangle$ of the probe is defined in terms of a suspension-averaged viscosity: $\langle \zeta \rangle = 6\pi \langle \eta \rangle R$ where $\langle \eta \rangle$ is known as the microviscosity of the suspension [37, 38]. In the absence of any hydrodynamic interactions or interparticle forces, the microviscosity of a passive suspension is $\langle \eta \rangle = \eta_s(1 + \phi^{ex})$, where the excluded volume fraction is $\phi^{ex} = \phi(1 + R/a)^2/2$. The effect of the bath particles is characterized

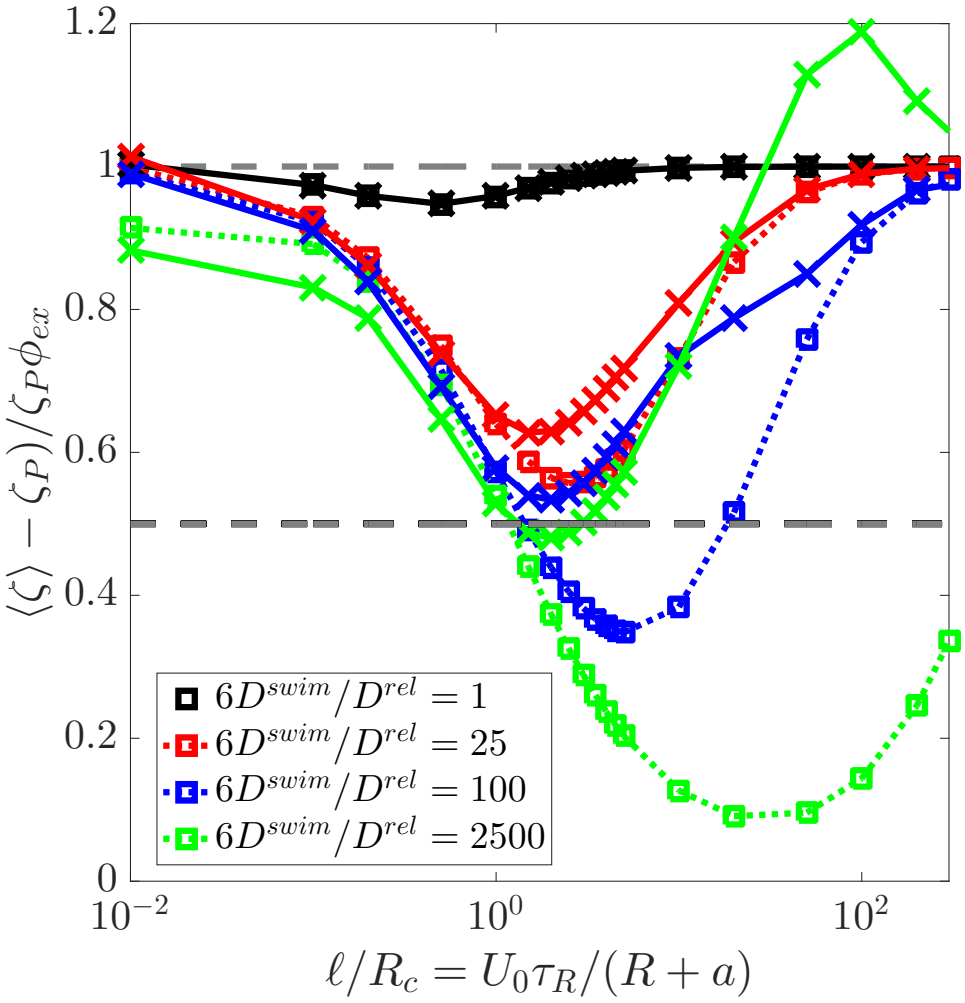

Figure 3.3: Particle contribution to the probe drag ($d = 3$) scaled by its value in a passive suspension $\zeta_P\phi^{ex}$. The Stokes drag of the probe is ζ_P, and the excluded volume fraction of the suspension is $\phi^{ex} = 2\pi a(R+a)^2 n^\infty/3$, where n^∞ is the number density, a is the swimmer size, and R is the probe size. This scaled drag contribution is plotted as a function of $\ell/R_c \equiv U_0\tau_R/(R+a)$, where U_0 is the speed of the swimmers, and τ_R is their reorientation time. Different colors indicate different strengths of swimming: $6D^{swim}/D^{rel} = U_0^2\tau_R/D^{rel}$, where D^{rel} is the relative thermal diffusivity. Squares are for the closure $\boldsymbol{Q' = 0}$ and crosses are for the closure $\boldsymbol{B' = 0}$. The dashed lines serve as guides for the eye.

by the intrinsic microviscosity $\eta^{micro} \equiv (\langle\zeta\rangle - \zeta_P)/\zeta_P\phi^{ex}$, where $\zeta_P = 6\pi\eta_s R$ is the probe's Stokes drag coefficient. The intrinsic microviscosity is a scalar constant independent of the volume fraction.

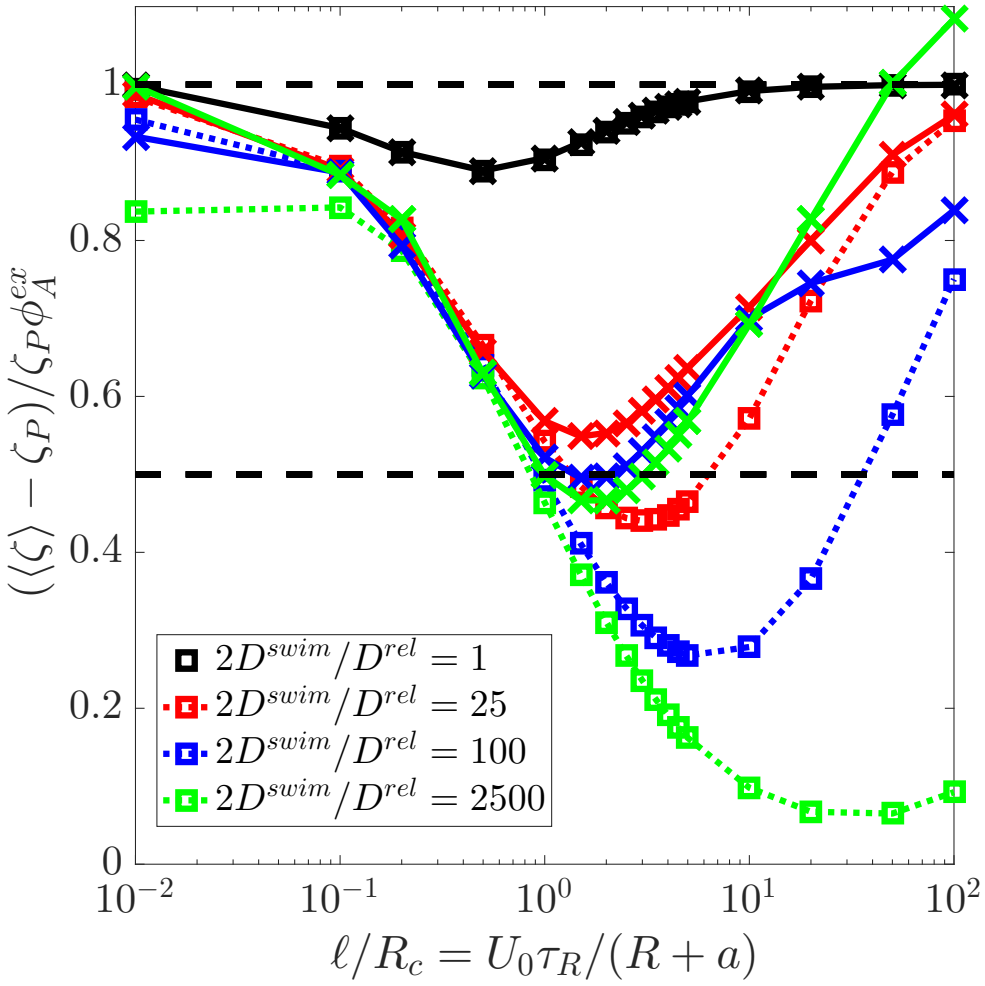

Figure 3.4: Particle contribution to the probe drag ($d = 2$) scaled by its value in a passive suspension $\zeta_P\phi_A^{ex}$. The Stokes drag of the probe is ζ_P, and the excluded area fraction of the suspension is $\phi_A^{ex} = 2\pi a(R+a)n_A^{\infty}$, where n_A^{∞} is the areal number density, a is the swimmer size, and R is the probe size. This scaled drag contribution is plotted as a function of $\ell/R_c \equiv U_0\tau_R/(R+a)$, where U_0 is the speed of the swimmers, and τ_R is their reorientation time. Different colors indicate different strengths of swimming: $2D^{swim}/D^{rel} = U_0^2\tau_R/D^{rel}$, where D^{rel} is the relative thermal diffusivity. Squares are for the closure $\boldsymbol{Q'} = \mathbf{0}$ and crosses are for the closure $\boldsymbol{B'} = \mathbf{0}$. The dashed lines serve as guides for the eye.

Swim-thinning

Dimensional analysis of the governing equations for $\hat{\boldsymbol{u}} \cdot \hat{\boldsymbol{d}}^{(F)}$ reveals two dimensionless groups that determine the strength of activity in the linear-response regime: $Pe_s = U_0R_c/D^{rel}$ and $\gamma^2 = (d-1)R_c^2/D^{rel}\tau_R$. The first is a Péclet number relating the strength of swimming to the strength of Brownian motion, and the second com-

pares the rate of thermal diffusion to the reorientation time of the swimmers. In terms of the time scales discussed in the calculation of $\langle \boldsymbol{D} \rangle$ in Chapter 2, $Pe_s = \tau_D/\tau_{adv}$ and $\gamma^2 = (d-1)\tau_D/\tau_R$, where $\tau_D = R_c^2/D^{rel}$ and $\tau_{adv} = R_c/U_0$. Alternatively, we can define these groups in terms of three length scales: the run length $\ell = U_0\tau_R$, the microscopic length $\delta = \sqrt{D^{rel}\tau_R}$, and the contact length R_c ($Pe_s = \ell R_c/\delta^2$ and $\gamma^2 = (d-1)R_c^2/\delta^2$). Figs. 3.3 and 3.4 show that the qualitative dependence of η^{micro} on the ratio ℓ/R_c is the same for all activity levels—constant values of $\ell/\delta = \sqrt{D^{swim}/D^{rel}} \sim \sqrt{k_s T_s/k_B T}$.

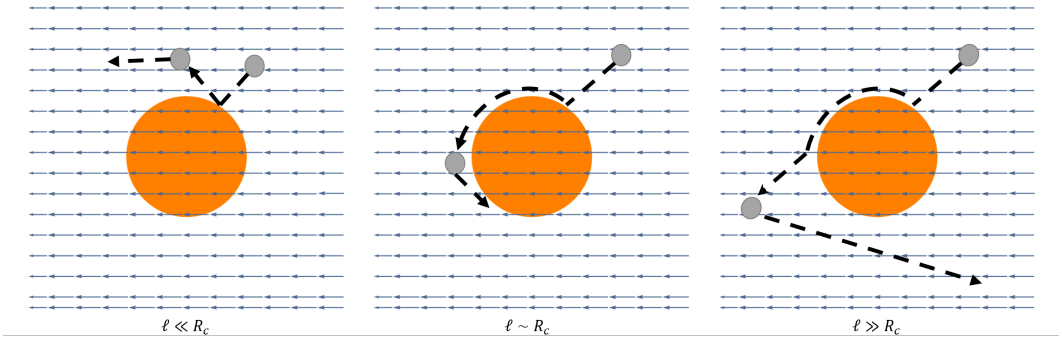

Figure 3.5: Sketch of swimmer trajectories upon collision with the probe particle for various regimes of $\ell/R_c = U_0\tau_R/(R+a)$, where U_0 is the speed of the swimmer, τ_R is its reorientation time, a is its size, and R is the size of the probe. The background arrows indicate the direction of fluid flow.

The limit $\ell/R_c \ll 1$ is known as the continuum limit. The run-length of the swimmers is small compared to the size of the probe, thus from the probe's perspective the swimmers are simply "hot" Brownian particles diffusing through the fluid with an active self-diffusivity $D_T + D^{swim}$. When they collide with the probe due to the advective flux (see Fig. 3.5, left), they can immediately reorient and diffuse away from the probe. Thus, even though the number density of particles at the surface may be large $n_0 \sim n^\infty(1 + D^{swim}/D_T)$, the advective disturbance is balanced by the diffusive restoring flux $(D_T + D^{swim})\nabla n'$. The microviscosity is

$$\eta^{micro} = 1 - \frac{\sqrt{3}}{2}\frac{\ell}{R_c}, \tag{3.25}$$

which is what we find in passive suspensions, minus a small correction that reflects swim-thinning of the suspension.

In the opposite limit the run length of the swimmers is far larger than the contact length $\ell \gg R_c$. When a swimmer collides with the probe, it slides along the contact surface until it is able to swim away again with the same orientation (see Fig. 3.5,

right). This is a consequence of the no-flux boundary condition. The swimmer does not reorient during its contact with the probe, and thus the particles do not accumulate at the surface of the probe $n_0 \sim n^\infty$. In this case, the weak advective perturbation is simply perturbing a suspension from a uniform microstructure, and the microviscosity is

$$\eta^{micro} = 1 - \frac{2}{9} Pe_s^2, \tag{3.26}$$

the passive suspension microviscosity with a small correction for swim-thinning when ℓ/R_c is large but finite. Note that Pe_s is actually small when ℓ/δ is fixed but ℓ/R_c is allowed to become asymptotically large.

In the intermediate regime—$\ell/R_c \sim O(1)$, illustrated in the center panel of Fig. 3.5—the behavior is different. When a swimmer collides with the probe, it slides along the surface as it does when $\ell/R_c \gg 1$, but it may still be near the probe when it reorients. For example, a swimmer approaching the front of the probe may collide and then slide around to the back of the probe. Once there, it can either reorient and swim away from the probe, or it can collide with the probe again and push it along—the latter scenario would result in a microviscosity *less* than one would find in a passive suspension. The opposite would be true of a particle approaching the rear of the swimmer—it could swim away in front or reorient and hit the probe, thereby increasing the microviscosity. When $\ell/R_c \sim O(1)$ we find

$$\eta^{micro} = \sqrt{8}/Pe_s, \tag{3.27}$$

which approaches zero as $Pe_s \to \infty$. This simply means that the weak advective disturbance causes more swimmers to collide with the front of the probe and then slide to the back than vice-versa. Some of these swimmers reorient and push the probe along, decreasing the microviscosity.

It should be noted that this particular limit of the microviscosity—$\ell/R_c \sim O(1)$—is sensitive to the equation closure, as indicated by the difference between square symbols and crosses in Figs. 3.3 and 3.4 (for a detailed discussion, see Chapter 4). If nematic order is included, η^{micro} approaches as constant value slightly less than $1/2$, as $Pe_s \to \infty$, which is consistent with finite element calculations of $\hat{P}_{1/1}$ that do not rely on the moments expansion in $\boldsymbol{q}$. Additionally, the overshoot in the approach to the large ℓ/R_c value seen in Figs. 3.4 and 3.3 at large D^{swim}/D^{rel} is a result of the closure $\boldsymbol{B'} = 0$. It is not seen with the closure $\boldsymbol{Q'} = 0$ or in finite-element calculations (Chapter 4).

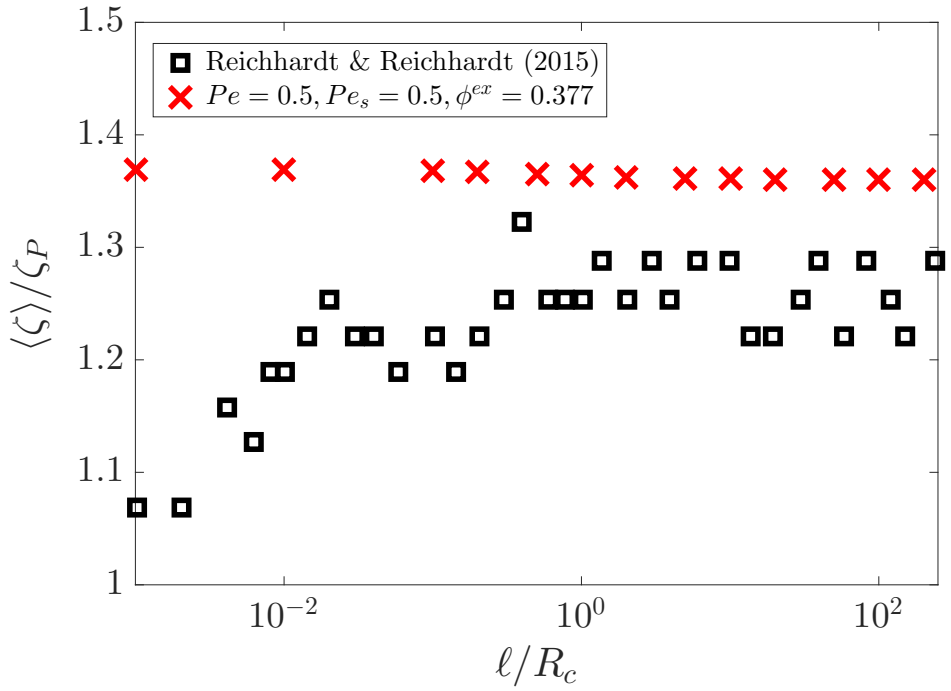

Figure 3.6: Comparison between our theoretical predictions (red crosses) and the simulations of [29] (black squares).

In the absence of any hydrodynamic interactions, activity decreases the excess drag coming from the bath particles, but the microviscosity is never reduced below the viscosity of the embedding solvent, $\langle\eta\rangle > \eta_s$. This agrees with previous simulations which compute an *decreased* mobility in an active bath without hydrodynamic interactions [29]. Curiously, Reichhardt & Reichhardt find that the mobility monotonically decreases with ℓ/R_c at fixed Pe_s [29], the opposite of what we find here (see Fig. 3.6). The reasons for this discrepancy are not clear, though it should be noted that their simulations neglect Brownian motion (which is strong when the external force is weak) and are not dilute ($\phi^{ex} \geq 0.377$) which can significantly impact the motion of the ABPs. These findings of an effective drag coefficient greater than the Stokes drag stand in contrast to many theoretical predictions and measurements of reduced shear viscosity in bacterial suspensions [20, 21, 23, 39] and reduced microviscosity in an active nematic [22], which would require a negative intrinsic microviscosity. We discuss possible reasons for this discrepancy at the end of this chapter.

Connections to a GSESR

In colloidal suspensions of passive particles near equilibrium, the FDT is satisfied: $\langle\zeta\rangle\langle D\rangle = k_BT$. For example, in a dilute Brownian suspension of hard spheres in the absence of HI, Squires and Brady found $\langle\zeta\rangle = \zeta_P(1 + \phi^{ex})$, and Zia and Brady later showed $\langle D\rangle = D_P(1 - \phi^{ex})$ using generalized Taylor dispersion theory [31, 38]. The product is $\langle\zeta\rangle\langle D\rangle = k_BT$ to $O(\phi^{ex})^2$. It is well-known that active matter breaks local detailed balance by virtue of its continuous conversion of chemical into mechanical energy; thus, the FDT does not necessarily apply to these systems [24].

For a non-equilibrium suspension, we quantify the departures from the theorem with the field variable $\boldsymbol{d}'$, which characterizes the fluctuations of the probe particle due to non-equilibrium effects—in this case, the activity of the bath particles. The long-time dispersion of the tracer particle resulting from these fluctuations can be thought of in terms of an excess suspension energy E^{act}, such that $\langle\boldsymbol{D}\rangle = (k_BT + E^{act})\langle\boldsymbol{M}^{\boldsymbol{UF}}\rangle$. We want to determine if E^{act} depends on particle activity only, or if it also depends on the suspension geometry/microstructure.

The excess energy of the suspension has three limiting behaviors, corresponding to the three different decorrelation time scales for the tracer diffusion problem [27].

(1) When the time τ over which the probe velocity correlations become decorrelated is the dictated by Brownian motion $\tau = \tau_D \equiv R_c^2/D^{rel}$, probe fluctuations are induced by the swimming bath particles, but the fluctuations are sufficiently weak that they decay on the time scale of Brownian diffusion. Using the results of the preceeding section and Chatper 2, we find

$$E^{act} = \frac{17}{54} k_BTPe_s^2\phi^{ex}, \tag{3.28}$$

regardless of the swimmer-to-probe size ratio a/R (when $a/R \ll 1$ the bare volume fraction ϕ takes the place of the excluded volume fraction ϕ^{ex}). One could also predict the scaling behavior of E^{act} using the same kinematic arguments to those used to predict the active contribtuion to the probe's LTSD [27].

(2) When swimming is strong compared to Brownian motion, the decorrelation time scale for probe fluctuations is $\tau = \tau_{adv} = R_c/U_0$. The swimmers are bombarding the probe so rapidly that the resulting fluctuations become decorrelated on the time it takes for a swimmers to traverse the distance R_c. The detailed calculations give:

$$E^{act} = \frac{1}{3\sqrt{3}} F^{swim} R \left(\frac{2 + \sqrt{2\tau_D/\tau_R}}{1 + \sqrt{2\tau_D/\tau_R}} \right) \phi^{ex}, \tag{3.29}$$

where $F^{swim} = \zeta_s U_0$ is the swim force, and ζ_s is the (Stokes) drag coefficient of the swimmer. In this limit the run length of a swimmer, $\ell \equiv U_0 \tau_R$, is large compared to the pair size R_c, and a swimmer collides with the probe before it is able to traverse its full run length. The swimmer pushes the probe with force $F^{swim} = \zeta_s U_0$, but is only able to move it a distance of R on average. Just as in the diffusion-controlled regime, the result is insensitive to the swimmer-probe size ratio a/R. It manifests only in ϕ^{ex}, which simply becomes ϕ for point tracers.

(3) When Brownian motion is weak compared to the swimmers' reorientations, the decorrelation time is set by the reorientation time: $\tau = \tau_R$. In this "continuum" limit, the run length is small compared to the contact length $\ell/R_c \ll 1$, so the probe sees the swimmers as effectively Brownian particles with an active self-diffusivity $D^{act} = D_T + D^{swim}$. The excess energy is then

$$E^{act} = k_s T_s \frac{R}{R_c} \phi^{ex}, \tag{3.30}$$

just as in the simple result for a single ABP. In the limit $a/R \to 0$, $E^{act} = k_s T_s \phi^{ex}$ and in the limit $a/R \to \infty$, $E^{act} = k_s T_s \phi$. The probe experiences many small kicks of $O(k_B T)$ from the solvent molecules, and kicks of $O(k_s T_s)$ from the swimmers. The volume fraction dependence of E^{act} necessarily reflects the fact that the active fluctuations come from the particles only, whereas thermal fluctuations come from the solvent.

In general, the fluctuation-dissipation relation in active systems reads

$$\langle \boldsymbol{D} \rangle \cdot \langle \boldsymbol{M}^{\boldsymbol{UF}} \rangle^{-1} = k_B T \boldsymbol{I} + \boldsymbol{E}^{\boldsymbol{act}}(a/R, \phi, \ell/R_c, \ldots) \tag{3.31}$$

which is a weaker statement than the FDT for equilibrium systems. Indeed though $\boldsymbol{E}^{\boldsymbol{act}}$ is isotropic in the case studied in this chapter, it may be anisotropic in other scenarios. This active "temperature" does not depend only on the activity of the suspension (i.e. on U_0, τ_R only), but also on the particle sizes a and R and the concentration ϕ. Only in the continuum limit $\ell/R_c \to 0$ do we find that the product $\langle \boldsymbol{D} \rangle \cdot \langle \boldsymbol{M}^{\boldsymbol{UF}} \rangle^{-1}$ depends solely activity of the bath particles $k_s T_s$—in this limit the probe is large enough that the random active motion of the bath particles is instantaneous and microscopic on the scale of its own motion, just like in an equilibrium suspension. Finally, though this section specifically addresses 3-D systems, the same physical arguments are expected to apply in 2-D.

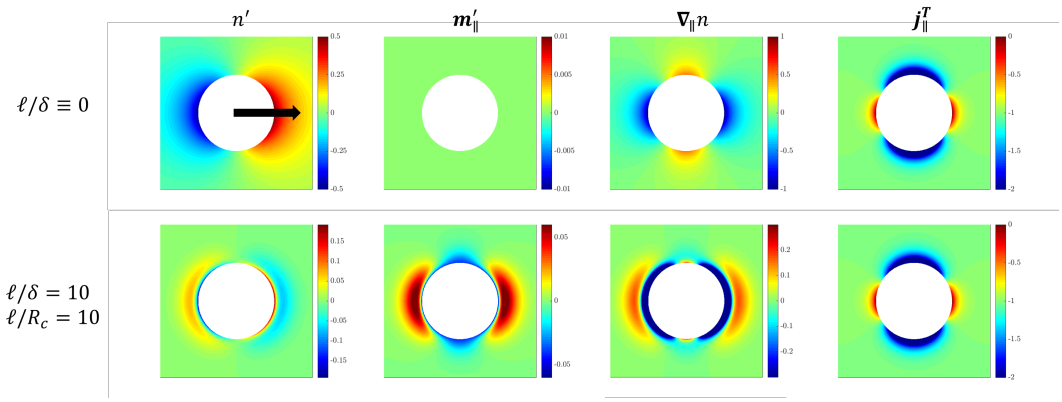

Figure 3.7: Contour plots of the 3-D (axisymmetric) perturbed microstructure for weak external forcing; the direction of the external force is indicated with a solid black arrow. The background green colors indicates a uniform microstructure fluctuation: $n', \boldsymbol{m'} \sim 0$. Red (warm) colors indicate an accumulation of particles, and blues (cold colors) indicate a depletion. For the polar order $\boldsymbol{m}'_{\parallel}$, concentration gradient $\nabla_{\parallel} n'$, and flux $\boldsymbol{j}^T_{\parallel}$, the color indicates how strongly the field is aligned with (reds) or against (blues) the external force.

3.3 Microstructure

We now examine the microstructural underpinnings of the probe drag. When the probe is stationary ($F^{ext} = 0$), the microstructure is isotropic, and in the absence of activity the number density is uniform. When the probe is set into motion, the microstructure is perturbed from its isotropic steady state. This perturbed structure determines the microviscosity. In a suspension of passive Brownian particles, Brownian motion gives rise to a diffusive dipole that balances the advective disturbance of the probe, resulting in a particle accumulation in front ($\hat{\boldsymbol{u}} \cdot \boldsymbol{n} > 0$) of the probe, and a depletion of equal magnitude behind ($\hat{\boldsymbol{u}} \cdot \boldsymbol{n} < 0$) the particle. (The disturbance to the polar order is identically zero for a passive bath.) The flux of (passive) particles relative to the probe $j^T_{\parallel} \equiv (\hat{\boldsymbol{u}} \cdot \boldsymbol{j^T})/(U^{probe} n^{\infty}) = -n_0 - \nabla_{\parallel} n'$ is quadrupolar: Brownian motion drives particles along $\hat{\boldsymbol{u}}$ to compensate for the wake left by advection (recall that n_0 is the number density around a stationary probe, and note that we define $\nabla_{\parallel} = \hat{\boldsymbol{u}} \cdot \boldsymbol{\nabla}$). At the poles $\hat{\boldsymbol{u}} \cdot \boldsymbol{n} = 0$, and the flux goes against the external motion $-\hat{\boldsymbol{u}}$ because the concentration gradient changes sign.

In active suspensions, Brownian motion must now balance perturbations due to both advection and swimming. Because the rotational and translational motion are coupled through the polar (and nematic) order, there are two distinct boundary-layers that arise from activity: one that is a distance $\lambda^{-1} = \delta/\sqrt{2(1/6(\ell/\delta)^2 + 1)}$ away from the probe surface (in 3-D), and another that is a distance δ from the probe surface, where $\delta = \sqrt{D^{rel}\tau_R}$ and $\ell = U_0\tau_R$. The number density n' is screened by λ, and the

polar order $\boldsymbol{m}'$ is screened by both λ and $1/\delta$, [40] resulting in "nested" boundary-layers. The second row of Fig. 3.7 provides a clear picture of this boundary-layer within another boundary-layer phenomenon.

The most noteworthy aspect of the structure is that the concentration disturbance n' is now non-monotonic with distance from the probe surface. In the innermost region, $r - R_c \sim O(1/\lambda)$, Brownian motion balances the flux due to self propulsion $Pe_s\boldsymbol{m}'$, but only the screened terms $\sim e^{-(r-R_c)\lambda}/r$ contribute. In the region $r - R_c \sim O(1/\delta)$, we see something very different: Brownian motion must now balance terms $\sim e^{-(r-R_c)/\delta}/r$ in the polar order, which are of the *opposite* sign. In the far-field $r \gg \delta, \lambda^{-1}$, we return to the long-ranged advective-diffusive dipole response (which is weak). Interestingly, though the polar order (and thus the gradient in number density) are non-monotonic in r, the flux of swimmers relative to the probe is monotonic, and exhibits precisely the same qualitative behavior as in the absence of activity—overall, Brownian motion is still trying to compensate for the wake left by the advective motion, and the swimmers assist Brownian motion because of their desire to be near the probe's surface.

Effects of closure

Figures 3.3 and 3.4 reveal that the closure of the Smoluchowski equation seems to make a larger quantitative difference than in previous studies [27, 33, 34, 40]; this may be explained by simple geometric arguments. When the probe is stationary the only vector with which the swimmers may align is the probe's outward-pointing unit normal $\boldsymbol{n}$, and the polar order (whether the swimmers are moving toward or away from the probe) is the most important ordered field. The nematic order would contain terms proportional to $\boldsymbol{nn}$ and $\boldsymbol{I}$, which do not significantly affect the kinetic boundary-layer structure, even if the probe were of some arbitrary shape [40]. With the introduction of an external force (or orienting field) in a fixed direction $\hat{\boldsymbol{u}}$, the swimmers may now be swimming toward or away from the probe $\boldsymbol{m'} \sim \hat{\boldsymbol{u}} \cdot \boldsymbol{n}\,\boldsymbol{n}$ or with or against the external field $\boldsymbol{m'} \sim \hat{\boldsymbol{u}}$, as the solution in Appendix C reveals. This implies that the nematic order may have terms proportional to $\hat{\boldsymbol{u}}\boldsymbol{n}$, $(\hat{\boldsymbol{u}} \cdot \boldsymbol{n})\boldsymbol{I}$, and $(\hat{\boldsymbol{u}} \cdot \boldsymbol{n})\,\boldsymbol{nn}$. These correlations between the external force director $\hat{\boldsymbol{u}}$ and the unit normal of the surface $\boldsymbol{n}$ must make a more significant quantitative impact in this problem.

We plot the non-zero components of the nematic order fluctuation in Fig. 3.8. Indeed we find small but not negligible components of $\boldsymbol{Q}'$ that indicate the presence

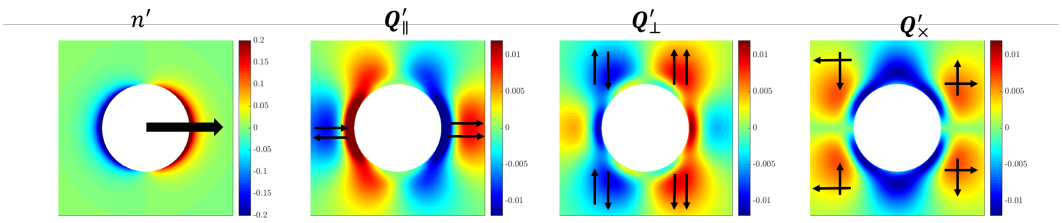

Figure 3.8: Contour plots of the 3-D (axisymmetric) perturbed microstructure for weak external forcing. The background green colors indicates a uniform microstructure fluctuation: $n', \boldsymbol{m}', \boldsymbol{Q}' \sim 0$. Red (warm) colors indicate an accumulation of particles, and blues (cold colors) indicate a depletion. For the nematic order $\boldsymbol{Q}'$, the color indicates how strongly the swimmers' alignments are correlated—small black arrows are included to help with visualizing the three components of $\boldsymbol{Q}'$: $Q'_{\parallel} = \hat{\boldsymbol{u}} \cdot \boldsymbol{Q}' \cdot \hat{\boldsymbol{u}}$, where $\hat{\boldsymbol{u}} = \boldsymbol{e}_z$ is the unit vector in the direction of the external force (as indicated in the concentration disturbance plot), $Q'_{\perp} = \boldsymbol{e}_{\perp} \cdot \boldsymbol{Q}' \cdot \boldsymbol{e}_{\perp}$, where $\boldsymbol{e}_{\perp} = \cos\psi \boldsymbol{e}_x + \sin\psi \boldsymbol{e}_y$, and $Q'_{\times} = \boldsymbol{e}_{\perp} \cdot \boldsymbol{Q}' \cdot \hat{\boldsymbol{u}}$. The azimuthal coordinate is ψ.

of apolar order in the suspension. The parallel apolar ordering $Q'_{\parallel}$, which represents apolar ordering along the direction of probe motion, is the most pronounced. The swimmers are diverging in front of the probe—the particles closer to the surface tend to move away and the particles further out in the same layer will tend to move toward the surface—and are converging behind it. This qualitatively supports the structural features seen in the polar order in Fig. 3.7. The activity brings particles into the wake and pushes them out of the way in front, leading to a reduction in the viscous drag. The nematic order will thus quantitatively change the microstructure, but does not qualitatively change particle motion.

3.4 Conclusions

Using generalized Taylor dispersion theory, we showed that the fluctuation-dissipation theorem (FDT) does not hold for generic active matter systems, though the long-time self-diffusivity and self-mobility are formally identical. We constructed a generalized Stokes-Einstein-Sutherland relation that says the effective diffusivity of a tracer particle is inversely proportional to the effective drag through the active medium, and the energy that the probe must dissipate depends on the activity of the swimmers as well as the suspension structure. In one special case—the continuum limit, where the run length of the swimmer is much smaller than the center-to-center separation of the probe and swimmer upon contact $\ell \ll R_c$—the energy dissipated depends only on $k_B T$ and the bath particle activity $k_s T_s$. In finding the effective fluctuation-dissipation relation, we necessarily calculated the linear viscous response of an active suspension to a tracer particle being dragged by a fixed external force. We

find that the suspension, in the absence of hydrodynamic interactions (HI), is uniformly swim-thinning. The microviscosity reaches a minimum value of $\sim 1/2$ that seen in passive suspensions when the run length and contact length are commensurate $\ell \sim R_c$. The precise value of the minimum predicted microviscosity will depend on the closure of the Smoluchowski equation.

Notably, we did not find a negative microviscosity in this investigation—the swimmers always increase the effective suspension microviscosity no matter how active they become, as demonstrated in simulations [29] but in contrast to measurements of the microviscosity of an active nematic [22]. There are two explanations for this. First, we have implicitly assumed a fixed-force mode of microrheology in using generalized Taylor dispersion theory. Negative suspension viscosities are precluded in this mode of measurement because a negative viscosity would result in the speed of the probe increasing until the effective drag was once again positive [39]. In the absence of hydrodynamic interactions (HI) however, the difference between the fixed-force and fixed-velocity microviscosity is simply a factor of R_c/a. Second, in neglecting HI we do not consider any effects related to the swimmers' gait, as in previous theoretical investigations [21, 22]. We expect that hydrodynamic interactions are essential to finding the observed viscosity reduction in active suspensions. Even in the case where the swimmers exert no hydrodynamic stress on the fluid, Takatori and Brady showed that the swim stress—the macroscopic mechanical stress associated with the random run-and-tumble motion of the active particles—is affected by an ambient viscometric flow, and indeed they predict a viscosity reduction in active suspensions regardless of swimming gait or shape of the swimmers [39]. We examine the effects of HI in Chapter 8.

In Chapter 5, we will examine the viscous response when the external force on the probe particle is large compared to the thermal restoring force $F^{ext} \gg k_B T/a$. In Chapter 9, we discuss the problem of "fixed probe" microrheology—the viscous response measured by a fixed probe in a bath of particles whose motion is biased by an applied external field.

Appendix

A: Generalized Taylor dispersion theory in non-equilibrium systems

Consider a suspension of N particles embedded in a Newtonian fluid. The suspension dynamics may be described by a Smoluchowski equation for $P_N(\{\boldsymbol{x}_\alpha\}, t)$, the probability of finding the N-particles in some phase-space configuration $\{\boldsymbol{x}_\alpha\}$ at

time t ($\boldsymbol{x}_\alpha$ is taken to represent the laboratory frame position and orientation of each particle):

$$\frac{\partial P_N}{\partial t} + \sum_{\alpha=1}^{N} \nabla_\alpha \cdot \boldsymbol{j}_{\boldsymbol{\alpha}} = 0, \tag{3.32}$$

with the general constitutive expression for the flux $\boldsymbol{j}_\alpha$:

$$\boldsymbol{j}_{\boldsymbol{\alpha}} = \boldsymbol{U}_\alpha P_N - \sum_{\beta=1}^{N} \boldsymbol{D}_{\boldsymbol{\alpha\beta}} \cdot \nabla_\beta P_N. \tag{3.33}$$

The thermal diffusivity of particle α relative to β is described by $\boldsymbol{D}_{\alpha\beta} = k_B T \boldsymbol{M}^{\boldsymbol{UF}}_{\boldsymbol{\alpha\beta}}$, where $\boldsymbol{M}^{\boldsymbol{UF}}_{\boldsymbol{\alpha\beta}}$ is the hydrodynamic mobility [30, 41]. We take $\boldsymbol{U}_\alpha$ to represent both translational and angular velocities of the particles, and $\boldsymbol{F}_\alpha$ to represent both forces and torques. We have explicitly written the particle fluxes arising from Brownian motion; the velocity $\boldsymbol{U}_{\boldsymbol{\alpha}}$ contains all other contributions to the particle motion, whether it be from activity, external forces or flows, or interparticle forces.

To probe the suspension properties, we select a test particle at $\boldsymbol{x}_1 \equiv \boldsymbol{z}$, and re-write the equation in terms of particle coordinates relative to the test particle $\boldsymbol{r}_\alpha = \boldsymbol{x}_\alpha - \boldsymbol{x}_1$.

$$\frac{\partial P_N}{\partial t} + \nabla_z \cdot \boldsymbol{j}_{\boldsymbol{1}} + \sum_{\alpha=1}^{N} \nabla_{r_\alpha} \cdot (\boldsymbol{j}_{\boldsymbol{\alpha}} - \boldsymbol{j}_{\boldsymbol{1}}) = 0, \tag{3.34}$$

where

$$\boldsymbol{j}_{\boldsymbol{1}} = \boldsymbol{U}_{\boldsymbol{1}} P_N - \boldsymbol{D}_{\boldsymbol{11}} \cdot \nabla_z P_N - \sum_{\alpha=1}^{N} (\boldsymbol{D}_{\boldsymbol{1\alpha}} - \boldsymbol{D}_{\boldsymbol{11}}) \cdot \nabla_{r_\alpha} P_N, \tag{3.35}$$

$$\boldsymbol{j}_{\boldsymbol{\alpha}} = \boldsymbol{U}_{\boldsymbol{\alpha}} P_N - \boldsymbol{D}_{\boldsymbol{\alpha 1}} \cdot \nabla_z P_N - \sum_{\beta=1}^{N} (\boldsymbol{D}_{\boldsymbol{\alpha\beta}} - \boldsymbol{D}_{\boldsymbol{\alpha 1}}) \cdot \nabla_{r_\beta} P_N, \tag{3.36}$$

according to the chain rule[1].

Fluctuations in the test-particle coordinate $\boldsymbol{z}$ are unbounded[2], so we may take a Fourier transform with respect to $\boldsymbol{z}$ derive:

$$\frac{\partial \hat{P}_N}{\partial t} + i\boldsymbol{k} \cdot \hat{\boldsymbol{j}}_{\boldsymbol{1}} + \sum_{\alpha=1}^{N} \nabla_{r_\alpha} \cdot (\hat{\boldsymbol{j}}_{\boldsymbol{\alpha}} - \hat{\boldsymbol{j}}_{\boldsymbol{1}}) = 0, \tag{3.37}$$

[1] For simplicity it is assumed that the relative rotations can be written in this manner. Indeed, this is a true statement in 2-D (see Chapter 4), though it is not as simple in 3-D [42].

[2] One can imagine allowing the orientation coordinate to be unbounded by defining it on a Riemann surface without any branch points. Alternatively, one could take a Finite Fourier Transform with respect to $\boldsymbol{q}_1$. The details are not important for the discussion here.

where

$$\hat{\boldsymbol{j}}_{\mathbf{1}} = \boldsymbol{U}_{\mathbf{1}}\hat{P}_N - i\boldsymbol{k}\cdot\boldsymbol{D}_{\mathbf{11}}\hat{P}_N - \sum_{\alpha=1}^{N}(\boldsymbol{D}_{\mathbf{1}\alpha} - \boldsymbol{D}_{\mathbf{11}})\cdot\nabla_{r_\alpha}\hat{P}_N, \tag{3.38}$$

$$\hat{\boldsymbol{j}}_{\boldsymbol{\alpha}} = \boldsymbol{U}_{\boldsymbol{\alpha}}\hat{P}_N - i\boldsymbol{k}\cdot\boldsymbol{D}_{\boldsymbol{\alpha}\mathbf{1}}\hat{P}_N - \sum_{\beta=1}^{N}(\boldsymbol{D}_{\boldsymbol{\alpha}\boldsymbol{\beta}} - \boldsymbol{D}_{\boldsymbol{\alpha}\mathbf{1}})\cdot\nabla_{r_\beta}\hat{P}_N. \tag{3.39}$$

We have assumed that the velocity of the test particle is independent of its absolute position $\boldsymbol{z}$. This may not be true if, for example, the particle experiences motion due to an external potential fixed in the laboratory frame [38].

We may average the N-particle equation over the relative configurations of the $N-1$ other particles to get an equation of motion for the test particle

$$\frac{\partial\hat{P}_1}{\partial t} + i\boldsymbol{k}\cdot\langle\hat{\boldsymbol{j}}_{\mathbf{1}}\rangle_{N-1} = 0, \tag{3.40}$$

which makes use of the condition that there be no relative particle flux at contact or at infinity: $\boldsymbol{n}_{\mathbf{1}\boldsymbol{\alpha}}\cdot(\hat{\boldsymbol{j}}_{\boldsymbol{\alpha}} - \hat{\boldsymbol{j}}_{\mathbf{1}}) = 0$, where $\boldsymbol{n}_{\mathbf{1}\boldsymbol{\alpha}}$ is the unit vector pointing from particle 1 to particle α along the line of center. The average flux of the test particle is

$$\begin{aligned}\frac{\langle\hat{\boldsymbol{j}}_{\mathbf{1}}\rangle_{N-1}}{\hat{P}_1} = &\int \boldsymbol{U}_{\mathbf{1}}\hat{P}_{N-1/1}d\boldsymbol{r}_{\boldsymbol{\alpha}} - i\boldsymbol{k}\cdot\int \boldsymbol{D}_{\mathbf{11}}\hat{P}_{N-1/1}d\boldsymbol{r}_{\boldsymbol{\alpha}}\\ &- \int\sum_{\alpha=1}^{N}(\boldsymbol{D}_{\mathbf{1}\alpha} - \boldsymbol{D}_{\mathbf{11}})\cdot\nabla_{r_\alpha}\hat{P}_{N-1/1}\,d\boldsymbol{r}_{\boldsymbol{\alpha}},\end{aligned} \tag{3.41}$$

which has been simplified by the substitution $\hat{P}_N = \hat{P}_1(\boldsymbol{k},t)\hat{P}_{N-1/1}(\boldsymbol{k},\{\boldsymbol{r}_\alpha\},t)$. The long-time self-diffusivity of the test particle will be determined by the long wave length (small $\boldsymbol{k}$) fluctuations in its position so we expand the relative microstructure with respect to $i\boldsymbol{k}$: $\hat{P}_{N-1/1} = \hat{P}^{(0)}_{N-1/1} + i\boldsymbol{k}\cdot\hat{\boldsymbol{d}}^{(\boldsymbol{k})} + O(k^2)$. From this we can define an effective dispersion relation:

$$\langle\hat{\boldsymbol{j}}_{\mathbf{1}}\rangle_{N-1} \equiv [\langle\boldsymbol{U}^{\boldsymbol{probe}}\rangle - i\boldsymbol{k}\cdot\langle\boldsymbol{D}\rangle + ...]\hat{P}_1, \tag{3.42}$$

where

$$\langle\boldsymbol{U}^{\boldsymbol{probe}}\rangle = \int \boldsymbol{U}_{\mathbf{1}}\hat{P}^{(0)}_{N-1/1}d\boldsymbol{r}_{\boldsymbol{\alpha}} - \int\sum_{\alpha=1}^{N}(\boldsymbol{D}_{\mathbf{1}\alpha} - \boldsymbol{D}_{\mathbf{11}})\cdot\nabla_{r_\alpha}\hat{P}^{(0)}_{N-1/1}\,d\boldsymbol{r}_{\boldsymbol{\alpha}}, \tag{3.43}$$

$$\langle\boldsymbol{D}\rangle = \int \boldsymbol{D}_{\mathbf{11}}\hat{P}^{(0)}_{N-1/1}d\boldsymbol{r}_{\boldsymbol{\alpha}} - \int \boldsymbol{U}_{\mathbf{1}}\hat{\boldsymbol{d}}^{(\boldsymbol{k})}d\boldsymbol{r}_{\boldsymbol{\alpha}} + \int\sum_{\alpha=1}^{N}(\boldsymbol{D}_{\mathbf{1}\alpha} - \boldsymbol{D}_{\mathbf{11}})\cdot\nabla_{r_\alpha}\hat{\boldsymbol{d}}^{(\boldsymbol{k})}\,d\boldsymbol{r}_{\boldsymbol{\alpha}}. \tag{3.44}$$

This is a generalization of the 2-particle result for equilibrium suspensions derived in [31]; recall that $\boldsymbol{U}_1$ can have non-equilibrium contributions, which contribute to the diffusivity through $\hat{\boldsymbol{d}}^{(\boldsymbol{k})}$. Note that the last integral in Eqn. 3.44 is convergent for a quadrupolar fluctuation field, and conditionally convergent for a dipolar fluctuation. We return to this point later.

Consider separately the motion of the test particle due to an applied external force: $\boldsymbol{U}_1 = \boldsymbol{U}_{\mathbf{1}}^{(\mathbf{0})} + \boldsymbol{M}_{\mathbf{11}}^{\boldsymbol{UF}} \cdot \boldsymbol{F}^{\boldsymbol{ext}}$, where $\boldsymbol{U}_{\mathbf{1}}^{(\mathbf{0})}$ can still contain contributions from shear flow, activity, etc. The average velocity of the test particle is now

$$\langle \boldsymbol{U}^{\boldsymbol{probe}} \rangle = \int (\boldsymbol{U}_{\mathbf{1}}^{(\mathbf{0})} + \boldsymbol{M}_{\mathbf{11}}^{\boldsymbol{UF}} \cdot \boldsymbol{F}^{\boldsymbol{ext}}) \hat{P}^{(0)}_{N-1/1} \, d\boldsymbol{r}_{\boldsymbol{\alpha}} - \int \sum_{\alpha=1}^{N} (\boldsymbol{D}_{\mathbf{1}\boldsymbol{\alpha}} - \boldsymbol{D}_{\mathbf{11}}) \cdot \nabla_{r_\alpha} \hat{P}^{(0)}_{N-1/1} \, d\boldsymbol{r}_{\boldsymbol{\alpha}}. \tag{3.45}$$

If the external force is weak, we can also do a regular perturbation expansion of the microstructure in moments of the force: $\hat{P}^{(0)}_{N-1/1} = \hat{P}^{(0,0)}_{N-1/1} - \boldsymbol{F}^{\boldsymbol{ext}} \cdot \hat{\boldsymbol{d}}^{(\boldsymbol{F})} + O(F^{ext})^2$. The fluctuation field arising from the external force has units of length per energy; one could also define the wave vector $\boldsymbol{F}^{\boldsymbol{ext}}/k_B T$ instead so that the units of $\hat{\boldsymbol{d}}^{(\boldsymbol{F})}$ are also length. The average test particle velocity is

$$\begin{aligned} \langle \boldsymbol{U}^{\boldsymbol{probe}} \rangle = & \left(\int \boldsymbol{U}_{\mathbf{1}}^{(\mathbf{0})} \hat{P}^{(0,0)}_{N-1/1} d\boldsymbol{r}_\alpha - \int \sum_{\alpha=1}^{N} (\boldsymbol{D}_{\mathbf{1}\boldsymbol{\alpha}} - \boldsymbol{D}_{\mathbf{11}}) \cdot \nabla_{r_\alpha} \hat{P}^{(0,0)}_{N-1/1} \, d\boldsymbol{r}_{\boldsymbol{\alpha}} \right) \\ & + \boldsymbol{F}^{\boldsymbol{ext}} \cdot \left(\int \boldsymbol{M}_{\mathbf{11}}^{\boldsymbol{UF}} \hat{P}^{(0,0)}_{N-1/1} d\boldsymbol{r}_{\boldsymbol{\alpha}} - \int \boldsymbol{U}_{\mathbf{1}}^{(\mathbf{0})} \hat{\boldsymbol{d}}^{(\boldsymbol{F})} d\boldsymbol{r}_{\boldsymbol{\alpha}} \right. \\ & \left. + \int \sum_{\alpha=1}^{N} (\boldsymbol{D}_{\mathbf{1}\boldsymbol{\alpha}} - \boldsymbol{D}_{\mathbf{11}}) \cdot \nabla_{r_\alpha} \hat{\boldsymbol{d}}^{(\boldsymbol{F})} \, d\boldsymbol{r}_{\boldsymbol{\alpha}} \right). \end{aligned} \tag{3.46}$$

If we define $\langle \boldsymbol{U}^{\boldsymbol{probe}} \rangle \equiv \langle \boldsymbol{U}^{\boldsymbol{drift}} \rangle + \langle \boldsymbol{M}^{\boldsymbol{UF}} \rangle \cdot \boldsymbol{F}^{\boldsymbol{ext}}$, then we have an expression for $\langle \boldsymbol{U}^{\boldsymbol{drift}} \rangle$ that is formally identical to Eqn. 3.43, and an expression for $\langle \boldsymbol{M}^{\boldsymbol{UF}} \rangle$ that is formally identical to Eqn. 3.44. From this generalized Taylor dispersion perspective, dispersion driven by Brownian motion of the bath particles is equivalent to dispersion driven by an applied external force $\boldsymbol{F}^{\boldsymbol{ext}} = -i\boldsymbol{k}k_B T$

B: Governing equations for the fluctuation fields

The fluctuation-dissipation theorem for colloidal suspensions requires that the long-time self-diffusivity is proportional to the hydrodynamic mobility $\langle \boldsymbol{D} \rangle = k_B T \langle \boldsymbol{M}^{\boldsymbol{UF}} \rangle$ —a result derived by Einstein, Sutherland, and von Smoluchowski independently [41, 43, 44]. Qualitatively, this states that the random fluctuating motion of a test particle is related to the effective drag that the test particle would feel if it

were pulled through the fluid by an external force. Though the expressions for the mobility and diffusivity are formally identical (modulo a factor of k_BT), the fluctuation-dissipation theorem is satisfied only if $\hat{\boldsymbol{d}}^{(\boldsymbol{k})} = k_BT\hat{\boldsymbol{d}}^{(F)}$. We can derive equations for the fluctuation fields from Eqn. 3.37 from substitution of Eqn. 3.40 and $\hat{P}_N = \hat{P}_1(\boldsymbol{k},t)\hat{P}_{N-1/1}(\boldsymbol{k},\{\boldsymbol{r}_\alpha\},t)$:

$$\frac{\partial \hat{P}_{N-1/1}}{\partial t} + \sum_{\alpha=1}^{N} \nabla_{r_\alpha} \cdot (\hat{\boldsymbol{j}}_{\boldsymbol{\alpha}} - \hat{\boldsymbol{j}}_{\mathbf{1}}) = i\boldsymbol{k} \cdot ([\langle \hat{\boldsymbol{j}}_{\mathbf{1}} \rangle_{N-1}/\hat{P}_1]\hat{P}_{N-1/1} - \hat{\boldsymbol{j}}_{\mathbf{1}}) \tag{3.47}$$

with boundary conditions of no relative flux at contact and infinite separation:

$$\boldsymbol{n}_{\mathbf{1}\boldsymbol{\alpha}} \cdot (\hat{\boldsymbol{j}}_{\boldsymbol{\alpha}} - \hat{\boldsymbol{j}}_{\mathbf{1}}) = 0. \tag{3.48}$$

Thermal fluctuations

The governing equations for $P^{(0)}_{N-1/1}$ are

$$\frac{\partial \hat{P}^{(0)}_{N-1/1}}{\partial t} + \sum_{\alpha=2}^{N} \nabla_{r_\alpha} \cdot \left([\boldsymbol{U}_{\boldsymbol{\alpha}} - \boldsymbol{U}_{\mathbf{1}}]\hat{P}^{(0)}_{N-1/1} - \boldsymbol{D}^{\boldsymbol{rel}}_{\boldsymbol{\alpha\beta}} \cdot \nabla_{r_\beta} \hat{P}^{(0)}_{N-1/1} \right) = 0, \tag{3.49}$$

$$\sum_{\alpha=2}^{N} \boldsymbol{n}_{\mathbf{1}\boldsymbol{\alpha}} \cdot \left([\boldsymbol{U}_{\boldsymbol{\alpha}} - \boldsymbol{U}_{\mathbf{1}}]\hat{P}^{(0)}_{N-1/1} - \boldsymbol{D}^{\boldsymbol{rel}}_{\boldsymbol{\alpha\beta}} \cdot \nabla_{r_\beta} \hat{P}^{(0)}_{N-1/1} \right) = 0, \tag{3.50}$$

where $\boldsymbol{D}^{\boldsymbol{rel}}_{\boldsymbol{\alpha\beta}} \equiv \sum_{\beta=2}^{N} (\boldsymbol{D}_{\boldsymbol{\alpha\beta}} - \boldsymbol{D}_{\boldsymbol{\beta}\mathbf{1}} - \boldsymbol{D}_{\mathbf{1}\boldsymbol{\alpha}} + \boldsymbol{D}_{\mathbf{11}})$ and the fluctuation field is governed by

$$\begin{aligned} \frac{\partial \hat{\boldsymbol{d}}^{(\boldsymbol{k})}}{\partial t} + \sum_{\alpha=2}^{N} \nabla_{r_\alpha} \cdot \left([\boldsymbol{U}_{\boldsymbol{\alpha}} - \boldsymbol{U}_{\mathbf{1}}]\hat{\boldsymbol{d}}^{(\boldsymbol{k})} - \boldsymbol{D}^{\boldsymbol{rel}}_{\boldsymbol{\alpha\beta}} \cdot \nabla_{r_\beta} \hat{\boldsymbol{d}}^{(\boldsymbol{k})} \right) &= \hat{P}^{(0)}_{N-1/1} (\langle \boldsymbol{U}^{\boldsymbol{probe}} \rangle - \boldsymbol{U}_{\mathbf{1}}) \\ +2 \sum_{\alpha=1}^{N} (\boldsymbol{D}_{\mathbf{1}\boldsymbol{\alpha}} - \boldsymbol{D}_{\mathbf{11}}) \cdot \nabla_{r_\alpha} \hat{P}^{(0)}_{N-1/1} + \hat{P}^{(0)}_{N-1/1} \sum_{\alpha=1}^{N} \nabla_{r_\alpha} \cdot (\boldsymbol{D}_{\mathbf{1}\boldsymbol{\alpha}} - \boldsymbol{D}_{\mathbf{11}}) \end{aligned} \tag{3.51}$$

with the no-flux condition

$$\sum_{\alpha=2}^{N} \boldsymbol{n}_{\mathbf{1}\boldsymbol{\alpha}} \cdot \left([\boldsymbol{U}_{\boldsymbol{\alpha}} - \boldsymbol{U}_{\mathbf{1}}]\hat{\boldsymbol{d}}^{(\boldsymbol{k})} - \boldsymbol{D}^{\boldsymbol{rel}}_{\boldsymbol{\alpha\beta}} \cdot \nabla_{r_\beta} \hat{\boldsymbol{d}}^{(\boldsymbol{k})} \right) = \sum_{\alpha=2}^{N} \boldsymbol{n}_{\mathbf{1}\boldsymbol{\alpha}} \cdot (\boldsymbol{D}_{\mathbf{1}\boldsymbol{\alpha}} - \boldsymbol{D}_{\mathbf{11}}) \hat{P}^{(0)}_{N-1/1}. \tag{3.52}$$

If we integrate Eqn. 3.51 with respect to $\boldsymbol{r}_\alpha$, apply the no-flux boundary condition 3.52, and make use of $\int \hat{P}_{N-1/1} d\boldsymbol{r}_{\boldsymbol{\alpha}} = 1$, then we find the same equation for $\langle \boldsymbol{U}^{\boldsymbol{probe}} \rangle$ as given in Eqn. 3.43 [45].

For the simplest case of pair-wise interactions between hard spheres at equilibrium, $\hat{\boldsymbol{d}}^{(\boldsymbol{k})} = -(1/4)\boldsymbol{r}/r^3$. The fluctuation field is dipolar, and thus the integral determining

the effective diffusivity is conditionally convergent. Using the divergence theorem, one can convert the integral to a surface integral at particle contact and infinity:

$$-\int D_{11}\nabla_r \hat{\boldsymbol{d}}^{(\boldsymbol{k})}\, d\boldsymbol{r} = \int_{S_c} D_{11}\boldsymbol{n}\hat{\boldsymbol{d}}^{(\boldsymbol{k})} dS + \int_{S_\infty} D_{11}\boldsymbol{n}\hat{\boldsymbol{d}}^{(\boldsymbol{k})} dS. \tag{3.53}$$

Recognizing the singular nature of the small $\boldsymbol{k}$ expansion at large interparticle distance r, we assume that the integral over S_∞ is zero, when in fact it should precisely cancel the contribution from the surface. This is because the dipolar solution is technically not the correct far-field form for $\hat{\boldsymbol{d}}^{(\boldsymbol{k})}$. Our small $\boldsymbol{k}$ expansion of the microstructure is regular within a distance $\boldsymbol{r}_\alpha \sim \boldsymbol{k}^{-1}$ from the test particle, but there is a convective-diffusive boundary-layer at large distances[3]. The correct far-field solution is really a screened dipole (making the surface integral over S_∞ unconditionally convergent). If one wanted to consider these boundary-layer effects, one could solve the boundary-layer problem for all $\boldsymbol{k}$ using matched asymptotic expansions, evaluate the average flux (3.38), and *then* take the limit for small $\boldsymbol{k}$ (see [46]).

External fluctuations

The equation for the unforced microstructure $\hat{P}^{(0,0)}_{N-1/1}$ is the same as Eqn. 3.49 for the forced microstructure:

$$\frac{\partial \hat{P}^{(0,0)}_{N-1/1}}{\partial t} + \sum_{\alpha=2}^{N} \nabla_{r_\alpha} \cdot \left([\boldsymbol{U}^{\boldsymbol{(0)}}_{\boldsymbol{\alpha}} - \boldsymbol{U}^{\boldsymbol{(0)}}_{\boldsymbol{1}}]\hat{P}^{(0,0)}_{N-1/1} - \boldsymbol{D}^{\boldsymbol{rel}}_{\boldsymbol{\alpha\beta}} \cdot \nabla_{r_\beta} \hat{P}^{(0,0)}_{N-1/1} \right) = 0 \tag{3.54}$$

$$\sum_{\alpha=2}^{N} \boldsymbol{n}_{\boldsymbol{1\alpha}} \cdot \left([\boldsymbol{U}^{(0)}_{\boldsymbol{\alpha}} - \boldsymbol{U}^{\boldsymbol{(0)}}_{\boldsymbol{1}}]\hat{P}^{(0,0)}_{N-1/1} - \boldsymbol{D}^{\boldsymbol{rel}}_{\boldsymbol{\alpha\beta}} \cdot \nabla_{r_\beta} \hat{P}^{(0,0)}_{N-1/1} \right) = 0, \tag{3.55}$$

but the fluctuation field is

$$\frac{\partial \hat{\boldsymbol{d}}^{(F)}}{\partial t} + \sum_{\alpha=2}^{N} \nabla_{r_\alpha} \cdot \left([\boldsymbol{U}^{\boldsymbol{(0)}}_{\boldsymbol{\alpha}} - \boldsymbol{U}^{\boldsymbol{(0)}}_{\boldsymbol{1}}]\hat{\boldsymbol{d}}^{(F)} - \boldsymbol{D}^{\boldsymbol{rel}}_{\boldsymbol{\alpha\beta}} \cdot \nabla_{r_\beta} \hat{\boldsymbol{d}}^{(F)} \right)$$
$$= \sum_{\alpha=2}^{N} \nabla_{r_\alpha} \cdot (\boldsymbol{M}^{\boldsymbol{UF}}_{\boldsymbol{1\alpha}} - \boldsymbol{M}^{\boldsymbol{UF}}_{\boldsymbol{11}})\hat{P}^{(0,0)}_{N-1/1} \tag{3.56}$$

[3]This is similar to Whitehead's paradox for small (but finite) Reynolds number (Re) corrections tot Stokes drag law—the inertial terms in the Navier-Stokes equations are only small within a distance of $1/Re$ of the particle surface.

with the no-flux condition

$$\sum_{\alpha=2}^{N} \boldsymbol{n_{1\alpha}} \cdot \left([\boldsymbol{U_\alpha} - \boldsymbol{U_1^{(0)}}] \hat{\boldsymbol{d}}^{(F)} - \boldsymbol{D_{\alpha\beta}^{rel}} \cdot \nabla_{r_\beta} \hat{\boldsymbol{d}}^{(F)} \right)$$
$$= \sum_{\alpha=2}^{N} \boldsymbol{n_{1\alpha}} \cdot (\boldsymbol{M_{1\alpha}^{UF}} - \boldsymbol{M_{11}^{UF}}) P^{(0,0)}_{N-1/1}. \tag{3.57}$$

The governing equations for the two different fluctuation fields are clearly different. Notably, the governing equation for $\hat{\boldsymbol{d}}^{(\boldsymbol{F})}$ is not forced by the the average velocity.

Indeed, we find the following condition for the fluctuation-dissipation theorem to be satisfied ($\langle \boldsymbol{D} \rangle = k_B T \langle \boldsymbol{M^{UF}} \rangle$): the local probe velocity

$$\boldsymbol{U^{probe}} = \boldsymbol{U_1} - \sum_{\alpha=1}^{N} (\boldsymbol{D_{1\alpha}} - \boldsymbol{D_{11}}) \cdot \nabla_{r_\alpha} \ln \hat{P}^{(0)}_{N-1/1}, \tag{3.58}$$

must be everywhere equal to the average probe velocity as givenn in Eqn. 3.43. This can only be true if both $\boldsymbol{U^{probe}}$ and $\hat{P}^{(0)}_{N-1/1}$ are spatially uniform, or if $\boldsymbol{U^{probe}} = 0$. For the equilibrium, hard-sphere suspension studied in [31], the probability distribution $\hat{P}^{(0)}_{N-1/1}$ is uniform, and $\boldsymbol{U^{probe}} = 0$; the theorem is satisfied. This would also be satisfied for the Boltzmann distribution $\hat{P}^{(0)}_{N-1/1} = P_0 e^{-V(\boldsymbol{r}_\alpha)/k_B T}$:

$$\langle \boldsymbol{U^{probe}} \rangle = \boldsymbol{U_1} + \sum_{\alpha=1}^{N} (\boldsymbol{M_{1\alpha}^{UF}} - \boldsymbol{M_{11}^{UF}}) \cdot \nabla_{r_\alpha} V. \tag{3.59}$$

The second term will precisely cancel the velocity of particle one due to interparticle forces. If there are no other forces acting on the test particle (e.g. no shear), then the fluctuation dissipation relation is again satisfied.

Quantifying departures from the FD Theorem

We define a difference field between force-induced and thermally-induced fluctuations: $\hat{\boldsymbol{d}}^{(\boldsymbol{k})} = k_B T \hat{\boldsymbol{d}}^{(\boldsymbol{F})} + \boldsymbol{d'}$, and assert that $\boldsymbol{F^{ext}} = -i\boldsymbol{k} k_B T$. We can then subtract the equations for the thermal and external fluctuations to find

$$\frac{\partial \boldsymbol{d'}}{\partial t} + \sum_{\alpha=2}^{N} \nabla_{r_\alpha} \cdot \left([\boldsymbol{U_\alpha} - \boldsymbol{U_1^{(0)}}] \boldsymbol{d'} - \boldsymbol{D_{\alpha\beta}^{rel}} \cdot \nabla_{r_\beta} \boldsymbol{d'} \right)$$
$$= \hat{P}^{(0,0)}_{N-1/1} (\boldsymbol{U^{probe}} - \boldsymbol{U_1}) + \sum_{\alpha=1}^{N} (\boldsymbol{D_{1\alpha}} - \boldsymbol{D_{11}}) \cdot \nabla_{r_\alpha} \hat{P}^{(0,0)}_{N-1/1} \tag{3.60}$$

with the boundary condition

$$\sum_{\alpha=2}^{N} \boldsymbol{n_{1\alpha}} \cdot \left([\boldsymbol{U_\alpha} - \boldsymbol{U_1^{(0)}}] \boldsymbol{d'} - \boldsymbol{D_{\alpha\beta}^{rel}} \cdot \nabla_{r_\beta} \boldsymbol{d'} \right) = 0. \tag{3.61}$$

For suspensions that satisfy fluctuation-dissipation, the right-hand side of Eqn. 3.60 is zero, and the boundary condition allows the null solution $\boldsymbol{d'} = 0$.

C: Microstructure, $\boldsymbol{Q'} = 0$

The governing equations for the microrheology problem in d dimensions are

$$\nabla_r \cdot [U_0 \boldsymbol{m'} - D^{rel} \nabla n'] = \boldsymbol{M^{UF}} \cdot \boldsymbol{F^{ext}} \cdot \nabla n_0, \tag{3.62}$$

$$\nabla_r \cdot [U_0 \boldsymbol{I} n'/d - D^{rel} \nabla \boldsymbol{m'}] + (d-1) D_R \boldsymbol{m'} = \boldsymbol{M^{UF}} \cdot \boldsymbol{F^{ext}} \cdot \nabla \boldsymbol{m_0}, \tag{3.63}$$

with the boundary conditions

$$\boldsymbol{n} \cdot [U_0 \boldsymbol{m'} - D^{rel} \nabla n'] = \boldsymbol{n} \cdot \boldsymbol{M^{UF}} \cdot \boldsymbol{F^{ext}} n_0, \; r = R_c, \tag{3.64}$$

$$\boldsymbol{n} \cdot [U_0 \boldsymbol{I} n'/d - D^{rel} \nabla \boldsymbol{m'}] = \boldsymbol{n} \cdot \boldsymbol{M^{UF}} \cdot \boldsymbol{F^{ext}} \boldsymbol{m_0}, \; r = R_c, \tag{3.65}$$

$$n', \boldsymbol{m'} \sim \boldsymbol{0}, \; r \to \infty. \tag{3.66}$$

The natural dimensionless groups that arise in scaling the equations are the swim Péclet number $Pe_s = U_0 R_c / D^{rel}$, the rotational parameter $\gamma^2 = (d-1) D_R R_c^2 / D^{rel}$, and the Péclet number $Pe = U^{probe} R_c / D^{rel}$. In this chapter, $Pe \ll 1$ but Pe_s and γ^2 may take any non-negative value.

The unit vector $\hat{\boldsymbol{u}}$ points in the direction of the applied external force (or the probe's prescribed external velocity), and the solutions for n_0 are known, [33]

$$\frac{n_0^{3D}}{n^\infty} = 1 + \frac{Pe_s^2/3}{\gamma^2 + 2(1+\lambda)} \frac{e^{-\lambda(r-1)}}{r}, \tag{3.67}$$

$$\frac{n_0^{2D}}{n_A^\infty} = 1 + \frac{2\left(\frac{\ell}{\delta}\right)^2 K_0(\lambda(r-1))}{K_0(\lambda(r-1))\left[2 - \left(\frac{\ell}{\delta}\right)^2\right] + K_2(\lambda(r-1))\left[2 + \left(\frac{\ell}{\delta}\right)^2\right]}, \tag{3.68}$$

where K_n is the nth modified Bessel function of the second kind, $\lambda = \sqrt{Pe_s^2/d + \gamma^2}$ and the polar order is proportional to the gradient in the number density $\boldsymbol{m_0} = Pe_s^{-1} \nabla n_0$. Note that λ is dimensionless here, but has units of inverse length in the main text. The governing equations are linear and may be solved via the same screened harmonic decomposition methods used to determine the equilibrium solution [27]. The only difference here is that both governing equations are now forced by the divergence of the equilibrium advective flux, and so one must find a particular solution in addition to the homogeneous solutions found via the multipole expansion.

In 3-D the concentration disturbance n' in terms of two undetermined coefficients is

$$n' = \hat{\boldsymbol{u}} \cdot \boldsymbol{n}\Bigg(B_1 \frac{1}{r^2} - \frac{\frac{1}{9}Pe_s^4/\lambda^4}{2(\lambda+1)+\gamma^2} e^{-\lambda(r-1)}\Big(\frac{\lambda}{r} + \frac{1}{r^2}\Big) - A_1 \frac{Pe_s}{\lambda^2} e^{-\lambda(r-1)}\Big(\frac{\lambda}{r} + \frac{1}{r^2}\Big) \\ - \frac{\frac{1}{3}Pe_s^2/\lambda^2}{2(\lambda+1)+\gamma^2}\Big(\frac{1}{3}\frac{Pe_s^2}{\lambda^2} + 1\Big) e^{-\lambda(r-1)}\Big(\frac{3}{4\lambda^2}\frac{1}{r^2} + \frac{3}{4\lambda}\frac{1}{r} + \frac{1}{2}\Big)\Bigg), \tag{3.69}$$

where the coefficients A_1 and B_1 are coupled to the polar order disturbance:

$$\begin{aligned}
\boldsymbol{m}' = {} & C_1 e^{-\gamma(r-1)} \hat{\boldsymbol{u}} \cdot \Big\{ \frac{\boldsymbol{I}}{r} - \frac{1}{\gamma^2}\Big[\Big(3\frac{\boldsymbol{nn}}{r^3} - \frac{\boldsymbol{I}}{r^3}\Big) + \gamma\Big(3\frac{\boldsymbol{nn}}{r^2} - \frac{\boldsymbol{I}}{r^2}\Big) + \gamma^2\frac{\boldsymbol{nn}}{r}\Big]\Big\} \\
& - \frac{1}{Pe_s}\frac{1}{2(\lambda+1)+\gamma^2} e^{-\lambda(r-1)} \hat{\boldsymbol{u}} \cdot \Big[\Big(3\frac{\boldsymbol{nn}}{r^3} - \frac{\boldsymbol{I}}{r^3}\Big) + \lambda\Big(3\frac{\boldsymbol{nn}}{r^2} - \frac{\boldsymbol{I}}{r^2}\Big) + \lambda^2\frac{\boldsymbol{nn}}{r}\Big] \\
& - \frac{\frac{1}{3}Pe_s/\lambda^2}{2(\lambda+1)+\gamma^2} e^{-\lambda(r-1)} \hat{\boldsymbol{u}} \cdot \Big[\Big(3\frac{\boldsymbol{nn}}{r^3} - \frac{\boldsymbol{I}}{r^3}\Big) + \lambda\Big(3\frac{\boldsymbol{nn}}{r^2} - \frac{\boldsymbol{I}}{r^2}\Big) + \lambda^2\frac{\boldsymbol{nn}}{r}\Big] \\
& + \frac{1}{2(\lambda+1)+\gamma^2}\frac{2\lambda^2-\gamma^2}{\lambda^2 Pe_s}\Big(\frac{1}{3}\frac{Pe_s^2}{\lambda^2} + 1\Big) e^{-\lambda(r-1)} \hat{\boldsymbol{u}} \cdot \Big[\Big(3\frac{\boldsymbol{nn}}{r^3} - \frac{\boldsymbol{I}}{r^3}\Big) \\
& + \lambda\Big(3\frac{\boldsymbol{nn}}{r^2} - \frac{\boldsymbol{I}}{r^2}\Big) + \lambda^2\frac{\boldsymbol{nn}}{r}\Big] + B_1\frac{1}{3}\frac{Pe_s}{\gamma^2}\hat{\boldsymbol{u}} \cdot \Big(3\frac{\boldsymbol{nn}}{r^3} - \frac{\boldsymbol{I}}{r^3}\Big) \\
& + \frac{1}{\lambda^2} A_1 e^{-\lambda(r-1)} \hat{\boldsymbol{u}} \cdot \Big[\Big(3\frac{\boldsymbol{nn}}{r^3} - \frac{\boldsymbol{I}}{r^3}\Big) + \lambda\Big(3\frac{\boldsymbol{nn}}{r^2} - \frac{\boldsymbol{I}}{r^2}\Big) + \lambda^2\frac{\boldsymbol{nn}}{r}\Big] \\
& + \frac{\frac{1}{3}Pe_s}{2(\lambda+1)+\gamma^2}\Big(\frac{1}{3}\frac{Pe_s^2}{\lambda^2} + 1\Big) e^{-\lambda(r-1)} \hat{\boldsymbol{u}} \cdot \Big[\frac{3}{4\lambda^2}(\lambda r + 1)\Big(\frac{\boldsymbol{I}}{r^3} - 3\frac{\boldsymbol{nn}}{r^3}\Big) \\
& + \frac{1}{2}\Big(\frac{\boldsymbol{I}}{r} - \frac{\boldsymbol{nn}}{r}\Big) - \lambda\boldsymbol{nn}\Big(\frac{3}{4\lambda^2 r} + \frac{1}{2}\Big)\Big].
\end{aligned} \tag{3.70}$$

The coeffcients A_1, B_1, and C_1 are determined by the no-flux boundary condition at particle contact. This results in a linear system of three equations that may be solved

to find algebraic expressions for n':

$$2B_1\Big(1+\frac{Pe_s^2}{3\gamma^2}\Big)-2C_1Pe_s\Big(\frac{1+\gamma}{\gamma^2}\Big)=1-2C_0\frac{(1+\lambda)}{\lambda^4} \tag{3.71}$$

$$\begin{aligned}B_1\frac{Pe_s}{\gamma^2}-C_1\Big(2+\frac{3}{\gamma^2}+\frac{3}{\gamma}+\gamma\Big)+A_1\Big(1+\frac{3}{\lambda}+\frac{3}{\lambda^2}\Big)=\frac{C_0}{\lambda^2}\Big[\Big(\frac{3}{\lambda^2}+\frac{3}{\lambda}+1\Big)\\ \times\Big(1+\frac{3}{Pe_s^2}-\frac{3(2\lambda^2-\gamma^2)^2}{\lambda^6Pe_s^2}\Big)-\Big(1+\frac{Pe_s^2}{3\lambda^2}\Big)\Big(\frac{1}{2}+\frac{9}{4\lambda^2}+\frac{3}{2\lambda}+\frac{\lambda}{2}=\frac{3(1+\lambda)}{4\lambda}\Big)\Big]\end{aligned} \tag{3.72}$$

$$\begin{aligned}&-B_1Pe_s\Big(\frac{\gamma^2+9}{3\gamma^2}\Big)+C_1\Big(4+\frac{9}{\gamma^2}+\frac{9}{\gamma}+\gamma\Big)-A_1\Big(\lambda+4+\frac{9}{\lambda}+\frac{9}{\lambda^2}\Big)+A_1\frac{(1+\lambda)Pe_s^2}{3\lambda^2}\\ &\quad-\frac{C_0(1+\lambda)}{2\lambda^2}-\frac{C_0}{\lambda^4}(2\lambda^2-\gamma^2)\Big(\frac{5}{4}+\frac{27}{4\lambda^2}+\frac{9}{2\lambda}+\frac{5\lambda}{4}+\frac{\lambda^2}{2}+\frac{9(1+\lambda)}{4\lambda}\Big)\\ &\quad-C_0(9+9\lambda+4\lambda^2+\lambda^3)\Big(-\frac{1}{\lambda^4}-\frac{3}{\lambda^2(Pe_s^2)}+\frac{(2\lambda^2-\gamma^2)^2}{\lambda^6(\lambda^2-\gamma^2)}\Big)\\ &\quad=\frac{Pe_s}{3}\Big[\frac{C_0Pe_s^3(1+\lambda)}{3\lambda^6}+\frac{C_0(2\lambda^2-\gamma^2)}{\lambda^4}\Big(\frac{1}{2}+\frac{3(1+\lambda}{4\lambda^2}\Big)\Big],\end{aligned} \tag{3.73}$$

where we define $C_0 = (Pe_s^2/3)/(\gamma^2 + 2(1+\lambda))$ for brevity.

The analysis in $d = 2$ follows precisely the same formula, but the solution will be in terms of gradients of the modified Bessel function $K_0(\lambda r)$ [33].

The intrinsic microviscosity is determined by n':

$$\begin{aligned}\eta^{micro} &= 2\Big[B_1-\frac{\frac{1}{9}Pe_s^4/\lambda^4}{2(\lambda+1)+\gamma^2}(\lambda+1)-A_1\frac{Pe_s}{\lambda^2}(\lambda+1)\\ &\quad-\frac{\frac{1}{3}Pe_s^2/\lambda^2}{2(\lambda+1)+\gamma^2}\Big(\frac{1}{3}\frac{Pe_s^2}{\lambda^2}+1\Big)\Big(\frac{3}{4\lambda^2}+\frac{3}{4\lambda}+\frac{1}{2}\Big)\Big],\end{aligned} \tag{3.74}$$

where we have left the expression in terms of the coefficients A_1 and B_1 for both brevity and generality—this construction for the microstructure is valid even when the contact boundary condition is not one of no translational flux. When $Pe_s = 0$, $n' = B_1\hat{\boldsymbol{u}}\cdot\boldsymbol{n}/r^2$ and $B_1 = 1/2$, so $\eta^{micro} = 1$.

BIBLIOGRAPHY

[1]R. Kubo, "The fluctuation-dissipation theorem", Reports Prog. Phys. **29**, 255 (1966).

[2]H. B. Callen, and T. A. Welton, "Irreversibility and Generalized Noise*", Phys. Rev. **83**, 34–40 (1951).

[3]J. F. Brady, "The long-time self-diffusivity in concentrated colloidal dispersions", J. Fluid Mech. **272**, 109 (1994).

[4]S. Ramaswamy, "The Mechanics and Statistics of Active Matter", Annu. Rev. Condens. Matter Phys. **1**, 323–345 (2010).

[5]M. C. Marchetti, J. F. Joanny, S. Ramaswamy, T. B. Liverpool, J. Prost, M. Rao, and R. A. Simha, "Hydrodynamics of soft active matter", Rev. Mod. Phys. **85**, 1143–1189 (2013).

[6]S. C. Takatori, and J. F. Brady, "Towards a thermodynamics of active matter", Phys. Rev. E - Stat. Nonlinear, Soft Matter Phys. **91**, 1–7 (2015).

[7]A. P. Solon, M. E. Cates, and J. Tailleur, "Active brownian particles and run-and-tumble particles: A comparative study", Eur. Phys. J. Spec. Top. **224**, 1231–1262 (2015).

[8]S. C. Takatori, and J. F. Brady, "A theory for the phase behavior of mixtures of active particles", Soft Matter **11**, 7920–7931 (2015).

[9]X.-l. Wu, and A. Libchaber, "Particle Diffusion in a Quasi-Two-Dimensional Bacterial Bath", Phys. Rev. Lett. **84**, 3017–3020 (2000).

[10]M. J. Kim, and K. S. Breuer, "Enhanced diffusion due to motile bacteria", Phys. Fluids **16**, 1–5 (2004).

[11]G. Miño, T. E. Mallouk, T. Darnige, M. Hoyos, J. Dauchet, J. Dunstan, R. Soto, Y. Wang, A. Rousselet, and É. Clément, "Enhanced diffusion due to active swimmers at a solid surface", Phys. Rev. Lett. **106**, 1–4 (2011).

[12]A. Jepson, V. a. Martinez, J. Schwarz-Linek, A. Morozov, and W. C. K. Poon, "Enhanced diffusion of nonswimmers in a three-dimensional bath of motile bacteria", Phys. Rev. E - Stat. Nonlinear, Soft Matter Phys. **88**, 3–7 (2013).

[13]G. Miño, J. Dunstan, A. Rousselet, É. Clément, and R. Soto, "Induced Diffusion of Tracers in a Bacterial Suspension: Theory and Experiments", J. Fluid Mech. **729**, 20 (2013).

[14]J.-L. Thiffeault, and S. Childress, "Stirring by swimming bodies", Phys. Lett. Sect. A Gen. At. Solid State Phys. **374**, 3487–3490 (2010).

[15]D. O. Pushkin, and J. M. Yeomans, "Fluid mixing by curved trajectories of microswimmers", Phys. Rev. Lett. **111**, 1–5 (2013).

[16]A. Morozov, and D. Marenduzzo, “Enhanced diffusion of tracer particles in dilute bacterial suspensions.”, Soft Matter **10**, 2748–58 (2014).

[17]R. Jeanneret, D. O. Pushkin, V. Kantsler, and M. Polin, “Entrainment dominates the interaction of microalgae with micron-sized objects”, Nat. Commun. **7**, 12518 (2016).

[18]Y. Hatwalne, S. Ramaswamy, M. Rao, and R. A. Simha, “Rheology of Active-Particle Suspensions”, Phys. Rev. Lett. **92**, 1–4 (2004).

[19]B. M. Haines, I. S. Aronson, L. V. Berlyand, and D. A. Karpeev, “Effective viscosity of dilute bacterial suspensions: a two-dimensional model.”, Phys. Biol. **5**, 046003 (2008).

[20]A. Sokolov, and I. S. Aranson, “Reduction of viscosity in suspension of swimming bacteria”, Phys. Rev. Lett. (2009) 10.1103/PhysRevLett.103.148101.

[21]D. Saintillan, “Extensional rheology of active suspensions”, Phys. Rev. E - Stat. Nonlinear, Soft Matter Phys. **81** (2010).

[22]G. Foffano, J. S. Lintuvuori, A. N. Morozov, K. Stratford, M. E. Cates, and D. Marenduzzo, “Bulk rheology and microrheology of active fluids”, Eur. Phys. J. E **35** (2012) 10.1140/epje/i2012-12098-5.

[23]H. M. López, J. Gachelin, C. Douarche, H. Auradou, and É. Clément, “Turning Bacteria Suspensions into Superfluids”, Phys. Rev. Lett. **115**, 028301 (2015).

[24]D. T. N. Chen, A. W. Lau, L. A. Hough, M. F. Islam, M. Goulian, T. C. Lubensky, and A. G. Yodh, “Fluctuations and rheology in active bacterial suspensions”, Phys. Rev. Lett. **99**, 1–4 (2007).

[25]T. V. Kasyap, D. L. Koch, and M. Wu, “Hydrodynamic tracer diffusion in suspensions of swimming bacteria”, Phys. Fluids **26**, 081901 (2014).

[26]A. E. Patteson, A. Gopinath, P. K. Purohit, and P. E. Arratia, “Particle diffusion in active fluids is non-monotonic in size.”, Soft Matter **12**, 2365–72 (2016).

[27]E. W. Burkholder, and J. F. Brady, “Tracer diffusion in active suspensions”, Phys. Rev. E - Stat. Nonlinear, Soft Matter Phys. (2017) 10.1103/PhysRevE.95.052605,

[28]G. Foffano, J. S. Lintuvuori, K. Stratford, M. E. Cates, and D. Marenduzzo, “Colloids in active fluids: Anomalous microrheology and negative drag”, Phys. Rev. Lett. **109**, 1–5 (2012).

[29]C. Reichhardt, and C. J. O. Reichhardt, “Active microrheology in active matter systems: Mobility, intermittency, and avalanches”, Phys. Rev. E - Stat. Nonlinear, Soft Matter Phys. **91**, 1–7 (2015).

[30]S. Kim, and S. J. Karilla, *Microhydrodynamics : Principles and Selected Applications* (1991).

[31]R. N. Zia, and J. F. Brady, "Single-particle motion in colloids: force-induced diffusion", J. Fluid Mech. **658**, 188–210 (2010).

[32]J. F. Brady, and J. F. Morris, "Self-diffusion in sheared suspensions", J. Fluid Mech. **312**, 223–252 (1996).

[33]W. Yan, and J. F. Brady, "The force on a body in active matter", J. Fluid Mech. **6**, 1–11 (2015).

[34]E. W. Burkholder, and J. F. Brady, "Do hydrodynamic interactions affect the swim pressure?", Soft Matter **14**, 3581–3589 (2018),

[35]D. Saintillan, and M. J. Shelley, "Theory of Active Suspensions", in *Complex fluids biol. syst.* Edited by S. Spagnolie, (Springer, New York, 2015) Chap. 9, pp. 319–355.

[36]D. Saintillan, and M. J. Shelley, "Active suspensions and their nonlinear models", Comptes Rendus Phys. **14**, 497–517 (2013).

[37]A. S. Khair, and J. F. Brady, "Single particle motion in colloidal dispersions: a simple model for active and nonlinear microrheology", J. Fluid Mech. **557**, 73 (2006).

[38]T. M. Squires, and J. F. Brady, "A simple paradigm for active and nonlinear microrheology", Phys. Fluids **17**, 1–21 (2005).

[39]S. C. Takatori, and J. F. Brady, "Superfluid Behavior of Active Suspensions from Diffusive Stretching", Phys. Rev. Lett. **118**, 018003 (2017).

[40]W. Yan, and J. F. Brady, "Soft Matter The curved kinetic boundary layer of active matter", Soft Matter **14**, 279–290 (2017).

[41]A. Einstein, "Neue Bestimmung der Moleküldimensionen", Ann. Phys., 1–5 (1906).

[42]M. Gruber, "Active microrheology of ellipsoidal probes", 2017.

[43]W. Sutherland, "A dynamical theory of diffusion for non-electrolytes and the molecular mass of albumin", Philos. Mag. Ser. 6 **9**, 781–785 (1905).

[44]M. von Smoluchowski, "Zur kinetischen Theorie der Brownschen Molekularbewegung und der Suspensionen", Ann. Phys. **326**, 756–780 (1906).

[45]H. Brenner, "A general theory of Taylor dispersion phenomena IV . Direct Coupling Effects", Chem. Eng. Commun., 355–379 (1982).

[46]J. M. Rallison A N, and D. E. J. Hinch, "The effect of particle interactions on dynamic light scattering from a dilute suspension", J. Fluid Mech **167**, 131–168 (1986).

Chapter 4

CLOSURE OF THE FIELD EQUATIONS

While the aim of the previous chapter was principally to address the effects of activity on the microviscosity, it raises an issue central to our theoretical approach to active materials—the validity of the field equations. The N-particle Smoluchowski equation is always exact; it is simply a statement that the probability distribution of particles is a conserved quantity. For an isolated, isotropic active Brownian particle (ABP) in an unbounded fluid, this equation reduces to

$$\frac{\partial P}{\partial t} + \nabla_x \cdot \boldsymbol{j}^{\boldsymbol{T}} + \nabla_q \cdot \boldsymbol{j}^{\boldsymbol{R}} = 0, \tag{4.1}$$

where the translational flux $\boldsymbol{j}^{\boldsymbol{T}} = \boldsymbol{U_0} P - D_T \nabla_x P$, and the rotary flux $\boldsymbol{j}^{\boldsymbol{R}} = -\tau_R^{-1} \nabla_q P$. The self-propulsive velocity of the ABP (swimmer) is $\boldsymbol{U_0} = U_0 \boldsymbol{q}$, its reorientation time is τ_R, and its Stokes-Einstein-Sutherland diffusivity is D_T; the particle's position and orientation in the laboratory frame are $\boldsymbol{x}$ and $\boldsymbol{q}$, respectively. Substantial progress has been made using a simple expansion of the probability distribution P in moments of the swimmer orientation $\boldsymbol{q}$:

$$P = n(\boldsymbol{x}, t) + \boldsymbol{q} \cdot \boldsymbol{m}(\boldsymbol{x}, t) + (\boldsymbol{qq} - \boldsymbol{I}/d) : \boldsymbol{Q}(\boldsymbol{x}, t) + \ldots \tag{4.2}$$

where d is the spatial dimension [1]. This expansion of the probability distribution in solid surface harmonics allows us to take a mean field approach with respect to the orientation of the swimmer and solve coupled field equations in position space only. As noted by Saintillan and Shelley [2], the advective flux of the swimmers $U_0 \boldsymbol{q}$ (as well as other terms associated with $\boldsymbol{j}^{\boldsymbol{R}}$ when hydrodynamic interactions are included) requires that any equation for the ith moment of P also depends on the $i + 1$th moment (and sometimes $i + 2$). Thus we need a closure for higher order moments to make any progress in this fashion.

For problems near equilibrium—meaning the microstructure is nearly isotropic—the most common assumption is to say that all higher order moments are isotropic:

$$\langle \boldsymbol{qq} \rangle = \frac{1}{d} \boldsymbol{I} n \tag{4.3}$$

$$\langle \boldsymbol{qqq} \rangle = \frac{1}{d+2} \boldsymbol{\alpha} \cdot \boldsymbol{m} \tag{4.4}$$

$$\langle \boldsymbol{qqqq} \rangle = \frac{1}{d(d+2)} \boldsymbol{\alpha} n + \frac{1}{2(d+4)} \boldsymbol{\kappa} : \boldsymbol{Q} \ldots, \tag{4.5}$$

where $\boldsymbol{\alpha}$ is the fourth-order isotropic tensor and $\boldsymbol{\kappa}$ is the sixth-order isotropic tensor in d dimensions. Closures 4.3 and 4.4 are used in previous chapters to truncate the tensor harmonic expansion of P, and in previous calculations of the force on a boundary [3], as well as other works [4, 5]. Other closures include Doi's *ad hoc* quadratic closure $\langle \boldsymbol{qqqq} \rangle = \langle \boldsymbol{qq} \rangle^2 / n$ [6], commonly used for liquid crystals. More rigorous approaches developed by Hinch and Leal link the fourth-moment to the second moment through the rate-of-strain tensor for the background fluid flow $\boldsymbol{E}$ [7]. This has been used to model active filaments with nematic order but no polar order (similar to passive Brownian ellipsoids) [8].

Isotropic closures—which amount to a truncation of the expansion of P in tensor harmonics of $\boldsymbol{q}$—are derived such that there can be no steady state tensorial order in the absence of spatial fluctuations: an unbounded suspension at steady state should be isotropic. For calculations of the force on a boundary, assuming isotropic nematic order $\boldsymbol{Q} = 0$ correctly predicts the number density profile near the wall. This remains true in the presence of hydrodynamic interactions, as they do not substantially influence the geometry of the problem (Chapter 6). From a purely mathematical perspective, we only need an accurate prediction of the zeroth moment n to compute the pressure at the wall. Assuming $\boldsymbol{Q} = 0$ correctly predicts the number density, but not the polar order $\boldsymbol{m}$ (see Fig 4.4). However, the important dynamic feature—that the polar order indicates that the swimmers move toward the wall on average—is captured with this closure. If we needed to compute a vector quantity—which would directly or indirectly depend on the polar order—we need to include $\boldsymbol{Q}$ so that the prediction of $\boldsymbol{m}$ is correct. Indeed one could deduce that numerically accurate predictions for $\boldsymbol{Q}$ would require calculation of $\boldsymbol{B} = \langle \boldsymbol{qqq} \rangle - \boldsymbol{\alpha} \cdot \boldsymbol{m}/(d+2)$.

These closures are also limited in their ability to predict the precise shape of the distribution. Indeed if one is interested in the spatial distribution or time evolution of $n, \boldsymbol{m}$ or $\boldsymbol{Q}$, even more moments beyond $\boldsymbol{B}$ may be required to correctly predict the profiles. One alternative approach that circumvents this is to explicitly include the effects of long-ranged spatial fluctuations in the equation closures. For example, if one is interested in the diffusion of ABPs, one could "slave" the polar order to gradients in n and $\boldsymbol{Q}$:

$$\boldsymbol{m} = -\frac{U_0 \tau_R}{d(d-1)} \nabla n + \frac{U_0 \tau_R}{(d-1)} \boldsymbol{\nabla} \cdot \boldsymbol{Q}, \tag{4.6}$$

which gives the physically correct diffusion coefficient in the equation for the number density $(U_0^2 \tau_R / d(d-1) + D_T) \nabla^2 n = 0$ (neglecting the nematic order $\boldsymbol{Q} = 0$).

Similarly, if one is interested in the spatiotemporal evolution of $\boldsymbol{Q}$ (perhaps to look at transient behavior of the swim stress), an appropriate closure might be to also "slave" $\boldsymbol{B}$ to gradients in n and $\boldsymbol{Q}$:

$$\boldsymbol{B} \sim U_0\tau_R(\boldsymbol{\nabla}\cdot\boldsymbol{\alpha}n + \boldsymbol{\nabla}\cdot\boldsymbol{\kappa} : \boldsymbol{Q}). \tag{4.7}$$

These closures are similar in spirit to Hinch and Leal's linking of the fourth-moment to the rate-of-strain tensor, as the microstructure is clearly not isotropic in the presence of an ambient, steady flow-field.

In this chapter, we consider a test problem—the linear microrheology of an active suspension confined to an interface—and systematically investigate the effects of various closures on the computed probability distribution and its physically relevant moduli. We examine two isotropic closures, $\boldsymbol{Q} = \boldsymbol{0}$ and $\boldsymbol{B} = \boldsymbol{0}$, and a simple closure linking the nematic order to gradients in the polar order:

$$\boldsymbol{Q} = -\frac{\ell}{16}[\nabla\boldsymbol{m} + (\nabla\boldsymbol{m})^{\dagger} - \boldsymbol{I}(\nabla\cdot\boldsymbol{m})], \tag{4.8}$$

and compare this to predictions of the microviscosity from solving the full Smoluchowski equation in position and orientation space.

4.1 Full smoluchowski equation: no closure

Consider the motion of a probe particle through a suspension of ABPs; the dynamics are described by

$$\frac{\partial P_2}{\partial t} + \nabla_{x_P}\cdot\boldsymbol{j}_{\boldsymbol{P}}^{\boldsymbol{T}} + \nabla_{x_s}\cdot\boldsymbol{j}_{\boldsymbol{s}}^{\boldsymbol{T}} + \nabla_{q_P}\cdot\boldsymbol{j}_{\boldsymbol{P}}^{\boldsymbol{R}} + \nabla_{q_s}\cdot\boldsymbol{j}_{\boldsymbol{s}}^{\boldsymbol{R}} = 0, \tag{4.9}$$

where $P_2(\boldsymbol{x}_P, \boldsymbol{x}_s, \boldsymbol{q}_P, \boldsymbol{q}_s, t)$ is the probability of finding the probe at position $\boldsymbol{x}_P$ pointing in the direction $\boldsymbol{q}_P$, and the swimmer at position $\boldsymbol{x}_s$ pointing in the direction $\boldsymbol{q}_s$ at time t. We wish to re-write the equation in terms of a conditional probability of finding the swimmer at some point $(\boldsymbol{r}, \boldsymbol{q})$ in phase space, given that the probe is at the point $(\boldsymbol{z}, \boldsymbol{p})$. Transforming the position-space equations into a relative coordinate frame is simple vector addition—$\boldsymbol{z}' \equiv \boldsymbol{x}_P$, $\boldsymbol{r}' \equiv \boldsymbol{x}_s - \boldsymbol{x}_P$—but moving into a frame where the swimmer rotates relative to the probe requires a matrix operator $\boldsymbol{R}(\boldsymbol{q}_P)$ that rotates these position vectors into the appropriate frame: $\boldsymbol{z} = \boldsymbol{z}', \boldsymbol{r} = \boldsymbol{R}\cdot\boldsymbol{r}', \boldsymbol{p} = \boldsymbol{q}_P, = \boldsymbol{q} = \boldsymbol{R}\cdot\boldsymbol{q}_s$. In microrheology problem, the direction of the probe velocity (or external force) $\hat{\boldsymbol{u}}$ determines the orientation of the probe, so we require $\boldsymbol{R}(\boldsymbol{q}_P)\cdot\boldsymbol{q}_{\boldsymbol{P}} = \hat{\boldsymbol{u}}$ [9]. For $d = 2$, this rotation is parametrized only by the polar angle. In 3-D, the rotation matrix would be defined in the same manner, but we would

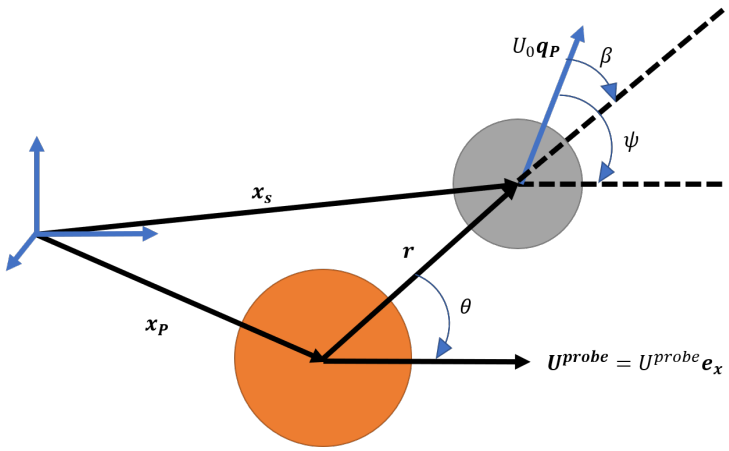

Figure 4.1: Sketch of the probe-swimmer coordinate system. The probe has a position $\boldsymbol{x}_P$ and orientation $\boldsymbol{e}_x$ in the fixed coordinate frame. The swimmer has a position $\boldsymbol{x}_s$ and orientation $\boldsymbol{q}_s$ (parametrized by the angle ψ) in the fixed frame. The relative separation between the particles is $\boldsymbol{r}$, and the polar angle of the swimmer's position with respect to the probe is θ. The orientation of the swimmer relative to the probe is parametrized by the angle $\beta = \psi - \theta$.

require both a polar and azimuthal coordinate to parametrize the rotation. The 3-D rotation is not unique.

For simplicity, we will assume that we are working in two-dimensions, and that the probe is moving in the x-direction $\hat{\boldsymbol{u}} = \boldsymbol{e}_x$ (see Fig. 4.1). The unit normal of the probe—the unit vector pointing along $\boldsymbol{r}'$—is thus given by $\boldsymbol{n} = \cos\theta \boldsymbol{e}_x + \sin\theta \boldsymbol{e}_y$. We can assume that $\boldsymbol{z}'$ is at the origin. The orientation of the swimmer is $\boldsymbol{q}_s = \cos\psi \boldsymbol{e}_x + \sin\psi \boldsymbol{e}_y$. The fluxes of each particle are now as follows:

$$\boldsymbol{j}_{\boldsymbol{P}}^{\boldsymbol{T}} = U^{probe}\boldsymbol{e}_x P - D_P \nabla'_z P + D_P \nabla'_r P \tag{4.10}$$

$$\boldsymbol{j}_{\boldsymbol{s}}^{\boldsymbol{T}} = U_0 \boldsymbol{q}_s P - D_T \nabla'_r P \tag{4.11}$$

$$\boldsymbol{j}_{\boldsymbol{P}}^{\boldsymbol{R}} = -D_R \nabla_{q_P} P \tag{4.12}$$

$$\boldsymbol{j}_{\boldsymbol{s}}^{\boldsymbol{R}} = -\frac{1}{\tau_R} \nabla_{q_s} P, \tag{4.13}$$

where D_P is the thermal translational diffusivity of the probe, and D_R is the probes rotational diffusivity. In this chapter we have chosen to represent changes in reorientation by gradients with respect to $\boldsymbol{q}_P$ and $\boldsymbol{q}_s$; Brenner showed that $\nabla_R^2 = \nabla_q^2$, so either representation is equivalent in the final equation [10]. For the microvicosity, we are not concerned with fluctuations in the absolute position (and orientation) of the probe)—more care is needed when computing the effects of activity on the effective long-time self-diffusivity of the probe. All rotations are isometries and members of the special orthogonal group $SO(d)$; consequently $\boldsymbol{R}^{-1} = \boldsymbol{R}^{\dagger}$ and the

dot product is invariant under rotation. Thus, we circumvent the need to write the flux expressions in rotating coordinates, and may write down the final, scalar equation:

$$\frac{\partial P}{\partial t} + U_0\Big(\cos(\psi-\theta)\frac{\partial P}{\partial r} + \frac{\sin(\psi-\theta)}{r}\frac{\partial P}{\partial \theta}\Big) - U^{probe}\Big(\cos\theta\frac{\partial P}{\partial r} - \frac{\sin\theta}{r}\frac{\partial P}{\partial \theta}\Big) \\ -D^{rel}\nabla_r^2 P - \frac{1}{\tau_R}\frac{\partial^2 P}{\partial \psi^2} - D_R\frac{\partial^2 P}{\partial \theta^2} = 0, \tag{4.14}$$

which is effectively expressed as a function of r, θ, and the angle $\beta \equiv \psi - \theta$:

$$\frac{\partial P}{\partial t} + U_0\Big(\cos\beta\frac{\partial P}{\partial r} - \frac{\sin\beta}{r}\frac{\partial P}{\partial \beta} + \frac{\sin\beta}{r}\frac{\partial P}{\partial \theta}\Big) - U^{probe}\Big(\cos\theta\frac{\partial P}{\partial r} - \frac{\sin\theta}{r}\frac{\partial P}{\partial \theta} \\ +\frac{\sin\theta}{r}\frac{\partial P}{\partial \beta}\Big) - D^{rel}\Big(\frac{\partial^2 P}{\partial r^2} + \frac{1}{r}\frac{\partial P}{\partial r} + \frac{1}{r^2}\frac{\partial^2 P}{\partial \beta^2} + \frac{1}{r^2}\frac{\partial^2 P}{\partial \theta^2}\Big) \\ -(\tau_R^{-1} + D_R)\frac{\partial^2 P}{\partial \beta^2} - D_R\frac{\partial^2 P}{\partial \theta^2} = 0. \tag{4.15}$$

The derivatives with respect to β are lost if one does not carefully consider the transformation to a frame rotating with the probe.

At equilibrium $U^{probe} \equiv 0$ and there can be no dependence on the angle θ, as there is no symmetry breaking without directed motion. For small perturbations away from equilibrium, we know that the probability distribution should take the form $P = P_0(r,\beta) + Pe\cos\theta f(r,\beta)$, where $Pe = U^{probe}R_c/D^{rel}$. So we now do a moments expansion in θ rather than in β. Indeed this is most appropriate when we allow the magnitude of activity to be arbitrary, but consider only small perturbations due to external forces.

The equilibrium governing equations are:

$$Pe_s\Big(\cos\beta\frac{\partial P_0}{\partial r} - \frac{\sin\beta}{r}\frac{\partial P_0}{\partial \beta}\Big) - \frac{\partial^2 P_0}{\partial r^2} - \frac{1}{r}\frac{\partial P_0}{\partial r} - \Big(\frac{1}{r^2} + \gamma^2\Big)\frac{\partial^2 P_0}{\partial \beta^2} = 0, \tag{4.16}$$

$$Pe_s\cos\beta P_0 - \frac{\partial P_0}{\partial r} = 0,\ r = 1, \tag{4.17}$$

$$P_0 \sim n^\infty/2\pi, r \to \infty, \tag{4.18}$$

where $Pe_s = U_0R_c/D^{rel}$, $\gamma^2 = R_c^2/D^{rel}(\tau_R - D_R^{-1})$. The $O(Pe)$ equations are

$$Pe_s\Big(\cos\beta\frac{\partial f}{\partial r} - \frac{\sin\beta}{r}\frac{\partial f}{\partial \beta}\Big) - \frac{\partial P_0}{\partial r} - \frac{\partial^2 f}{\partial r^2} - \frac{1}{r}\frac{\partial f}{\partial r} + \frac{f}{r^2} - \Big(\frac{1}{r^2} + \gamma^2\Big)\frac{\partial^2 f}{\partial \beta^2} = 0, \tag{4.19}$$

$$Pe_s\cos\beta f - P_0 - \frac{\partial f}{\partial r} = 0,\ r = 1, \tag{4.20}$$

$$P_1 \sim 0, r \to \infty. \tag{4.21}$$

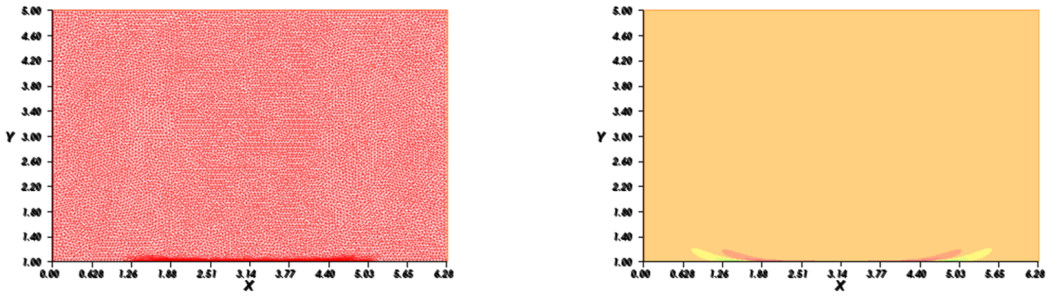

Figure 4.2: Example of adapted finite-element mesh and solution for $\ell/\delta = 50$ and $\ell/R_c = 10$. The y-coordinate is the dimensionless interparticle separation distance r and the x-axis is the angle of the swimmer relative to the probe β.

The governing equation for f is obtained by multiplying the full $O(Pe)$ equation by $\cos\theta$ and integrating with respect to θ. Thus, the microviscosity will simply be $\eta^{micro} = \phi_A^{ex} \int f(1,\beta)d\beta$, and the osmotic pressure $\Pi = n^{\infty} k_B T \int P_0(1,\beta)d\beta$.

Three dimensions

If the probe and swimmer have azimuthal coordinates ϕ and ζ respectively, then one can write the azimuthal variations respect to ϕ and $\alpha = \zeta - \phi$, for example:

$$\begin{aligned} \boldsymbol{q}\cdot\boldsymbol{\nabla}_{\boldsymbol{r}} &= (\cos\psi\cos\theta + \sin\psi\sin\theta\cos\alpha)\frac{\partial}{\partial r} + (\sin\theta\cos\psi - \sin\psi\cos\theta\cos\alpha)\frac{1}{r}\frac{\partial}{\partial\theta} \\ &\quad + \frac{1}{r}\frac{\sin\psi}{\sin\theta}\sin\alpha\left(\frac{\partial}{\partial\phi} - \frac{\partial}{\partial\alpha}\right), \end{aligned} \tag{4.22}$$

where we can easily integrate over any $\phi-$dependence. The problem is not easily expressed in terms of the relative polar angle β unless $\alpha = 0$; the problem is generally not axisymmetric in the rotating coordinate system.

4.2 Finite-element results, $d = 2$

Finite-element solutions for $P_0(r,\beta)$ and $f(r,\beta)$ are done in FreeFEM++ [11], which uses a standard Galerkin P2-FEM method with adaptive mesh refinement. An example mesh is plotted in Fig. 4.2, which is adapted to best fit the sharp gradients in the solution for $f(r,\beta)$. From P_0 and f, we can directly compute the various moments of P as a Fourier series expansion:

$$P(r,\theta,\beta) = \sum_{i=0}^{\infty} a_i(r,\theta)\cos(i\beta) + b_i(r,\theta)\sin(i\beta), \tag{4.23}$$

where

$$a_i(r,\theta) = \frac{1}{\pi}\int P\cos(i\beta)d\beta \tag{4.24}$$

$$b_i(r,\theta) = \frac{1}{\pi}\int P\sin(i\beta)d\beta \tag{4.25}$$

and i is some positive integer (in the special case of a_0, the coefficient of the integral is $1/2\pi$). These coefficients in the series expansions are the moments in the field equations introduced previously: $n = a_0$, $\boldsymbol{m} = a_1\boldsymbol{e_r} + b_1\boldsymbol{e_\theta}$, etc.

Equilibrium probability distribution

At equilibrium, we can compute the effective osmotic pressure of the suspension from the number density of particles at the surface of the probe: $\Pi = n^\infty k_B T \int P(r = R_c, \beta)d\beta$. Yan and Brady concluded that truncating the series at $i = 1$ was sufficient to capture the correct behavior of the osmotic pressure (as verified by Brownian dynamics simulations), and that including the term $i = 2$ made only a small quantitative difference in the result (this is also the case when hydrodynamic interactions are included; see Chapter 6) [3].

In Fig. 4.3, we compare the probability distribution at the probe surface $P_0(1,\beta)$ to approximations by various moments. While the finite difference approximations of P_0 agree reasonably well with the computed approximations, the agreement is not exact. One notices that the polar order is over-predicted if $\boldsymbol{Q} = 0$, severely under-predicted with $\boldsymbol{Q} \sim \nabla\boldsymbol{m}$, but almost exact if $\boldsymbol{B} = 0$. Similarly, the nematic order is under-predicted in the absence of the third moment $\boldsymbol{B}$. It is worth noting that it is not the shape of the probability distribution that matters for computing the pressure, only the area under the curve, which is relatively insensitive to the closure. The fact that the distribution is peaked at $\beta = \pi$ tells us that the swimmers are, on average, swimming toward the probe, as predicted by simulations [3]. We also note that the severe truncation of the series expansion says that the probability distribution is negative around $\beta = 0$ and $\beta = 2\pi$. While it is impossible to have a negative probability of finding the swimmer at an orientation $\beta = 0$, we needn't be concerned unless this approximation results in a negative number density $\int P_0 d\beta < 0$ at any point in space (it does not).

Curiously, the closure $\boldsymbol{Q} \sim \nabla\boldsymbol{m}$ matches the shape of the probability distribution, but the peak is much less pronounced than in in either of the isotropic closures. This is likely due to the enhanced diffusion of the polar order field associated with this closure: instead of D_T, $\boldsymbol{m}$ now diffuses with an effective diffusivity

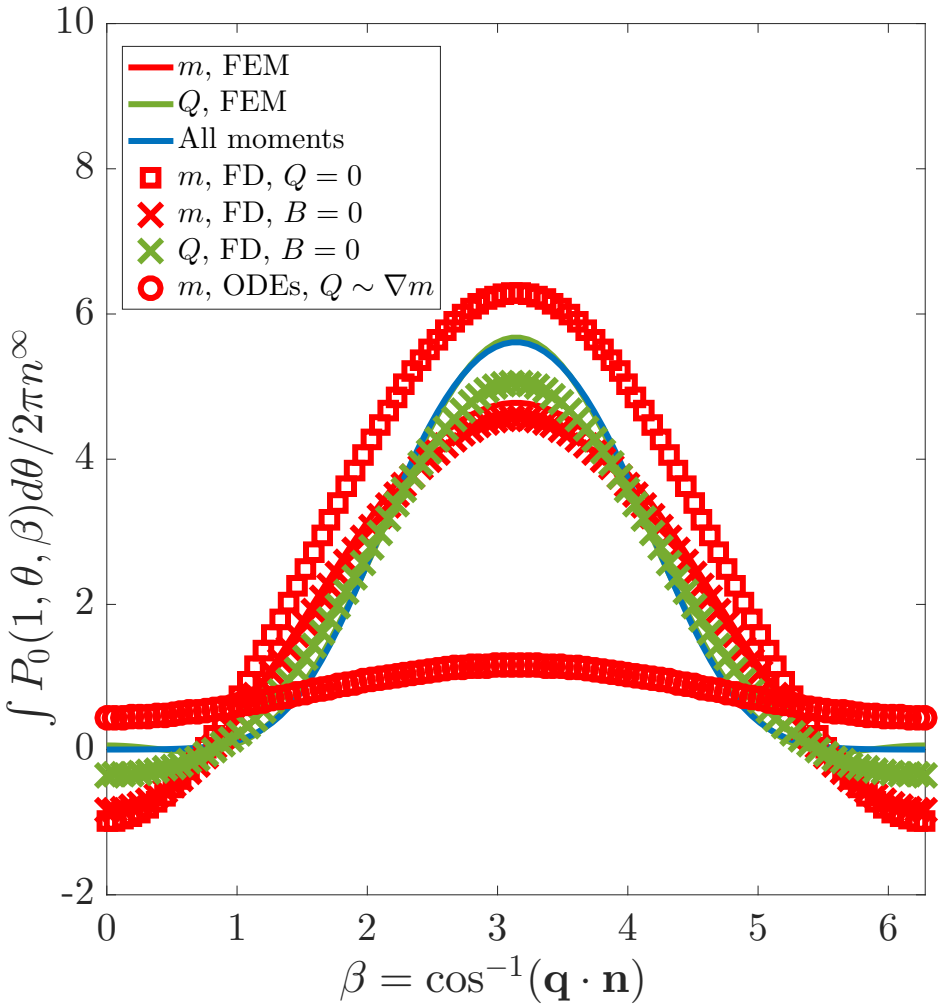

Figure 4.3: Equilibrium distribution contact as a function of the angle of the swimmer relative to the probe unit normal β: $\int P_0(1, \theta, \beta) d\theta / 2\pi n^\infty$ for $\ell/\delta = 10, \ell/R_c = 3$. Solid lines are moments derived from the full solution for P, square symbols are mean-field predictions for $\boldsymbol{Q} = 0$, crosses are the mean-field predictions for $\boldsymbol{B} = 0$, and circles are for the closure $\boldsymbol{Q} \sim \nabla \boldsymbol{m}$. The red data truncate the series expansion at $i = 2$, green data truncate at $i = 3$ and the blue line contains all moments.

$D_T + U_0^2 \tau_R / 16$. This reduces the screening length λ by a factor of $\sqrt{1 + (\ell/\delta)^2/16}$, and thus exaggerates the effective truncation of the run length when $\ell/R_c \gtrsim O(1)$ and under-predicts the number density accumulation at the probe surface.

Linear response

In Fig. 4.4 we plot the microviscosity as a function of ℓ/R_c for various closures. Even the simplest closure $\boldsymbol{Q} = 0$ correctly captures the limiting behavior for $\ell/R_c \to 0$ and $\ell/R_c \to \infty$, and the qualitative shape of the distribution. Allowing for fluctuations

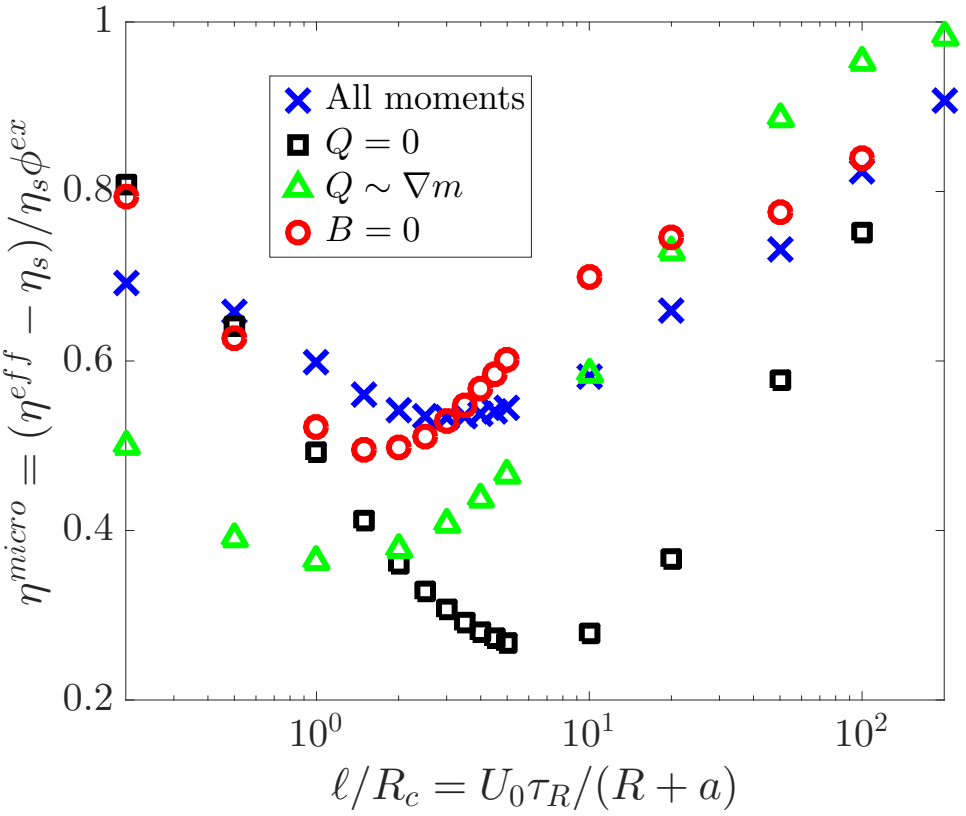

Figure 4.4: Microviscosity ($d = 2$) as a function of ℓ/R_c at $\ell/\delta = 10$ for various closures of the moments expansion of P. The squares and crosses are from finite difference solutions of the 2-D governing equations in MATLAB, and the circles are from finite element simulations of the full Smoluchowski equation in FreeFEM++ [11].

in nematic order by slaving $\boldsymbol{Q}$ to $\nabla \boldsymbol{m}$ improves the quantitative accuracy, but $\boldsymbol{B} = 0$ provides the best quantitative match to the exact solution. All closures capture the trend with respect to ℓ/R_c. We can check the limiting behaviors in microviscosity from a boundary-layer analysis similar to the one used to compute the microviscosity at large Pe in Chapter 5. Equations 4.16 and 4.19 can be rewritten in terms of a boundary-layer coordinate $Y = Pe_s(r-1)$ when $Pe_s \gg 1$. If $\gamma/Pe_s \ll 1$ ($\ell/R \gg 1$), then one finds that the microviscosity approaches 1 as $Pe_s \to \infty$. Near the viscosity minimum, we must retain terms $\sim O(\gamma/Pe_s)^2$ to capture the minimum properly; unfortunately even the boundary-layer equations are no longer analytically tractable in this case.

In Fig. 4.5 we plot $\int P_1(1,\theta,\beta)d\theta$ as a function of the angle of swimming relative to the probe particle β. We see that, though the equilibrium distribution P_0 is matched

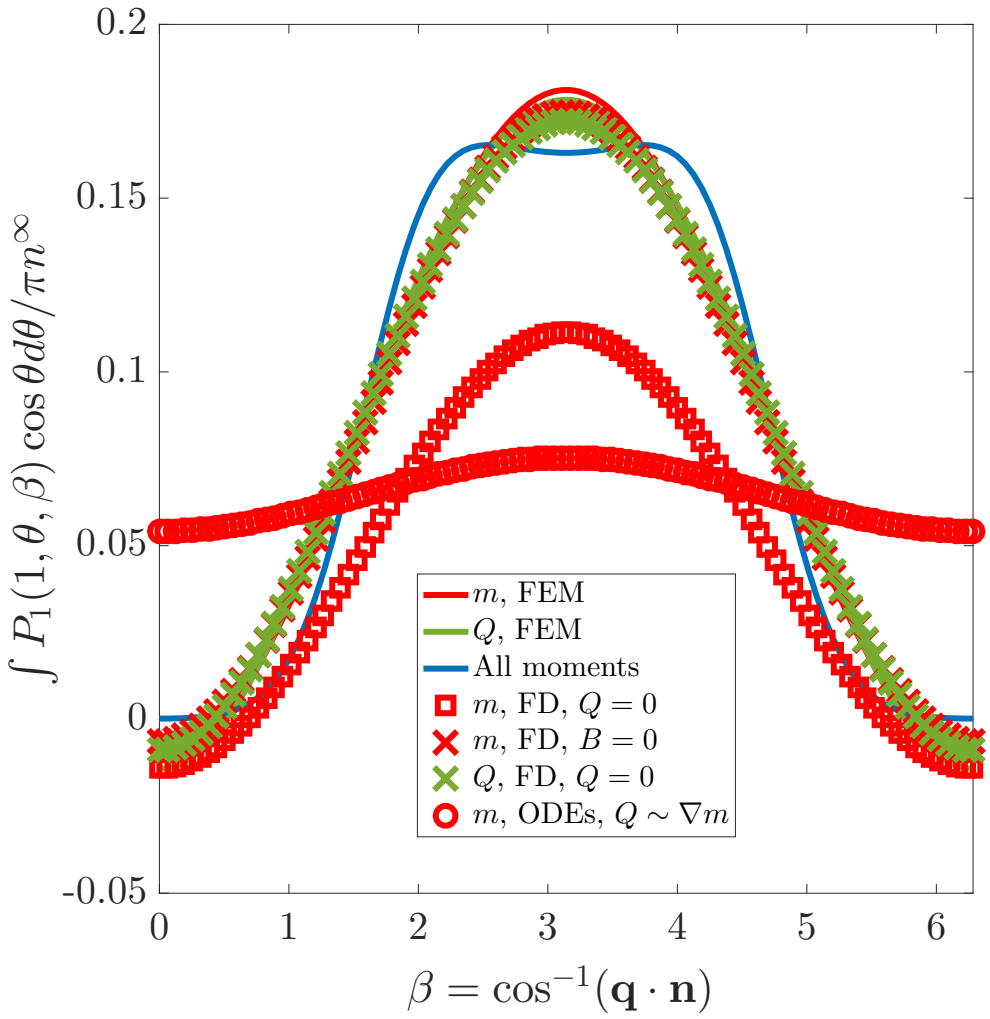

Figure 4.5: Linear disturbance to P as a function of β for various closures at $\ell/\delta = 10$, $\ell/R_c = 3$. The legend is the same as that in Fig. 4.3.

almost exactly by setting $a_i, b_i = 0$, $i \geq 3$, one must retain $i = 3$ to match the distribution for the $O(Pe)$ perturbation. At first glance this seems to indicate that $\boldsymbol{B}$ is fundamental to the microrheology problem, but the relationship is more nuanced than that. For the force on a boundary, all that is required to properly capture the dynamics is that the maximum of P_0 with respect to β be at $\beta = \pi$, such that the swimmers are pointing inward toward the probe surface. To determine correct value of the force on the boundary, we only require that the area under the curve is correct, not a precise match in shape. In the microrheology problem, we also only require the correct area under the curve to determine the microviscosity. This is matched with only three moments (see Fig. 4.5), but not with n and $\boldsymbol{m}$ only. As discussed in the introduction, $\boldsymbol{m}$ is fundamental to the calculation of the average probe velocity,

which determines η^{micro}. Thus, $\boldsymbol{Q}$ is necessary to compute the correct profile for $\boldsymbol{m}$, though $\boldsymbol{Q}$ itself is also well predicted by $\boldsymbol{B} = 0$ closure. Again, the closure linking $\boldsymbol{Q}$ and $\nabla\boldsymbol{m}$ results in a much more uniform probability distribution, though it predicts the microviscosity quite well.

The higher order-moments ($i \geq 3$) of the distribution change the qualitative shape of f with respect to β. We see two peaks slightly offset from $\beta = \pi$. As $Pe_s \to \infty$, these peaks separate and P more closely resembles a top-hat distribution distributed across $\pi/2 \leq \beta < 3\pi/2$, rather than the delta function $\delta(\beta - \pi)$ one might find in the same limit for the equilibrium distribution. A top-hat distribution simply says that there is an equal chance of the swimmer colliding with the probe at any angle. When $\ell > R_c$, a swimmer coming from far away (in the isotropic bulk) may not collide with the probe, let alone collide head-on ($\beta = \pi$). Indeed, the distribution indicates that the swimmer has the same probability of a head-on collision $\beta = \pi$ as a glancing blow with the probe.

4.3 Conclusions

In this chapter, we systematically investigated the effects of closure on both the physical moduli and the probability distribution for the 2-D microrheology problem. Finite-element calculations and boundary-layer analysis of the governing equations for $P(r, \boldsymbol{q})$ agree nearly perfectly with finite-difference calculations using the orientational moments $n, \boldsymbol{m}, \boldsymbol{Q}$ in their predictions of the microviscosity. Though we notice a qualitative difference in the shape of $P(r, \beta)$ predicted by the two different methods, this does not lead to substantial differences in the physical quantities of interest.

We conclude that including nematic order $\boldsymbol{Q}$ is necessary for correct quantitative predictions of the microviscosity in active suspensions, and that the closure $\boldsymbol{B} = 0$ seems to provide the best agreement. Because the viscosity depends on the volume-averaged diffusive flux of swimmers—thus yielding a direct connection to the polar order—we require $\boldsymbol{Q}$ in order to correctly predict $\boldsymbol{m}$ and moreover we require short-ranged fluctuations in $\boldsymbol{Q}$ for a quantitatively correct solution. For the remainder of this thesis we will use the orientation-averaged field equations with the closure $\boldsymbol{B} = 0$ to describe the system dynamics. When hydrodynamic interactions are included, there is no change to the geometric structure of the problem, and thus we expect the closure $\langle \boldsymbol{qqq} = \boldsymbol{\alpha} \cdot \boldsymbol{m}/5$ to remain sufficient. In the case of active and non-linear microrheology,we also expect this closure to remain valid because $\boldsymbol{q}$ will

be prinicipally aligned with the background flow in the direction $\hat{\boldsymbol{u}}$ (in this limit, even $\boldsymbol{Q} = 0$ would work equally well).

There are instances where appropriate closure for the field equations is not as simple. Preliminary investigations of the short-time diffusive behavior of active Brownian particles confined to line source indicate that higher order moments such as $\boldsymbol{B}$ may be necessary to match the results given by Brownian dynamics simulations. In addition, if one were interested in the transient dynamics of the suspension stress, one fundamentally requires knowledge of $\boldsymbol{Q}$. Thus far, our analysis indicates that this would require one to compute $\boldsymbol{B}$ in order to capture the correct behavior of $\boldsymbol{Q}$. In these scenarios, more sophisticated closures that capture the problem dynamics (e.g. coupling between the microstructure and the background flow) may be necessary if one is to use a mean-field approach to describe the suspension mechanics.

Appendix

A: Boundary-layer analysis for large $Pe_s, \ell/R_c$

When $Pe_s \gg 1$, an $O(Pe_s^{-1})$ thin boundary-layer forms near the surface of the probe. Outside this boundary-layer, the probability distribution is approximately uniform $P \sim n^{\infty}/2\pi$. (There may be an intermediate region—an outer boundary-layer—if $\gamma \gg 1$, which would change the outer solution we match to. This is discussed in Chapter 3 and [12]). In the inner region $Y = Pe_s(r-1) \sim O(1)$, and the radial gradients are amplified. At equilibrium, the accumulation of probability at the probe surface is $O(Pe_s)$, thus we write $P_0 = Pe_s g_0 + g_1 + O(Pe_s^{-1})$. The leading order governing equations for P_0 are:

$$\frac{\partial^2 g_0}{\partial Y^2} - \cos\beta \frac{\partial g_0}{\partial Y} + \left(\frac{\gamma}{Pe_s}\right)^2 \frac{\partial^2 g_0}{\partial \beta^2} = 0, \tag{4.26}$$

$$\frac{\partial g_0}{\partial Y} - \cos\beta g_0 = 0,\ Y = 0, \tag{4.27}$$

$$g_0 \sim 0,\ Y \to \infty, \tag{4.28}$$

which tells us $g_0 = A(\beta) exp(Y\cos\beta)$ in the limit where $\gamma/Pe_s \ll 1$. Note that this is true when $\cos\beta < 0$, i.e. the swimmers are moving toward the probe surface. To determine the function $A(\beta)$, one must solve the $O(1)$ governing equations:

$$\frac{\partial^2 g_1}{\partial Y^2} + \frac{\partial g_0}{\partial Y} - \cos\beta \frac{\partial g_1}{\partial Y} + \sin\beta \frac{\partial g_0}{\partial \beta} = 0, \tag{4.29}$$

$$\frac{\partial g_1}{\partial Y} - \cos\beta g_1 = 0,\ Y = 0, \tag{4.30}$$

$$g_1 \sim 1/2\pi,\ Y \to \infty, \tag{4.31}$$

which are identical (up to a factor of 2) to those from the large Pe microrheology problem in passive suspensions. The function A is thus governed by the ordinary differential equation

$$-\frac{1}{2\pi}\cot\beta\cos\beta = A(\beta)(\cot\beta + \tan\beta) + \frac{dA}{d\beta}, \tag{4.32}$$

which gives $A = -\cos\beta/2\pi$. Thus the equilibrium distribution is

$$P_0 = \frac{1}{2\pi}(1 - Pe_s\cos\beta e^{Y\cos\beta}) + O(1). \tag{4.33}$$

The $O(Pe)$ solution follows a similar procedure, though we note that f should be $O(1)$, thus $f = f_0 + Pe_s^{-1} f_1$. The governing equation for f_0 is

$$\frac{\partial^2 f_0}{\partial Y^2} - \cos\beta\frac{\partial f_0}{\partial Y} + D\frac{\partial g_0}{\partial Y} = 0, \tag{4.34}$$

which yields $f_0 = (B(\beta) - Y\cos\beta/2\pi)e^{Y\cos\beta}$. As before, we must go to the next order in the expansion of f, which gives a similar ODE as that for A:

$$0 = (B(\beta) - (2\pi)^{-1})(\cot\beta + \tan\beta) + \frac{d(B(\beta) - (2\pi)^{-1})}{d\beta}. \tag{4.35}$$

The only solution that remains bounded at $\beta = \pi, 2\pi$ yields

$$f = \frac{1}{2\pi}(1 - Y\cos\beta)e^{Y\cos\beta}, \tag{4.36}$$

which gives $\eta^{micro} = 1$. This agrees with the predictions from the fluctuation-dissipation arguments and field equations in Chapter 3.

BIBLIOGRAPHY

[1]D. Saintillan, and M. J. Shelley, "Theory of Active Suspensions", in *Complex fluids biol. syst.* Edited by S. Spagnolie, (Springer, New York, 2015) Chap. 9, pp. 319–355.

[2]D. Saintillan, and M. J. Shelley, "Active suspensions and their nonlinear models", Comptes Rendus Phys. **14**, 497–517 (2013).

[3]W. Yan, and J. F. Brady, "The force on a body in active matter", J. Fluid Mech. **6**, 1–11 (2015).

[4]A. Baskaran, and M. C. Marchetti, "Statistical mechanics and hydrodynamics of bacterial suspensions", Proc. Natl. Acad. Sci. U. S. A. **106**, 15567–15572 (2009).

[5]T. Brotto, J. B. Caussin, E. Lauga, and D. Bartolo, "Hydrodynamics of confined active fluids", Phys. Rev. Lett. **110**, 1–5 (2013).

[6]M. Doi, and S. F. Edwards, "Dynamics of rod-like macromolecules in concentrated solution. Part 2", J. Chem. Soc. Faraday Trans. 2 Mol. Chem. Phys. **74**, 918–932 (1978).

[7]E. J. Hinch, and L. G. Leal, "The effect of Brownian motion on the rheological properties of a suspensions of non-spherical particles", J. Fluid Mech. **52**, 683–712 (1972).

[8]F. G. Woodhouse, and R. E. Goldstein, "Spontaneous circulation of confined active suspensions", Phys. Rev. Lett. **109** (2012) 10.1103/PhysRevLett.109.168105.

[9]M. Gruber, "Active microrheology of ellipsoidal probes", 2017.

[10]H. Brenner, "Rheology of a dilute suspension of dipolar spherical particles in an external field", J. Colloid Interface Sci. **32**, 141–158 (1970).

[11]F. Hecht, O. Pironneau, J. Morice, A. Le Hyaric, K. Ohtsuka, and P. Jolivet, *FreeFem++*, Paris, France, 2017.

[12]W. Yan, and J. F. Brady, "Soft Matter The curved kinetic boundary layer of active matter", Soft Matter **14**, 279–290 (2017).

Chapter 5

ACTIVE AND NONLINEAR MICRORHEOLOGY IN ACTIVE SUSPENSIONS

The focus of many theoretical and experimental investigations in soft-matter physics has turned to the dynamic behavior of colloidal suspensions of self propelled particles, an example of active matter. These systems pose an interesting challenge, as their constituents are able to generate their own internal stresses and drive a suspension out of equilibrium without the influence of external forces [1, 2]. Typical thermodynamic relations between quantities such as temperature, chemical potential, and free energy are not valid in these non-equilibrium systems—indeed it has even been debated what the "temperature" of these systems might be [3–5]. Despite these complications, active systems have well-defined pressure-volume phase diagrams that seem to obey simple physical models reminiscent of equilibrium systems. These phase diagrams predict interesting physical phenomena such as segregation into non-equilibrium mechanical phases of higher and lower concentration [3, 6–9].

In Chapter 3, we united the idea of an effective "thermodynamics" of active matter with the well-studied problem of tracer-diffusion in active suspensions to study the fluctuation-dissipation theorem (FDT) in non-equilibrium systems. For colloidal suspensions at equilibrium, the FDT states that the long-time self-diffusivity of a tracer particle is equal to the Boltzmann energy times the average self-mobility in the suspension: $\langle \boldsymbol{D} \rangle = k_B T \langle \boldsymbol{M}^{\boldsymbol{UF}} \rangle$. The FDT is not satisfied even in the simplest active systems, but by quantifying deviations from the theorem, we showed that one can still write a generalized Stokes-Einstein-Sutherland relation (GSESR) for active matter: $\langle \boldsymbol{D} \rangle = (k_B T + E^{act}) \langle \boldsymbol{M}^{\boldsymbol{UF}} \rangle$. In the continuum limit, where the run length of the swimmers ℓ is small compared to the probe size R, E^{act} depends only on the activity of the swimmers $k_s T_s$. In general, however, E^{act} depends on the microstructure of the suspension.

Examining the FDT in active matter required solving the linear microrheology problem—determining the average viscous response of an active suspension when weakly perturbed from its (non-equilibrium) steady state by the motion of a tracer particle. This naturally leads one to question what the viscoelastic response of active matter suspensions is when they are subjected to nonlinear microscopic

deformations—when the external force is comparable to or much larger than k_BT. Microrheology is an ideal framework for analyzing the suspension mechanics of active systems because it does not require large sample volumes, which may be prohibitively expensive or experimentally unrealizable for active biological materials, and it can probe micro-scale heterogeneities in the material structure [10]. For example, the interior of a cell may be modeled as a concentrated colloidal dispersion, and many of the constituents of this dispersion are self-propelled (i.e. motor proteins). Understanding how the activity of biocolloids affects the micro-mechanics of such systems promises to give greater understanding of fundamental cellular processes, such as cellular reproduction where cytoskeletal filaments undergo directed motion by motor proteins in preparation for mitosis—how would the active motion of other cellular components affect the force required to move these filaments? Enhanced understanding of these biological processes may enable more effective drug delivery and gene therapy at the cellular level [11, 12].

Microrheology is different from macrorheology, where a large volume of material is sheared between two surfaces and the viscous properties are then inferred from the bulk material relaxation. Both methods are valid tools for probing the rheology of complex materials, but they measure fundamentally different things: macrorheology measures the material response at length scales on the order of the gap distance between two surfaces (usually in the range of a few millimeters), whereas microrheology measures the material response on the order of the probe size (a few microns). One may also use two-point microrheology in order to induce deformations on length scales larger than the probe size and infer the mechanical properties on this mesoscale by cross-correlating the fluctuating motion of two probes [13]. There are also differences at the microstructural level between the two methods: macrorheology applies some ambient, homogeneous shear to the suspension (quadrupolar forcing), whereas microrheological deformations are dipolar and inhomogeneous because they arise from a point force on the probe. Though the two methods measure distinct viscoelastic properties that may not necessarily agree with one another [14], agreement between the Einstein viscosity correction and microviscosity has been found in the limit of a large probe particle moving in a suspension of point bath particles, as would be expected [15]. But qualitatively, macrorheology and microrheology show the same behavior more broadly.

Macroscopic measurements of the shear-viscosity of active suspensions have shown the potential for highly active suspensions of tail-actuated swimmers under weak

shear to reach a superfluid-like state, in which the total shear stress measured by bulk rheometry is zero—or even negative [16]! Most theoretical models of this behavior are constructed for suspensions of anisotropic particles, wherein the hydrodynamic stress of a pusher or puller will either decrease or increase the apparent viscosity, respectively [17]. These effects are hydrodynamic in origin, and reflect the interaction of the swimmer with the fluid under shear, not the interaction between swimmers in suspension. Additionally, they do not account for the swim stress generated by the particle's self-propulsion that is distinct from the hydrodynamic stress generated by pushing or pulling [8]. Takatori and Brady [18] showed that this negative shear viscosity may be explained from a deviatoric swim stress that arises from diffusive stretching of the swimmer's active random walk by the bulk flow.

Reductions in the zero-shear viscosity of active suspensions thus give rise to non-Newtonian suspension rheology, even at the single-particle level. The shear viscosity of the suspension depends on the ratio of the shear-rate $\dot{\gamma}$ to the rotary diffusion rate τ_R^{-1} of the swimmers $Pe = \dot{\gamma}\tau_R$. When $Pe \ll 1$ swimming is dominant and the active particles may greatly reduce the zero-shear Newtonian plateau [16–18]. When $Pe \gg 1$, the fluid flow is able to overwhelm the active random motion of the swimmers and align them with the rate of strain field—this gives Einstein's (or Hinch's, depending on the particle shape) familiar correction to the shear viscosity for a single particle [19, 20]. Takatori and Brady's model shows that this transition is non-monotonic in Pe—thus the suspension goes from being Newtonian in the absence of activity (at the single-particle level) to non-monotonically shear thickening [18]. In passive colloidal suspensions, shear-thickening can only arise at the pair-level, and is usually attributed to lubrication interactions or frictional contact forces between particles [21, 22]. As we observed a reduction in the microviscosity (compared to an equivalent suspension of passive particles) in Chapter 3, we expect that it may be possible to find (non-monotonic) force-thickening of the suspension on the micro-scale as well—without any hydrodynamic effects!

The fundamental physical problem in microrheology is to compute (1) the average velocity of a particle as it is dragged through a suspension by an external force $\boldsymbol{F}^{ext}$, or (2) the average force required to make a particle translate through the suspension with velocity $\boldsymbol{U}^{probe}$. The former mode is referred to as fixed-force microrheology and the latter is the fixed-velocity mode; in an experimental system the true mode of probing may lie somewhere in between (say, if the probe is being moved by an optical trap of finite potential depth). The differences are discussed in depth in previous

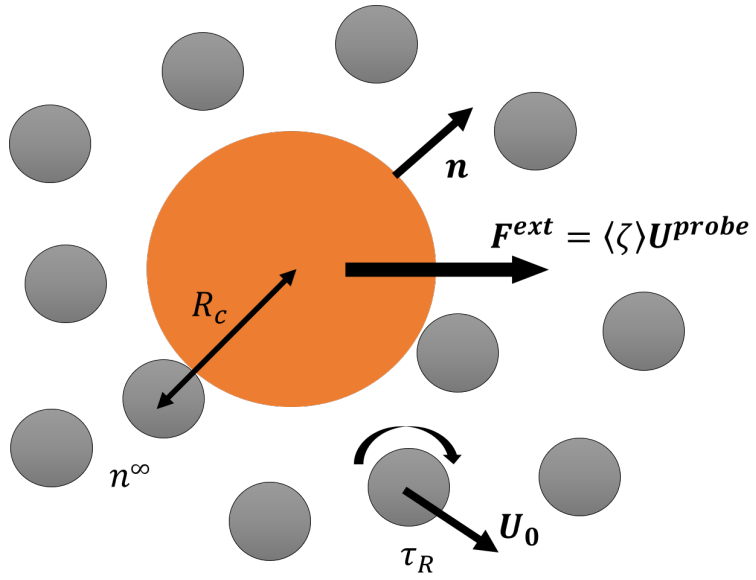

Figure 5.1: Schematic of the model system: a Brownian probe particle of size R immersed in a suspension of active Brownian particles (ABPs) with size a at number density n^∞—the center-to-center separation distance upon a collision is denoted by $R_c = R + a$. The ABPs swim in a direction $\boldsymbol{q}$ at speed U_0; $\boldsymbol{q}$ changes randomly on a time scale characterized by τ_R. The probe translates under the action of some external force $\boldsymbol{F}^{ext} = \langle\zeta\rangle\boldsymbol{U}^{probe}$, which may be constant or specified such that the resulting probe velocity $\boldsymbol{U}^{probe}$ is constant. The force and velocity are related by the effective drag coefficient $\langle\zeta\rangle$.

works on microrheology in passive systems, but in the absence of hydrodynamic interactions, the two modes differ only by a geometric factor [23, 24].

Consider a Brownian probe particle of size R moving through a dilute suspension comprised of a Newtonian solvent with viscosity η_s and bath particles of size a at some number density n^∞, as depicted in Fig. 5.1. The average velocity of the probe as it moves through the suspension is

$$\langle \boldsymbol{U}^{probe} \rangle = \boldsymbol{U}^{Stokes} - \frac{1}{\zeta_P} k_B T \int \boldsymbol{n} P_N dS, \tag{5.1}$$

in the absence of any hydrodynamic interactions or interparticle forces [14, 23, 25]. The probe's Stokes drag coefficient is $\zeta_P = 6\pi\eta_s R$, its velocity in a Newtonian solvent is $\boldsymbol{U}^{Stokes}$ and its outward-pointing unit normal is $\boldsymbol{n}$. P_N is the joint N-particle probability distribution for the bath particles surrounding the probe. In the linear-response regime the velocity reduction due to collisions with the bath particles is linear in the applied external force: $\langle \boldsymbol{U}^{probe} \rangle - \boldsymbol{U}^{Stokes} \sim -\boldsymbol{F}^{ext}\langle\mu\rangle$, where $\langle\mu\rangle$ is the probe mobiliy. For the fixed-velocity mode $\langle \boldsymbol{F}^{ext} \rangle - \boldsymbol{F}^{Stokes} \sim \langle\zeta\rangle \boldsymbol{U}^{probe}$, where $\boldsymbol{F}^{Stokes} = \zeta_P \boldsymbol{U}^{Stokes}$; we define an effective drag coefficient $\langle\zeta\rangle = 6\pi\langle\eta\rangle R$, where $\langle\eta\rangle$ is the microviscosity of the suspension [23]. In the absence of hydro-

dynamic interactions, $\langle\mu\rangle = 1/\langle\zeta\rangle$, but this is not true in general. The effects of interparticle interactions (and thus, activity) are characterized by the intrinsic microviscosity $\eta^{micro} = (\langle\zeta\rangle - \zeta_P)/\zeta_P\phi^{ex}$, where $\phi^{ex} = 2\pi a(R+a)^2 n^\infty/3$ is the excluded volume fraction. (The excluded area fraction is $\phi_A^{ex} = 2\pi a(R+a)n_A^\infty$ and n_A^∞ is the areal number density of swimmers.) Even though this linear force-velocity relation is only guaranteed near equilibrium, we use the same definition for the nonlinear response [23]. Thus the effective drag $\langle\zeta\rangle$ (and mobility $\langle\mu\rangle$) and intrinsic microviscosity η^{micro} may now be functions of the external force or probe velocity: $\langle \boldsymbol{U}^{\boldsymbol{probe}}\rangle - \boldsymbol{U}^{\boldsymbol{Stokes}} \sim -\boldsymbol{F}^{\boldsymbol{ext}}\langle\mu(F^{ext})\rangle$.

In the next section we write down a Smoluchowski equation that describes the dynamics of a passive Brownian probe particle moving through a suspension of active Brownian particles (ABPs). We then discuss the microstructure and nonlinear microrheological behavior of these model suspensions: they may be (non-monotonically) force-thinning or (non-monotonically) force-thickening depending on the ratio of the probe speed to the swim speed, even in the absence of hydrodynamic effects. We conclude with a discussion of future work in the microrheology of active suspensions.

5.1 Theoretical framework

We consider a dispersion of $N-1$ swimmers and one passive probe particle of size R with thermal Stokes-Einstein-Sutherland (SES) diffusivity D_P in a Newtonian solvent with viscosity η_s. The swimmers are modeled as active Brownian particles (ABPs) with size a, (constant) swim speed U_0, thermal SES diffusivity D_T, and a characteristic reorientation time τ_R. The probe moves at speed U^{probe} due to an applied external force F^{ext}; either the force or probe speed may be fixed. We will neglect hydrodynamic interactions (HI) in this chapter. The dynamics of this suspension are described by a Smoluchowski equation in position and orientation space:

$$\frac{\partial P_N}{\partial t} + \sum_{i=1}^{N} \nabla_{\boldsymbol{x}_i} \cdot \boldsymbol{j}_i^T + \sum_{i=1}^{N} \nabla_{R_i} \cdot \boldsymbol{j}_i^R = 0, \tag{5.2}$$

which is simply a conservation statement for $P_N(\{\boldsymbol{x}_i\}, \{\boldsymbol{q}_i\}; t)$, the time-dependent N-particle probability distribution of the suspension that depends on the positions ($\boldsymbol{x}_i$) and orientations ($\boldsymbol{q}_i$) of each particle. The rotational operator ∇_{R_i} is given by $\boldsymbol{q}_i \times \nabla_{\boldsymbol{q}_i}$ for an axisymmetric particle.

When the suspension is sufficiently dilute ($\phi = 4\pi n^\infty a^3/3 \ll 1$ in three dimensions

or $\phi_A = 4\pi a^2 n_A^\infty \ll 1$ in two-dimensions, where n^∞ is the constant volumetric number density of swimmers and n_A^∞ is a constant areal number density of swimmers for $d = 2$) only the pair-wise interactions between the probe and a single swimmer matter. Thus, one can write a Smoluchowski equation for the pair-level probability distribution, $P_2(\boldsymbol{x}_P, \boldsymbol{x}_s, \boldsymbol{q}_P, \boldsymbol{q}_s; t)$, where the position and orientation of both the probe $(\boldsymbol{x}_P, \boldsymbol{q}_P)$ and swimmer $(\boldsymbol{x}_s, \boldsymbol{q}_s)$ are in the laboratory frame. It can be shown that long-wavelength fluctuations in the probe's position do not affect its average speed to leading order, [26, 27] thus we can average over the phase space of the probe and write the Smoluchoski equation in a relative coordinate frame

$$\frac{\partial P_{1/1}(\boldsymbol{r}, \boldsymbol{q}; t)}{\partial t} + \nabla_r \cdot (\boldsymbol{j}_{\boldsymbol{s}}^{\boldsymbol{T}} - \boldsymbol{j}_{\boldsymbol{P}}^{\boldsymbol{T}}) + \nabla_{q_s} \cdot \boldsymbol{j}_s^R = 0, \tag{5.3}$$

where $P_2(\boldsymbol{x}_P, \boldsymbol{x}_s, \boldsymbol{q}_P, \boldsymbol{q}_s; t) = P_{1/1}(\boldsymbol{r}, \boldsymbol{q}; t) P_1(\boldsymbol{z}, \boldsymbol{q}_P; t)$ and we have defined $\boldsymbol{z} = \boldsymbol{x}_P$, $\boldsymbol{r} = \boldsymbol{x}_{\boldsymbol{s}} - \boldsymbol{x}_{\boldsymbol{P}}$, and $\boldsymbol{q} = \boldsymbol{q}_s$. $\boldsymbol{j}_{\boldsymbol{s}}^{\boldsymbol{P}}$ is the translational flux of the probe, and $\boldsymbol{j}_{\boldsymbol{s}}^{\boldsymbol{T}}$ and $\boldsymbol{j}_{\boldsymbol{s}}^{\boldsymbol{R}}$ are the translational and rotational fluxes of the swimmer, respectively. The probability distribution for the probe particle P_1 is not explicitly needed to compute the average probe velocity or diffusivity (see Chapter 3). The translational and rotational flux of the swimmer relative to the probe are:

$$\boldsymbol{j}^{\boldsymbol{T}} \equiv \boldsymbol{j}_{\boldsymbol{s}}^{\boldsymbol{T}} - \boldsymbol{j}_{\boldsymbol{P}}^{\boldsymbol{T}} = (U_0 \boldsymbol{q} - \boldsymbol{U}^{\boldsymbol{probe}}) P_{1/1} - D^{rel} \nabla_r P_{1/1}, \tag{5.4}$$

$$\boldsymbol{j}_s^R = -\frac{1}{\tau_R} \nabla_{\boldsymbol{q}} P_{1/1}, \tag{5.5}$$

where $D^{rel} = D_P + D_T$ for a fixed external force and $D^{rel} = D_T$ when the velocity of the probe is fixed. The probe and swimmer interact via excluded volume interactions and thus the particles may not pass through one another upon a collision: $\boldsymbol{n} \cdot \boldsymbol{j}^{\boldsymbol{T}} = 0$, at $|\boldsymbol{r}| = R_c \equiv R + a$, where $\boldsymbol{n}$ is the outward pointing unit normal of the probe.

We solve the Smoluchowski equation using the familiar method popularized by Saintillan and Shelley [28] and expand the pair-distribution function in terms of orthogonal tensor harmonics in $\boldsymbol{q}$:

$$\begin{aligned} P_{1/1}(\boldsymbol{r}, \boldsymbol{q}; t) = n(\boldsymbol{r}; t) + \boldsymbol{q} \cdot \boldsymbol{m}(\boldsymbol{r}; t) + (\boldsymbol{qq} - \boldsymbol{I}/d) : \boldsymbol{Q}(\boldsymbol{r}; t) \\ + (\boldsymbol{qqq} - \boldsymbol{\alpha} \cdot \boldsymbol{q}/(d+2)) \odot \boldsymbol{B} + ..., \end{aligned} \tag{5.6}$$

where d is the spatial dimension ($d = 2, 3$ in this chapter) and $\boldsymbol{\alpha}$ is the fourth-order isotropic tensor. The zeroth moment, n is the concentration field, $\boldsymbol{m}$ is the polar order, $\boldsymbol{Q}$ is the nematic order, and so on [28, 29]. In light of the results in Chapter 4 pertaining to the appropriate closure of these equations for the linear-response microrheology problem, we make the closure $\boldsymbol{B} = 0$, or $\langle \boldsymbol{qqq} \rangle = \boldsymbol{\alpha} \cdot \langle \boldsymbol{q} \rangle / (d+2)$.

Applying the moments-averaging procedure to the governing equation and boundary conditions for $P_{1/1}$ yields a system of coupled PDEs governing the steady microstructure:

$$\nabla_r \cdot [U_0 \boldsymbol{m} - D^{rel} \nabla n - \boldsymbol{U^{probe}} n] = 0 \tag{5.7}$$

$$\nabla_r \cdot [U_0(\boldsymbol{I} n/d + \boldsymbol{Q}) - D^{rel} \nabla \boldsymbol{m} - \boldsymbol{U^{probe}} \boldsymbol{m}] + (d-1) D_R \boldsymbol{m} = 0, \tag{5.8}$$

$$\nabla_r \cdot [U_0(\boldsymbol{\alpha} \cdot \boldsymbol{m}/(d+2) - \boldsymbol{I}\boldsymbol{m}/d) - D^{rel} \nabla \boldsymbol{Q} - \boldsymbol{U^{probe}} \boldsymbol{Q}] + 2d D_R \boldsymbol{Q} = 0. \tag{5.9}$$

At the probe surface there can be no translational flux, and far from the probe the suspension can exhibit no order:

$$\boldsymbol{n} \cdot \langle \boldsymbol{j}^{\boldsymbol{T}} \rangle_{\boldsymbol{q}} = \boldsymbol{n} \cdot \langle \boldsymbol{q}\boldsymbol{j}^{\boldsymbol{T}} \rangle_{\boldsymbol{q}} = \boldsymbol{n} \cdot \langle (\boldsymbol{q}\boldsymbol{q} - \boldsymbol{I}/d)\boldsymbol{j}^{\boldsymbol{T}} \rangle_{\boldsymbol{q}} = 0, \; r = R_c \tag{5.10}$$

$$n \sim n^{\infty}, \boldsymbol{m} \sim \boldsymbol{0}, \boldsymbol{Q} \sim \boldsymbol{0}, \; r \to \infty. \tag{5.11}$$

The solution to these equations must be obtained numerically, which we do using a second-order finite difference scheme [14]. When non-dimensionalized on the contact length R_c, the governing equations reveal three dimensionless groups: (1) an external Péclet number $Pe = U^{probe} R_c / D^{rel} = F^{ext}/(k_B T/a)$, (2) a swim Péclet number $Pe_s = U_0 R_c / D^{rel}$, and (3) a rotational parameter $\gamma^2 = (d-1) R_c^2 / D^{rel} \tau_R$ that compares reorientation to translational diffusion. These groups reflect the four different length scales in the problem: the contact length R_c, the run length of the swimmers $\ell = U_0 \tau_R$, the microscopic length $\delta = \sqrt{D^{rel} \tau_R}$ (the distance the particles diffuse in a time τ_R) and the advective length $L^{adv} = U^{probe} \tau_R$.

5.2 Nonlinear microrheology

In the absence of activity, colloidal suspensions are known to force-thin from the low Pe Newtonian plateau of $\eta^{micro} = 1$ to a high Pe plateau of $1/2$ (in the absence of HI). Force-thinning is the microrheological analog of shear-thinning. The probe is moving quickly through the suspension and accumulates $\sim O(Pe)$ particles in an $O(Pe^{-1})$ thin boundary-layer on its front side, but a long-ranged wake is left behind the probe where the number density is zero. The net effect is to have a finite microviscosity that is half the value found when $Pe \to 0$ [23]; this is independent of the dimensionality of the problem ($d = 2, 3$). The microviscosity is a monotonically decreasing function of Pe and the onset of force-thinning goes as Pe^2 [23]. In the viscosity-force plots in this chapter, this passive result is given by a dotted gray line for comparison.

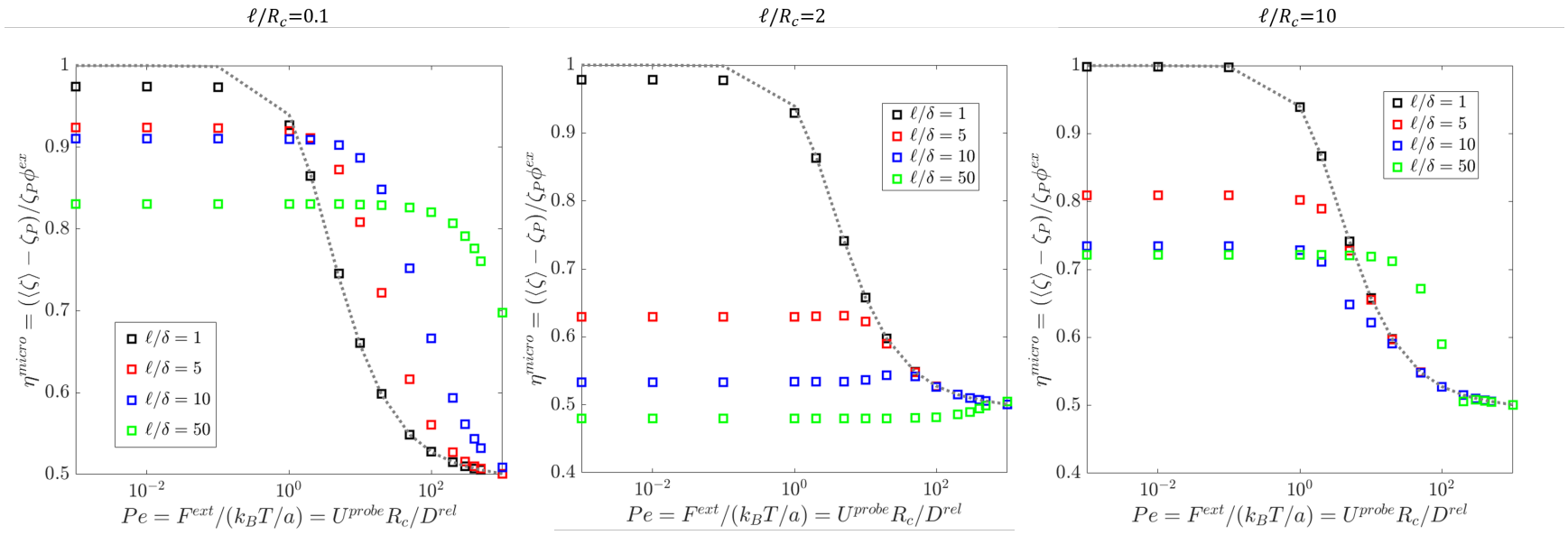

Figure 5.2: Nonlinear intrinsic microviscosity ($d = 3$) η^{micro} plotted as a function of $Pe = U^{probe}R_c/D^{rel}$ for various ℓ/R_c. The probe's speed is U^{probe}, D^{rel} is the relative thermal, $R_c = R + a$, where R is the probe size, a is the swimmer size, U_0 is the speed of the swimmers, and τ_R is their reorientation time. Different colors indicate different strengths of swimming: $\ell/\delta = \sqrt{U_0^2\tau_R/D^{rel}}$.

In Chapter 3, we concluded that activity lowers the intrinsic microviscosity, and indeed η^{micro} asymptotes to a value slightly less than $1/2$ as $\ell/\delta \to \infty$ for $\ell/R_c \sim O(1)$ in the linear response regime. This low-shear plateau is always lower than that found in a passive suspension, and indeed might even be lower than the large Pe plateau found in passive suspensions. When $Pe \to \infty$, we expect that we must recover the passive suspension result because the swimming is obscured by advection, indicating there must be a region where a highly active suspension is force-thickening even in the absence of any interparticle hydrodynamic interactions (HI), contact frictional forces, or fluid disturbances arising from self-propulsion. This purely active, mechanical effect arising from steric interactions between the swimmers and probe can be seen in the middle panel of Fig. 5.2 for $\ell/\delta = 50$ and $\ell/R_c = 2$. The suspension is "Newtownian" for a wide range of Pe and then thickens to meet the passive viscous response, thinning again as $Pe \to \infty$. In the same panel, we also see non-monotonic force-thinning of the suspension for slightly lower activity levels $\ell/\delta = 10$; the trend is the same as the green curve ($\ell/\delta = 50$), but the low-Pe plateau is higher than the $Pe \to \infty$ plateau. Indeed another possibility one could imagine is that the microviscosity could be completely independent of Pe at particular activity levels (e.g. $\ell/\delta \sim 20$, $\ell/R_c = 2$). Previous experiments that measure the shear viscosity of a bacterial suspension using a rotating colloidal probe have found the same result [30]. This rich rheological behavior could be exploited in material design—for example adding particles with a certain activity level to slightly increase the viscosity of a fluid while keeping it Newtonian.

These are special cases of the more general trend depicted in Fig. 5.2 that the activity of the suspensions widens the weak-force Newtonian plateau. In Fig. 5.3, we plot the microviscosity as a function of Pe at fixed Pe_s—increasing Pe is equivalent to increasing U^{probe} while U_0 remains fixed. We see that the width of the weak-force plateau is an increasing function of ℓ/R_c at fixed Pe_s; there is also this plateau widening as ℓ/δ increases at fixed ℓ/R_c in Fig. 5.2. The weak-force plateau is notoriously difficult to measure by either experiment or simulation; the widening of the plateau would allow one to make a linear response measurement at much higher probe speeds, where the average velocity (or force) is more readily distinguishable from Brownian fluctuations.

The widening of the low-force plateau leads to an interesting behavior in the continuum limit $\ell/R_c \ll 1$: the suspension force-thins, but the viscosity is higher in the active suspension than the passive suspension in the force-thinning regime (see

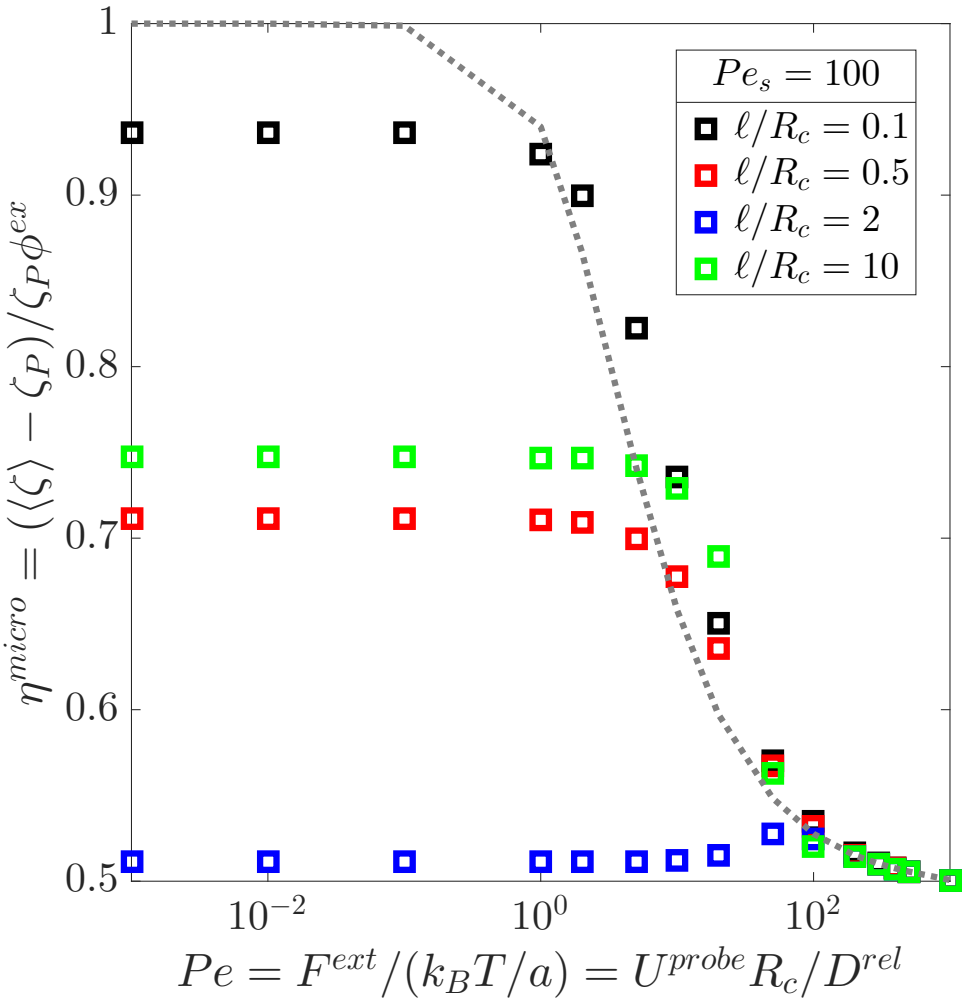

Figure 5.3: Nonlinear apparent microviscosity ($d = 3$) η^{micro}, scaled by its passive value plotted as a function of $Pe = U^{probe}R_c/D^{rel}$ for $Pe_s = U_0R_c/D^{rel} = 100$. The swimmers' speed is U_0, D^{rel} is the relative thermal diffusivity of the probe-swimmer pair, and the center-to-center separation of a probe-swimmer pair at contact is R_c. Different colors indicate different values of ℓ/R_c.

Fig. 5.2, left). Indeed one would expect this due to the widening of the plateau at large Pe_s. An additional feature to this trend is evidenced in the right-hand panel of Fig. 5.2: the width of the plateau increases with $\gamma^2/Pe^2 = (\delta/L^{adv})^2$ in addition to $Pe_s/Pe = \ell/L^{adv}$. When either of these ratios is large or $O(1)$, it means that the distance the particle pair diffuses or a bath particle swims in a time τ_R is comparable to the distance the probe is moved in the same time—thus activity and/or diffusion are able to fill in the wake left by the probe and maintain the low force plateau, as indicated by the microstructures discussed in the next section.

5.3 Suspension microstructure

In Fig. 5.4 we show the microstructural underpinnings of these phenomena at a fixed activity level $D^{swim}/D^{rel} \sim k_s T_s / k_B T \sim 100$; this corresponds to the $\ell/\delta = 10$ (blue) lines in Fig. 5.2. When the advective disturbance is weak ($Pe \ll 1$), we see a nearly uniform concentration of swimmers around the probe, reflecting a balance between activity and thermal diffusion. As Pe_s increases, we see that the number density at the probe surface increases and the active-diffusive boundary layer gets thinner. This uniform concentration increase is not responsible for the change in the microviscosity: there is a dipolar concentration disturbance of $O(Pe)$ that determines the drag on the probe. Activity reduces the probe drag over that one would find in a passive suspension (as evidenced by the viscosity surface). When the run length of the swimmers is comparable to the probe size, a swimmer colliding with the probe will slide along the surface and then have the opportunity to reorient and push the probe along or further hinder its motion. The weak advective disturbance results in more swimmers pushing the probe and thus the microviscosity is less than that found in a passive suspension.

When Pe is increased to 5 the $O(Pe)$ disturbance to the microstructure becomes more visible—particularly at lower values of Pe_s. Note that there is still a net accumulation of swimmers in front of and behind the probe, but advection starts to distort this structure more. When $Pe_s = 1000$, this distortion is almost imperceptible because the bath particles can still swim fast enough to keep up with the probe—thus force-thinning is barely observable at large Pe_s, as discussed in the previous section.

At $Pe = 100$ there is a well developed wake behind the probe $n = 0$ and an $O(Pe)$ accumulation of bath particles on the front face of the probe. The viscosity plots belie a simpler structure than those observed—the viscosity at $Pe_s = 50$ is nearly indistinguishable from the high-shear viscosity plateau, but we clearly observe a triangular wake behind the probe, as opposed to the more parabolic wake observed at larger Pe, and in passive suspensions [23, 26]. The formation of this triangular wake appears to occur at $Pe_s \sim Pe$ (see panel (e)), where advection and swimming are similar in magnitude, and the shape indicates that the swimmers are trying to fill in the advective void left behind the probe. Adjacent to this wake we also see symmetric "shocks" of concentration where the advective-diffusive boundary-layer separates from the probe and the swimmers are actually moving away from the wake. We see similar structures at $Pe_s = 1000$ and $Pe \sim O(100)$, though the contrast between these shocks and the wake is not quite as abrupt. Interestingly, one can

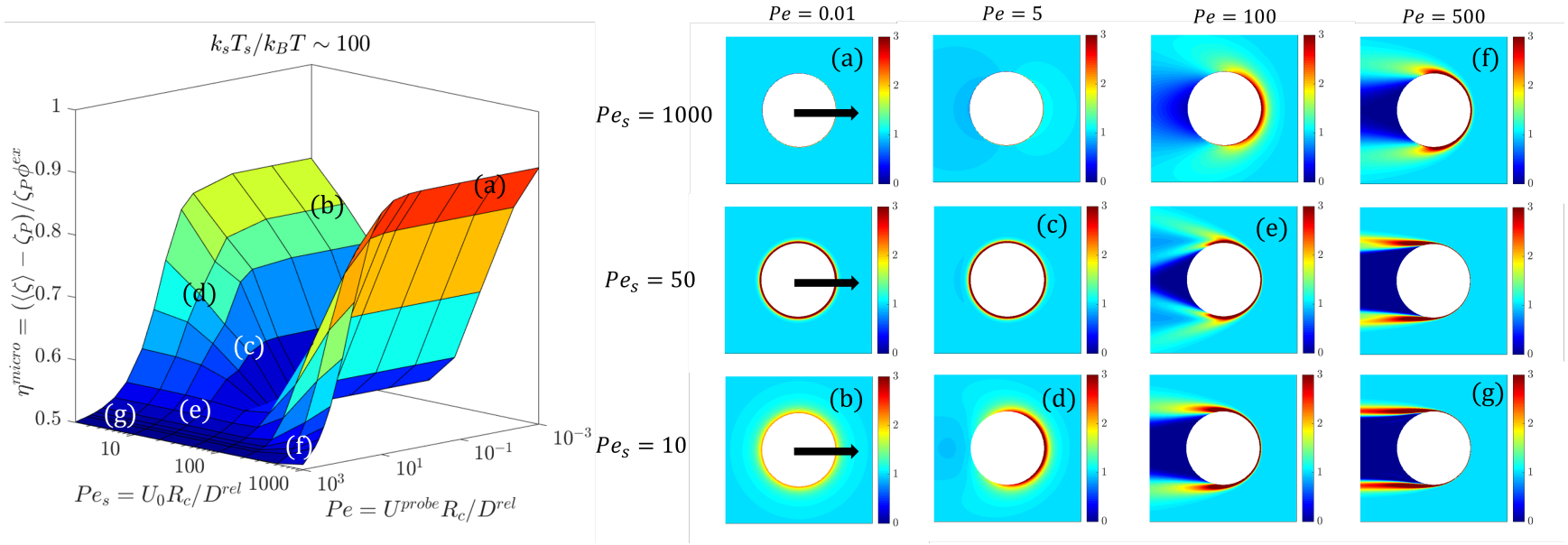

Figure 5.4: RIGHT: Microviscosity as a function of th external Péclet number $Pe = F^{ext}/(k_B T/a)$, where F^{ext} is the external force moving the probe (indicated by the black arrow) and a is the size of the bath particles, and the swim Péclet number $Pe_s = U_0 R_c/D^{rel}$ where U_0 is the swim speed, R_c is the center-to-center separation distance of a swimmer and the probe upon contact, and D^{rel} is the relative translational diffusivity of the pair. The activity level is fixed at $\ell/\delta = 10$ ($k_s T_s/k_B T \sim 100$). LEFT: Contour plots of the 3-D (axisymmetric) microstructure for various degrees external forcing Pe and activity levels Pe_s. The background light blue color indicates a uniform microstructure: $n = n^{\infty}, \boldsymbol{m} = 0$. Red (warm) colors indicate an accumulation of particles, and darker blues (cold colors) indicate a depletion.

see that the viscous response where these structures are found is indistinguishable from the response of a passive suspension. This is because the number density at the surface has not changed from what one would find in the absence of swimming, only the wake structure.

Fig. 5.5 focuses on the structures and viscosity when advection is strong ($Pe = 100$) and swimming is within an order of magnitude of the advective response. When $\ell/R_c = 0.1$, the structure is nearly indistinguishable from a passive suspension. This is not because swimming is weak ($U_0 \sim U^{probe}$), rather it is because the swimmers reorient so quickly that they are not able to fill the $O(R_c)$ size wake left by the advection of the probe—they can only move a distance $\ell \ll R_c$ before changing their direction. This is reflected in the viscous behavior—the right-hand side of Fig. 5.5 is invariant with U_0/U^{probe} and small ℓ/R_c.

This figure also reinforces the observation that U_0/U^{probe} is important to the rheological behavior of active suspensions, but that it is not a complete description of activity. Increasing ℓ/R_c in Fig. 5.5 shows a range of rich behaviors underpinning viscous response. When $U^{probe} = U_0$, one can actually see the swim-diffusive boundary layer detach from the rear of the probe as ℓ/R_c increases in (h). These are plots of the stationary probability distribution, so this detached layer persists and "hovers" behind the probe. This reflects a splitting of the advective-diffusive wake due to the swimmers' desire to be at the probe's surface, but advection starting to overwhelm them. This structure pinpoints the spot on the corresponding curve in Fig. 5.3 where force-thinning begins.

Fig. 5.5 also reveals that the triangular wake and "shocks" of concentration arise only when the probe velocity slightly exceeds the bare swim speed—the swimmers are not quite able to keep up with the probe, but they still distort the shape of its wake by trying to swim into the depleted areas. In the last column of Fig. 5.4 and 5.5 the swimmers can no longer keep up with the probe, and we see the characteristic $O(Pe)$ long wake behind the probe, with the accumulation boundary-layer separating from the probe at the poles $\hat{\boldsymbol{u}} \cdot \boldsymbol{n} = 0$. This shape is constant across the activity levels we depict in Figs. 5.4 and 5.5; however the accumulation boundary-layer "tails" are shorter when Pe_s is larger (or equivalently, ℓ/R_c is smaller)—c.f. (f) and (g) in Fig. 5.4. This is simply another physical manifestation of the activity trying to compensate for the advective disturbance—the swimmers want to swim with the probe so the advective wake is simply not as long. As before, the change in the long-ranged wake structure does not affect the number density at the surface, thus

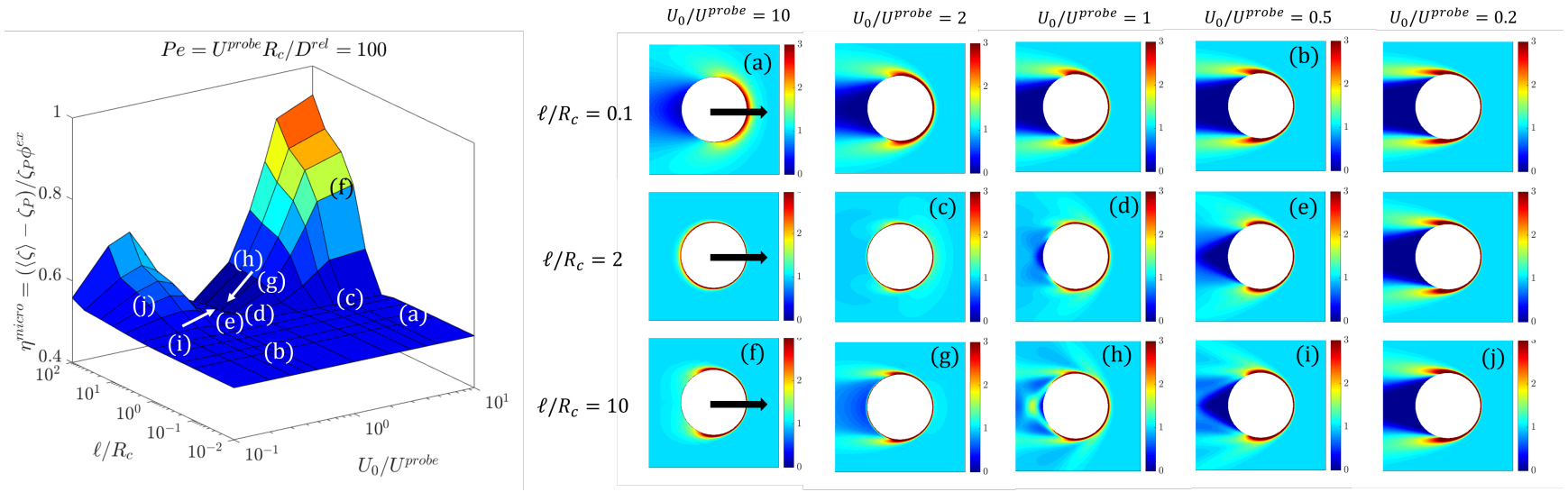

Figure 5.5: RIGHT: Microviscosity at $Pe = 100$ as a function of ℓ/R_c and U_0/U^{probe} where U_0 is the swim speed of the bath particles and U^{probe} is the speed of the probe. LEFT: Contour plots of the 3-D (axisymmetric) microstructure at $Pe = 100$ for various ratios of U_0/U^{probe}. The rows vary the value of ℓ/R_c as in Fig. 5.2. The background light blue color indicates a uniform microstructure: $n = n^{\infty}, \boldsymbol{m} = 0$. Red (warm) colors indicate an accumulation of particles, and darker blues (cold colors) indicate a depletion.

the microviscosity is the same as one would find in passive suspensions here.

5.4 Conclusions

Using familiar frameworks from the study of passive colloidal suspensions, we investigated the nonlinear microrheology of a suspension of ABPs. We find that the suspension, in the absence of hydrodynamic interactions, swim-thins regardless of the hydrodynamic propulsion mechanism of the swimmer when $Pe \ll 1$. We found that this low-Pe Newtonian plateau persists for a wide range of Péclet numbers, and that the width of the Newtonian plateau is set by the swimmers' activity. The persistence of this plateau reflects the fact that the swimmers are able to fill in the void created by the probe's advective motion when $U_0 > U^{probe}$ and $\ell \gtrsim R_c$. If the run length is short compared to the size of the probe's wake, the swimmers will reorient before they are able to reach the probe even when $U_0 \gtrsim U^{probe}$; in this limit the wake (and viscous response) resembles that of a passive suspension. When $U_0 \ll U^{probe}$, the effects of activity vanish and we recover the familiar high Pe plateau from previous work on passive suspensions [23]. Most of these effects are predictive; there are no experimental studies to-date that measure the microviscosity of an active suspension, though there is a computational study examining various phase behaviors in the microrheology problem [31]. Reichhardt & Reichhardt compute the mobility of a probe in an active bath (neglecting hydrodynamic interactions and Brownian motion), and find *reduced* probe mobility, even at low volume fractions. This is consistent with our findings that the intrinsic microviscosity is positive in the absence of HI.

Hydrodynamic interactions in passive suspensions have been shown to cause quantitative changes in the non-equilibrium mechanical properties of a suspension, and more importantly produce qualitatively different behaviors. The most notable example of this is that near-field hydrodynamic interactions lead to force-thickening of the suspension at high shear rates [14, 21]. In active suspensions, hydrodynamic interactions have been shown to alter the particle-phase pressure [32] and shear viscosity [16, 18, 30, 33], but these effects do not alter the problem's boundary-layer structure [32]. The same balances between advection, diffusion, and activity seen here are expected to hold, but the parameters D^{rel}, τ_R, and F^{ext} or U^{probe} will now depend on the strength of hydrodynamic interactions through familiar mobility formalisms in low Reynolds number fluid-mechanics [34]. Incorporation of the hydrodynamics does not require us to say anything about the propulsive mechanism of the bath particles, though the framework presented in previous works is readily

modified to include specifications of the swimmers' gait. We will discuss the role of HI in more detail in the remainder of this thesis.

Appendix

A: Boundary-layer analysis, $Pe \gg 1$

When advection is strong $Pe \gg 1$, there will be a thin boundary-layer $O(Pe^{-1})$ at the surface of the probe when diffusion balances advection. For simplicity, we assume that, outside the advective-diffusive boundary-layer, the microstructure is uniform $n = 1$ and $\boldsymbol{m} = 0$; the effects of activity are contained within the advective-diffusive layer. We choose a boundary-layer coordinate Y, such that $Y = Pe(r-1)$, thus amplifying all of the gradients in the governing equations by Pe. We then expand the concentration and polar order in powers of Pe^{-1}: $n = Pen_0 + n_1 + O(Pe^{-1}), \boldsymbol{m} = Pe\boldsymbol{m_0} + \boldsymbol{m_1} + O(Pe^{-1})$. Due to the advective build-up of bath particles near the surface, the leading order terms must scale with the Péclet number.

In the boundary-layer, the governing equations reduce to

$$\frac{\partial n_0}{\partial Y} + \mu n_0 = \frac{Pe_s}{Pe} m_{r,0}, \tag{5.12}$$

$$\frac{\partial^2 m_{r,0}}{\partial Y^2} + \mu \frac{\partial m_{r,0}}{\partial Y} - \frac{\gamma^2}{Pe^2} m_{r,0} = \frac{1}{3}\frac{Pe_s}{Pe}\frac{\partial n_0}{\partial Y} \tag{5.13}$$

$$\frac{\partial m_{r,0}}{\partial Y} + \mu m_{r,0} = \frac{1}{3}\frac{Pe_s}{Pe} n_0, Y = 0 \tag{5.14}$$

$$m_{r,0} \sim 0, Y \to \infty, \tag{5.15}$$

$$\frac{\partial^2 m_{\mu,0}}{\partial Y^2} + \mu \frac{\partial m_{\mu,0}}{\partial Y} - \frac{\gamma^2}{Pe^2} m_{\mu,0} = 0 \tag{5.16}$$

$$\frac{\partial m_{\mu,0}}{\partial Y} + \mu m_{\mu,0} = 0, Y = 0 \tag{5.17}$$

$$m_{mu,0} \sim 0, Y \to \infty, \tag{5.18}$$

where $\mu \equiv \hat{\boldsymbol{u}} \cdot \boldsymbol{n}$ and m_r and m_μ are the radial and angular components of the polar order. Because $m_{\mu,0}$ is de-coupled from n_0 and $m_{r,0}$, we may assume that it is unimportant at $O(Pe)$ and derive a third-order equation for n_0 by substituting

Eqn. 5.12 into Eqn. 5.13:

$$\begin{aligned} \frac{\partial^3 n_0}{\partial Y^3} + 2\mu\frac{\partial^2 n_0}{\partial Y^2} + \mu^2\frac{\partial n_0}{\partial Y} - \frac{\lambda^2}{Pe^2}\frac{\partial n_0}{\partial Y} - \frac{\gamma^2}{Pe^2}\mu n_0 = 0 \\ \frac{\partial^2 n_0}{\partial Y^2} + 2\mu\frac{\partial n_0}{\partial Y} + \mu^2 n_0 = \frac{1}{3}\left(\frac{Pe_s}{Pe}\right)^2 n_0, Y = 0 \\ n_0 \sim 0, \qquad \frac{\partial n_0}{\partial Y} + \mu n_0 \sim 0, Y \to \infty, \end{aligned} \tag{5.19}$$

which has exponential solutions $f(\mu, \lambda, \gamma, Pe)e^{g(\mu,\lambda,\gamma,Pe)Y}$. The function g is given by solutions to the characteristic equation

$$g(g+\mu)^2 = \frac{\gamma^2 + g\lambda^2}{Pe^2}. \tag{5.20}$$

This equation will have three roots, one of which leads to an unphysical exponential growth. The other two roots are exponentially screened, oscillating functions of $\lambda/Pe, \gamma/Pe$, and μ.

We neglect terms of $O(\gamma/Pe)$ to reduce the order of the characteristic equation (using the no-flux boundary condition). In doing this we assume that $L^{adv} = U^{probe}\tau_R \gg \delta$: the distance moved by the probe in τ_R is much greater than distance the pair moves by Brownian motion in the same time. This could also be realized with smooth swimmers that do not reorient $\tau_R \to \infty$. This assumption is reasonable for a fast-moving probe that is similar in size to or much larger than the swimmers. Indeed the numerical analysis seems to indicate that γ does not substantially affect the force-dependent behavior of the suspension.

We can solve the reduced characteristic equation for n_0:

$$n_0 = A(\mu)e^{-Y(\mu+\lambda/Pe))} + B(\mu)e^{-Y(\mu-\lambda/Pe))}, \tag{5.21}$$

where $\lambda/Pe = Pe_s/\sqrt{3}Pe$ as $\gamma/Pe \to 0$. This gives the correct result in the limit $\lambda/Pe \to 0$ and decays as $e^{-\lambda(r-1)}$ when activity dominates advection.

To find the functions $A(\mu)$ and $B(\mu)$, one must go to the next order in Pe^{-1}. When one does this, we find:

$$n_0 \sim 1 + \frac{1}{2}(Pe\mu + \lambda)e^{-(r-1)(Pe\mu+\lambda)}, \tag{5.22}$$

when $\lambda/Pe > |\mu|$. When $\lambda/Pe < |\mu|$, the concentration of bath particles behind the probe ($\mu < 0$) is zero, and in front of the probe ($\mu > 0$), we find that the accumulation of particles is:

$$n_0 = 1 + \frac{1}{4}(Pe\mu + \lambda)e^{-(r-1)(Pe\mu+\lambda)} + \frac{1}{4}(Pe\mu - \lambda)e^{-(r-1)(Pe\mu-\lambda)}. \tag{5.23}$$

This microviscosity is thus:

$$\eta^{micro} = \frac{1}{2}\left[1 + \left(\frac{\lambda}{Pe}\right)^3\right], \lambda < Pe \tag{5.24}$$

$$\eta^{micro} = 1, \lambda > Pe. \tag{5.25}$$

The first result indicates that the suspension must force-thin when $Pe \gg 1$, but the thinning goes as $(\lambda/Pe)^3$. Activity increases the concentration of bath particles inside the advective-diffusive boundary-layer, increasing the the total drag on the probe. The second indicates that, when external forcing is strong, but swimming stronger, the microviscosity is equal to 1—the linear-response value for $Pe_s/\gamma \gg 1$. Even though the suspension is being strongly driven from equilibrium by an external force, the swimmers are fast enough to fill in the wake left by the probe, so the suspension remains Newtonian. When the external force increases, the swimmers can no longer keep up, and we approach the result for a passive suspension [23]

B: 2-D Results

For completeness, we include the results for the microviscosity in 2-D in Fig. 5.6. There are no qualitative structural differences compared to the 3-D problem, only quantitative differences.

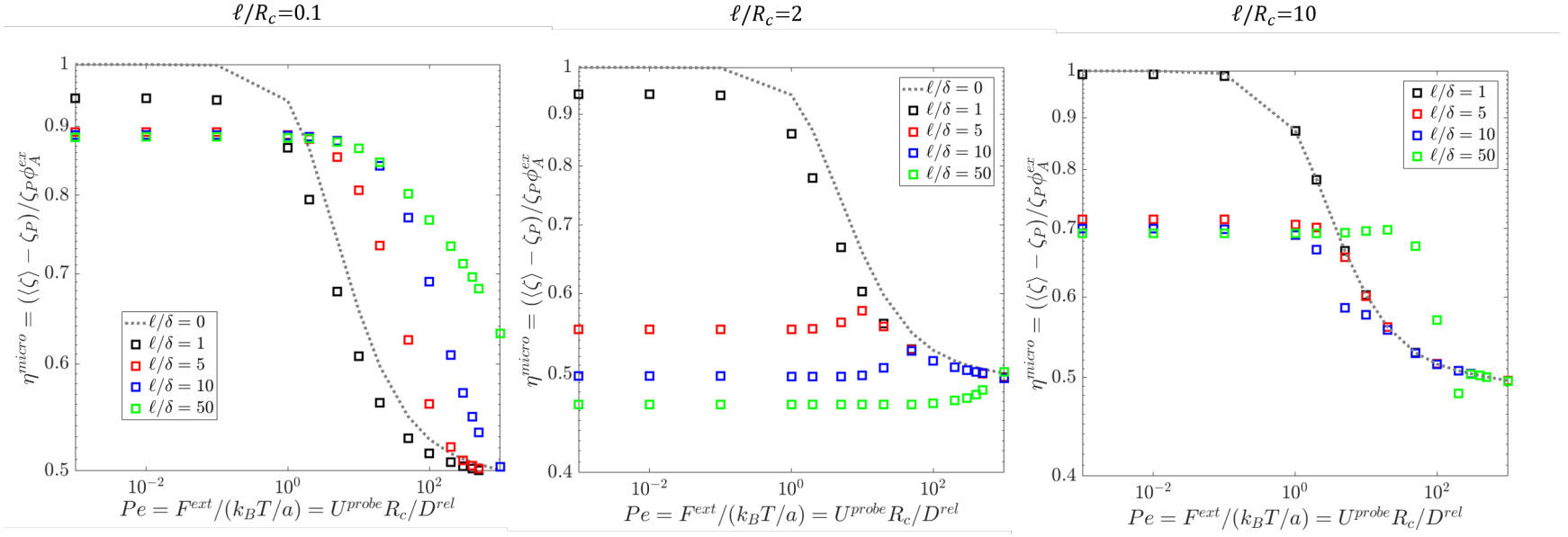

Figure 5.6: Nonlinear apparent microviscosity ($d = 2$) η^{micro} plotted as a function of $Pe = U^{probe}R_c/D^{rel}$ for various ℓ/R_c. Legend is the same as in Fig. 5.2

BIBLIOGRAPHY

[1]S. Ramaswamy, "The Mechanics and Statistics of Active Matter", Annu. Rev. Condens. Matter Phys. **1**, 323–345 (2010).

[2]M. C. Marchetti, J. F. Joanny, S. Ramaswamy, T. B. Liverpool, J. Prost, M. Rao, and R. A. Simha, "Hydrodynamics of soft active matter", Rev. Mod. Phys. **85**, 1143–1189 (2013).

[3]A. P. Solon, M. E. Cates, and J. Tailleur, "Active brownian particles and run-and-tumble particles: A comparative study", Eur. Phys. J. Spec. Top. **224**, 1231–1262 (2015).

[4]S. C. Takatori, and J. F. Brady, "A theory for the phase behavior of mixtures of active particles", Soft Matter **11**, 7920–7931 (2015).

[5]S. C. Takatori, and J. F. Brady, "Towards a thermodynamics of active matter", Phys. Rev. E - Stat. Nonlinear, Soft Matter Phys. **91**, 1–7 (2015).

[6]J. Tailleur, and M. E. Cates, "Statistical mechanics of interacting run-and-tumble bacteria", Phys. Rev. Lett. **100**, 3–6 (2008).

[7]M. E. Cates, D. Marenduzzo, I. Pagonabarraga, and J. Tailleur, "Arrested phase separation in reproducing bacteria creates a generic route to pattern formation", Proc. Natl. Acad. Sci. U. S. A. **107**, 11715–11720 (2010).

[8]S. C. Takatori, W. Yan, and J. F. Brady, "Swim pressure: Stress generation in active matter", Phys. Rev. Lett. **113**, 1–5 (2014).

[9]Y. Fily, and M. C. Marchetti, "Athermal phase separation of self-propelled particles with no alignment", Phys. Rev. Lett. **108**, 1–5 (2012).

[10]T. M. Squires, and T. G. Mason, "Fluid Mechanics of Microrheology", Annu. Rev. Fluid Mech. **42**, 413–438 (2010).

[11]D. Wirtz, "Particle-tracking microrheology of living cells: principles and applications.", Annu. Rev. Biophys. **38**, 301–326 (2009).

[12]S. Ebbens, "Active colloids: Progress and challenges toward realising autonomous applications", Curr. Opin. Colloid Interface Sci. **21**, 14–23 (2016).

[13]J. C. Crocker, and B. D. Hoffman, *Multiple-Particle Tracking and Two-Point Microrheology in Cells*, 2007.

[14]A. S. Khair, and J. F. Brady, "Single particle motion in colloidal dispersions: a simple model for active and nonlinear microrheology", J. Fluid Mech. **557**, 73 (2006).

[15]N. J. Hoh, "Effects of Particle Size Ratio on Single Particle Motion in Colloidal Dispersions", PhD thesis (California Institute of Technology, 2013).

[16]H. M. López, J. Gachelin, C. Douarche, H. Auradou, and É. Clément, "Turning Bacteria Suspensions into Superfluids", Phys. Rev. Lett. **115**, 028301 (2015).

[17]D. Saintillan, "The Dilute Rheology of Swimming Suspensions: A Simple Kinetic Model", Exp. Mech. **50**, 1275–1281 (2010).

[18]S. C. Takatori, and J. F. Brady, "Superfluid Behavior of Active Suspensions from Diffusive Stretching", Phys. Rev. Lett. **118**, 018003 (2017).

[19]A. Einstein, "Neue Bestimmung der Moleküldimensionen", Ann. Phys., 1–5 (1906).

[20]E. J. Hinch, and L. G. Leal, "The effect of Brownian motion on the rheological properties of a suspensions of non-spherical particles", J. Fluid Mech. **52**, 683–712 (1972).

[21]J. Bergenholtz, J. F. Brady, and M. Vicic, "The non-Newtonian rheology of dilute colloidal suspensions", J. Fluid Mech. **456**, 239–275 (2002).

[22]N. J. Wagner, and J. F. Brady, "Shear thickening in colloidal dispersions", Phys. Today **62**, 27–32 (2009).

[23]T. M. Squires, and J. F. Brady, "A simple paradigm for active and nonlinear microrheology", Phys. Fluids **17**, 1–21 (2005).

[24]J. W. Swan, and R. N. Zia, "Active microrheology: Fixed-velocity versus fixed-force", Phys. Fluids **25** (2013) 10.1063/1.4818810.

[25]J. F. Brady, "Brownian motion, hydrodynamics, and the osmotic pressure", J. Chem. Phys. **98**, 3335 (1993).

[26]R. N. Zia, and J. F. Brady, "Single-particle motion in colloids: force-induced diffusion", J. Fluid Mech. **658**, 188–210 (2010).

[27]N. J. Hoh, and R. N. Zia, "The impact of probe size on measurements of diffusion in active microrheology", Lab Chip **16**, 3114–3129 (2016).

[28]D. Saintillan, and M. J. Shelley, "Theory of Active Suspensions", in *Complex fluids biol. syst.* Edited by S. Spagnolie, (Springer, New York, 2015) Chap. 9, pp. 319–355.

[29]D. Saintillan, and M. J. Shelley, "Active suspensions and their nonlinear models", Comptes Rendus Phys. **14**, 497–517 (2013).

[30]A. Sokolov, and I. S. Aranson, "Reduction of viscosity in suspension of swimming bacteria", Phys. Rev. Lett. (2009) 10.1103/PhysRevLett.103.148101.

[31]C. Reichhardt, and C. J. O. Reichhardt, "Active microrheology in active matter systems: Mobility, intermittency, and avalanches", Phys. Rev. E - Stat. Nonlinear, Soft Matter Phys. **91**, 1–7 (2015).

[32]E. W. Burkholder, and J. F. Brady, "Do hydrodynamic interactions affect the swim pressure?", Soft Matter **14**, 3581–3589 (2018),

[33]D. Saintillan, “Extensional rheology of active suspensions”, Phys. Rev. E - Stat. Nonlinear, Soft Matter Phys. **81** (2010).

[34]S. Kim, and S. J. Karilla, *Microhydrodynamics : Principles and Selected Applications* (1991).

Chapter 6

HYDRODYNAMIC INTERACTIONS IN ACTIVE SUSPENSIONS

This chapter includes content from the appendix of our previously published article:

[1]E. W. Burkholder, and J. F. Brady, "Do hydrodynamic interactions affect the swim pressure?", Soft Matter **14**, 3581–3589 (2018),

6.1 Suspension mechanics and the swim force

Consider a colloidal dispersion of N particles in a Newtonian solvent of viscosity η and density ρ. The particles are sufficiently small that (1) they may be subject to fluctuating thermal forces and torques from the solvent, and (2) their motion is at low Reynolds number, thus allowing us to neglect particle and fluid inertia in the equations of motion. The suspension dynamics are described by a Smoluchoski equation for P_N, the time-dependent probability distribution of particle positions $\boldsymbol{x_\alpha}$, and orientations $\boldsymbol{q_\alpha}$:

$$\frac{\partial P_N}{\partial t} + \sum_{\alpha=1}^{N} \nabla_{\boldsymbol{x}_\alpha} \cdot \boldsymbol{j_\alpha^T} + \sum_{\alpha=1}^{N} \nabla_{R_\alpha} \cdot \boldsymbol{j_\alpha^R} = 0, \tag{6.1}$$

where $\boldsymbol{x}_\alpha$ is the position of particle α in the laboratory frame, and ∇_{R_α} is the appropriate rotational operator for particle α. The translational flux of particle α is $\boldsymbol{j}_\alpha^T = \boldsymbol{U_\alpha} P_N$ and its rotational flux is $\boldsymbol{j_\alpha^R} = \boldsymbol{\Omega_\alpha} P_N$, where $\boldsymbol{U}_\alpha$ and $\boldsymbol{\Omega}_\alpha$ are, respectively, the velocity and angular velocity of particle α.

Because we are at low Reynolds number, all particles are force- and torque-free. In active suspensions, this means that the swim force [1] (plus any other forces acting on the particle) is (are) balanced by the hydrodynamic drag. Consider the simple example of two particles subject only to active and hydrodynamic drag forces:

$$0 = -\boldsymbol{R_{11}^{FU}} \cdot \boldsymbol{U_1} - \boldsymbol{R_{12}^{FU}} \cdot \boldsymbol{U_2} + \boldsymbol{F_1^{swim}}, \tag{6.2}$$

$$0 = -\boldsymbol{R_{21}^{FU}} \cdot \boldsymbol{U_1} - \boldsymbol{R_{22}^{FU}} \cdot \boldsymbol{U_2} + \boldsymbol{F_2^{swim}}. \tag{6.3}$$

The tensor $\boldsymbol{R_{\alpha\beta}^{FU}}$ is the resistance tensor that gives the hydrodynamic force on particle α due to the velocity of particle β. Analaogus expressions may be written for the

torque balance. Suppose particle 2 is an active Brownian particle (ABP) that moves with the undisturbed velocity $\boldsymbol{U}_2^0$ regardless of the presence of particle 1. From the force balance we have $\boldsymbol{F}_1^{swim} = \boldsymbol{R}_{12}^{FU} \cdot \boldsymbol{U}_2^0$ and $\boldsymbol{F}_2^{swim} = \boldsymbol{R}_{22}^{FU} \cdot \boldsymbol{U}_2^0$, and thus

$$0 = -\boldsymbol{R}_{11}^{FU} \cdot \boldsymbol{U}_1 - \boldsymbol{R}_{12}^{FU} \cdot (\boldsymbol{U}_2 - \boldsymbol{U}_2^0), \tag{6.4}$$

$$0 = -\boldsymbol{R}_{21}^{FU} \cdot \boldsymbol{U}_1 - \boldsymbol{R}_{22}^{FU} \cdot (\boldsymbol{U}_2 - \boldsymbol{U}_2^0), \tag{6.5}$$

whose solution is simply $\boldsymbol{U}_1 = 0$ and $\boldsymbol{U}_2 = \boldsymbol{U}_2^0$ as desired. It may seem surprising that particle 1 experiences a swim force due to the motion of the active particle 2, especially so because we are saying that particle 2 moves with the undisturbed motion $\boldsymbol{U}_2^0$ and particle 1 does not move at all! But in the resistance formulation of the problem, where forces and torques can be superimposed, things are different than the perhaps more familiar mobility perspective where the velocities are expressed in terms of the forces, and one must proceed carefully. Stokes flow is unique and so either prospective—resistance or mobility—is fine.

In this simple 2-particle example, if there were other forces acting on the particles the force balances would become

$$0 = -\boldsymbol{R}_{11}^{FU} \cdot \boldsymbol{U}_1 - \boldsymbol{R}_{12}^{FU} \cdot (\boldsymbol{U}_2 - \boldsymbol{U}_2^0) + \boldsymbol{F}_1^{other}, \tag{6.6}$$

$$0 = -\boldsymbol{R}_{21}^{FU} \cdot \boldsymbol{U}_1 - \boldsymbol{R}_{22}^{FU} \cdot (\boldsymbol{U}_2 - \boldsymbol{U}_2^0) + \boldsymbol{F}_2^{other}, \tag{6.7}$$

and the velocities of the two particles would now be

$$\begin{pmatrix} \boldsymbol{U}_1 \\ \boldsymbol{U}_2 - \boldsymbol{U}_2^0 \end{pmatrix} = \begin{pmatrix} \boldsymbol{R}_{11}^{FU} & \boldsymbol{R}_{12}^{FU} \\ \boldsymbol{R}_{21}^{FU} & \boldsymbol{R}_{22}^{FU} \end{pmatrix}^{-1} \cdot \begin{pmatrix} \boldsymbol{F}_1^{other} \\ \boldsymbol{F}_2^{other} \end{pmatrix}, \tag{6.8}$$

The 'other' forces can be of any type because we can superimpose forces at low Reynolds numbers.

In going forward for compactness we employ the notation $\boldsymbol{\mathcal{U}}_{\boldsymbol{\alpha}} = (\boldsymbol{U}_{\boldsymbol{\alpha}}, \boldsymbol{\Omega}_{\boldsymbol{\alpha}})$, and $\boldsymbol{\mathcal{F}}_{\boldsymbol{\alpha}} = (\boldsymbol{F}_{\boldsymbol{\alpha}}, \boldsymbol{L}_{\boldsymbol{\alpha}})$, where $\boldsymbol{L}_{\boldsymbol{\alpha}}$ is the torque acting on particle α. We generalize this idea to write the velocity of any particle α relative to some background flow $\boldsymbol{\mathcal{U}}_{\boldsymbol{\alpha}}^{\infty}$:

$$\boldsymbol{\mathcal{U}}_{\boldsymbol{\alpha}} = \boldsymbol{\mathcal{U}}_{\boldsymbol{\alpha}}^{\boldsymbol{0}} + \boldsymbol{\mathcal{U}}_{\boldsymbol{\alpha}}^{\infty} + \sum_{\beta=1}^{N} \boldsymbol{\mathcal{R}}_{\boldsymbol{\alpha\beta}}^{-\boldsymbol{1}} \cdot \boldsymbol{\mathcal{F}}_{\beta}, \tag{6.9}$$

where $\boldsymbol{\mathcal{F}}_{\boldsymbol{\beta}}$ is the sum of all other forces and torques acting on particle β and $\boldsymbol{\mathcal{R}}$ is the grand resistance tensor [2]. Particles may be subject to forces and torques from Brownian motion, interparticle potentials, shear, external sources (e.g. gravity),

and even additional swim forces: $\mathcal{F} = \mathcal{F}^B + \mathcal{F}^P + \mathcal{F}^{ext} + \mathcal{F}^{shear} + (\mathcal{F}^{swim})'$. The swim force necessary to produce the undisturbed swim velocity $\mathcal{U}_\alpha^0$ has already been accounted for in (6.9).

For a fixed-velocity swimmer hydrodynamics do not influence the swim speed $\mathcal{U}_\alpha^0$, but they can influence the motion, $\mathcal{U}_\alpha$, caused by hydrodynamic interactions (HI) with other particles or boundaries. We emphasize that HI *will* influence particle motion due to swim forces above and beyond the fundamental swim force. For example, stresslet swimmers have an additional swim force, $(\mathcal{F}^{swim})'$, that affects the motion of another particle.

Furthermore, a swimmer may change its orientation q_α through a random stochastic process that need not be due to Brownian motion or HI: the swimmer can "decide" to change its direction (perhaps in response to an external stimulus, or by moving its flagella). This reorientation process produces no flow, and is not coupled to the motion of other particles. The simplest system thus has no swim angular velocity $\Omega_\alpha^0 = 0$, but there can be reorientation arising from rotary Brownian motion and this stochastic reorientation, the latter of which we model as $\tau_R^{-1} \cdot \nabla_R \ln P_N$, where τ_R is the reorientation time.

We now specify the form of the other forces/torques acting on the particles. The Brownian forces/torques have the familiar form $\mathcal{F}^B = -k_B T \nabla \ln P_N$, and we will assume that the interparticle force is conservative $\mathcal{F}^P = -k_B T \nabla V$, where V is the dimensionless interparticle potential and the gradients are with respect to both position and orientation of the particles. The full expression for the flux of a particle is thus

$$\begin{aligned} j_\alpha = (\mathcal{U}_\alpha^0 + \mathcal{U}_\alpha^\infty)P + \mathcal{U}_\alpha^{ext} P + \mathcal{U}_\alpha^{shear} P + (\mathcal{U}_\alpha^{swim})' P \\ -k_B T \sum_{\beta=1}^{N} \mathcal{R}^{-1} \cdot (\nabla V + \nabla \ln P) P - \tau_R^{-1} \cdot \nabla P. \end{aligned} \tag{6.10}$$

The "other" particle velocities are $\mathcal{U}_\alpha^{ext} = \mathcal{R}^{-1} \cdot \mathcal{F}^{ext}$ (e.g. particles sedimenting due to gravity), $\mathcal{U}_\alpha^{shear} = \mathcal{R}^{-1} \cdot \mathcal{R}_{FE} : \mathcal{E}^\infty$, and $(\mathcal{U}_\alpha^{swim})' = \mathcal{R}^{-1} \cdot (\mathcal{F}^{swim})'$. For the additional swim force one must model the hydrodynamics of the desired swimming mechanism. For example, a stresslet swimmer exerts a force dipole on the embedding fluid, which can cause a second particle to translate and rotate, but does not impact its own motion (which is already accounted for by $\mathcal{U}_\alpha^0$. Thus, the motion of particle α due to a stresslet swimmer β would be $(U_\alpha^{swim})' = \sigma_\beta K(x_\alpha - x_\beta) \cdot (q_\beta q_\beta - \frac{1}{3} I)$, where K is the Stokes flow stresslet singularity function (the double layer potential),

and σ_β is the magnitude of the stresslet. Finally we note that the form of the resistance functions are independent of the particle orientations for spheres.

6.2 Single-particle, equilibrium problems

For the problem of a single particle in the presence of a no-flux boundary, the Smoluchowski equation reduces to

$$\frac{\partial P}{\partial t} + \nabla_{\boldsymbol{x}} \cdot \boldsymbol{j}^{\boldsymbol{T}} + \nabla_{\boldsymbol{R}} \cdot \boldsymbol{j}^{\boldsymbol{R}} = 0, \tag{6.11}$$

where $\nabla_{\boldsymbol{R}} = \boldsymbol{q} \times \boldsymbol{\nabla}_{\boldsymbol{q}}$ and $P(\boldsymbol{x}, \boldsymbol{q}, t)$ is the probability of finding a particle at position $\boldsymbol{x}$ with orientation $\boldsymbol{q}$ at a time t. The translational and rotational fluxes of the swimmer are

$$\boldsymbol{j}^{\boldsymbol{T}} = U_0 \boldsymbol{q} P - \boldsymbol{D}^{\boldsymbol{TT}} \cdot \nabla_{\boldsymbol{x}} P - \boldsymbol{D}^{\boldsymbol{TR}} \cdot \nabla_R P, \tag{6.12}$$

$$\boldsymbol{j}^{\boldsymbol{R}} = -\boldsymbol{D}^{\boldsymbol{RT}} \cdot \nabla_{\boldsymbol{x}} P - (\boldsymbol{D}^{\boldsymbol{RR}} + \tau_R^{-1} \boldsymbol{I}) \cdot \nabla_R P. \tag{6.13}$$

The above expressions make use of the fact that the hard-core potential vanishes everywhere in space and manifests only as a condition of no translational flux, $\boldsymbol{n} \cdot \boldsymbol{j}^T = 0$, at the boundary. This boundary condition applies at some distance Δa (a is the swimer size) away from the no-slip boundary for the fluid. This is the commonly used excluded annulus model [3], and allows one to smoothly tune from complete HI ($\Delta \to 0$) and no HI ($\Delta \to \infty$).

There are several relevant problems in which the geometry is axisymmetric: a spherical swimmer near an infinite flat wall, a spherical swimmer between two flat plates, and a spherical swimmer outside and inside of a spherical cavity. We employ the notation of Kim and Karrila [2] for the mobility functions in an axysmmetric geometry:

$$\boldsymbol{D}^{\boldsymbol{TT}} = \frac{k_B T}{6\pi\eta a}\left(x^a \boldsymbol{nn} + y^a (\boldsymbol{I} - \boldsymbol{nn}) \right) \tag{6.14}$$

$$\boldsymbol{D}^{\boldsymbol{RR}} = \frac{k_B T}{8\pi\eta a^3}\left(x^c \boldsymbol{nn} + y^c (\boldsymbol{I} - \boldsymbol{nn}) \right) \tag{6.15}$$

$$\boldsymbol{D}^{\boldsymbol{RT}} = (\boldsymbol{D}^{\boldsymbol{TR}})^\dagger = \frac{k_B T}{4\pi\eta a^2} y^b \boldsymbol{\epsilon} \cdot \boldsymbol{n}, \tag{6.16}$$

where $\boldsymbol{\epsilon}$ is the unit-alternating tensor and $\boldsymbol{n}$ is a unit vector defining the axis of symmetry. The diffusivities follow the Einstein relation $\boldsymbol{D} = k_B T \boldsymbol{\mathcal{R}}^{-1}$, where $\boldsymbol{D}^{\boldsymbol{TT}} = k_B T \boldsymbol{M}^{\boldsymbol{UF}}$, $\boldsymbol{D}^{\boldsymbol{RT}} = (\boldsymbol{D}^{\boldsymbol{TR}})^\dagger = k_B T \boldsymbol{M}^{\boldsymbol{\Omega F}}$, and $\boldsymbol{D}^{\boldsymbol{RR}} = k_B T \boldsymbol{M}^{\boldsymbol{\Omega L}}$, and

$\boldsymbol{M^{UF}}, \boldsymbol{M^{\Omega F}}$, and $\boldsymbol{M^{\Omega L}}$ are the familiar mobility tensors [2]. For the simplest problem of neutral swimmers (or 'movers'), the only effect of HI is to introduce anisotropy in the thermal diffusivities.

We use a moments expansion of P to derive general equations governing the suspension structure:

$$P = n(\boldsymbol{x}, t) + \boldsymbol{m}(\boldsymbol{x}, t) \cdot \boldsymbol{q} + \boldsymbol{Q}(\boldsymbol{x}, t) : (\boldsymbol{qq} - \tfrac{1}{3}\boldsymbol{I}) + ..., \tag{6.17}$$

where n is the concentration field $\boldsymbol{m}$ is the polar order and $\boldsymbol{Q}$ is the nematic order [4]. At steady-state, the concentration field is described by

$$\frac{\partial}{\partial x_i}\left[U_0 m_i - D_{ij}^{TT}\frac{\partial n}{\partial x_j}\right] = 0, \tag{6.18}$$

the polar order is described by

$$\begin{aligned}\frac{\partial}{\partial x_i}\Bigg[U_0\Big(Q_{pi} + \frac{1}{3}\delta_{pi}n\Big) + D_{ij}^{TT}\frac{\partial m_p}{\partial x_j} + D_{ij}^{TR}\epsilon_{jkp}m_k\Bigg] \\ + D_{ij}^{RT}\epsilon_{ikp}\frac{\partial m_k}{\partial m_j} + D_{ii}^{RR}m_p - D_{ip}^{RR}m_i + \frac{2}{\tau_R}m_p = 0,\end{aligned} \tag{6.19}$$

and the nematic order is described by

$$\begin{aligned}\frac{\partial}{\partial x_i}\Bigg[\frac{U_0}{5}\Big(\alpha_{qpsi} - \frac{5}{3}\delta_{ps}\delta_{qi}\Big)m_q - D_{ij}^{TT}\frac{\partial Q_{ps}}{\partial x_j} \\ + D_{ij}^{TR}(\epsilon_{jkp}Q_{sk} + \epsilon_{jks}Q_{pk})\Bigg] + D_{ij}^{RT}\frac{\partial}{\partial x_j}\Big(\epsilon_{ikp}Q_{sk} \\ + \epsilon_{iks}Q_{pk}\Big) - D_{ij}^{RR}(\epsilon_{iks}\epsilon_{jmp} + \epsilon_{ikp}\epsilon_{jms})Q_{km} \\ + D_{ij}^{RR}(2\delta_{ij}Q_{ps} - \delta_{js}Q_{ip} - \delta_{jp}Q_{is}) + \frac{6}{\tau_R}Q_{ps} = 0,\end{aligned} \tag{6.20}$$

where we have made the closure that $\langle \boldsymbol{qqq} \rangle = \boldsymbol{\alpha} \cdot \boldsymbol{m}/5$ and $\boldsymbol{\alpha}$ is the fourth-order isotropic tensor [5, 6]. We can reduce the system of equations to coupled ODEs using linearity arguments: $n = f(r)$, $\boldsymbol{m} = g(r)\boldsymbol{n}$, $\boldsymbol{Q} = h(r)\boldsymbol{nn} + k(r)(\boldsymbol{I} - \boldsymbol{nn})$ (or $f(z)$, $g(z)\boldsymbol{e_z}$, and $h(z)\boldsymbol{e_z e_z} + k(z)(\boldsymbol{I} - \boldsymbol{e_z e_z})$ in 1D geometries).

Infinite flat plate

We consider a single swimmer near an infinite plane wall. Though the swimmers are still free to move and rotate in 3-D, all variations will occur in the direction

normal to the wall e_z. The governing equations reduce to

$$\frac{d}{dz}\left(x^a(z)D^{TT}\frac{df}{dz}\right) - U_0\frac{dg}{dz} = 0, \tag{6.21}$$

$$\frac{d}{dz}\left(x^a(z)D^{TT}\frac{dg}{dz}\right) - \frac{U_0}{3}\frac{df}{dz} - U_0\frac{dh}{dz} \\ -2\tau_R^{-1}g(z) - 2y^c(z)D^{RR}g(z) = 0, \tag{6.22}$$

$$\frac{d}{dz}\left(x^a(z)D^{TT}\frac{dh}{dz}\right) - \frac{4}{15}U_0\left(\frac{dg}{dz} - g(z)\right) \\ -6\tau_R^{-1}h(z) - 4y^c(z)D^{RR}(h(z) - k(z)) = 0, \tag{6.23}$$

$$\frac{d}{dz}\left(x^a(z)D^{TT}\frac{dk}{dz}\right) + \frac{2}{15}U_0\left(\frac{dg}{dz} - g(z)\right) \\ -6\tau_R^{-1}k(z) + 2y^c(z)D^{RR}(h(z) - k(z)) = 0, \tag{6.24}$$

and the no-flux boundary conditions are

$$x^a(z)D^{TT}\frac{df}{dz} - U_0 g(z) = 0, \tag{6.25}$$

$$x^a(z)D^{TT}\frac{dg}{dz} - \frac{U_0}{3}f(z) - U_0 h(z) = 0, \tag{6.26}$$

$$x^a(z)D^{TT}\frac{dh}{dz} - \frac{4}{15}U_0 g(z) = 0, \tag{6.27}$$

$$x^a(z)D^{TT}\frac{dk}{dz} + \frac{2}{15}U_0 g(z) = 0. \tag{6.28}$$

In the above we have factored out the mobility functions $x^a(z)$, etc., and therefore the constant diffusivities from (6.14-6.16) are $D^{TT} = k_BT/6\pi\eta a$, $D^{RR} = k_BT/8\pi\eta a^3$ and $D^{RT} = D^{TR} = k_BT/4\pi\eta a^2$.

For a single flat wall, we apply the no-flux conditions at the hard-repulsion boundary $z = a(1+\Delta)$, and say that the suspension has no long-range order: $f \to 1, g \to 0, h \to 0, k \to 0$, as $z \to \infty$. The functions $x^a(z)$ and $y^c(z)$ are have been tabulated by Swan and Brady using the Stokesian dynamics method [7] and by others using the method of reflections and fast-multipole methods [8–10]. We use the far-field forms of the functions given in [7], and the near-field forms from Goldman et al. and Bossis et al. [11, 12].

Outside a sphere

The second problem is a swimmer outside a spherical cavity of radius R. The structure is similar to the flat-plate problem, but the governing equations retain

some additional terms due to the curvature:

$$\frac{d}{dr}\left(x^a(r)D^{TT}\frac{df}{dr}\right) + x^a(r)D^{TT}\frac{2}{r}\frac{df}{dr} - U_0\left(\frac{dg}{dr} + \frac{2}{r}g(r)\right) = 0, \tag{6.29}$$

$$\frac{d}{dr}\left(x^a(r)D^{TT}\frac{dg}{dr}\right) + x^a(r)D^{TT}\frac{2}{r}\frac{dg}{dr} - \frac{2}{r^2}y^a(r)D^{TT}g(r) - \frac{4}{r}y^b(r)D^{RT}g(r) - \frac{U_0}{3}\frac{df}{dr} - U_0\frac{dh}{dr} - \frac{2U_0}{r}(h(r) - k(r)) - 2(\tau_R^{-1} + y^c(r)D^{RR})g(r) = 0, \tag{6.30}$$

$$\frac{d}{dr}\left(x^a(r)D^{TT}\frac{dh}{dr}\right) + x^a(r)d^{TT}\frac{2}{r}\frac{dh}{dr} - \frac{4}{r^2}y^a(r)D^{TT}h(r) + \frac{4}{r^2}y^a(r)D^{TT}k(r) - \frac{8}{r}y^b(r)D^{RT}(h(r) - k(r)) - \frac{4}{15}U_0\left(\frac{dg}{dr} - \frac{g(r)}{r}\right) - 6\tau_R^{-1}h(r) - 4y^c(r)D^{RR}(h(r) - k(r)) = 0, \tag{6.31}$$

$$\frac{d}{dr}\left(x^a(r)D^{TT}\frac{dk}{dr}\right) + x^a(r)d^{TT}\frac{2}{r}\frac{dk}{dr} + \frac{2}{r^2}y^a(r)D^{TT}h(r) - \frac{2}{r^2}y^a(r)D^{TT}k(r) - \frac{8}{r}y^b(r)D^{RT}(h(r) - k(r)) + \frac{2}{15}U_0\left(\frac{dg}{dr} - \frac{g(r)}{r}\right) - 6\tau_R^{-1}k(r) + 2y^c(r)D^{RR}(h(r) - k(r)) = 0. \tag{6.32}$$

The no-flux boundary conditions are

$$x^a(r)D^{TT}\frac{df}{dr} - U_0g(r) = 0, \tag{6.33}$$

$$x^a(r)D^{TT}\frac{dg}{dr} - \frac{U_0}{3}f(r) - U_0h(r) = 0, \tag{6.34}$$

$$x^a(r)D^{TT}\frac{dh}{dr} - \frac{4}{15}U_0g(r) = 0, \tag{6.35}$$

$$x^a(r)D^{TT}\frac{dk}{dr} + \frac{2}{15}U_0g(r) = 0. \tag{6.36}$$

which are applied at $r = (R + a)(1 + \Delta)$. There is no long-range order far from the sphere.

For the motion of a swimmer outside a sphere, the mobility functions needed are a bit different than the standard two-sphere mobility functions in [2]. The spherical

cavity of radius R is held fixed ($\boldsymbol{U}_1 = 0$, $\boldsymbol{\Omega}_1 = 0$) and the external force $\boldsymbol{F}^{ext}$ and torque $\boldsymbol{L}^{ext}$ necessary can be found from Eqns. 5.6 and 5.7. Thus, even though we are only interested in the motion of the swimmer relative to the cavity, this is fundamentally a two-particle problem, and

$$\boldsymbol{\mathcal{F}}_{\mathbf{1}}^{\boldsymbol{ext}} = \boldsymbol{\mathcal{R}}_{\mathbf{12}}^{\boldsymbol{\mathcal{FU}}} \cdot (\boldsymbol{\mathcal{R}}_{\mathbf{22}}^{\boldsymbol{\mathcal{FU}}})^{-1} \cdot \boldsymbol{\mathcal{F}}_{\mathbf{2}}^{\boldsymbol{other}} - \boldsymbol{\mathcal{F}}_{\mathbf{1}}^{\boldsymbol{other}}, \tag{6.37}$$

which is then substituted into Eqn. 6.9. This does not change the structure of the equations, it only impacts the precise definitions of x^a, y^a, y^b, and y^c in the system of ODEs that must be solved.

The only 'other' forces to be considered in the above equation are from thermal fluctuations; thus all the effects appear in the diffusive terms of the Smoluchowski equation. From the force balances, one can show that

$$\begin{aligned}
\boldsymbol{D}^{\boldsymbol{TT}} &= \boldsymbol{D}_{\mathbf{22}}^{\boldsymbol{TT}} + \boldsymbol{D}_{\mathbf{21}}^{\boldsymbol{TT}} \cdot (\boldsymbol{R}_{\mathbf{12}}^{\boldsymbol{FU}} \cdot (\boldsymbol{\mathcal{R}}_{\mathbf{22}})_{UF}^{-1} + \boldsymbol{R}_{\mathbf{12}}^{\boldsymbol{F\Omega}} \cdot (\boldsymbol{\mathcal{R}}_{\mathbf{22}})_{\Omega F}^{-1}) \\
&\quad + \boldsymbol{D}_{\mathbf{21}}^{\boldsymbol{TR}} \cdot (\boldsymbol{R}_{\mathbf{12}}^{\boldsymbol{LU}} \cdot (\boldsymbol{\mathcal{R}}_{\mathbf{22}})_{UF}^{-1} + \boldsymbol{R}_{\mathbf{12}}^{\boldsymbol{L\Omega}} \cdot (\boldsymbol{\mathcal{R}}_{\mathbf{22}})_{\Omega F}^{-1}) \qquad (6.38) \\
\boldsymbol{D}^{\boldsymbol{TR}} &= \boldsymbol{D}_{\mathbf{22}}^{\boldsymbol{TR}} + \boldsymbol{D}_{\mathbf{21}}^{\boldsymbol{TR}} \cdot (\boldsymbol{R}_{\mathbf{12}}^{\boldsymbol{LU}} \cdot (\boldsymbol{\mathcal{R}}_{\mathbf{22}})_{UL}^{-1} + \boldsymbol{R}_{\mathbf{12}}^{\boldsymbol{L\Omega}} \cdot (\boldsymbol{\mathcal{R}}_{\mathbf{22}})_{\Omega L}^{-1}) \\
&\quad + \boldsymbol{D}_{\mathbf{21}}^{\boldsymbol{TT}} \cdot (\boldsymbol{R}_{\mathbf{12}}^{\boldsymbol{FU}} \cdot (\boldsymbol{\mathcal{R}}_{\mathbf{22}})_{UL}^{-1} + \boldsymbol{R}_{\mathbf{12}}^{\boldsymbol{F\Omega}} \cdot (\boldsymbol{\mathcal{R}}_{\mathbf{22}})_{\Omega L}^{-1}) \qquad (6.39) \\
\boldsymbol{D}^{\boldsymbol{RR}} &= \boldsymbol{D}_{\mathbf{22}}^{\boldsymbol{RR}} + \boldsymbol{D}_{\mathbf{21}}^{\boldsymbol{RR}} \cdot (\boldsymbol{R}_{\mathbf{12}}^{\boldsymbol{LU}} \cdot (\boldsymbol{\mathcal{R}}_{\mathbf{22}})_{UL}^{-1} + \boldsymbol{R}_{\mathbf{12}}^{\boldsymbol{L\Omega}} \cdot (\boldsymbol{\mathcal{R}}_{\mathbf{22}})_{\Omega L}^{-1}) \\
&\quad + \boldsymbol{D}_{\mathbf{22}}^{\boldsymbol{RT}} \cdot (\boldsymbol{R}_{\mathbf{12}}^{\boldsymbol{FU}} \cdot (\boldsymbol{\mathcal{R}}_{\mathbf{22}})_{UL}^{-1} + \boldsymbol{R}_{\mathbf{12}}^{\boldsymbol{F\Omega}} \cdot (\boldsymbol{\mathcal{R}}_{\mathbf{22}})_{\Omega L}^{-1}), \qquad (6.40)
\end{aligned}$$

and $\boldsymbol{D}^{\boldsymbol{RT}} = -\boldsymbol{D}^{\boldsymbol{TR}}$ by symmetry. The proper components of the tensor $(\boldsymbol{\mathcal{R}}_{\mathbf{22}})^{-1}$ are

$$(\boldsymbol{\mathcal{R}}_{\mathbf{22}})_{UF}^{-1} = (\boldsymbol{R}_{\mathbf{22}}^{\boldsymbol{FU}} - \boldsymbol{R}_{\mathbf{22}}^{\boldsymbol{F\Omega}} \cdot (\boldsymbol{R}_{\mathbf{22}}^{\boldsymbol{L\Omega}})^{-1} \cdot \boldsymbol{R}_{\mathbf{22}}^{\boldsymbol{LU}})^{-1} \tag{6.41}$$

$$(\boldsymbol{\mathcal{R}}_{\mathbf{22}})_{\Omega F}^{-1} = -(\boldsymbol{R}_{\mathbf{22}}^{\boldsymbol{L\Omega}})^{-1} \cdot \boldsymbol{R}_{\mathbf{22}}^{\boldsymbol{LU}} \cdot (\boldsymbol{R}_{\mathbf{22}}^{\boldsymbol{FU}} - \boldsymbol{R}_{\mathbf{22}}^{\boldsymbol{F\Omega}} \cdot (\boldsymbol{R}_{\mathbf{22}}^{\boldsymbol{L\Omega}})^{-1} \cdot \boldsymbol{R}_{\mathbf{22}}^{\boldsymbol{LU}})^{-1} \tag{6.42}$$

$$(\boldsymbol{\mathcal{R}}_{\mathbf{22}})_{\Omega L}^{-1} = (\boldsymbol{R}_{\mathbf{22}}^{\boldsymbol{L\Omega}} - \boldsymbol{R}_{\mathbf{22}}^{\boldsymbol{LU}} \cdot (\boldsymbol{R}_{\mathbf{22}}^{\boldsymbol{FU}})^{-1} \cdot \boldsymbol{R}_{\mathbf{22}}^{\boldsymbol{F\Omega}})^{-1}, \tag{6.43}$$

and, as before $(\boldsymbol{\mathcal{R}}_{\mathbf{22}})_{\Omega F}^{-1} = -(\boldsymbol{\mathcal{R}}_{\mathbf{22}})_{UL}^{-1}$ by symmetry [2].

The effective mobility functions may be expressed in the resistance formulation above, or via an equivalent formulation in terms of the component mobility functions only. The explicit forms for the latter formulation follow from rearranging the

Smoluchowski equation outlined in section 6.1.

$$x^a = x^a_{22} - \frac{4\beta}{(1+\beta)^2}\frac{x^a_{21}x^a_{12}}{x^a_{11}}, \tag{6.44}$$

$$y^a = y^a_{22} - \frac{48\beta}{(1+\beta)^4}\frac{(y^b_{12})^2}{y^c_{11}} - \frac{\beta}{y^c_{11}}\left[\frac{(\frac{2}{(1+\beta)}y^a_{12}y^c_{11} - \frac{12}{(1+\beta)^2}y^b_{11}y^b_{21})^2}{y^a_{11}y^c_{11} - 3(y^b_{11})^2}\right], \tag{6.45}$$

$$y^b = y^b_{22} - \frac{32\beta^2}{(1+\beta)^5}\frac{y^b_{21}y^c_{12}}{y^c_{11}} - \frac{1}{y^c_{11}}\left[\frac{\frac{2}{(1+\beta)}y^a_{21}y^c_{11} - \frac{12}{(1+\beta)^2}y^b_{12}y^b_{11}}{y^a_{11}y^c_{11} - 3(y^b_{11})^2}\right] \times\left(\frac{8\beta^2}{(1+\beta)^3}y^c_{12}y^b_{11} - \frac{4\beta^2}{(1+\beta)^2}y^b_{21}y^c_{11}\right), \tag{6.46}$$

$$x^c = x^c_{22} - \frac{64\beta^3}{(1+\beta)^6}\frac{x^c_{12}x^c_{12}}{x^c_{11}}, \tag{6.47}$$

$$y^c = y^c_{22} - \frac{64\beta^3}{(1+\beta)^6}\frac{y^c_{21}y^c_{12}}{y^c_{11}} - \frac{6}{8}\frac{\beta^3}{y^c_{11}}\left[\frac{(\frac{8}{(1+\beta)^2}y^b_{21}y^c_{11} - \frac{16}{(1+\beta)^3}y^c_{21}y^b_{11})^2}{y^a_{11}y^c_{11} - 3(y^b_{11})^2}\right], \tag{6.48}$$

where $\beta = a/R$ is the size ratio of the swimmer to the cavity. The needed mobility functions are now expressed in terms of the standard two-sphere functions, which can be found in [2, 13, 14]. Note that in the limit $\beta \to 0$ only the functions x^a_{22}, etc. remain, but care is needed to reduce these expressions to the flat-wall limit as the swimmer would always be "close" to the wall. The far field forms for x^a_{22}, etc. in [2] assume that the interparticle separation distance $r - (a + R) \gg R$, but the flat wall problem assumes that $R \to \infty$ first, making it impossible to have the have the particle a distance $z = r - (a + R) \gg R$ from the wall.

The notion of lubrication interactions—$\Delta \ll 1$—for squirmers becomes tricky if the organism's surface is deforming on a length scale comparable to the gap between the particles. Rather than use a no-slip condition on a deformed surface, Ishikawa and coworkers did a lubrication analysis assuming an effective slip velocity at the squirmer's surface. We neglect these in our analysis, as this would be associated with the mobility functions for $(\boldsymbol{F}^{swim})'$, not the fundamental run-and-tumble active motion. Additionally, lubrication interactions associated with this force contribute terms $\sim O(-\ln\Delta)$ to the force on the passive sphere, which is negligible compared to the $O(1/\Delta)$ contribution from Brownian fluctuations.

As a final note, the lubrication forms for x^c are not given in the work of Jeffrey and Onishi, as the "scope for applications is limited," and indeed is not necessary for computing the force/pressure on a stationary spherical cavity [14]. From Jef-

frey's original work on rotations of solid bodies [15], the complementary resistance function X^C is nearly unity even at small interparticle separations ($\Delta \sim 0.2$). As this function is needed in later calculations, we simply assume that the far-field form of this is always valid, as the functions x^a, y^a, and y^c are the most important. Squirming corrections to x^c are $O(\Delta)$ for small Δ [16].

Force on a sphere

Finally we are interested in the force necessary to hold the spherical cavity fixed. Although there is no net force, via the force we can define the pressure. The force on the cavity, when averaged over the orientation of the swimmer, is given by

$$\langle \boldsymbol{F}^{\boldsymbol{ext}} \rangle_q = -k_B T \left\{ \left(\frac{X^A_{12}}{X^A_{22}} + 1 \right) \boldsymbol{nn} + \left[\frac{Y^A_{12} Y^C_{22} - Y^B_{12} Y^B_{22}}{Y^C_{22} Y^A_{22} - (Y^B_{22})^2} + 1 \right] (\boldsymbol{I} - \boldsymbol{nn}) \right\} \cdot \nabla_r \ln n, \quad (6.49)$$

because contributions from thermal torques do not contribute to the orientation-averaged force. The Brownian forces and torques on the cavity in Eqn. 6.37 do not enter in the Smoluchowski equation, but they must still be considered when computing the average external force on the cavity. We follow Squires and Brady [17] and may write the suspension-averaged force:

$$\begin{aligned} \langle \boldsymbol{F}^{\boldsymbol{ext}} \rangle = &- \int_{S^c} \boldsymbol{n} \left(1 + \frac{X^A_{12}}{X^A_{22}} \right) n(\Delta) dS \\ &+ \int_V \boldsymbol{n} \left[\frac{d}{dr} \left(\frac{X^A_{12}}{X^A_{22}} \right) + \frac{2}{r} \left(\frac{X^A_{12}}{X^A_{22}} - \left[\frac{Y^A_{12} Y^C_{22} - Y^B_{12} Y^B_{22}}{Y^C_{22} Y^A_{22} - (Y^B_{22})^2} \right] \right) \right] n(r) dV, \quad (6.50) \end{aligned}$$

noting that the appropriate weighting is the deviation from the uniform number density. The first term is a surface integral of this number density deviation over the cavity's surface, and the second term results from the divergence of the relative mobility. By symmetry this force is zero for an isotropic distrubtion of the particles. The force can no longer be given by the simple relation $\boldsymbol{F} = \int \boldsymbol{n} k_B T n(\boldsymbol{x}) dS$, as in the special case of a flat wall. Indeed, this is true for inactive Brownian suspensions as well [17, 18].

6.3 External perturbations

For the microrheology problem, we can readily use the formalism given in section 6.1 to incorporate an external force $\boldsymbol{F}^{\boldsymbol{ext}}$ driving the motion of a test particle (labeled

particle 1) in the presence of a swimmer (labeled particle 2):

$$\frac{\partial}{\partial x_i}\left[U_0 m_i + M_{ij}^{UF} F_j^{ext} n - D_{ij}^{TT}\frac{\partial n}{\partial x_j}\right] = 0, \tag{6.51}$$

$$n_i\left[U_0 m_i + M_{ij}^{UF} F_j^{ext} n - D_{ij}^{TT}\frac{\partial n}{\partial x_j}\right] = 0, r = R_c, \tag{6.52}$$

$$n \sim n^{\infty}, r \to \infty, \tag{6.53}$$

$$\frac{\partial}{\partial x_i}\left[U_0\left(Q_{pi} + \frac{1}{3}\delta_{pi} n\right) + M_{ij}^{UF} F_j^{ext} m_p + D_{ij}^{TT}\frac{\partial m_p}{\partial x_j} + D_{ij}^{TR}\epsilon_{jkp} m_k\right] \tag{6.54}$$

$$-M_{ij}^{\Omega F} F_j^{ext}\epsilon_{ikp} m_k + D_{ij}^{RT}\epsilon_{ikp}\frac{\partial m_k}{\partial x_j} + D_{ii}^{RR} m_p - D_{ip}^{RR} m_i + \frac{2}{\tau_R} m_p = 0,$$

$$n_i\left[U_0\left(Q_{pi} + \frac{1}{3}\delta_{pi} n\right) + M_{ij}^{UF} F_j^{ext} m_p + D_{ij}^{TT}\frac{\partial m_p}{\partial x_j} + D_{ij}^{TR}\epsilon_{jkp} m_k\right], = 0, r = R_c \tag{6.55}$$

$$m_p \sim 0, r \to \infty, \tag{6.56}$$

$$\frac{\partial}{\partial x_i}\left[\frac{U_0}{5}\left(\alpha_{qpsi} - \frac{5}{3}\delta_{ps}\delta_{qi}\right) m_q + M_{ij}^{UF} F_j^{ext} Q_{ps} - D_{ij}^{TT}\frac{\partial Q_{ps}}{\partial x_j}\right. \tag{6.57}$$

$$\left. + D_{ij}^{TR}(\epsilon_{jkp} Q_{sk} + \epsilon_{jks} Q_{pk})\right] - M_{ij}^{\Omega F} F_j^{ext}(\epsilon_{ikp} Q_{sk} + \epsilon_{iks} Q_{pk})$$

$$+ D_{ij}^{RT}\frac{\partial}{\partial x_j}\left(\epsilon_{ikp} Q_{sk} + \epsilon_{iks} Q_{pk}\right) + \frac{6}{\tau_R} Q_{ps}$$

$$- D_{ij}^{RR}(\epsilon_{iks}\epsilon_{jmp} + \epsilon_{ikp}\epsilon_{jms}) Q_{km} + D_{ij}^{RR}(2\delta_{ij} Q_{ps} - \delta_{js} Q_{ip} - \delta_{jp} Q_{is}) = 0,$$

$$n_i\left[\frac{U_0}{5}\left(\alpha_{qpsi} - \frac{5}{3}\delta_{ps}\delta_{qi}\right) m_q + M_{ij}^{UF} F_j^{ext} Q_{ps} - D_{ij}^{TT}\frac{\partial Q_{ps}}{\partial x_j}\right.$$

$$\left. + D_{ij}^{TR}(\epsilon_{jkp} Q_{sk} + \epsilon_{jks} Q_{pk})\right] = 0, r = R_c, \tag{6.58}$$

$$Q_{ps} \sim 0, r \to \infty, \tag{6.59}$$

where the diffusivities and mobilities will differ for fixed-force or fixed velocity probe motion. In this dissertation it is assumed that we can apply an external torque to prevent the probe from rotating, as this allows us to circumvent the formalism associated with writing the Smoluchowski equation in a coordinate frame that rotates with the Brownian fluctuations of the probe. This is a relatively simple problem in 2-D (there is only relative angle to consider), but becomes more complicated in

3-D. For a more detailed discussion, see Chapter 4. The external torque required to prevent the probe from rotating is

$$\boldsymbol{L}^{ext} = -(\boldsymbol{M}_{\mathbf{11}}^{\boldsymbol{\Omega L}})^{-1} \cdot [\boldsymbol{M}_{\mathbf{11}}^{\boldsymbol{\Omega F}} \cdot \boldsymbol{F}^{ext} + (\boldsymbol{D}_{\mathbf{11}}^{\boldsymbol{RT}} - \boldsymbol{D}_{\mathbf{12}}^{\boldsymbol{RT}}) \cdot \nabla_r \ln P - \boldsymbol{D}_{\mathbf{12}}^{\boldsymbol{RR}} \cdot \nabla_R \ln P], \tag{6.60}$$

which will affect the diffusivity and mobility tensors used in the field equations.

Fixed-force

We again make use of the linearity of Stokes flow to pose a microrheology problem where the probe does not rotate, but its translational velocity may fluctuate due to collisions with the bath particles. The effective mobility and diffusivity tensors for the Smoluchowski equation are thus

$$\boldsymbol{M}^{\boldsymbol{UF}} = [\boldsymbol{M}_{\mathbf{21}}^{\boldsymbol{UF}} - \boldsymbol{M}_{\mathbf{11}}^{\boldsymbol{UF}} - (\boldsymbol{M}_{\mathbf{21}}^{\boldsymbol{UL}} - \boldsymbol{M}_{\mathbf{11}}^{\boldsymbol{UL}}) \cdot (\boldsymbol{M}_{\mathbf{11}}^{\boldsymbol{\Omega L}})^{-1} \cdot \boldsymbol{M}_{\mathbf{11}}^{\boldsymbol{\Omega F}}], \tag{6.61}$$

$$\boldsymbol{M}^{\boldsymbol{\Omega F}} = [\boldsymbol{M}_{\mathbf{21}}^{\boldsymbol{\Omega F}} - \boldsymbol{M}_{\mathbf{21}}^{\boldsymbol{\Omega L}} \cdot (\boldsymbol{M}_{\mathbf{11}}^{\boldsymbol{\Omega L}})^{-1} \cdot \boldsymbol{M}_{\mathbf{11}}^{\boldsymbol{\Omega F}}], \tag{6.62}$$

$$\boldsymbol{D}^{\boldsymbol{TR}} = (\boldsymbol{D}_{\mathbf{22}}^{\boldsymbol{TR}} - \boldsymbol{D}_{\mathbf{12}}^{\boldsymbol{TR}}) - (\boldsymbol{M}_{\mathbf{21}}^{\boldsymbol{UL}} - \boldsymbol{M}_{\mathbf{11}}^{\boldsymbol{UL}}) \cdot (\boldsymbol{M}_{\mathbf{11}}^{\boldsymbol{\Omega L}})^{-1} \cdot \boldsymbol{D}_{\mathbf{12}}^{\boldsymbol{RR}}, \tag{6.63}$$

$$\boldsymbol{D}^{\boldsymbol{RT}} = (\boldsymbol{D}_{\mathbf{22}}^{\boldsymbol{RT}} - \boldsymbol{D}_{\mathbf{21}}^{\boldsymbol{RT}}) - \boldsymbol{M}_{\mathbf{21}}^{\boldsymbol{\Omega L}} \cdot (\boldsymbol{M}_{\mathbf{11}}^{\boldsymbol{\Omega L}})^{-1} \cdot (\boldsymbol{D}_{\mathbf{11}}^{\boldsymbol{RT}} - \boldsymbol{D}_{\mathbf{12}}^{\boldsymbol{RT}}), \tag{6.64}$$

$$\begin{aligned}\boldsymbol{D}^{\boldsymbol{TT}} &= (\boldsymbol{D}_{\mathbf{22}}^{\boldsymbol{TT}} + \boldsymbol{D}_{\mathbf{11}}^{\boldsymbol{TT}} - \boldsymbol{D}_{\mathbf{12}}^{\boldsymbol{TT}} - \boldsymbol{D}_{\mathbf{21}}^{\boldsymbol{TT}}) \\ &\quad + (\boldsymbol{M}_{\mathbf{21}}^{\boldsymbol{UL}} - \boldsymbol{M}_{\mathbf{11}}^{\boldsymbol{UL}}) \cdot (\boldsymbol{M}_{\mathbf{11}}^{\boldsymbol{\Omega L}})^{-1} \cdot (\boldsymbol{D}_{\mathbf{11}}^{\boldsymbol{RT}} - \boldsymbol{D}_{\mathbf{12}}^{\boldsymbol{RT}}),\end{aligned} \tag{6.65}$$

$$\boldsymbol{D}^{\boldsymbol{RR}} = \boldsymbol{D}_{\mathbf{22}}^{\boldsymbol{RR}} - \boldsymbol{M}_{\mathbf{21}}^{\boldsymbol{\Omega L}} \cdot (\boldsymbol{M}_{\mathbf{11}}^{\boldsymbol{\Omega L}})^{-1} \cdot \boldsymbol{D}_{\mathbf{12}}^{\boldsymbol{RR}}; \tag{6.66}$$

note that $\boldsymbol{D}^{\boldsymbol{RT}} = (\boldsymbol{D}^{\boldsymbol{TR}})^{\dagger}$. The mobility functions—as defined previously— are

$$x^a = \frac{x_{22}^a + \beta x_{11}^a}{1+\beta} - \frac{4\beta x_{12}^a}{(1+\beta)^2}, \tag{6.67}$$

$$y^a = \frac{y_{22}^a + \beta y_{11}^a}{1+\beta} - \frac{4\beta y_{12}^a}{(1+\beta)^2} - \frac{48\beta}{(1+\beta)^5} \frac{\left(y_{21}^b - \frac{(1+\beta)^2}{4} y_{11}^b\right)^2}{y_{11}^c}, \tag{6.68}$$

$$y^b = \left(y_{22}^b - \frac{4\beta^2}{(1+\beta)^2} y_{12}^b\right)\left(1 - \frac{8}{(1+\beta)^3} \frac{y_{12}^c}{y_{11}^c}\right), \tag{6.69}$$

$$x^c = x_{22}^c - \frac{64\beta^3}{(1+\beta)^6} \frac{(x_{21}^c)^2}{x_{11}^c}, \tag{6.70}$$

$$y^c = y^c_{22} - \frac{64\beta^3}{(1+\beta)^6}\frac{(y^c_{21})^2}{y^c_{11}}, \tag{6.71}$$

$$\tilde{x}^a_{21} = \left(\frac{2\beta}{(1+\beta)^2}x^a_{12} - x^a_{11}\right), \tag{6.72}$$

$$\tilde{y}^a_{21} = \left(\frac{2\beta}{(1+\beta)^2}y^a_{21} - y^a_{11}\right) - \frac{3\beta}{(1+\beta)^3}\frac{y^b_{11}}{y^c_{11}}\left(y^b_{21} - \frac{(1+\beta)^2}{4}y^b_{11}\right), \tag{6.73}$$

$$\tilde{y}^b_{21} = y^b_{21} - \frac{2y^c_{21}y^b_{11}}{(1+\beta)y^c_{11}}, \tag{6.74}$$

where we have defined $\tilde{y}^b_{21}$, $\tilde{x}^a_{21}$, and $\tilde{y}^a_{21}$ as the composite mobility functions for the terms linear in $\boldsymbol{F^{ext}}$: $\boldsymbol{M^{UF}} = \tilde{x}^a_{21}\boldsymbol{nn} + \tilde{y}^a_{21}(\boldsymbol{I} - \boldsymbol{nn})$, $\boldsymbol{M^{\Omega F}} = \tilde{y}^b_{21}\boldsymbol{\epsilon}\cdot\boldsymbol{n}$.

The average speed of the probe particle under the action of $\boldsymbol{F^{ext}}$, $\boldsymbol{L^{ext}}$ is

$$\begin{aligned}\langle \boldsymbol{U^{probe}}\rangle \;=\; & \int [\boldsymbol{M^{UF}_{11}} - \boldsymbol{M^{UL}_{11}}\cdot(\boldsymbol{M^{\Omega L}_{11}})^{-1}\cdot\boldsymbol{M^{\Omega F}_{11}}]\cdot\boldsymbol{F^{ext}} n\, dV \\ & - \int \nabla\cdot[\boldsymbol{D^{TT}_{11}} - \boldsymbol{D^{TT}_{12}} + \boldsymbol{M^{UL}_{11}}\cdot(\boldsymbol{M^{\Omega L}_{11}})^{-1}\cdot(\boldsymbol{D^{RT}_{11}} - \boldsymbol{D^{RT}_{12}})] n\, dV \\ & + \int \boldsymbol{n}\cdot[\boldsymbol{D^{TT}_{11}} - \boldsymbol{D^{TT}_{12}} + \boldsymbol{M^{UL}_{11}}\cdot(\boldsymbol{M^{\Omega L}_{11}})^{-1}\cdot(\boldsymbol{D^{RT}_{11}} - \boldsymbol{D^{RT}_{12}})] n\, dS,\end{aligned} \tag{6.75}$$

where each line reflects the hydrodynamic, Brownian, and interparticle contributions to the velocity, respectively. The term in the second integral—the divergence of the effective probe diffusivity—gives a scalar function similar to Batchelor's $W(r)$ for passive colloidal suspensions [13]. For spherical particles, the interparticle velocity is determined only by $\boldsymbol{D^{TT}_{11}}$.

Fixed-velocity

When the probe moves with a fixed speed, one can derive the required force $\boldsymbol{F^{ext}}$ (and torque $\boldsymbol{L^{ext}}$) such that $\boldsymbol{U^{probe}}$ remains constant in the flux expressions:

$$\begin{aligned}\boldsymbol{F^{ext}} = & [\boldsymbol{M^{UF}_{11}} - \boldsymbol{M^{UL}_{11}}\cdot(\boldsymbol{M^{\Omega L}_{11}})^{-1}\cdot\boldsymbol{M^{\Omega F}_{11}}]^{-1}\cdot\{\boldsymbol{U^{probe}} \\ & -[(\boldsymbol{D^{TT}_{12}} - \boldsymbol{D^{TT}_{11}}) + \boldsymbol{M^{UL}_{11}}\cdot(\boldsymbol{M^{\Omega L}_{11}})^{-1}\cdot(\boldsymbol{D^{RT}_{11}} - \boldsymbol{D^{RT}_{12}})]\cdot\nabla_r \ln P \\ & -[\boldsymbol{D^{TR}_{12}} - \boldsymbol{M^{UL}_{11}}\cdot(\boldsymbol{M^{\Omega L}_{11}})^{-1}\cdot\boldsymbol{D^{RR}_{12}}]\cdot\nabla_R \ln P\}.\end{aligned} \tag{6.76}$$

The problem of the fixed spherical cavity in the previous section is simply a special case of the fixed-velocity microrheology problem where $\boldsymbol{U^{probe}} = 0$. Indeed the diffusivity tensors in this problem will be identical to those derived in the previous

section. The mobility functions for the terms linear in $\boldsymbol{F^{ext}}$ are

$$\tilde{x}^a_{21} = \left(\frac{2}{(1+\beta)}\frac{x^a_{21}}{x^a_{11}} - 1\right), \tag{6.77}$$

$$\tilde{y}^a_{21} = \frac{\left[y^c_{11}\left(\frac{2}{(1+\beta)}y^a_{21} - y^a_{11}\right) - \frac{y^b_{11}}{3}\left(\frac{4}{(1+\beta)}y^b_{21} - y^b_{11}\right)\right]}{y^a_{11}y^c_{11} - 3(y^b_{11})^2}, \tag{6.78}$$

$$\tilde{y}^b_{21} = \frac{y^b_{21}y^c_{11} + \frac{2}{(1+\beta)}y^c_{21}y^b_{11}}{y^a_{11}y^c_{11} - 3(y^b_{11})^2}. \tag{6.79}$$

We previously defined the average force on the probe—the quantity of interest in the fixed-velocity microrheology problem—in the absence of probe motion. When the probe moves with a prescribed speed $\boldsymbol{U^{probe}}$ the average force is precisely the same, with the additional hydrodynamic contribution

$$\langle \boldsymbol{F^{ext}} \rangle^H = \int [\boldsymbol{M^{UF}_{11}} - \boldsymbol{M^{UL}_{11}} \cdot (\boldsymbol{M^{\Omega L}_{11}})^{-1} \cdot \boldsymbol{M^{\Omega F}_{11}}]^{-1} \cdot \boldsymbol{U^{probe}} n \, dV. \tag{6.80}$$

6.4 Anisotropic particles

While some biological swimmers are spherical (e.g. *Volvox*), the majority of them are anisotropic. *E. Coli* and *B. subtilis* are both prolate spheroids, and many species of hydrozoan jellyfish have an oblate spheroidal medusa.[1] We consider the interactions between a spherical probe and an axisymmetric (spheroidal) swimmer. The isolated Stokes-Einstein-Sutherland diffusivities of the swimmers are now

$$\boldsymbol{D^{TT}} = D^{TT}[k^T_{\parallel}\boldsymbol{qq} + k^T_{\perp}(\boldsymbol{I} - \boldsymbol{qq})], \tag{6.81}$$

$$\boldsymbol{D^{RR}} = D^{RR}[k^R_{\parallel}\boldsymbol{qq} + k^R_{\perp}(\boldsymbol{I} - \boldsymbol{qq})], \tag{6.82}$$

and $\boldsymbol{D^{RT}} = (\boldsymbol{D^{TR}})^{\dagger} = 0$, where $D^{TT} = k_BT/3\pi\eta d$ and $D^{RR} = k_BT/\pi\eta d^3$ are the Stokes-Einstein-Sutherland diffusivities based on the diameter $d = 2a$ of the swimmer. The mobility functions $k_{\parallel}, k_{\perp}$ are functions of the swimmers length-to-diameter ratio—the aspect ratio—$\xi = L/d$ only [20]:

[1] Though most jellyfish are too large to be analyzed in the Stokes-flow regime, hydrozoan species can be much smaller, reaching only a few hundred microns in size [19].

$$k_{\parallel}^{T} = \frac{3}{4}\left(\frac{2\nu\xi^2 - \nu - \xi}{\xi^2 - 1}\right), \tag{6.83}$$

$$k_{\perp}^{T} = \frac{3}{8}\left(\frac{2\nu\xi^2 - 3\nu + \xi}{\xi^2 - 1}\right), \tag{6.84}$$

$$k_{\parallel}^{R} = \frac{3}{2}\left(\frac{\xi - \nu}{\xi^2 - 1}\right), \tag{6.85}$$

$$k_{\perp}^{R} = \frac{3}{2}\left(\frac{2\nu\xi^2 - 3\nu + \xi}{\xi^4 - 1}\right), \tag{6.86}$$

$$\nu = \begin{cases} \dfrac{\cosh^{-1}\xi}{\sqrt{\xi^2 - 1}}, & \xi > 1, \\ \dfrac{\cos^{-1}\xi}{\sqrt{1 - \xi^2}}, & \xi < 1, \end{cases} \tag{6.87}$$

where all functions are unity when $\xi = 1$.

These are the single-particle contributions to the mobility functions, and clearly do not represent the $\boldsymbol{q}$ dependent interactions between the swimmer and probe. In general, the grand mobility tensor would still be comprised of (anti)symmetric second-order tensors based on both $\boldsymbol{q}$ and $\boldsymbol{n}$—for example, $f(r)(\boldsymbol{qn} + \boldsymbol{nq})$. Indeed one would expect the mobility associated with the active hydrodynamic stress to also have some dependence on $\boldsymbol{q}$. These terms are not known analytically in Stokes flow, though in principal one could find them using the method of reflections with the singularity system for a sphere and an ellipsoid [2]. In this thesis we assume that the mobility functions are independent of the particle orientations $\boldsymbol{q}_\alpha$.

For simplicity, we consider the problem where the swimmers are small compared to the probe $a/R \ll 1$. One can show that the relative diffusivities simply become those for an isolated spheroidal swimmer in an infinite Newtonian fluid, and that the advective velocity of the swimmer relative to the probe is simply given by Stokes flow outside a translating sphere—the swimmer is a tracer particle [21]. DePuit and Squires have used this approach to compute the microviscosity in suspensions of slender, Brownian ellipsoids [22], but thus far, no investigations have systematically investigated the role of shape or hydrodynamic interactions in this problem.

Given the traceless definition of the nematic order $\boldsymbol{Q}$, it will prove more useful to write the diffusivity in terms of isotropic and traceless components

$$\boldsymbol{D}^{\boldsymbol{TT}} = \bar{D}\boldsymbol{I} + \Delta D(\boldsymbol{qq} - \boldsymbol{I}/3), \tag{6.88}$$

where $\bar{D} = D^{TT}(k_{\parallel}^{T} + 2k_{\perp}^{T})/3$ and $\Delta D = D^{TT}(k_{\parallel}^{T} - k_{\perp}^{T})$. The same decomposition may be applied to the rotary diffusivity, but only the perpendicular portion of this diffusivity affects the angular velocity of the swimmer by symmetry [20, 23]. This is *not* necessarily true when the swimmers have finite size and/or the axisymmetry of the problem is broken. When the size of the swimmers affects the hydrodynamic interactions, one can imagine a scenario where $|\boldsymbol{q}\cdot\boldsymbol{n}| = f(\phi)$, where ϕ is the azimuthal spatial coordinate. In this case, the fluid velocity disturbance arising from a rotation of the swimmer about its axis may not be axisymmetric with respect to the probe normal $\boldsymbol{n}$.

When one appropriately modifies the expressions for the translational and rotational fluxes, the governing equations are

$$\frac{\partial}{\partial x_i}\left[U_0 m_i - u_i^{Stokes} n - \bar{D}\frac{\partial n}{\partial x_i} - \Delta D\frac{\partial Q_{ij}}{\partial x_j}\right] = 0, \tag{6.89}$$

$$\begin{aligned}\frac{\partial}{\partial x_i}\Bigg[&U_0\Big(Q_{pi} + \frac{1}{3}\delta_{pi}n\Big) - u_i^{Stokes} m_p - \Big(\bar{D} - \frac{2}{15}\Delta D\Big)\frac{\partial m_p}{\partial x_i} + \frac{\Delta D}{5}\Big(\frac{\partial m_i}{\partial x_p} + \delta_{ip}\frac{\partial m_j}{\partial x_j}\Big)\Bigg]\\ &+ m_i\Omega_{ip}^{Stokes} - \frac{3}{5}Bm_iE_{ip}^{Stokes} + 2D^{RR}k_{\perp}^{R}m_p = 0,\end{aligned} \tag{6.90}$$

$$\begin{aligned}\frac{\partial}{\partial x_i}\Bigg[&\frac{U_0}{5}\Big(\alpha_{qpsi} - \frac{5}{3}\delta_{ps}\delta_{qi}\Big)m_q - u_i^{Stokes}Q_{ps} - \Big(\bar{D} - \frac{4\Delta D}{21}\Big)\frac{\partial Q_{ps}}{\partial x_j}\\ &-\frac{\Delta D}{45}\Big(3\delta_{ip}\delta_{js} + 3\delta_{is}\delta_{jp} - 2\delta_{ij}\delta_{sp}\Big)\frac{\partial n}{\partial x_j} - \frac{\Delta D}{21}\frac{\partial}{\partial x_j}\Big(3\delta_{ip}Q_{js} + 3\delta_{is}Q_{jp}\\ &+3\delta_{jp}Q_{is} + 3\delta_{js}Q_{ip} - 4\delta_{ps}Q_{ij}\Big)\Bigg] + 6D^{RR}k_{\perp}^{R}Q_{ps} - (Q_{pi}\Omega_{is}^{Stokes} - Q_{si}\Omega_{ip}^{Stokes})\\ &+B\Big(-\frac{2}{5}E_{ps}^{Stokes}n - \frac{3}{7}(Q_{pj}E_{js}^{Stokes} + E_{pj}^{Stokes}Q_{js}) + \frac{2}{7}\delta_{ps}E_{ij}^{Stokes}Q_{ij}\Big) = 0,\end{aligned} \tag{6.91}$$

where

$$u_i^{Stokes} = U_j^{probe}\left[\delta_{ij} - \frac{3}{4}\Big(\frac{\delta_{ij}}{r} + \frac{x_ix_j}{r^3}\Big) - \frac{1}{4}\Big(\frac{\delta_{ij}}{r^3} - 3\frac{x_ix_j}{r^5}\Big)\right], \tag{6.92}$$

$$\Omega_{ip}^{Stokes} = \frac{1}{2}\Big(\frac{\partial u_p^{Stokes}}{\partial x_i} - \frac{\partial u_i^{Stokes}}{\partial x_p}\Big) \qquad E_{ip}^{Stokes} = \frac{1}{2}\Big(\frac{\partial u_i^{Stokes}}{\partial x_p} + \frac{\partial u_p^{Stokes}}{\partial x_i}\Big),$$

characterize the velocity field for a translating sphere in Stokes flow. The Bretherton constant $B = (\xi^2 - 1)/(\xi^2 + 1)$ determines how the particle is aligned by the strain component of the velocity field [24, 25].

For the reader more familiar with nematic liquid crystals, many of the terms proportional to ΔD are reminiscent of terms associated with the excess free energy density of a liquid crystal. The "splay" of the active suspension appears in the polar order equation:

$$\frac{\Delta D}{5}\Big(\frac{\partial m_i}{\partial x_p} + \delta_{ip}\frac{\partial m_j}{\partial x_j}\Big), \tag{6.93}$$

and terms related to the "bending" of the nematic order appears in the concentration field as $\Delta D \nabla \cdot \boldsymbol{Q}$ and in the nematic order field as

$$\begin{aligned}\frac{\Delta D}{45}\Big(3\delta_{ip}\delta_{js} + 3\delta_{is}\delta_{jp} - 2\delta_{ij}\delta_{sp}\Big)\frac{\partial n}{\partial x_j} + \frac{\Delta D}{21}\frac{\partial}{\partial x_j}\Big(3\delta_{ip}Q_{js} + 3\delta_{is}Q_{jp} \\ +3\delta_{jp}Q_{is} + 3\delta_{js}Q_{ip} - 4\delta_{ps}Q_{ij}\Big).\end{aligned} \tag{6.94}$$

Because the particles are spheroidal and the problem is axisymmetric, the twist $(\boldsymbol{q} \cdot \nabla \times \boldsymbol{q})$ is zero.

Many active matter experiments are conducted at an interface (e.g. an air-water or oil-water interface, or the bottom of a container), and thus the particle dynamics are confined to two dimensions. Though there is not solution to Stokes equations in 2-D, one could imagine that there are still fully three-dimensional fluid flows associated with the swimmers' motion, even if they only move in a plane. In this spirit, we can also write down these governing equations for the case of swimmers moving in a plane, but the probe still creating the full 3-D fluid disturbance:

$$\frac{\partial}{\partial x_i}\left[U_0 m_i - u_i^{Stokes} n - \bar{D}\frac{\partial n}{\partial x_i} - \Delta D\frac{\partial Q_{ij}}{\partial x_j}\right] = 0, \tag{6.95}$$

$$\begin{aligned}\frac{\partial}{\partial x_i}\left[U_0\Big(Q_{pi} + \frac{1}{2}\delta_{pi}n\Big) - u_i^{Stokes} m_p - \Big(\bar{D} - \frac{1}{2}\Delta D\Big)\frac{\partial m_p}{\partial x_i} + \frac{\Delta D}{4}\Big(\frac{\partial m_i}{\partial x_p} + \delta_{ip}\frac{\partial m_j}{\partial x_j}\Big)\right] \\ +m_i\Omega_{ip}^{Stokes} - \frac{B}{2}m_i E_{ip}^{Stokes} + D^{RR}k_\perp^R m_p = 0,\end{aligned} \tag{6.96}$$

$$\begin{aligned}\frac{\partial}{\partial x_i}\Bigg[\frac{U_0}{4}\Big(\alpha_{qpsi} - 2\delta_{ps}\delta_{qi}\Big)m_q - u_i^{Stokes}Q_{ps} - \Big(\bar{D} - \frac{\Delta D}{3}\Big)\frac{\partial Q_{ps}}{\partial x_j} \\ -\frac{\Delta D}{8}\Big(\delta_{ip}\delta_{js} + \delta_{is}\delta_{jp} - \delta_{ij}\delta_{sp}\Big)\frac{\partial n}{\partial x_j} - \frac{\Delta D}{6}\frac{\partial}{\partial x_j}\Big(\delta_{ip}Q_{js} + \delta_{is}Q_{jp} \\ +\delta_{jp}Q_{is} + \delta_{js}Q_{ip} - 2\delta_{ps}Q_{ij}\Big)\Bigg] + 4D^{RR}k_\perp^R Q_{ps} - (Q_{pi}\Omega_{is}^{Stokes} - Q_{si}\Omega_{ip}^{Stokes}) \\ +B\Big(-\frac{1}{2}E_{ps}^{Stokes}\,n - \frac{1}{3}(Q_{pj}E_{js}^{Stokes} + E_{pj}^{Stokes}Q_{js}) + \frac{1}{3}\delta_{ps}E_{ij}^{Stokes}Q_{ij}\Big) = 0.\end{aligned} \tag{6.97}$$

One could achieve this experimentally by, for example, creating a fluid-fluid interface between fluids of the same viscosity, but drastically different densities. Particles density-matched to the denser fluid would settle to the interface. It is crucial that one still require $\partial u_i/\partial x_i = 0$ and $E_{ii}^{Stokes} = 0$ when implementing this scheme.

No-flux conditions

The no-flux boundary condition is complicated by the asphericity of the swimmers. Nitsche and Brenner [26] give the abstract no-flux condition for particles of arbitrary shape:

$$(\nabla_r S) \cdot \boldsymbol{j}^T + (\nabla_q S) \cdot \boldsymbol{j}^R = 0, \tag{6.98}$$

where S is the hypersurface that defines particle contacts in position and orientation space. This has been applied to problems of active fibers confined in an infinitely long channel [27], where the contact surface $S(\boldsymbol{r}, \boldsymbol{q})$ is simply parametrized by the distance from the wall z and the orientation angle of the (2-D) swimmer θ.

In three dimensions, the unit normal of this surface is more complex:

$$\nabla_r S = \boldsymbol{n} \cdot \Big(\boldsymbol{I} - (d/2)[\xi\, \boldsymbol{qq} + (\boldsymbol{I} - \boldsymbol{qq})] \Big) \tag{6.99}$$

$$\nabla_q S = \Big((L - d) + \frac{1}{4}(d^2 - L^2) \Big) [\boldsymbol{q}(\boldsymbol{n} \cdot \boldsymbol{q})^2 - \boldsymbol{n}(\boldsymbol{q} \cdot \boldsymbol{n})], \tag{6.100}$$

and the point of contact is

$$R_c = R(1 + \Delta) + (L/2)\boldsymbol{n} \cdot \boldsymbol{q} + (d/2)\sqrt{\boldsymbol{nn} : (\boldsymbol{I} - \boldsymbol{qq})}. \tag{6.101}$$

For simplicity, it is often assumed that the contact surface is itself spheroidal, so that the problem may be written in prolate or oblate spheroidal coordinates [28, 29]. In the limit of point swimmers one can approximate this by the conventional no-flux condition $\boldsymbol{n} \cdot \boldsymbol{j}^{\boldsymbol{T}} = 0$ with corrections $\sim O(L/R(1 + \Delta))$ or $O(d/R(1 + \Delta))$—the swimmers rotate freely at contact. The anisotropy of the translational diffusion still has an impact on the translational flux at the boundary through the coupling of n, $\boldsymbol{m}$, and $\boldsymbol{Q}$.

BIBLIOGRAPHY

[1]S. C. Takatori, W. Yan, and J. F. Brady, "Swim pressure: Stress generation in active matter", Phys. Rev. Lett. **113**, 1–5 (2014).

[2]S. Kim, and S. J. Karilla, *Microhydrodynamics : Principles and Selected Applications* (1991).

[3]W. B. Russel, "The Huggins coefficient as a means for characterizing suspended particles", J. Chem. Soc. Faraday Trans. 2 Mol. Chem. Phys. **80**, 31 (1984).

[4]D. Saintillan, and M. J. Shelley, "Theory of Active Suspensions", in *Complex fluids biol. syst.* Edited by S. Spagnolie, (Springer, New York, 2015) Chap. 9, pp. 319–355.

[5]D. Saintillan, and M. J. Shelley, "Active suspensions and their nonlinear models", Comptes Rendus Phys. **14**, 497–517 (2013).

[6]W. Yan, and J. F. Brady, "The force on a body in active matter", J. Fluid Mech. **6**, 1–11 (2015).

[7]J. W. Swan, and J. F. Brady, "Simulation of hydrodynamically interacting particles near a no-slip boundary", Phys. Fluids **19** (2011) 10.1063/1.2803837.

[8]B. Cichocki, R. B. Jones, R. Kutteh, and E. Wajnryb, "Friction and mobility for colloidal spheres in Stokes flow near a boundary: The multipole method and applications", J. Chem. Phys. **112**, 2548–2561 (2000).

[9]B. Cichocki, and R. B. Jones, "Image representation of a spherical particle near a hard wall", Phys. A Stat. Mech. its Appl. **258**, 273–302 (1998).

[10]G. S. Perkins, and R. B. Jones, "Hydrodynamic interaction of a spherical particle with a planar boundary I. Free surface", Phys. A Stat. Mech. its Appl. **171**, 575–604 (1991).

[11]A. J. Goldman, R. G. Cox, and H. Brenner, "Slow viscous motion of a sphere parallel to a plane wall—I Motion through a quiescent fluid", Chem. Eng. Sci. **22**, 637–651 (1967).

[12]G. Bossis, A. Meunier, and J. D. Sherwood, "Stokesian dynamics simulations of particle trajectories near a plane", Phys. Fluids A Fluid Dyn. **3**, 1853–1858 (1991).

[13]G. K. Batchelor, "Sedimentation in a dilute polydisperse system of interacting spheres. Part 1. General theory", J. Fluid Mech. **119**, 379 (1982).

[14]D. J. Jeffrey, and Y. Onishi, "Calculation of the resistance and mobility functions for two unequal rigid spheres in low-Reynolds-number flow", J. Fluid Mech. **139**, 261 (1984).

[15]G. Jeffrey, "On the steady motion of a solid of revolution in a viscous fluid", Proc. London Math. Soc. **2**, 327–338 (1915).

[16]T. Ishikawa, M. P. Simmonds, and T. J. Pedley, *Hydrodynamic interaction of two swimming model micro-organisms*, Vol. 568 (2006), p. 119.

[17]T. M. Squires, and J. F. Brady, "A simple paradigm for active and nonlinear microrheology", Phys. Fluids **17**, 1–21 (2005).

[18]J. F. Brady, "Particle motion driven by solute gradients with application to autonomous motion: continuum and colloidal perspectives", J. Fluid Mech. **667**, 216–259 (2011).

[19]S. P. Colin, and J. H. Costello, "Morphology, swimming performance and propulsive mode of six co-occurring hydromedusae.", J. Exp. Biol. **205**, 427–437 (2002).

[20]H. Brenner, "Rheology of a dilute suspension of axisymmetric Brownian particles", Int. J. Multiph. Flow **1**, 195–341 (1974).

[21]N. J. Hoh, "Effects of Particle Size Ratio on Single Particle Motion in Colloidal Dispersions", PhD thesis (California Institute of Technology, 2013).

[22]R. J. Depuit, and T. M. Squires, "Micro-macro-discrepancies in nonlinear microrheology: I. Quantifying mechanisms in a suspension of Brownian ellipsoids", J. Phys. Condens. Matter **24** (2012).

[23]J. K. G. Dhont, "Fundamental Equations of Motion", in *An introd. to dyn. colloids*, 1st ed. (Elsevier, 1996) Chap. 4, pp. 172–195.

[24]G. Jeffrey, "The motion of ellipsoidal particles immersed in a viscous fluid", Proc. R. Soc. A Math. Phys. Eng. Sci. **102**, 161–179 (1922).

[25]F. Bretherton, "The motion of rigid particles i n a shear flow at low Reynolds number", J. Fluid Mech., 284–304 (1962).

[26]J. M. Nitsche, and H. Brenner, "On the formulation of boundary conditions for rigid nonspherical Brownian particles near solid walls: Applications to orientation-specific reactions with immobilized enzymes", J. Colloid Interface Sci. **138**, 21–41 (1990).

[27]B. Ezhilan, and D. Saintillan, "Transport of a dilute active suspension in pressure-driven channel flow", J. Fluid Mech. **777**, 482–522 (2015).

[28]A. S. Khair, and J. F. Brady, "Microrheology of colloidal dispersions: Shape matters", J. Rheol. (N. Y. N. Y). **52**, 165 (2008).

[29]M. Gruber, "Active microrheology of ellipsoidal probes", 2017.

Chapter 7

FORCE ON A BOUNDARY: THE OSMOTIC PRESSURE

[1]E. W. Burkholder, and J. F. Brady, "Do hydrodynamic interactions affect the swim pressure?", Soft Matter **14**, 3581–3589 (2018),

Active matter systems—from chemically driven nanoparticles to crawling amoebas to humans crossing the street—share the ability to move autonomously. This autonomous motion can arise spontaneously or it may be in response to environmental influences, e.g. going towards food, light, or other organisms, and is inherently non-equilibrium. Such self-propulsion can result in fascinating dynamical and mechanical behavior such as spontaneous phase-separation [1–5] and apparent negative shear viscosities [6–9].

Despite the complexities of active systems, the minimal active Brownian particle (ABP) model has been successful in describing behaviors observed in real systems [1, 4, 5, 9–11]. ABPs move with a swim velocity $\boldsymbol{U}_0$, randomly reorient on a time scale τ_R, and are generally taken to be non-interacting. Historically, the ABP model has neglected hydrodynamic interactions (HI); this is often referred to as "dry" active matter [12]. Studies of HI among swimmers are minimal, and to-date, have primarily focused on their effect on shear rheology and diffusivity in suspensions of squirmers [7, 13–15], a notable exception is the work of Fielding [16] on the phase behavior in 2-D. No investigations have been made as to the effect of HI on the pressure in active systems.

Active motion is mechanically described by the swim force $\boldsymbol{F}^{swim}$—a stochastic, internal body force that a swimmer exerts on its embedding medium (or substrate) to propel itself [4, 17]. The mechanical stress associated with this active motion is $\boldsymbol{\sigma}^{swim} = -n\, sym\langle \boldsymbol{x}\boldsymbol{F}^{swim'}\rangle$, where n is the number density of swimmers, $\boldsymbol{x}$ is the particle position, the angle brackets represent a suspension average and sym refers to the symmetric part of the tensor. Here, $\boldsymbol{F}^{swim'} = \boldsymbol{F}^{swim} - \langle \boldsymbol{F}^{swim}\rangle$; the average swim force (which is proportional to the polar order) must be removed from the definition of the swim stress; only fluctuations in the force contribute to the stress. This swim stress is distinct from the hydrodynamic active particle stress arising from the dipolar (stresslet) velocity disturbance a swimmer creates due to its

force-free motion through the medium [7, 18–21]: $\boldsymbol{\sigma}^H = \sigma_0(3\boldsymbol{qq} - \boldsymbol{I})$, where σ_0 is proportional to the swimmer's force dipole, $\boldsymbol{q}$ is the direction of swimming and $\boldsymbol{I}$ is the isotopic tensor. This hydrodynamic active particle stress is traceless and does not contribute to the pressure. Takatori et al. [22] measured a substantially increased particle pressure in suspensions of Janus particles, which resulted from the swim pressure: $\Pi^{swim} = -tr(\boldsymbol{\sigma}^{swim})/3$.

The nature—and even the existence—of the swim stress and pressure has been a subject of substantial discussion in recent years. Of particular interest is the validity of the swim pressure as a state function and whether the trace of the swim stress is equivalent to the force per unit area exerted on a confining boundary [23, 24]. For a suspension of spherical, noninteracting ABPs, it has been shown that these two definitions of pressure are equivalent, but for more complex active particles the force per unit area the particles exert on the boundary may differ from the swim pressure in the bulk [23, 25]. It must be remembered, however, that the active particles are immersed in a medium, and the force on the confining boundaries has contributions from both the active particles and the pressure distribution in the embedding medium. That the 'partial' pressure exerted by one component in a two-component mixture can depend on the detailed interactions of that (or the other) component with a boundary should come as no surprise. It does have implications for measuring the particle pressure, however, as we discuss at the end.

7.1 Momentum balance

To see this, consider a suspension of particles between two solid walls in a Newtonian fluid. The motion is at low Reynolds number and therefore at each point in the fluid the divergence of the fluid stress tensor is zero: $\nabla \cdot \boldsymbol{\sigma}_f = 0$. Integrating over the entire fluid volume gives: $\int_L \boldsymbol{n} \cdot \boldsymbol{\sigma}_f dS + \int_R \boldsymbol{n} \cdot \boldsymbol{\sigma}_f dS + \sum \int_\alpha \boldsymbol{n} \cdot \boldsymbol{\sigma}_f dS = 0$, where the first integral is over the left (L) wall, the second over the right (R) wall, and the others over the surfaces of the active particles labeled α. The active particles undergo force-free motion and therefore $\int_\alpha \boldsymbol{n} \cdot \boldsymbol{\sigma}_f dS = 0$ for all particles between the two walls except those particles close enough to the right or left walls to experience an 'external' force from the wall. We can write this force as derivable from a potential, $-\nabla_\alpha V_{L,R}$, depending on the right or left wall. To make matters as simple as possible, which serves to reveal the essential physics, we take this wall-particle force to be a hard-particle, excluded volume, force with an amplitude of $k_B T$ for the

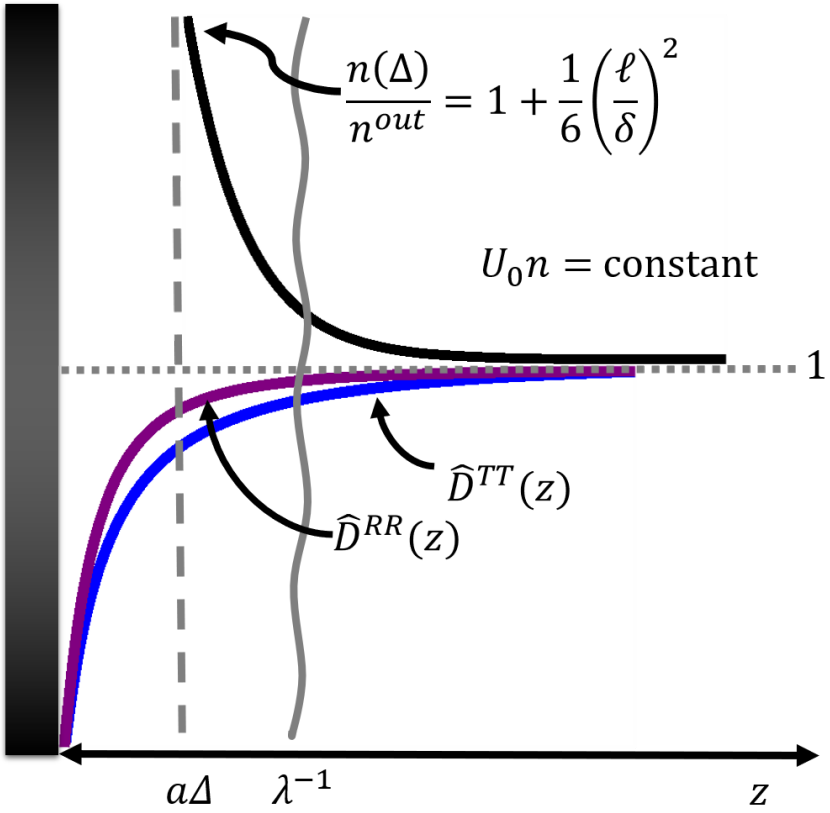

Figure 7.1: Schematic of the active-diffusive boundary-layer (BL) in a 1D geometry. The black line is the concentration profile of swimmers, λ^{-1} is the BL thickness, and $a\Delta$ is where the no-flux condition applies. The dimensionless translational and rotational diffusivities $\hat{D}^{TT}$ and $\hat{D}^{RR}$ are given by the blue (lower) and purple (upper) lines, respectively.

potential, where $k_B T$ is the thermal energy [1]. The hard-particle force projects out the number density in 'contact' with each wall and, allowing for the directions of the two normals, the over all force or momentum balance is

$$p_f^L + n^L k_B T = p_f^R + n^R k_B T, \tag{7.1}$$

where p_f^L is the pressure exerted on the left wall by the fluid ($\int_L \boldsymbol{n} \cdot \boldsymbol{\sigma}_f dS$) and n^L is the particle number density at the left wall, and similarly for the right wall.

The utility of this result is that we do not need to specify where the particles are, how they move, their shape, whether or not they experience a torque from the boundary, etc. In fact, the motion does not have to be a low Reynolds numbers, or even in a fluid; it could be particles crawling through an elastic medium. The macroscopic momentum balance must be satisfied. If, for whatever reason, there

[1] Any amplitude would be fine; choice of $k_B T$ is just helpful in connecting to passive Brownian particles.

are more particles near the wall on the right, then there will be a higher pressure in the fluid at the left wall then at the right wall. For 'passive' particles at steady state the only way for there to be a difference between the concentrations at the two walls is if the walls exert different forces on the particles. For active particles, however, the particles might simply 'like' one wall more than the other and therefore bias their force-free motion towards or away from one wall and consequently generate a compensating pressure distribution in the embedding medium as was shown by Yan & Brady [17].

Rather than speculate on what might make an active particle 'like' or 'dislike' a boundary, a simple model that demonstrates this effect is ABPs that interact hydrodynamically with a solid wall. The hydrodynamic interactions with a wall are the same as for passive Brownian particles [26, 27], and the familiar framework used to analyze suspensions of passive colloidal particles [28, 29] is easily extended to suspensions of active particles with any self-propulsion mechanism; the details are in Chapter 6.

7.2 Model system

Following the work of [25], consider a dispersion of ABPs of size a with fixed swim speed U_0 at number density n^∞ far from the wall in a Newtonian solvent of viscosity η and density ρ. The Reynolds number is small, $Re = \rho U_0 a/\eta \ll 1$, so the hydrodynamic force and torque on each particles is zero and the fluid obeys Stokes' equations. The ABPs are neutral swimmers (or "movers"), and thus exert no dipolar active hydrodynamic stress on the suspension in isolation [2], but are able to self-propel [18]. However, even neutral swimmers are still subject to the influence of hydrodynamic interactions with solid boundaries and other particles, and may thus have an active hydrodynamic stresslet associated with this interaction. We neglect such active hydrodynamic stresses in this chapter, as they do not contribute directly to the force on a boundary. These effects would manifest only as an effective mobility for the swim force, and a change in the reorientation rate (via the vorticity of the swimmer's fluid disturbance reflected off of the probe) in Eqns. 7.3-7.4 below.

We assume a dilute suspension so that the swimmers do not interact with one another; thus, the Smoluchowski equation for a single ABP applies:

$$\frac{\partial P}{\partial t} + \nabla_{\boldsymbol{x}} \cdot \boldsymbol{j}^{\boldsymbol{T}} + \nabla_{\boldsymbol{R}} \cdot \boldsymbol{j}^{\boldsymbol{R}} = 0, \tag{7.2}$$

[2] Michelin and Lauga [30] have shown that Janus particles can be made neutral swimmers by tuning their geometry

where $\nabla_{\boldsymbol{R}} = \boldsymbol{q} \times \boldsymbol{\nabla}_{\boldsymbol{q}}$ and $P(\boldsymbol{x}, \boldsymbol{q}, t)$ is the probability of finding a particle at position $\boldsymbol{x}$ with orientation $\boldsymbol{q}$ at a time t relative to the wall. The translational and rotational fluxes are

$$\boldsymbol{j}^{\boldsymbol{T}} = U_0 \boldsymbol{q} P - \boldsymbol{D}^{\boldsymbol{TT}} \cdot \nabla_{\boldsymbol{x}} P - \boldsymbol{D}^{\boldsymbol{TR}} \cdot \nabla_R P, \tag{7.3}$$

$$\boldsymbol{j}^{\boldsymbol{R}} = -\boldsymbol{D}^{\boldsymbol{RT}} \cdot \nabla_{\boldsymbol{x}} P - (\boldsymbol{D}^{\boldsymbol{RR}} + \tau_R^{-1} \boldsymbol{I}) \cdot \nabla_R P, \tag{7.4}$$

in the absence of external forces/torques and background flow.

The time scale τ_R is associated with active reorientations of the particle, which do not necessarily induce a rotational fluid flow—a spherical swimmer can simply "decide" to change its direction. The translational ($\boldsymbol{D}^{TT}$), rotational ($\boldsymbol{D}^{RR}$) and coupled ($\boldsymbol{D}^{\boldsymbol{RT}} = (\boldsymbol{D}^{\boldsymbol{TR}\dagger})$ diffusivities are independent of $\boldsymbol{q}$ for spherical particles but are functions of the distance z from the solid wall through the Einstein relation between diffusivity and hydrodynamic mobility $\boldsymbol{D} = k_B T \boldsymbol{M}$. For simple geometries such as a sphere near a plane wall or two adjacent spheres, $\boldsymbol{M}$ is known analytically as a function of separation [26, 28].

The swimmer interacts with the system boundary via an excluded-annulus potential which manifests as a no-flux condition at the boundary, $\boldsymbol{n} \cdot \boldsymbol{j}^{\boldsymbol{T}} = 0$, where $\boldsymbol{n}$ is the outward-pointing normal from the boundary (see Fig. 7.1). This potential is characterized by the nondimensional parameter Δ: for $\Delta \to \infty$, the particle remains sufficiently far from the boundary that the hydrodynamic interactions are unimportant and the problem is identical to that of [25]. For $\Delta \to 0$ the swimmer is allowed to come very close to the boundary and hydrodynamic lubrication interactions dominate. We solve (7.2) using the moments expansion method (i) without nematic order: $\langle \boldsymbol{qq} \rangle = \boldsymbol{I}/3$, and (ii) with nematic order with third moment given by $\langle \boldsymbol{qqq} \rangle = \langle \boldsymbol{\alpha} \cdot \boldsymbol{q} \rangle / 5$, where $\boldsymbol{\alpha}$ is the fourth-order isotropic tensor [25, 31]. Details may be found in Chapter 6. The equations were solved using the MATLAB boundary-value solver `bvp4c` to a relative error tolerance of 10^{-5}.

7.3 Flat plate

Consider first the problem of an ABP near an infinite flat plate as illustrated in Fig. 7.1. As shown by Yan & Brady [25] in the absence of HI ($\Delta \to \infty$), there is an accumulation boundary-layer at the no-flux surface where advective swimming, $U_0 \boldsymbol{q} P$, balances Brownian diffusion, $-D^{TT} \nabla P$. The resulting concentration profile is $n(z) \equiv \int P(z, \boldsymbol{q}) d\boldsymbol{q} = n^{\infty}(1 + \frac{1}{6}(\frac{\ell}{\delta})^2 e^{-\lambda(z - a(1+\Delta))})$, where z is measured from the no-slip surface. Here, n^{∞} is the uniform concentration far from the boundary, $\ell = U_0 \tau_R$

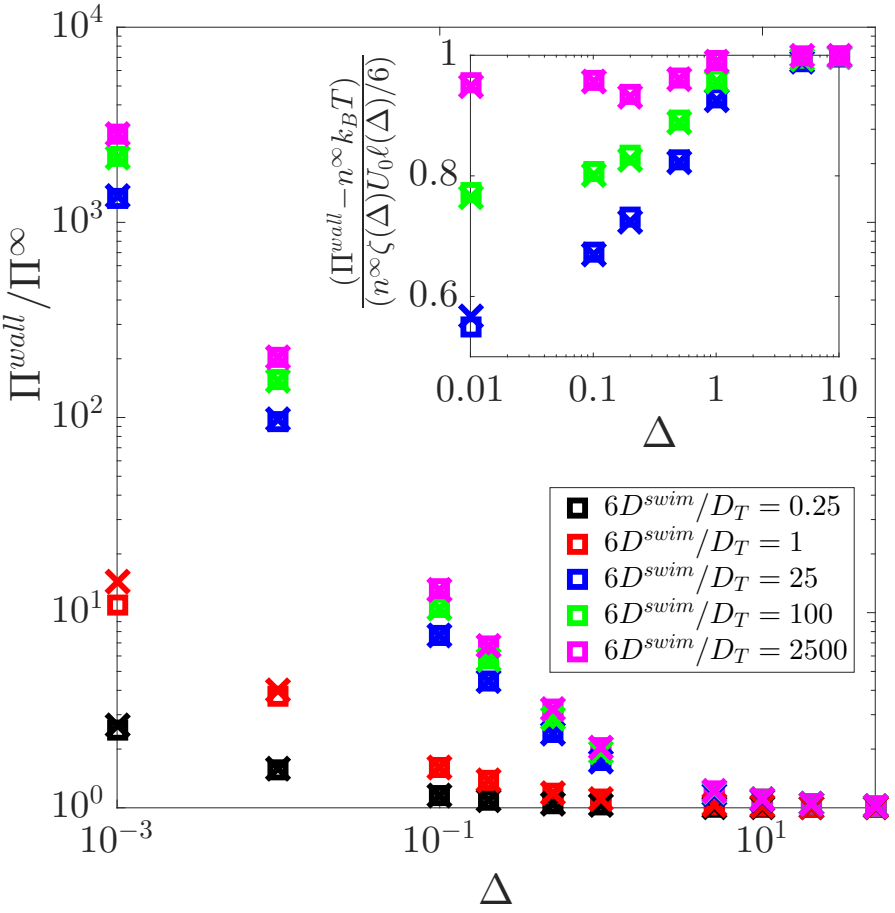

Figure 7.2: Pressure at the wall scaled by the bulk pressure $\Pi^{\infty} = n^{\infty}k_BT(1 + D^{swim}/D_T)$. The number density of swimmers is n^{∞} , D_T is the thermal diffusivity far from the wall, and D^{swim} is the swim diffusivity. This quantity is plotted against Δ, which characterizes the strength of HI; HI are strong for $\Delta \ll 1$, and weak for $\Delta \gg 1$. The square symbols indicate the pressure calculations neglecting the nematic order ($\langle \boldsymbol{qq} \rangle = \boldsymbol{I}/3$), and crosses include nematic order ($\langle \boldsymbol{qqq} \rangle = \langle \boldsymbol{\alpha} \cdot \boldsymbol{q} \rangle/5$, where $\boldsymbol{\alpha}$ is the fourth-order isotropic tensor. INSET: Active contribution to the wall pressure scaled by the prediction from the boundary-layer analyis: ζ is their translational drag, U_0 is the swimming speed, and ℓ is the run length of their active random walk.

is the run length, $\delta = \sqrt{D^{TT}\tau_R}$ is the diffusive size of the particle, the reorientation time is $\tau_R = 1/D^{RR}$, and the boundary-layer thickness $\lambda^{-1} = \delta/\sqrt{2[1 + (\ell/\delta)^2/6]}$.

The pressure the active particles exert on the wall is $\Pi^{wall} = n^W(a(1 + \Delta))k_BT = n^{\infty}k_BT(1 + (\ell/\delta)^2/6) = n^{\infty}(k_BT + k_sT_s)$, where we have defined the activity $k_sT_s = \zeta D^{swim}$, where $D^{swim} = U_0^2\tau_R/6$ is the swim diffusivity. Here, $\zeta = 6\pi\eta a$ is the (Stokes) drag coefficient for an isolated spherical particle ($k_BT = \zeta D^{TT}$). The pressure from the particles is the sum of the normal osmotic pressure of passive Brownian particles,

$\Pi^{osmo} = n^{\infty} k_B T$, plus the swim pressure, $\Pi^{swim} = n^{\infty} k_s T_s$, arising from activity. If the second wall (R) is far removed from the first (L) wall, we may superimpose the concentration distributions from the two walls [25], and the overall momentum balance (7.1) shows that the fluid pressure is uniform and its magnitude is arbitrary; only pressure differences are relevant for incompressible media.

The particle pressure on a flat wall Π^{wall} scaled by the bulk pressure Π^{∞} is plotted as a function of Δ in Fig. 7.2 from the solution of (7.2). When HI are unimportant ($\Delta \gg 1$) the pressure at the wall is equal to the bulk swim pressure for all activity levels: $6D^{swim}/D_T = (\ell/\delta)^2$, where $D_T = D^{TT}(\Delta \to \infty)$. When HI are strong, we predict a substantial increase in the swim pressure for high activity. Note that for low activity where thermal Brownian motion dominates, the pressure is independent of HI, as is well-known. Hydrodynamic interactions reduce the translational and rotational mobility of the swimmer near the wall, resulting in an increased accumulation of particles at the boundary and an increased particle pressure—the active particles remain longer at the wall ($1/D^{RR}$) and they push harder ($\zeta \sim 1/D^{TT}$).

We can predict the effects of HI using the a simple boundary-layer (BL) analysis, depicted in Fig. 7.1. When thermal diffusion is unimportant, (7.2) requires $U_0 n$ to be a spatial constant (in 1D). This does not satisfy the no-flux condition, however, and there is a BL of thickness λ^{-1} at the wall in which diffusion balances activity. In this layer the accumulation of particles still scales as $n^{out}(\ell/\delta)^2/6$, where n^{out} is the number density at the edge of the BL, but now ℓ and δ are functions of Δ because D^{TT} and D^{RR} decrease near the wall. For a thin BL, $\ell/\delta \gg 1$, only the behavior at Δ matters: $D^{TT}(z) = k_B T/\zeta(\Delta)$, $D^{RR}(z) = \tau_R^{-1}(\Delta)$, and the BL scaling gives $n(\Delta) = n^{\infty}(1 + U_0^2/6D^{TT}D^{RR}) = n^{\infty}(1 + \zeta(\Delta)U_0\ell(\Delta)/6k_B T)$—the run length and the drag are now functions of the strength of HI. When the boundary-layer is thicker ($\ell/\delta \sim O(1)$), spatial variations in D^{RR} and D^{TT} are important (see inset of Fig 7.2).

This result is easily generalized to include an athermal reorientation mechanism. If this active reorientation mechanism does not cause the fluid to rotate—the swimmer may simply move in a different direction–, one may add a term $\boldsymbol{\tau}_R^{-1} \cdot \nabla_R P$ to (7.4), where τ_R ($\neq 1/D^{RR}$) is independent of the strength of HI. For spherical movers:

$$\Pi^{wall} - n^{\infty} k_B T = \frac{n^{\infty}\zeta(\Delta)U_0^2\tau_R}{6[1 + \tau_R D^{RR}(\Delta)]} = \frac{n^{\infty}\zeta(\Delta)U_0\ell(\Delta)}{6}, \tag{7.5}$$

which is always larger than the bulk swim pressure Π^{swim}. Note that any reorientation mechanism for non-spherical particles will cause a fluid velocity disturbance; in this

case the rotary motion is captured by the same tensor $\boldsymbol{D^{RR}}$, but the magnitude of the disturbance will be $D^{RR} + \tau_R^{-1}$.

Owing to HI, the particle pressure at the wall exceeds that in the bulk, and because the suspension is incompressible, this difference must be balanced by a difference in the fluid pressure in accordance with the overall momentum balance (7.1). The fluid pressure at the wall is less than that in the bulk, $p_f^{wall} < p_f^{\infty}$, but this pressure difference does not cause the solvent to flow towards the wall as the swimmers are still executing their 'swim stokes.' The total pressure on the wall: $P^{wall} = p_f^{wall} + \Pi^{wall} = p_f^{\infty} + \Pi^{\infty}$ is constant everywhere in space, even though the particle-phase pressure may depend on the interactions with the container boundary. This applies generally to both "wet" and "dry" active matter systems when both the particles and the embedding medium/substrate are considered in the overall momentum balance [17].

7.4 Pressure on a fixed spherical body

To show that this phenomenon and boundary-layer balance are not restricted to the flat-wall geometry, we compute the pressure on the exterior of a fixed spherical cavity of radius R. In the absence of HI, $\Pi^{sphere} - n^{\infty}k_BT \sim n^{\infty}k_sT_s/[1 + \ell/\sqrt{3}R_c]$, where $R_c = (R+a)$: the pressure decreases as a function of ℓ/R_c. When $\ell \gtrsim R_c$, the swimmer will collide with the sphere before it is able to execute a full run length, thus reducing Π^{sphere} [25]. As with the flat plate, we find the same scaling:

$$\Pi^{sphere} - n^{\infty}k_BT = \frac{n^{\infty}\zeta(\Delta)U_0\ell(\Delta)/6}{1 + \ell(\Delta)/\sqrt{3}R_c}, \tag{7.6}$$

where ℓ, ζ, and R_c are appropriately modified to include the effects of HI: $R_c = (R + a)(1 + \Delta)$, $\zeta(\Delta) = k_BT/D^{TT}(\Delta)$, and $\ell = U_0\tau(\Delta)$. Note that the translation-rotation coupling is relevant in the spherical geometry, so $\tau(\Delta) = \tau_R/(1 + \tau_R D^{RR}(\Delta) + \tau_R D^{RT}(\Delta)/R_c)$.

We plot $\Pi^{sphere} - n^{\infty}k_BT$, scaled by our prediction for the flat plate (7.5), in Fig. 7.3; we take $\tau(\Delta) = 1/(D^{RR}(\Delta) + D^{RT}(\Delta)/R_c)$. As in the previous example, the inclusion of nematic order makes only a small quantitative difference (see Fig. 7.4). Eqn. (7.6) predicts the correct decay behavior when $\ell(\Delta) \gg R_c$, but we see that HI and the size ratio have a profound effect when $\ell(\Delta) \ll R_c$. As with the difference between (7.5) and the inset of Fig. 7.2, this is a result of the boundary-layer becoming thick; $\ell/\delta \lesssim O(1)$ in this region and thus the agreement is only good for large Δ. In Fig. 7.4, one can see that the closure makes only a small quantitative difference, even in the spherical geometry.

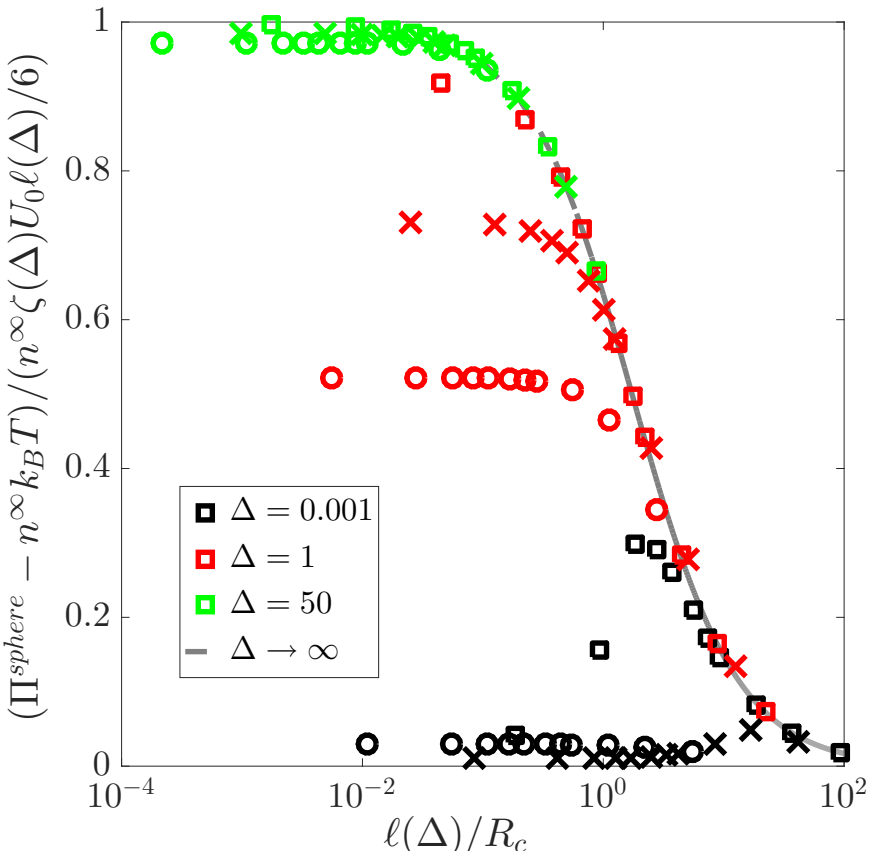

Figure 7.3: Active contribution to the pressure on a fixed spherical cavity of size R scaled by $n^\infty \zeta(\Delta) U_0 \ell(\Delta)/6$. The swimmer number density is n^∞, $k_B T$ is the thermal energy, ζ is the translational drag, U_0 is the swim speed, ℓ is the run length, and Δ characterizes the strength of hydrodynamic interactions (HI). We plot this against $\ell/R_c = U_0 \tau_R(\Delta)/(R + a)(1 + \Delta)$, where a is the size of the swimmer and $\tau_R(\Delta)$ is its (thermal) reorientation time. The colors represent different strengths of HI; square symbols are for $a/R = 1/8$, crosses are for $a/R = 1$, and circles are for $a/R = 8$. The dashed line is the analytical prediction from [25].

Without HI, one expects (and observes) that the spherical cavity agrees well with the flat wall as $a/R \to 0$, but taking this limit requires care. The far-field forms of $D^{TT}(\Delta)$ etc. for two spheres are tabulated in [28], and assume that the separation $r - (a + R) \gg R$. For a flat-wall, $R \to \infty$ independently, and these functions do not exactly approach the flat-wall limit because the swimmer's distance from the wall $z = r - (a + R)$ is always small. The spherical cavity problem is related to the microrheology of a passive particle in an active suspension, which is addressed in Chapter 6.

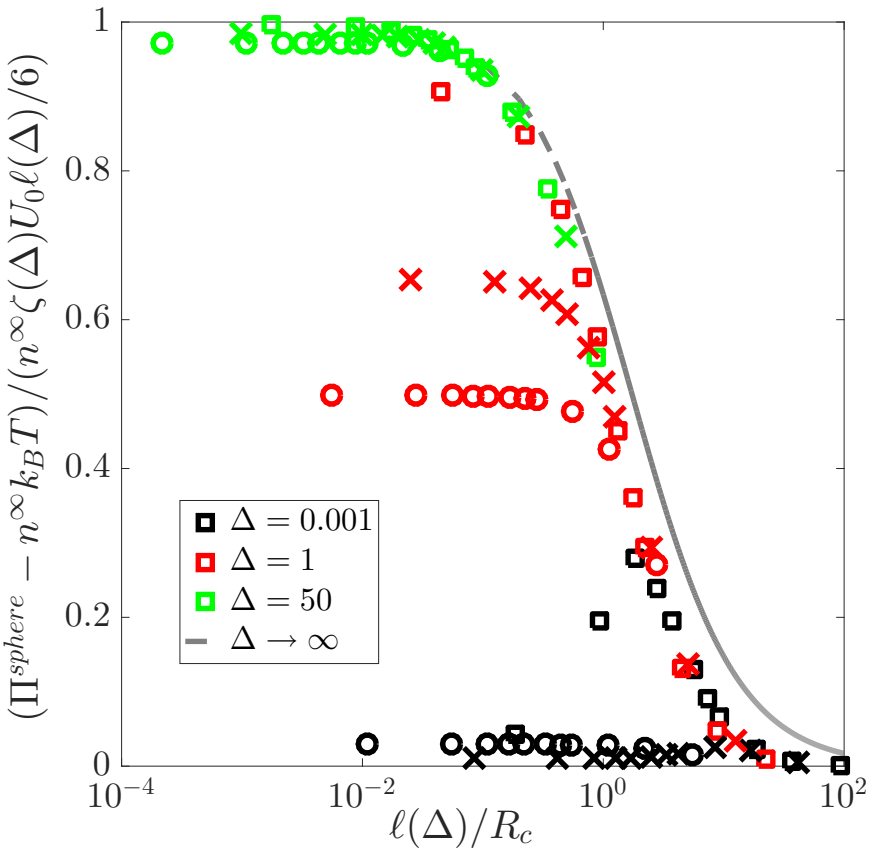

Figure 7.4: Same legend as Fig. 7.3 with $\boldsymbol{Q} \neq 0$.

7.5 Conclusions

We conclude that hydrodynamic interactions do indeed affect (increase) the swim pressure in active suspensions: the reduced mobility of the swimmers near solid boundaries results in an increased accumulation of particles over that when HI are unimportant. Despite this increase in the particle-phase pressure, the total mechanical pressure is unchanged by the presence of HI. If one connected a transducer to a solid plate to measure the average force on the wall, the measured force would reflect the contributions of both the solvent and the particles, which must always balance to give $P = p_f^\infty + \Pi^\infty$. If the boundary were instead a membrane (permeable to the solvent but not the particles) separating the suspension from a reservoir of pure solvent (in a u-tube manometer for example), the net force on the membrane would be given by the particle pressure at the wall, Π^{wall}, which *is* affected by HI. Because the fluid pressure is no longer spatially constant, measurement at a different spatial point where the suspension is homogeneous is necessary to determine the bulk swim pressure Π^∞.

The results in this chapter pertain to swimmers whose swim velocity $\boldsymbol{U}_0$ is fixed. For the flat-plate example, one could also determine the pressure for a suspension of *fixed-force* swimmers: $\boldsymbol{F}^{swim} = \boldsymbol{R}^{\boldsymbol{FU}} \cdot \boldsymbol{U_0}$. In this situation not only are the translational and rotational mobilities of the swimmer reduced near the wall, but U_0 is reduced as well. This would lead to a *decreased* particle pressure, but it is still captured by a simple scaling result: $\Pi^{wall} - n^{\infty} k_B T = n^{\infty} F^{swim} \ell(\Delta)/6$, where $\ell(\Delta) = F^{swim}\tau(\Delta)/\zeta(\Delta)$ just as in the fixed-kinematics problem addressed in this work. For other varieties of swimmers (e.g. pushers and pullers), one would need to include other terms representing the dipolar, quadrupolar, etc. disturbances to the fluid flow from swimming.

Finally, although we considered a hard-sphere force with the boundary, the general conclusions apply for any type of boundary-particle force.

BIBLIOGRAPHY

[1]J. Tailleur, and M. E. Cates, "Statistical mechanics of interacting run-and-tumble bacteria", Phys. Rev. Lett. **100**, 3–6 (2008).

[2]Y. Fily, and M. C. Marchetti, "Athermal phase separation of self-propelled particles with no alignment", Phys. Rev. Lett. **108**, 1–5 (2012).

[3]J. Bialké, H. Löwen, and T. Speck, "Microscopic theory for the phase separation of self-propelled repulsive disks", EPL **103**, 30008 (2013).

[4]S. C. Takatori, W. Yan, and J. F. Brady, "Swim pressure: Stress generation in active matter", Phys. Rev. Lett. **113**, 1–5 (2014).

[5]A. P. Solon, M. E. Cates, and J. Tailleur, "Active brownian particles and run-and-tumble particles: A comparative study", Eur. Phys. J. Spec. Top. **224**, 1231–1262 (2015).

[6]A. Sokolov, and I. S. Aranson, "Reduction of viscosity in suspension of swimming bacteria", Phys. Rev. Lett. (2009) 10.1103/PhysRevLett.103.148101.

[7]D. Saintillan, "The Dilute Rheology of Swimming Suspensions: A Simple Kinetic Model", Exp. Mech. **50**, 1275–1281 (2010).

[8]H. M. López, J. Gachelin, C. Douarche, H. Auradou, and É. Clément, "Turning Bacteria Suspensions into Superfluids", Phys. Rev. Lett. **115**, 028301 (2015).

[9]S. C. Takatori, and J. F. Brady, "Superfluid Behavior of Active Suspensions from Diffusive Stretching", Phys. Rev. Lett. **118**, 018003 (2017).

[10]M. E. Cates, D. Marenduzzo, I. Pagonabarraga, and J. Tailleur, "Arrested phase separation in reproducing bacteria creates a generic route to pattern formation", Proc. Natl. Acad. Sci. U. S. A. **107**, 11715–11720 (2010).

[11]E. W. Burkholder, and J. F. Brady, "Tracer diffusion in active suspensions", Phys. Rev. E - Stat. Nonlinear, Soft Matter Phys. (2017) 10.1103/PhysRevE.95.052605,

[12]M. C. Marchetti, J. F. Joanny, S. Ramaswamy, T. B. Liverpool, J. Prost, M. Rao, and R. A. Simha, "Hydrodynamics of soft active matter", Rev. Mod. Phys. **85**, 1143–1189 (2013).

[13]T. Ishikawa, M. P. Simmonds, and T. J. Pedley, *Hydrodynamic interaction of two swimming model micro-organisms*, Vol. 568 (2006), p. 119.

[14]T. V. Kasyap, D. L. Koch, and M. Wu, "Hydrodynamic tracer diffusion in suspensions of swimming bacteria", Phys. Fluids **26**, 081901 (2014).

[15]A. Morozov, and D. Marenduzzo, "Enhanced diffusion of tracer particles in dilute bacterial suspensions.", Soft Matter **10**, 2748–58 (2014).

[16]R. M. Navarro, and S. M. Fielding, "Clustering and phase behaviour of attractive active particles with hydrodynamics", Soft Matter **11**, 7525–7546 (2015).

[17]W. Yan, and J. F. Brady, "The swim force as a body force", Soft Matter **11**, 6235–6244 (2015).

[18]J. Bialké, "A spherical envelope approach to ciliary propulsion", J. Fluid Mech. **46**, 199 (1971).

[19]K. Drescher, R. E. Goldstein, N. Michel, M. Polin, and I. Tuval, "Direct measurement of the flow field around swimming microorganisms", Phys. Rev. Lett. **105**, 1–4 (2010).

[20]K. Drescher, J. Dunkel, L. H. Cisneros, S. Ganguly, and R. E. Goldstein, "Fluid dynamics and noise in bacterial cell – cell and cell – surface scattering", Proc. Natl. Acad. Sci. U. S. A. **108**, 10940–10945 (2011).

[21]D. L. Koch, and G. Subramanian, "Collective Hydrodynamics of Swimming Microorganisms: Living Fluids", Annu. Rev. Fluid Mech. **43**, 637–659 (2011).

[22]S. C. Takatori, R. De Dier, J. Vermant, and J. F. Brady, "Acoustic trapping of active matter", Nat. Commun. **7**, 10694 (2016).

[23]A. P. Solon, Y. Fily, A. Baskaran, M. E. Cates, Y. Kafri, M. Kardar, and J. Tailleur, "Pressure is not a state function for generic active fluids", Nat. Phys. **11**, 673–678 (2015).

[24]Y. Fily, Y. Kafri, A. P. Solon, J. Tailleur, and A. Turner, "Mechanical pressure and momentum conservation in dry active matter", ArXiv e-prints (2017).

[25]W. Yan, and J. F. Brady, "The force on a body in active matter", J. Fluid Mech. **6**, 1–11 (2015).

[26]J. W. Swan, and J. F. Brady, "Simulation of hydrodynamically interacting particles near a no-slip boundary", Phys. Fluids **19** (2011) 10.1063/1.2803837.

[27]A. J. Goldman, R. G. Cox, and H. Brenner, "Slow viscous motion of a sphere parallel to a plane wall—I Motion through a quiescent fluid", Chem. Eng. Sci. **22**, 637–651 (1967).

[28]S. Kim, and S. J. Karilla, *Microhydrodynamics : Principles and Selected Applications* (1991).

[29]T. M. Squires, and J. F. Brady, "A simple paradigm for active and nonlinear microrheology", Phys. Fluids **17**, 1–21 (2005).

[30]S. Michelin, and E. Lauga, "Geometric tuning of self-propulsion for Janus catalytic particles", Sci. Rep. **7**, 1–9 (2017).

[31]D. Saintillan, and M. J. Shelley, "Active suspensions and their nonlinear models", Comptes Rendus Phys. **14**, 497–517 (2013).

Chapter 8

PROBE MOTION IN ACTIVE SUSPENSIONS: FLUID-MEDIATED INTERACTIONS

Active suspensions—colloidal dispersions of particles that are able to self-propel through the conversion of chemical into mechanical energy—have many intriguing mechanical properties. Because these systems can generate their own internal stresses, they are far from equilibrium and exhibit fascinating dynamic behaviors such as spontaneous collective motion at sufficiently high concentrations [1–3]. Recent experiments [4] and kinetic models [5] have shown that active suspensions also have unusual rheological behavior. The shear viscosity of a suspension of *B. subtilis* was measured to be *lower* than the viscosity of the embedding solvent [4]. Theoretical descriptions that followed ascribed this viscosity reduction to the extensile hydrodynamic stress that the organisms exert on their environment to self-propel [5], and further predicted that the shear viscosity of the suspension would increase if the organisms exerted a contracticle hydrodynamic stress (e.g. *C. reihnhardtii*). Contractile swimmers are commonly called "pullers" and extensile swimmers are called "pushers[1]." Indeed models of swimmers' (specifically pushers') spontaneous collective motion describe that dynamic behavior as an instability that arises when the effective shear viscosity of the suspension is reduced to zero as a result of these hydrodynamic stresses [2].

However, recent experiments [7] and theory [8–10] have found that this transition to "superfluid-like" rhelogical behavior (i.e. zero shear viscosity) can happen at concentrations far below the predicted threshold concentration for the transition to collective behavior, and that the shear viscosity can even be negative![2]. The simple theory of [9] shows that this behavior is not dependent on the specific geometry or gait (pusher, puller, etc.) of the swimmers, rather the dominant contributor is the diffusive stretching of the swim stress $\boldsymbol{\sigma}^{swim}$—the mechanical stress that arises

[1] There is also a class of swimmers called "movers" or neutral swimmers which are able to self propel, but exert no hydrodynamic stress on the fluid as a result of this motion. These classes of swimmers are based on Blake's squirming model for locomotion of ciliated bodies [6].

[2] One may have a negative shear viscosity in a fixed strain-rate experiment. In a cylindrical couette rheometer this means that the applied torque will be opposite the direction of the fluid flow. In a fixed shear-stress experiment, a negative viscosity would cause the rheometer to speed up (and thus increase the shear rate) until the shear viscosity was no longer negative [9].

from the particles' active run-and-tumble motion—-by the ambient shear flow. The change in shear viscosity due to this swim stress is much larger than changes to the viscosity arising from the hydrodynamic stress a swimmer exerts on the fluid, which has been studied more extensively [5, 11–15].

As with the similarities between the shear viscosity and the microviscosity (the average drag on a colloidal tracer, interpreted as an effective viscosity) in a suspension of passive colloids [16–18], one might expect that this negative shear viscosity should have a microscopic analog. Indeed a negative microviscosity was found in suspensions of contractile active nematic fluids [19]. However, in Chapter 3, we found that the effective microviscosity of the suspension is never lower than that of the suspending solvent η_s in the linear response regime, in contrast to the experimental measurements and theoretical predictions of the effective shear-viscosity. While there is still one qualitative similarity—the random self-propulsive motion of the swimmers lower the microviscosity compared to that of a suspension of passive particles—we expect that hydrodynamic interactions must be important in determining the microrheological behavior in active fluids.

In suspensions of passive colloidal particles, hydrodynamic interactions are essential to finding quantitative agreement between macrorheology and microrheology. In the "continuum limit," where the colloidal probe being dragged through the suspension is much larger than the bath particles, the effective microviscosity is equal to the effective shear viscosity [18]. The physical picture in this limit is illustrated in Fig. 8.1: the bath particles are point tracers in the fluid flow created by the translating probe—the Stokes velocity outside a translating sphere. From a fluid-mechanical perspective, the force on the probe particle generates a Stokeslet velocity disturbance in the fluid that decays as $1/r$, where r is the distance from the center of the probe, scaled by its size R. This Stokeslet induces a Stresslet in the bath particles of magnitude β^3/r^2, where $\beta = a/R$ is the size ratio of the solute to the probe. This propagates a stresslet velocity disturbance back to the probe particle $\beta^3/r^2 \times 1/r^2 \sim \beta^3/r^4$, which hinders its motion. This propagated stresslet is responsible for the Einstein viscosity correction [18, 20] to the force required for the sphere to translate; there are no steric interactions between the probe and the "solute" in the bath. The effective viscosity measured in this continuum limit is known as the high-frequency shear viscosity η'_∞, which is equal to the steady shear viscosity for spherical bath particles.

The high-frequency shear viscosity is independent of the shape of the solute—

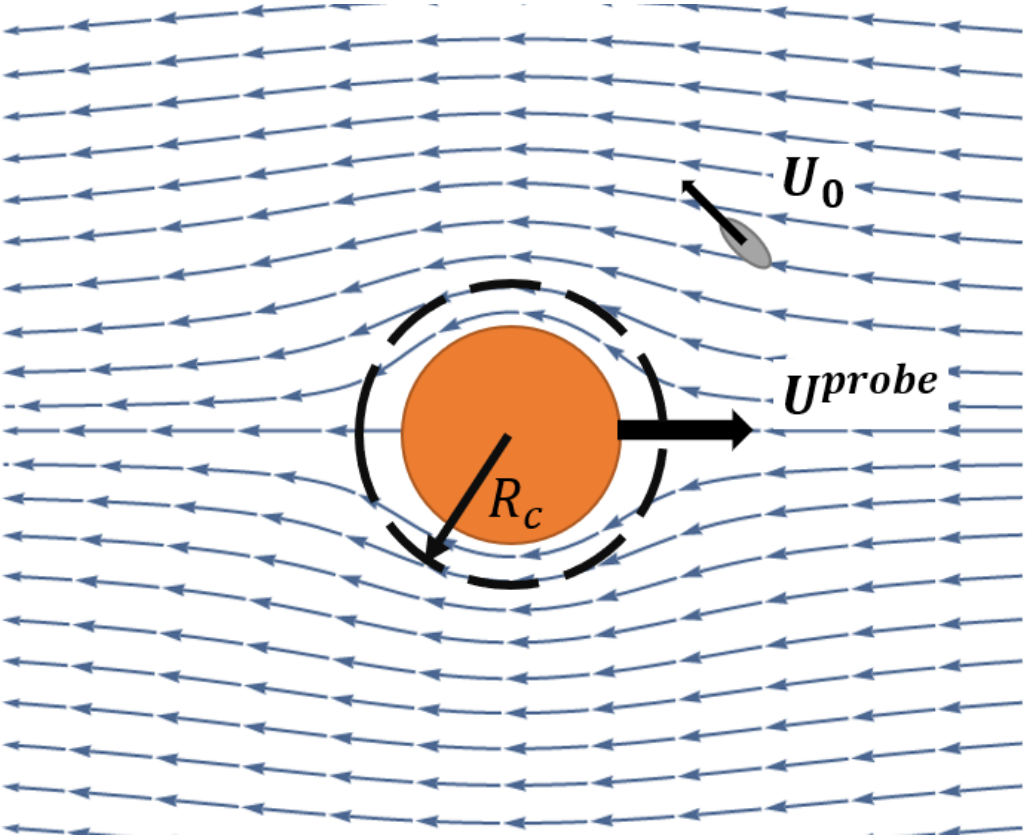

Figure 8.1: Sketch of a sphere of size R moving with velocity $\boldsymbol{U}^{\boldsymbol{probe}}$ through fluid containing a dilute dispersion of point ABPs with swim velocity $\boldsymbol{U}_0$. The probe-bath hydrodynamic interactions are modeled by an excluded annulus potential, which manifests as a no-flux condition at R_c. The fluid velocity stream-lines incdicated by the blue arrows are plotted in a probe-fixed reference frame.

a force-free solute particle may simply be represented by a point stresslet [21]. Indeed, under high-frequency oscillatory shear, one would expect the suspension to remain isotropic, and thus the orientation-averaged force (and η'_∞) remains the same regardless of shape. This is not the case for the *steady* shear viscosity of anisotropic particles. Under steady shear, the particles will become aligned with the ambient flow, leading to an anisotropic average stresslet that depends on the precise geometry of the particle. For passive axisymmetric particles described by a single orientation vector $\boldsymbol{q}$, this anisotropic stresslet always increases the effective shear viscosity, whether the particles are prolate or oblate spheroids [22, 23]. Investigations of particle geometry in the microrheology of colloidal suspensions have been limited to suspensions of needle-like Brownian ellipsoids [24, 25] or ellipsoidal probes in suspensions of spherical bath particles [26]. The effect of particle geometry on the microrheology of *active* suspensions warrants attention. Though there are many

examples of spherical swimmers—*Volvox* and synthetic Janus particles being the most common ones—many biological swimmers are anisotropic, including *E. Coli* and *B. Subtilis* which are commonly used in experiments on bacterial suspensions.

In this chapter we explore the effects of hydrodynamic interactions on the microrheology of active fluids. We first model a large probe translating through a bath of point swimmers with arbitrary aspect ratio. This allows us to investigate the physical mechanisms underpinning the microrheological material response, while keeping the fluid mechanics in the problem simple. We then investigate the effects of particle size, the mode of probe forcing, and the nonlinear response in a suspension of spherical swimmers using the formalisms derived in Chapter 6.

8.1 Model system

Consider a large spherical particle of size R and density ρ_P translating through a fluid of viscosity η_s and density ρ with some velocity $\boldsymbol{U}^{\boldsymbol{probe}}$; the external force acting on the probe is $\boldsymbol{F}^{ext}$. The Reynolds number $Re \equiv \rho U^{probe} R/\eta_s$ and Stokes number $St \equiv Re(\rho_P/\rho)$ are small, so the velocity of the fluid relative to the particle is the familiar Stokes velocity $\boldsymbol{u}^{\boldsymbol{Stokes}}$ (see Fig. 8.1) [21]. If the fluid also contains a dispersion of force-free point particles, then the velocity field in the fluid $\boldsymbol{u}^{\boldsymbol{Stokes}}$ remains unchanged, but one must now consider interactions between the probe particle and the solute via the joint probability density of finding a tracer particle at position $\boldsymbol{r}$ relative to the probe $P(\boldsymbol{r}, t)$ [18, 20]. Using a minimal model of hydrodynamic interactions that accounts only for the self-propulsive motion of a swimmer and neglects the velocity disturbance due to swimming, the same can be said in a suspension of active particles (Chapter 6).

Consider a suspension of active Brownian particles (ABPs) of diameter d and length L with a fixed swim speed U_0, rotary diffusivity $\boldsymbol{D}^{\boldsymbol{RR}}$ and thermal diffusivity $\boldsymbol{D}^{\boldsymbol{TT}}$—we neglect any fluid velocity disturbances associated with a particular swimming gait. For bodies of revolution, the isolated translational and rotational diffusivities can be expressed in terms of the diffusivity parallel and perpendicular to the particle orientation $\boldsymbol{q}$, $\boldsymbol{D}^{\boldsymbol{TT}} = D^T_{\parallel}\boldsymbol{qq} + D^T_{\perp}(\boldsymbol{I} - \boldsymbol{qq})$, $\boldsymbol{D}^{\boldsymbol{RR}} = D^R_{\parallel}\boldsymbol{qq} + D^R_{\perp}(\boldsymbol{I} - \boldsymbol{qq})$. We will assume that the direction of swimming coincides with $\boldsymbol{q}$, as is often observed[3] [23]. In the limit of $d/R, L/R \to 0$, the probability of finding the swimmer at some configuration relative to the probe $P(\boldsymbol{r}, \boldsymbol{q}, t)$ is determined by the following

[3]This need not be the case, one could also specify that swimming is in a different direction $\boldsymbol{q}'$. Determining this direction for ciliated swimmers or phoretic particles is a non-trivial problem, but all theory so far predicts swimming parallel or anti-parallel to $\boldsymbol{q}$ [27–31].

Smoluchowski equation:

$$\frac{\partial P(\boldsymbol{r},\boldsymbol{q},t)}{\partial t} + \nabla_{\boldsymbol{r}} \cdot \boldsymbol{j}^{\boldsymbol{T}} + \nabla_{\boldsymbol{q}} \cdot \boldsymbol{j}^{\boldsymbol{R}} = 0, \tag{8.1}$$

$$\boldsymbol{j}^{\boldsymbol{T}} = \boldsymbol{u}^{\boldsymbol{Stokes}} P + U_0 \boldsymbol{q} P - \boldsymbol{D}^{\boldsymbol{TT}} \cdot \nabla_{\boldsymbol{r}} P, \tag{8.2}$$

$$\boldsymbol{j}^{\boldsymbol{R}} = (\boldsymbol{\Omega}^{\boldsymbol{Stokes}} \cdot \boldsymbol{q} + B(\boldsymbol{I} - \boldsymbol{qq}) \boldsymbol{q} \cdot \boldsymbol{E}^{\boldsymbol{Stokes}}) P - \boldsymbol{D}^{\boldsymbol{RR}} \cdot \nabla_{\boldsymbol{q}} P, \tag{8.3}$$

where ∇_r is the gradient with respect to the distance from the center of the probe, and the rotational operator $\nabla_{\boldsymbol{q}}$ is the gradient with respect to the swimmer orientation. The Bretherton constant is given by $B = (\xi^2 - 1)/(\xi^2 + 1)$ [32, 33], where $\xi = L/d$ is the swimmer's length-to-diameter (aspect) ratio. For prolate swimmers $\xi > 1, B \in (0, 1]$, and for oblate swimmers $\xi < 1, B \in [-1, 0)$. The swimmer undergoes its active and thermal random walk, but its motion is biased by advection with the velocity field created by the motion of the probe particle $\boldsymbol{u}^{\boldsymbol{Stokes}}$; the swimmer's orientation is affected by the vorticity $\boldsymbol{\Omega}^{\boldsymbol{Stokes}} = [\boldsymbol{\nabla_r u}^{\boldsymbol{Stokes}} - (\boldsymbol{\nabla_r u}^{\boldsymbol{Stokes}})^{\dagger}]/2$ and straining field $\boldsymbol{E}^{\boldsymbol{Stokes}} = [\boldsymbol{\nabla_r u}^{\boldsymbol{Stokes}} + (\boldsymbol{\nabla_r u}^{\boldsymbol{Stokes}})^{\dagger}]/2$ in the fluid through Jeffrey's equation [33]. For simplicity, we do not specify the swimmer's gait in this problem, though it is simple to incorporate swimming gaits based on Blake's squirming model into the problem (see Chapter 6). Note that rotary diffusivity about the swimmer's axis of symmetry $D_{\parallel}^{R}$ does not affect the angular velocity of the swimmer, though this may not be true if one considers finite-size effects of the swimmers [23].

We solve these equations using the familiar expansion of P in solid harmonics of $\boldsymbol{q}$ [34]. This results in coupled mean-field equations for the number density $n(\boldsymbol{r}, t)$, polar order $\boldsymbol{m}(\boldsymbol{r}, t)$, and nematic order $\boldsymbol{Q}(\boldsymbol{r}, t)$ of the suspension. We make the closure $\langle \boldsymbol{qqq} \rangle = \boldsymbol{\alpha} \cdot \langle \boldsymbol{q} \rangle / 5$, where $\boldsymbol{\alpha}$ is the fourth-order isotropic tensor. This simple closure is sufficient to describe the microstructure in the absence of probe motion (Chapter 7) or in the absence of HI (Chapters 3-5), but is based on the assumption of an isotropic steady-state microstructure—it neglects any coupling between the disturbed microstructure and the fluid velocity field. When hydrodynamic interactions are considered, it is possible to have long-ranged, steady ordering of the suspension, similar to particles in a simple shear flow [22]. Unlike particles in a shear flow, however, there is no order at infinity, so in this chapter we will assume that this isotropic closure is sufficient, though future investigations might consider linking $\langle \boldsymbol{qqq} \rangle$ to the velocity disturbance of the probe to see if the added detail changes any findings presented here.

From the solution for $n, \boldsymbol{m}$, and $\boldsymbol{Q}$, we can compute the force required to keep the

velocity of the probe fixed:

$$\frac{\langle \boldsymbol{F}^{ext} \rangle}{6\pi\eta_s R} = \boldsymbol{U}^{probe} + \int \left[\left(\frac{1}{x^a} - 1 \right) \boldsymbol{nn} + \left(\frac{1}{y^a} - 1 \right) (\boldsymbol{I} - \boldsymbol{nn}) \right] \cdot \boldsymbol{U}^{probe} n(\boldsymbol{r}) d\boldsymbol{r} + \frac{k_B T}{6\pi\eta_s R} \int L(R_c) \boldsymbol{n}\, n(R_c) dS. \tag{8.4}$$

The external force is given by Stokes drag law, plus a hydrodynamic and an interparticle contribution. For bath particles with finite size, there will also be a Brownian contribution to the force arising from the divergence of the relative hydrodynamic mobility $\nabla \cdot \boldsymbol{M}^{\boldsymbol{UF}}$ (see Chapter 6). The Brownian contribution is $O(\beta)$, where $\beta = a/R$ is the swimmer-to-probe size ratio, and thus is neglected in the present discussion. The hydrodynamic contribution contained in the first integral depends on the mobility of the probe relative to its mobility in an unbounded fluid, which is contained in the mobility functions parallel (x^a) and transverse (y^a) to its outward pointing unit normal $\boldsymbol{n}$ [21]. Both x^a and y^a are functions of the distance from the center of the probe r (the origin in this coordinate frame), and the excluded annulus parameter Δ that characterizes the strength of hydrodynamic interactions [18, 35]. The second contribution is the drag force associated with probe-bath interactions, which depends only on the number density n at the no-flux probe surface $R_c = R(1 + \Delta)$, and the normal component of the fluid velocity field at the surface $L(R_c) = 1 - 3/(2(1 + \Delta)) + 1/(2(1 + \Delta)^3)$ [18].

8.2 Linear response

One can define the microviscosity from the effective drag force on the probe:

$$\frac{\langle \eta \rangle - \eta_s}{\eta_s} = \frac{|\langle \boldsymbol{F}^{ext} \rangle - \boldsymbol{F}^{\boldsymbol{Stokes}}|}{6\pi\eta_s R U^{probe}}, \tag{8.5}$$

where $\boldsymbol{F}^{\boldsymbol{Stokes}} = 6\pi\eta_s R \boldsymbol{U}^{\boldsymbol{probe}}$ is the Stokes drag force on the probe. We define the intrinsic microviscosity $\eta_i \equiv (\langle \eta \rangle - \eta_s)/\eta_s \phi^\star$ where $\phi^\star = (\pi n^\infty d^2 L/6)(1+\Delta)^3 = \phi(1 + \Delta)^3$. Those familiar with micellar solutions may know $\phi^\star$ as the wet volume fraction. The intrinsic microviscosity η_i is analogous to the Huggins coefficient for the steady shear viscosity, and has both a hydrodynamic contribution η_i^H and an interparticle contribution η_i^P (again, there would be a Brownian contribution η_i^B for swimmers with finite size). Note that $\eta_i \neq \eta^{micro}$ as defined in Chapters 3-5, though they only differ by a factor of $(1+\beta)^3/2\beta^2$. In the limit of point swimmers, the fixed-force and fixed-velocity microrheology problems are mathematically identical. All

that changes is the interpretation of the result—whether the swimmers increase (or decrease) the force required to keep the probe moving at a speed $\boldsymbol{U^{probe}}$, or how fast the probe moves under the action of $\boldsymbol{F^{ext}}$.

When the probe moves slowly compared to the rate of Brownian motion of the swimmers—characterized by a Péclet number $Pe = U^{probe}R_c/\bar{D} \ll 1$—we are in the linear-response regime and η_i is independent of U^{probe}. We have chosen $\bar{D} = (D_\parallel^T + 2D_\perp^T)/3$, the isotropic portion of $\boldsymbol{D^{TT}}$, as the scale for Brownian motion. For $Pe \ll 1$, the hydrodynamic microviscosity η_i^H depends only on the number density of swimmers around a stationary probe n_0 [18]:

$$\eta_{i,0}^H = \frac{8}{\beta^3\xi}\int_{r=1}^{\infty}\left(\frac{1}{x_{11}^a}+\frac{2}{y_{11}^a}-3\right)n_0(r)\,r^2\,dr, \tag{8.6}$$

and is equal to the high-frequency shear viscosity. The subscript 0 denotes that this quantity may be defined even in the absence of probe motion. The contribution due to interparticle collisions is

$$\eta_i^P = \frac{12(1+\beta)^3}{\beta^2\xi}\,\frac{L(\Delta)}{k_\parallel^T+2k_\perp^T}\,n'(r=1), \tag{8.7}$$

where $n' = (n-n_0)/Pe$ is the linear perturbation to the number density. The interparticle contribution to the effective microviscosity $\eta_i^P\phi^\star$ is proportional to the excluded volume fraction $\phi^{ex} = \phi^\star(1+\beta)^3/2\beta^2$, which is much larger than $\phi^\star$ when $\beta \ll 1$.

Hydrodynamic effects $\eta_{i,0}^H$

In Fig. 8.2, we plot the high frequency shear viscosity $\eta_{i,0}^H$ as a function of the bath activity $\ell/R = U_0/D_\perp^R R$. We assume that swimmer reorientations are due only to rotary Brownian motion, as this contribution is $O(1/\beta^2)$ larger than any active reorientation process. This viscosity contribution is an increasing function of activity; the increase is non-monotonic for prolate-spheroidal and spherical swimmers $\xi \geq 1$, and monotonic for oblate-spheroidal swimmers $\xi < 1$. Increasing the activity of the swimmers results in an increased concentration accumulation at the surface that scales as ℓ/R when $\ell \gg R$ [36]. When $\Delta \ll 1$, fluid friction makes it more difficult for the probe to move through this "cage" of bath particles (see Fig. 8.3), hence the increase in viscosity. There is a plateau at large ℓ/R as the $O(\ell/R)$ accumulation of particles at the probe surface is confined to a swim-diffusive boundary layer that is $O(R/\ell)$ thin. We note that $\eta_{i,0}^H$ is a monotonically decreasing function of Δ for all aspect ratios and activity levels, and increasing Δ does not substantially change the

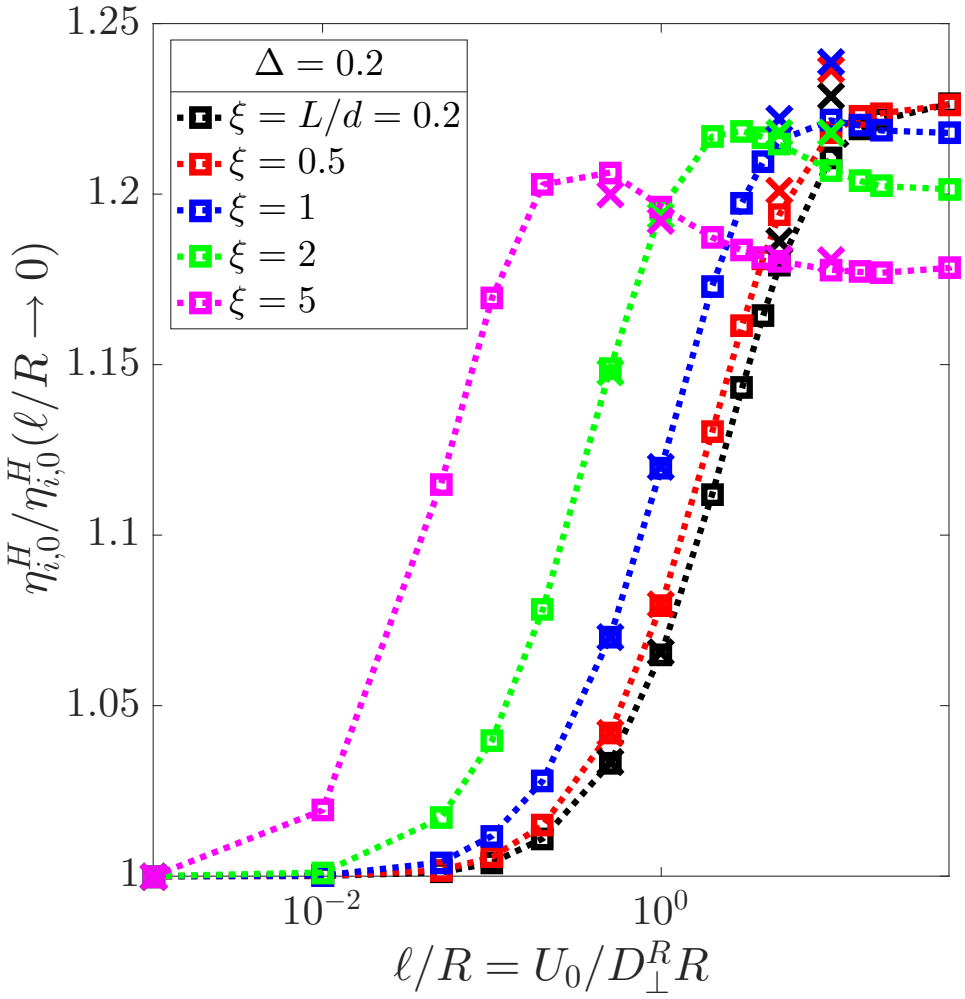

Figure 8.2: The hydrodynamic contribution to to the intrinsic microviscosity (in the absence of probe motion), scaled by the result for passive colloidal suspensions, is plotted as a function of the swimmers' activity $\ell/R = U_0/D^R_\perp R$, where U_0 is the swim speed, $D^R_\perp$ is the inverse reorientation time, and R is the size of the probe. Different colors represent different swimmer aspect ratios $\xi = L/d$. Hydrodynamic interactions are strong: $\Delta = 0.2$. Square symbols include anisotropy in the thermal diffusivity and crosses neglect it.

trend with respect to activity (see Appendix A), though at larger Δ, $\eta^H_{i,0}$ appears to be a monotonic function of activity for all ξ.

In the absence of activity, $\eta^H_{i,0}$ is independent of the particle geometry—the shape only enters into the volume fraction[4]. With the introduction of activity, particle

[4]When the swimmers have finite size, the self-mobility of the probe will be a function of the swimmer orientation $\boldsymbol{q}$, which will make $\eta^H_{i,0}$ a function of the particle geometry. We leave this to a future study, as it requires a lengthy calculation using the method of reflections and is not well-suited for analytical techniques [37, 38].

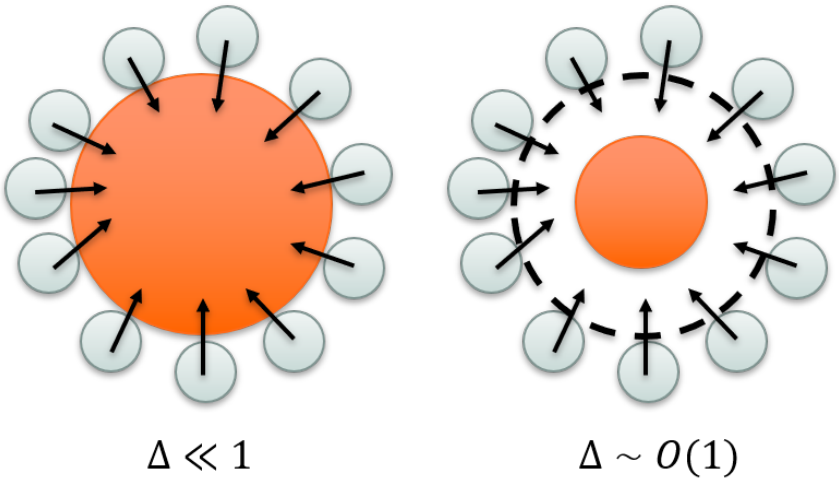

Figure 8.3: Sketch of the distribution and orientation of swimmers around the probe leading to the increase in the high-frequency shear viscosity $\eta^H_{i,0}$. Hydrodynamic interactions are strong for $\Delta \ll 1$ and moderate for $\Delta \sim O(1)$.

shape makes an appreciable difference (Fig. 8.2). Prolate-spheroidal and spherical swimmers show a maximum of $\eta^H_{i,0}$ with respect to activity for $\Delta \ll 1$, and this maximum shifts toward lower values of activity as the particles become more needle-like (ξ increases). The plateau at large activity is also shape-dependent—it is higher for oblate swimmers $\xi < 1$ and decreases as ξ increases for all Δ. In suspensions of passive needle-like particles, DePuit and Squires [24] make use of the reciprocal theorem to connect the suspension shear stress to the force on a translating body in a Newtonian fluid of the same viscosity, but this circumvents the need to explicitly compute $\eta^H_{i,0}$ and thus the effect of shape on the high-frequency shear viscosity is not discussed.

Fig. 8.2 also reveals that the anisotropy in the swimmers' thermal diffusivity $\Delta D \equiv D_{\parallel} - D_{\perp}$ has only a small quantitative effect on $\eta^H_{i,0}$. The crosses in Fig. 8.2 indicate solutions of the Smoluchowski equation where we let $\Delta D = 0$, but B vary with particle aspect ratio. Anisotropy in the diffusivity seems to have the largest effect at large ℓ/R_c, where gradients in the concentration field, polar order and nematic order are large. Setting $\Delta D = 0$ neglects some anisotropic diffusive terms (e.g. a number density flux due to the divergence of the nematic order, which is proportional to ΔD) that may become important in the boundary-layer balance between activity and diffusion at large ℓ/R_c.

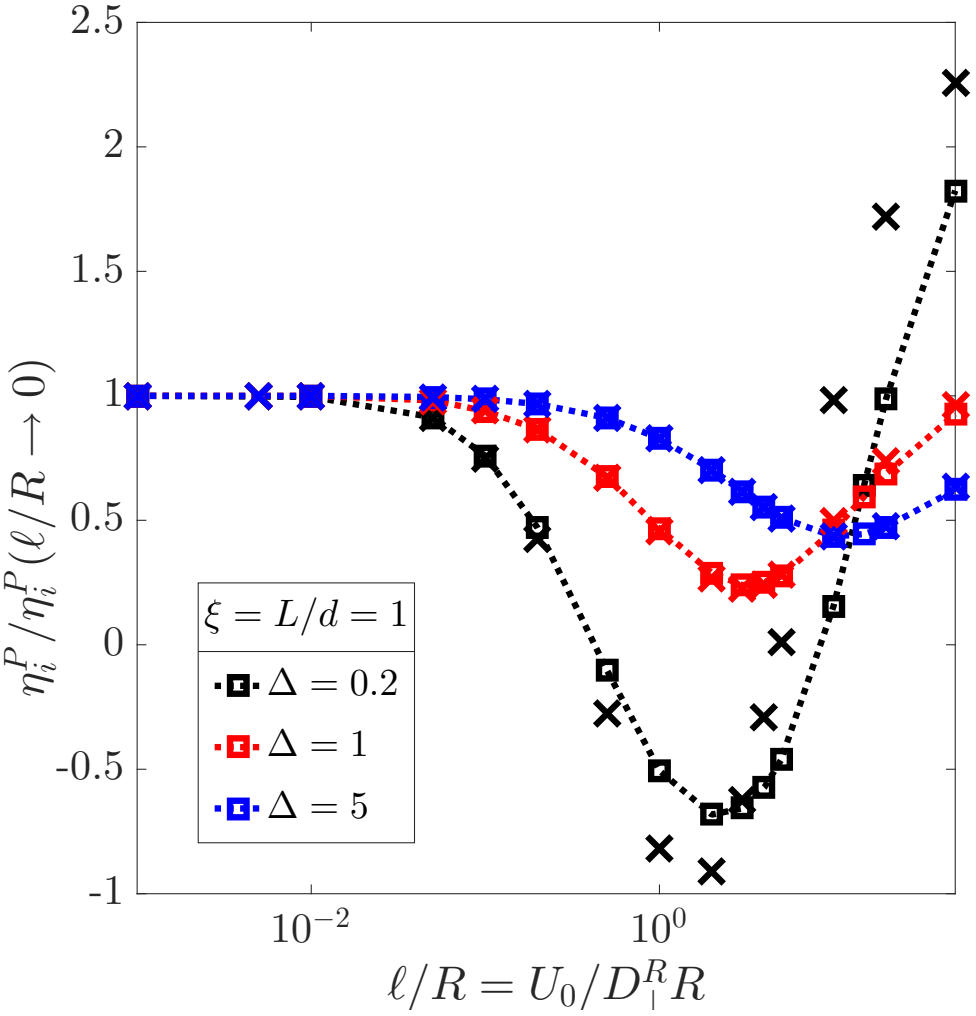

Figure 8.4: The interparticle contribution to the intrinsic microviscosity, scaled by the result for passive colloidal suspensions, plotted as a function of the (spherical) swimmers' activity $\ell/R = U_0/D_\perp^R R$, where U_0 is the swim speed, $D_\perp^R$ is the inverse reorientation time, and R is the size of the probe. Different colors represent different strengths of hydrodynamic interactions. Square symbols include fluid vorticity, and crosses neglect vorticity.

Interparticle effects η_i^P

We next examine the contribution that arises from direct probe-swimmer interactions η_i^P, which is plotted as a function of activity in Fig. 8.4 for spheres. Most noteworthy is the fact that we find negative contributions at moderate ℓ/R when HI are strong—the interparticle interactions *reduce* the microviscosity! Furthermore, we find this effect even if we neglect the reorientation of the swimmers due to fluid vorticity (because the swimmers are isotropic $\Delta D = 0, B = 0$ there is no strain-alignment either)—it is attributable only to advection and activity. This finding is curious. In

the absence of HI, the swimmers still advect with the (uniform) fluid flow $-\boldsymbol{U}^{\boldsymbol{probe}}$ yet η_i^P is always positive (albeit less than what one would measure in a suspension of passive particles). The only difference when HI are included is the spatial variation in the fluid velocity field $\boldsymbol{u}^{\boldsymbol{Stokes}}$.

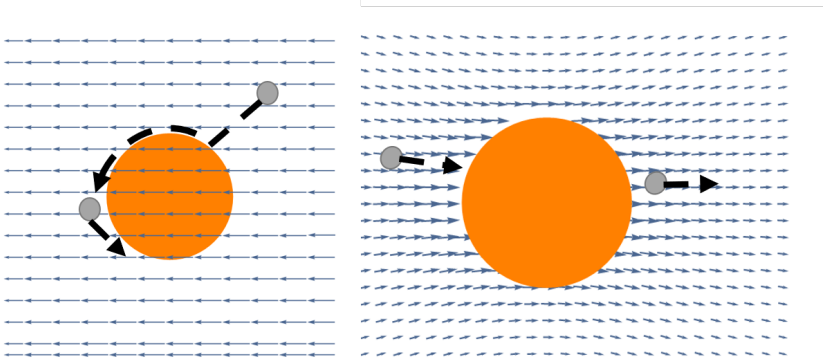

Figure 8.5: Sketch of a swimmer's trajectory around the probe when $\ell/R_c \sim O(1)$. The figure on the left illustrates flow in the absence of HI, and the figure on the right illustrates the additional fluid velocity disturbance of the probe when HI are included.

When a swimmer collides with the probe, it slides along the surface until it reorients (see Figs. 3.5 and 8.5). When ℓ/R is small, these collisions look like Brownian kicks of $O(k_sT_s)$, where $k_sT_s = \zeta_s U_0^2 \tau_R/6$ is the activity of the swimmers (ζ_s is the swimmer's Stokes drag coefficient). When $\ell/R \gg 1$, the swimmer will slide along the surface at the same orientation until it is able to continue swimming away from the probe. When the run length of the swimmers is commensurate with the size of the probe $\ell/R \sim O(1)$, the swimmer remains close enough to the probe that it may collide with the particle again after reorienting—if the swimmer is behind the probe it will push it along (decreasing the effective drag) and it will push agains the probe (increasing the effective drag) if it is in front of the probe. The symmetry-breaking provided by the constant fluid velocity field $-\boldsymbol{U}^{\boldsymbol{probe}}$ biases the swimmers to push the probe along (even in the absence of HI). This mechanism is consistent with negative values of η_i^P, but finding $\eta_i^P < 0$ requires that there be a deficit of swimmers in front of the probe, and an accumulation behind—this is not found in the absence of HI. This can be achieved with the assistance of the probe's fluid velocity disturbance $\boldsymbol{u}' = \boldsymbol{u}^{\boldsymbol{Stokes}} + \boldsymbol{U}^{\boldsymbol{probe}}$ (see Fig. 8.5, right): the swimmers are carried into the wake of the probe by this advective disturbance (and entrained), and are simultaneously pushed out of the way in front of the probe. There is now a concentration gradient of bath particles that gives rise to a net force in the same direction as probe motion $\hat{\boldsymbol{u}}$.

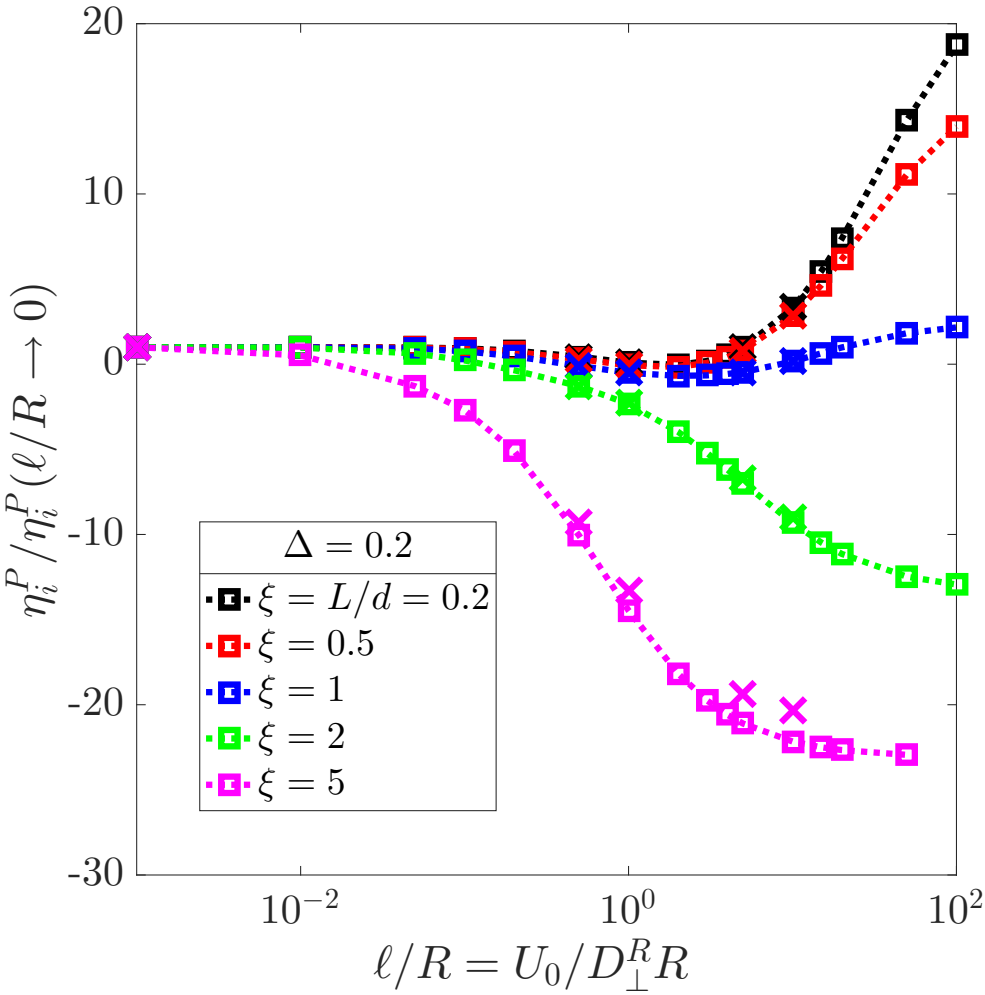

Figure 8.6: The interparticle contribution to the intrinsic microviscosity, scaled by the result for passive colloidal suspensions, plotted as a function of the swimmers' activity $\ell/R = U_0/D_\perp^R R$, where U_0 is the swim speed, $D_\perp^R$ is the inverse reorientation time, and R is the size of the probe. Different colors represent different swimmer aspect ratios $\xi = L/d$. Hydrodynamic interactions are strong: $\Delta = 0.2$. Square symbols include anisotropy in the thermal diffusivity and crosses neglect it.

This decrease in the interparticle intrinsic microviscosity is in competition with the increase in the high-frequency shear viscosity $\eta_{i,0}^H$. The hydrodynamic intrinsic microviscosity is $O(1)$, but $\eta_i^P \sim [L(\Delta)]^2/\beta^2$ which scales as (Δ^4/β^2) when HI are strong. One factor of $L(\Delta)$ comes from the hydrodynamic mobility in the definition of the force on the probe, and another comes from the no-flux boundary condition—the microstructural disturbance is forced by the advective flux $L(\Delta)\hat{\boldsymbol{u}}n_0$ at the probe surface. If a negative microviscosity is to be found then η_i^P must be large ($O(1/\phi^\star)$), which may be difficult given that it scales as Δ^4 when HI are strong and that η_i^P is

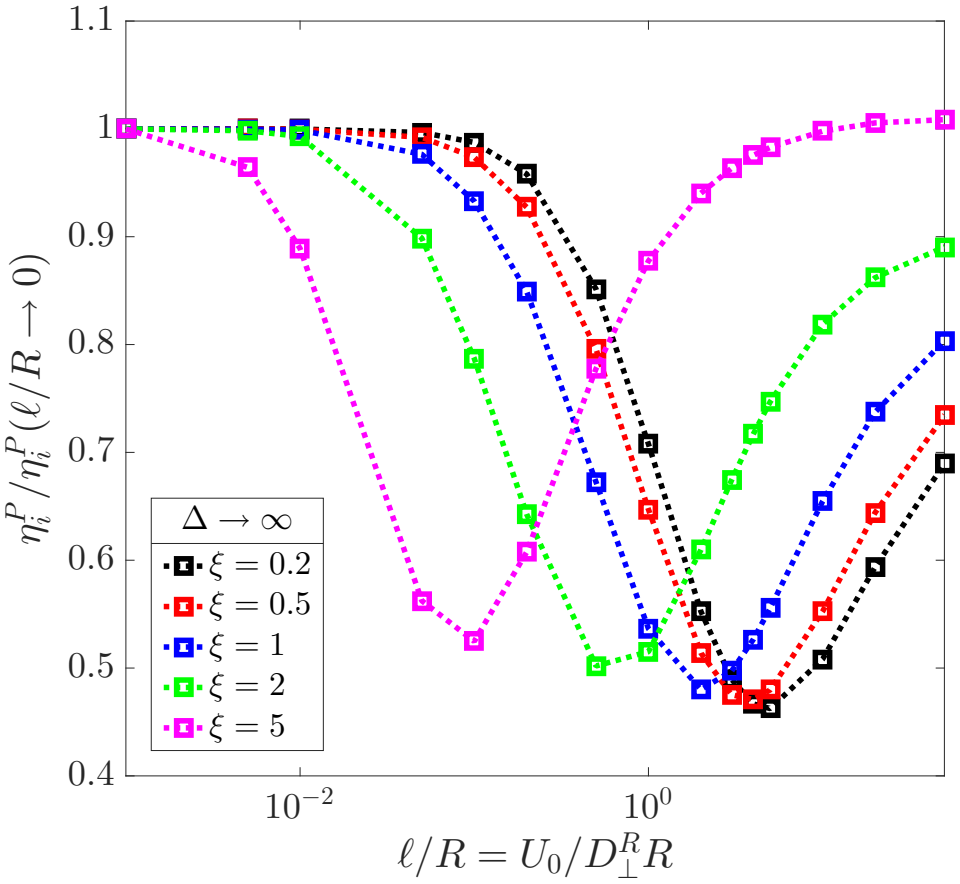

Figure 8.7: Intrinsic interparticle microviscosity, scaled by its value in passive-suspensions, as a function of ℓ/R for various aspect ratios in the absence of hydrodynamic interactions $\Delta \to \infty$.

a monotonically increasing function of Δ (see Appendix A). There may be a point where Δ is small enough that one finds $\eta_i^P < 0$, but Δ is still large enough that $\eta_i^P \sim O(1)$. Additionally, recall that the swimmers are very small $\beta \ll 1$: η_i^P may be comparable in size to $\eta_{i,0}^H$ if $\beta \ll \Delta$, a condition we impose on orientable particles to allow the particles to rotate freely at the no-flux boundary (see Chapter 6).

Though we find negative values of η_i^P even for spherical swimmers, the interparticle intrinsic microviscosity is strongly dependent on the the swimmer geometry, as evidenced by Fig. 8.6. The anisotropy of the swimmers introduces (1) anisotropy in the translational diffusivity and (2) alignment of the particles with the fluid rate-of-strain $\boldsymbol{E}^{\boldsymbol{Stokes}}$. When HI are weak, the strain-alignment terms vanish, but we still retain corrections to the diffusive flux for anisotropic particles (see Fig. 8.7). We recover $\eta_i^P = 1$ when $\ell/R_c \to 0$ as found in Chapter 3, but the plateau for

$\ell/R_c \to \infty$ appears to vary slightly with the particle aspect ratio. The interparticle intrinsic microviscosity retains a minimum with respect to activity, though the precise minimum value of η_i^P as well as the activity level ℓ/R depends on the shape of the particle (see Fig 8.7).

When HI are important, the strain-alignment effects dominate over the anisotropy in the thermal diffusivity—setting $\Delta D = 0$ while letting B vary with aspect ratio makes only a small, quantitative difference in the results (see Fig. 8.6). Analysis of the governing equations shows that the polar ordering due to strain-alignment is $\boldsymbol{m'} \sim B\boldsymbol{E}^{\boldsymbol{Stokes}} \cdot \boldsymbol{m_0}$, where $\boldsymbol{m_0}$ is the polar order in the absence of probe motion. This results in an additional flux of prolate-spheroidal swimmers with the flow (see the sketch, Fig. 8.8) and a flux of oblate-spheroidal swimmers against the flow. For

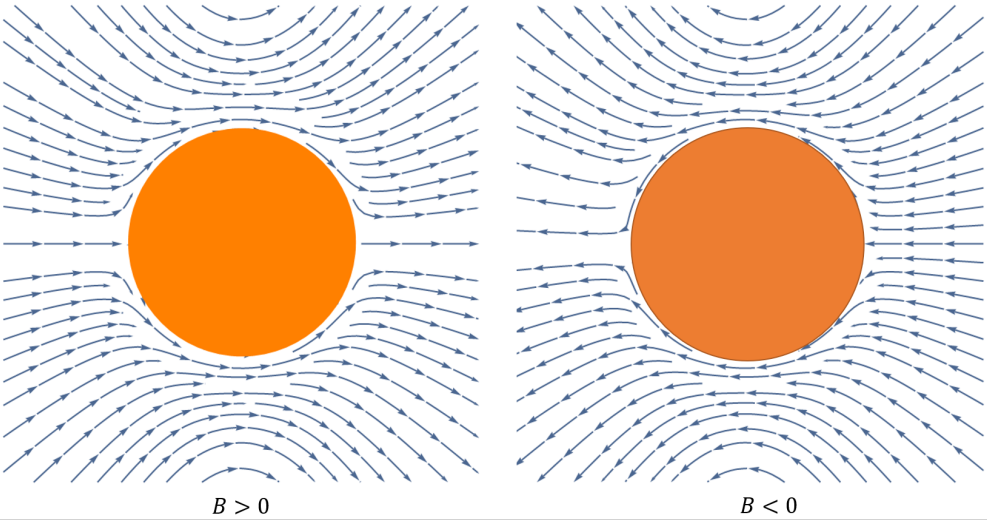

Figure 8.8: Sketch of the flux of swimmers due to strain-alignment in the fluid for prolate (left) and oblate (right) swimmers.

prolate swimmers, this enhances the depletion of swimmers in front of the probe and accumulation behind resulting from pure advection with the flow. (For oblate swimmers, there is an accumulation of particles in front of the probe and a deficit behind, as in the absence of HI.)

The straining motion tends to keep the swimmers aligned with (or against) the flow instead of randomly reorienting. For example, a swimmer behind the probe will find a streamline and swim along it until it collides with the probe, at which point it will push the probe along. It is now more difficult for random fluctuations in the swimmer orientation to take the swimmer along a different trajectory, so once

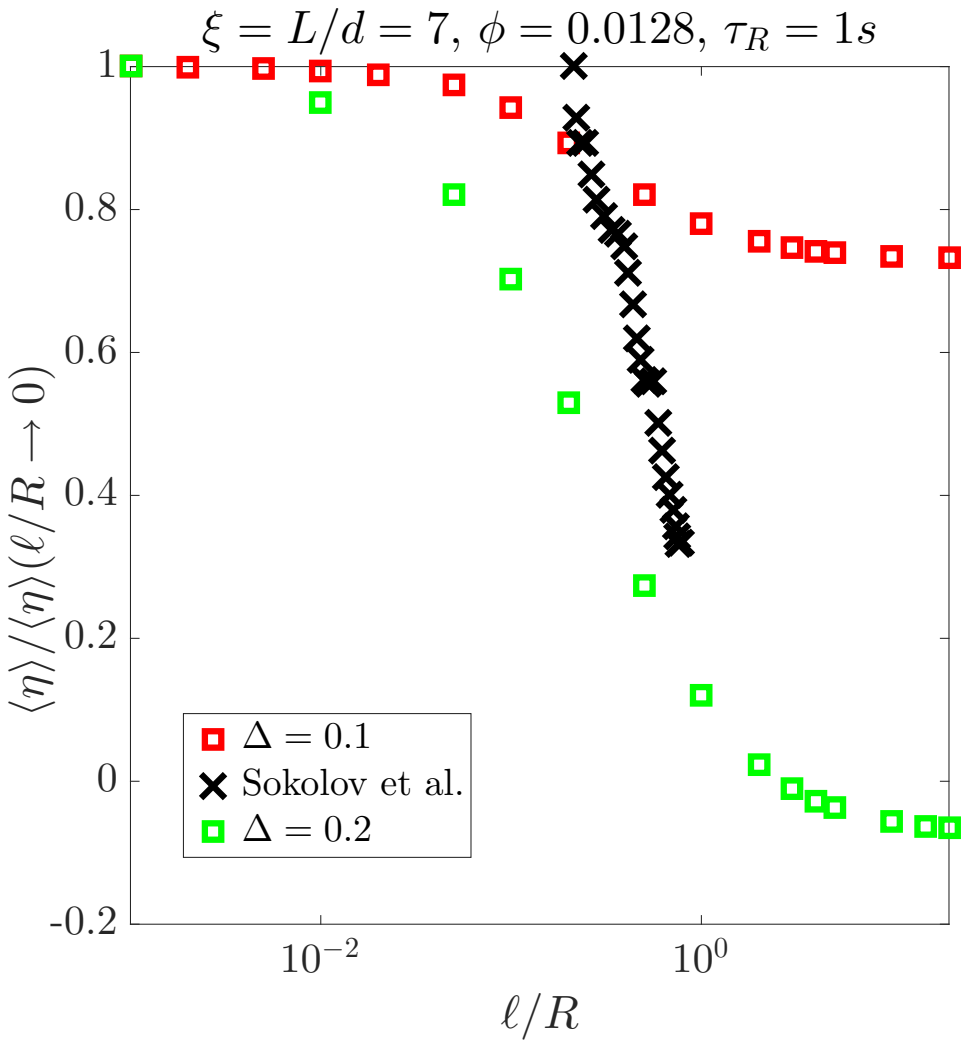

Figure 8.9: The effective viscosity of suspension of motile bacteria (*B. subtilis*), scaled by the effective viscosity of a suspension of nonmotile bacteria at the same concentration, plotted as a function of activity ℓ/R. The run-length is the product of the bacteria's swimming speed U_0 and reorientation time $\tau_R \sim 1s$. The probe size R is 50 μm, the aspect ratio of the bacteria is 7, and the number density of bacteria is $n^{\infty} \sim 1 \times 10^{10}$/mL. We compare the experimental data (in black) with predictions from our model for $\Delta = 0.1$ (red) and $\Delta = 0.2$ (green).

it starts pushing the probe it tends to stay there. Thus, the larger the run length of the swimmer, the further it can push the probe. Unlike the advective bias of the swimmers' random walk responsible for the viscosity reduction at $\ell/R_c \sim O(1)$, the reduction due to strain alignment thus becomes stronger at large ℓ/R_c.

Comparison with experiments and simulations

As a point of comparison, we first look at the experiments of Sokolov and Aronson, who determine the shear viscosity of a bacterial suspension using rotating-probe microrheology (see Fig 8.9). The experiments were done on suspensions of *B. subtilis* with $\xi = 7, \beta = 0.007$, and at volume fraction $\phi = 0.0128$. The reorientation time of the bacteria is not reported, though we assume value of $\sim O(1)s$, as reported in other experiments using wild-type *E. Coli* [39]. We further assume that $\Delta = 0.1 - 0.2$. Drescher et al. report this value as the hydrodynamic horizon for *E. Coli*—the distance beyond which hydrodynamic interactions are dominated by noise [40]. The comparison is imprecise at best, but the experiments measure (and our model predicts) a suspension viscosity much lower than that of the embedding solvent for highly active suspensions. In fact, our model predicts a negative microviscosity for highly active suspensions at $\Delta = 0.2$. A negative microviscosity means that the force required for the probe to translate at a fixed speed points *opposite* the direction of its own motion! This is a unique feature for fixed velocity (c.f. fixed strain rate) experiment. In a fixed-force (c.f. fixed shear-stress) experiment, the probe would speed up as the viscosity approached zero and the viscosity would then increase again. An interesting area of future study would be to determine if the probe could experience sustained phoretic motion due to the activity of the bath particles, and how that phoretic velocity depends on activity.

The data collected from Aronson's study are not expected to quantitatively match the predictions in this thesis. For one, the bacterial concentrations in [4] are in the range where suspension instabilities (the onset of collective motion) are predicted [2]. The proximity to the critical concentration for the onset of collective motion may explain the sharp dependence of the viscosity on the swim speed. Furthermore, Aronson's experiments measure the effective rotational drag on a probe that rotates due to a fixed external torque. This measures the shear viscosity of the suspension, not the microviscosity—there is no net force on the probe. Lastly the experimental study uses a fixed torque on the probe particle, which automatically precludes prediction of a steady negative viscosity, as the rotation rate of the probe would increase correspondingly until the effective viscosity became positive. There is of course the obvious reason that we have to estimate some physical properties of the bacteria, but this would not explain the drastic difference between our model and this experiment.

In the simulations of Foffano et al. [19], the authors compute the microviscosity of an active nematic suspension. Their continuum-level description neglects motility

of the active bath particles, and assumes that activity is completely described by the active stress exerted on the fluid (similar to calculations of the extensional viscosity [5]). Curiously, they find a negative microviscosity for a *contractile* active nematic, whereas all theories surrounding the bulk rheology predict reduced or negative shear viscosities only in suspensions of extensile swimmers. In [19], the negative microviscosity is the result of a fluid flow opposite the direction of probe motion that is generated by the active stress—a purely hydrodynamic effect. In our model, however, a negative microviscosity can only arise from interparticle effects (which are entirely absent in [19]) because we neglect the fluid velocity disturbances of the active particles. In future extensions of the model we consider here, it would be prudent to include the fluid velocity disturbance due to a stresslet swimmer. This would result in an additional hydrodynamic force on the probe (beyond the one considered here), which may also result in a negative microviscosity even in the absence of probe motion.

8.3 Finite size effects & fixed-force vs. fixed-velocity

For simplicity we have assumed that the swimmers are orientable point particles in the preceding analysis. For spherical swimmers we can relax the restriction on size, as the two-body mobility functions for spheres in Stokes flow are known [21, 41] for all β. The problem is formulated precisely in Chapter 6. We plot the linear-response microviscosity as a function of activity for various values of β in Fig. 8.10. We see that negative interparticle microviscosities are found only when $\beta \ll 1$, as our model neglects any hydrodynamic disturbance due to the self-propulsive motion of the swimmers. Were we to include these effects—e.g. those from the active hydrodynamic stresslet—we anticipate that the effects would be different because $\sigma_0 \sim \zeta_s U_0 a$. Pushers are predicted to lower the suspension viscosity, while pullers are predicted to increase it.

For point swimmers, the difference between the fixed-force and fixed-velocity modes of microrheology is a matter of physical interpretation—the mathematics are identical for the two problems, but one cannot find a negative microviscosity for a probe moving under the action of a fixed force. In the absence of hydrodynamic interactions, the difference between the two modes manifests only as a function of $(1 + \beta)$ in the expression for the microviscosity [16]. However, when one includes HI the dependence may be more complex. Swan and Zia showed that (for monodisperse suspensions $\beta = 1$), the ratio of the fixed velocity microviscosity to the fixed force microviscosity is a non-monotonic function of Δ, and a monotonically decreasing

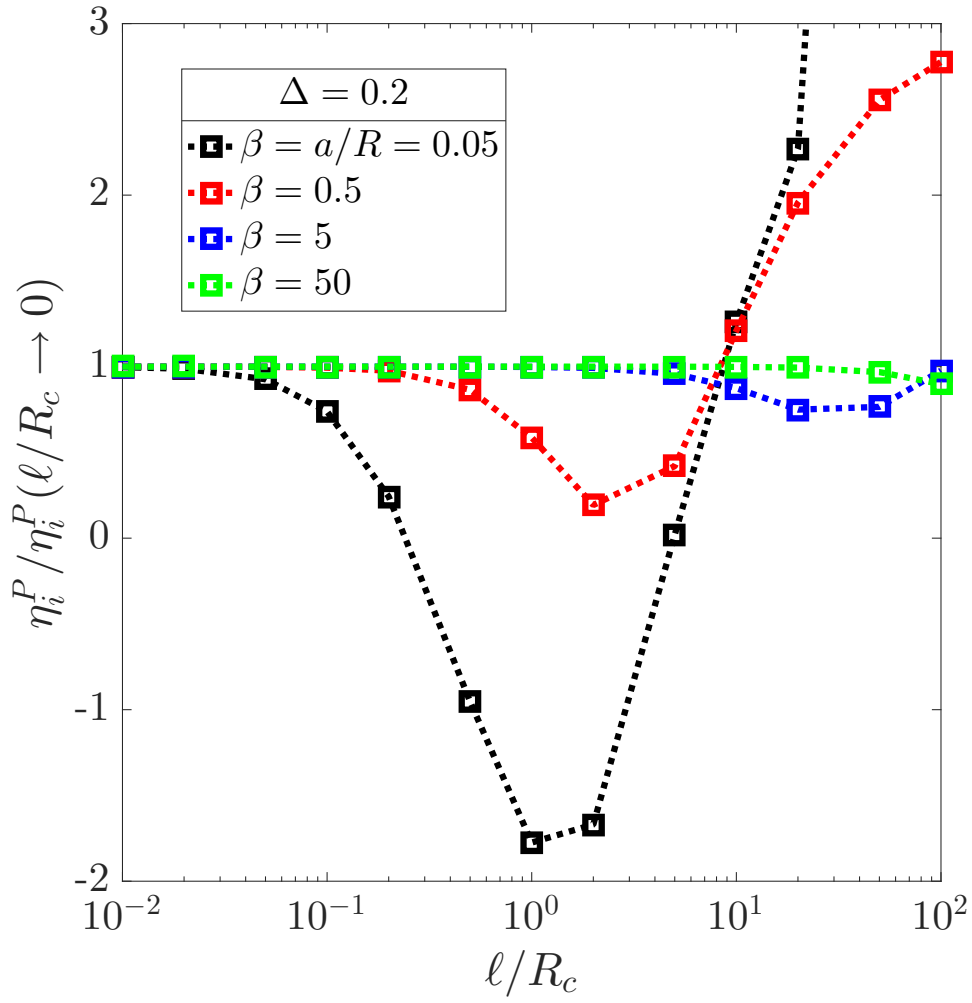

Figure 8.10: Intrinsic interparticle microviscosity (fixed-velocity mode) as a function of the swimmer activity ℓ/R_c for various swimmer-to-probe size ratios β. Hydrodynamic interactions are strong $\Delta = 0.2$, and the swimmers are spherical.

function of Pe, though the fixed-velocity microviscosity is always larger than its fixed-force counterpart. Almog and Brenner [42] examine the differences in η_i^H for fixed-force and fixed-velocity modes of motion in non-Brownian suspensions. To verify that the size ratio does not introduce any unexpected qualitative effects when Brownian motion is important ($Pe \ll 1$), we plot the viscosity ratio as a function of β for $Pe \to 0, \ell/R \to 0$ in Fig. 8.11. The viscosity ratio goes like $1 + \beta$ as predicted in the absence of HI [16], though there are deviations from this for $\beta \sim O(1)$ when HI are strong.

In Fig. 8.12 we plot the ratio of the fixed-velocity microviscosity increment $\Delta\eta_V = \langle\eta\rangle^V - \eta'_\infty$ (scaled by its value in the absence of activity) to the same quantity for the fixed-force

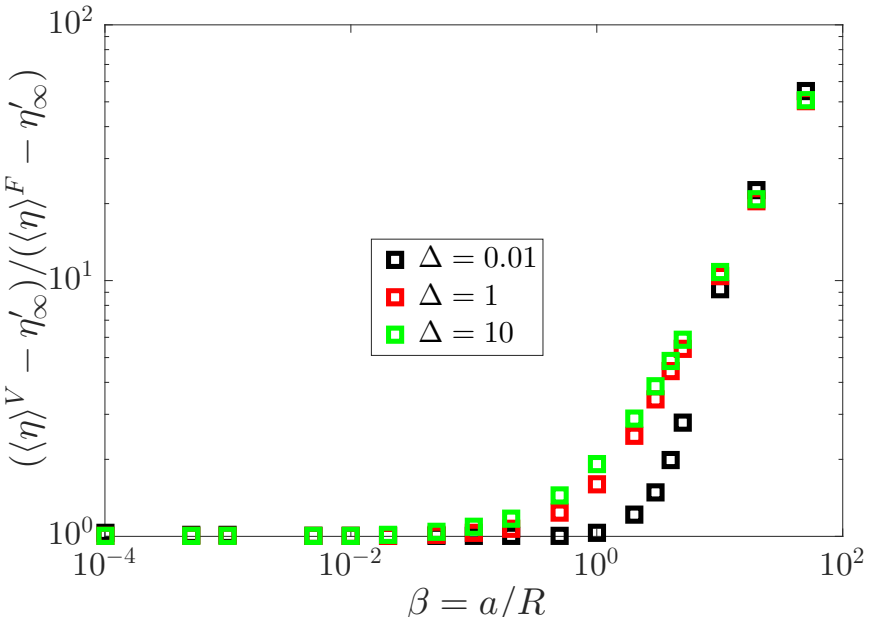

Figure 8.11: Ratio of the particle contribtuion to the fixed-velocity microviscosity $\langle\eta\rangle^V - \eta_s$ to the fixed-force particle contribution to the microviscosity $\langle\eta\rangle^F - \eta_s$ as a function of bath particle to probe size ratio $\beta = a/R$. Different colors indicate different strength of HI.

mode as a function of size ratio; the ratio of these two increments is called the viscosity ratio. When β is large, the two modes are in agreement and $\Delta\eta_V/\Delta\eta_F \sim (1+\beta)$ regardless of the strength of HI (different symbols) or activity level (different colors). Indeed when $\Delta \gg 1$, the activity has no impact on the fixed-force vs. fixed-velocity scaling. When $\Delta = 1$, we note that the fixed velocity increment may actually be *less* than the fixed force increment. This effect is exacerbated for $\Delta \ll 1$ and $\beta \ll 1$, where both activity and hydrodynamic interactions play important roles. The large fluctuations and non-monotonicity of the viscosity ratio reflect the viscosity increments becoming very small or negative. Whether or not these fluctuations are real or perhaps due to the choice of closure, neglect of the swimmers' fluid velocity disturbance, etc. remains an open question.

8.4 Nonlinear response

Sokolov and Aronson report that the viscosity is independent of external forcing for $U^{probe} < U_0$, similar to our predictions in the absence of HI (Chapter 5). This makes the linear-response regime easily accessible in very active suspensions. This is curiously not observed in the experiments of Lopez et al. [7] or the theory of Takatori and Brady [9] for the shear viscosity in active suspensions. In Fig. 8.13, we verify that the microviscosity is Newtonian over a wide range of Péclet number

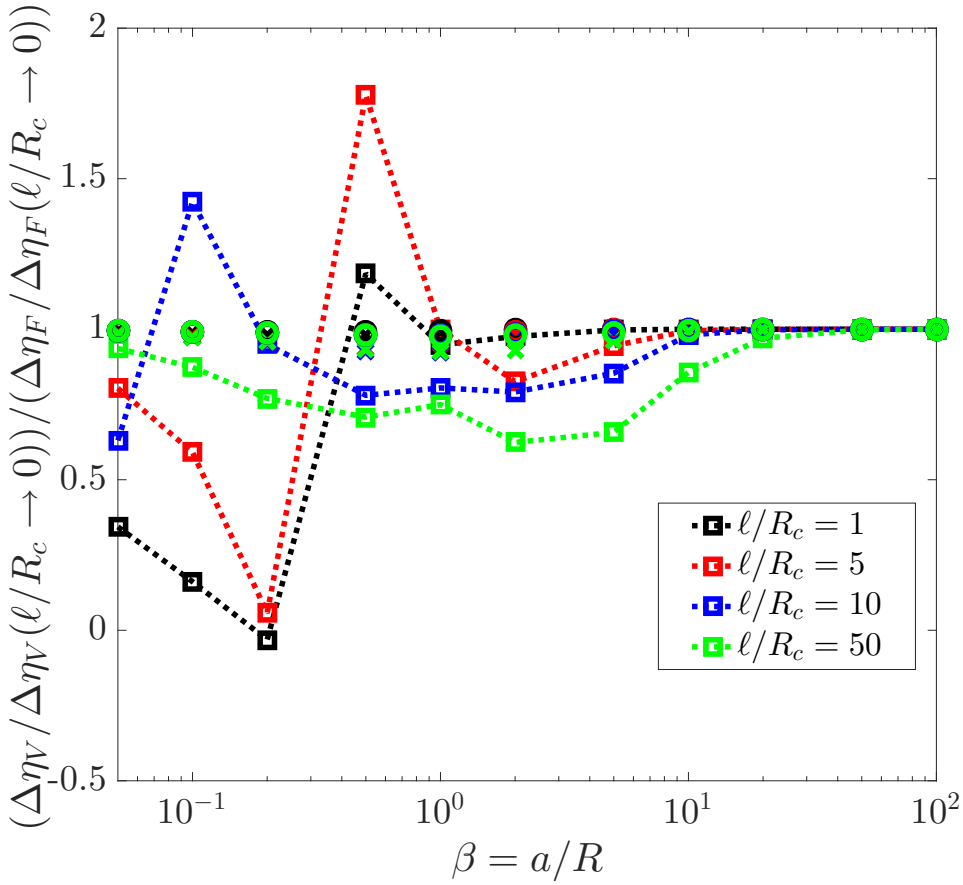

Figure 8.12: Viscosity ratio as a function of the swimmer-to-probe particle size ratio β. Different colors indicate different levels of activity, whereas the different symbols denote different values of Δ. Squares are $\Delta = 0.2$, crosses are $\Delta = 1$, and Circles are $\Delta = 5$.

for the test case $\beta \ll 1$, $\Delta = 0.2$ and $\ell/R = 1$. The widening of the small Pe Newtonian plateau is consistent across a range of particle aspect ratios. As before, the suspension is Newtonian until $U^{probe} \gtrsim U_0$, at which point the suspension transitions to the behavior one would expect in a suspension of passive particles[5]. Fig. 8.13 shows that this transition is smooth for oblate spheroidal swimmers, but there is a sharp jump for spherical swimmers and a singularity with respect to Pe for prolate swimmers. Brownian motion is weak, but finite at large Pe, so a true suspension instability seems unlikely. At the time of writing, it is not clear what is responsible for this discontinuity, though it does not appear to be a result of the closure of the Smoluchowski equation. It could be that an infinite number

[5]In the presence of hydrodynamic interactions, the large Pe plateau is a function of β and Δ. Indeed as $\Delta \to 0$, η_i does not reach a plateau as $Pe \to \infty$, but instead grows as a very weak function of Pe: $\eta_i \sim Pe^{0.21}$ [17, 18].

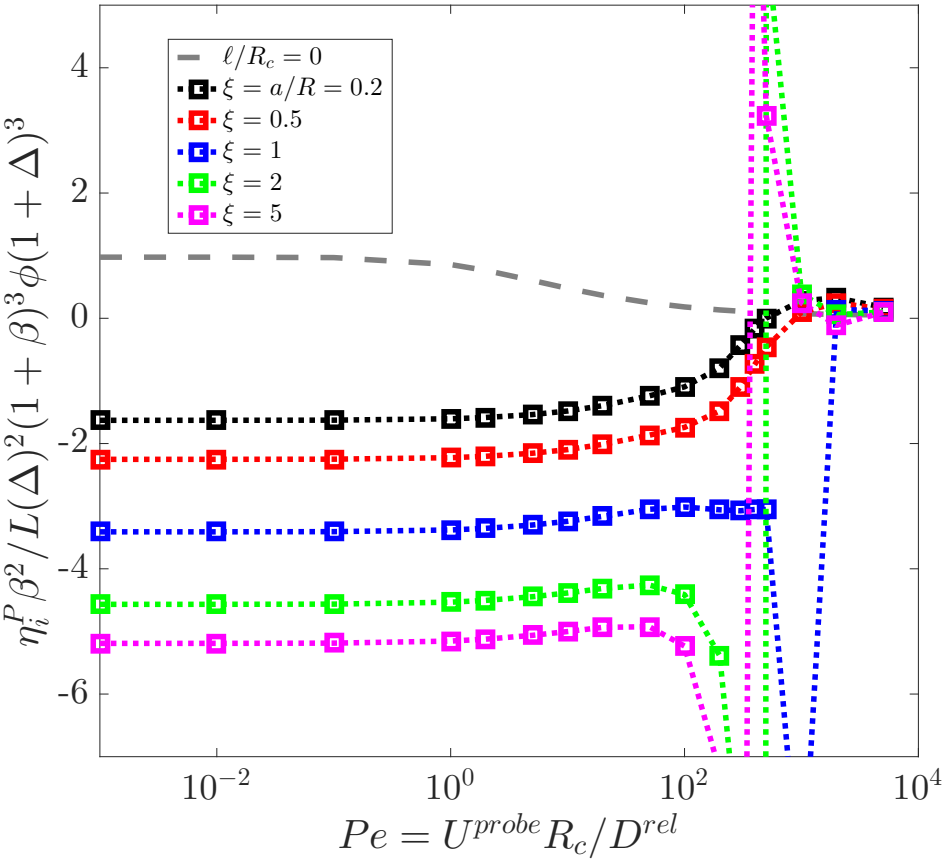

Figure 8.13: Intrinsic interparticle microviscosity (in pseudo-2-D) as a function of Pe, scaled by its $Pe \ll 1$ value in the absence of activity. The dashed grey line is a guide for the nonlinear response observed when $\ell/R = 0$, the symbols connected by dashed lines are at the activity level $\ell/R = 1$. Different colors represent different particle aspect ratios $\xi = L/d$.

of moments are needed to capture this transition properly, thus a finite-element or simulation based approach would be needed to verify the results.

For the sake of numerical precision, Fig. 8.13 was constructed using a pseudo-2-D approximation of the problem. As mentioned in Chapter 6, the essence of this approximation is that the particles only move and reorient in the plane, but the hydrodynamic disturbances are fully three-dimensional. Physically, this represents a situation where the particles sit at an interface between a dense and less dense fluid. The fluids density separate but have the same viscosity—e.g. salt-water and water—thus the particles stay at the interface when matched to the denser fluid, but a particle translating at this interface still induces the familiar Stokes velocity field $\boldsymbol{u}^{\boldsymbol{Stokes}}$. This approximation improves computational accuracy by i) reducing

the number of nematic order components that we need to calculate and ii) removes singularities (associated with the 3-D divergence operator) at the poles of the probe.

8.5 Conclusions

Using the framework developed in Chapter 6, we investigated the effects of interparticle hydrodynamic interactions on the effective microviscosity in active suspensions. Indeed, even in the simplest scenario where the size and hydrodynamic disturbances of the swimmers are neglected, we find that the microviscosity of the suspension may be negative depending on the level of activity, strength of HI, and swimmer shape. This decrease is entirely due to the interparticle contribution to the intrinsic microviscosity—the Brownian contribution is negligible, and the intrinsic hydrodynamic viscosity (or high-frequency shear viscosity) *increases* due to the accumulation of swimmers near the no-contact surface of the probe. While the negative interparticle microviscosity is principally due to the strain alignment of the swimmer with the direction of probe motion, it can also be explained simply by the advection of the swimmers with the fluid velocity field $\boldsymbol{u}^{\boldsymbol{Stokes}}$. The fluid vorticity appears to play a negligible role in this process, as it induces no net flux parallel to the probe's motion.

We also began to address some extensions of the simplest model: finite swimmer size (for spherical particles only), difference between fixed-force and fixed-velocity modes of microrheology, and the nonlinear response. When the swimmers are comparable to or larger than the probe, we no longer find a negative η_i^P. If we were to refine the model and include the stresslet disturbance due to swimmers' locomotion, we anticipate that this might change our findings. The difference between fixed-force and fixed-velocity microrheology in active suspensions is largely a matter of physical interpretation—a negative effective microviscosity is physically realizable only in the constant velocity mode. Indeed the viscosity ratio is unaffected by activity as β becomes large, but in the limit $\beta \ll 1$, the ratio fluctuates due to the interparticle contribution becoming negative. The physical results of the nonlinear analysis appear unchanged by hydrodynamic interactions: the suspension is Newtonian (with a much lower viscosity) until the probe speed exceeds the swim speed, at which point the suspension is indistinguishable from a suspension of passive colloids.

In future work on this topic, it would be interesting to investigate how the hydrodynamic effects seen here compare with those traditionally measured—the viscosity correction due to the swimmers' active stresslet. Takatori and Brady argue that

the swim-stress contribution to the suspension viscosity is much larger than the stresslet contribution when $\ell/R_c \gg 1$, thus the swimming gait is unimportant. The framework in Chapter 6 allows for one to easily incorporate the active stresslet into the microrheology problem. Additionally, it would be interesting to compute the effective diffusivity of the probe in the presence of hydrodynamic interactions (framework given in Chapter 3). One could then quantitatively investigate departures from the Stokes-Einstein-Sutherland relation, and compare to the departures found in the absence of HI.

Appendix

A: Additional figures of the intrinsic microviscosity in the linear-response regime $Pe \ll 1$

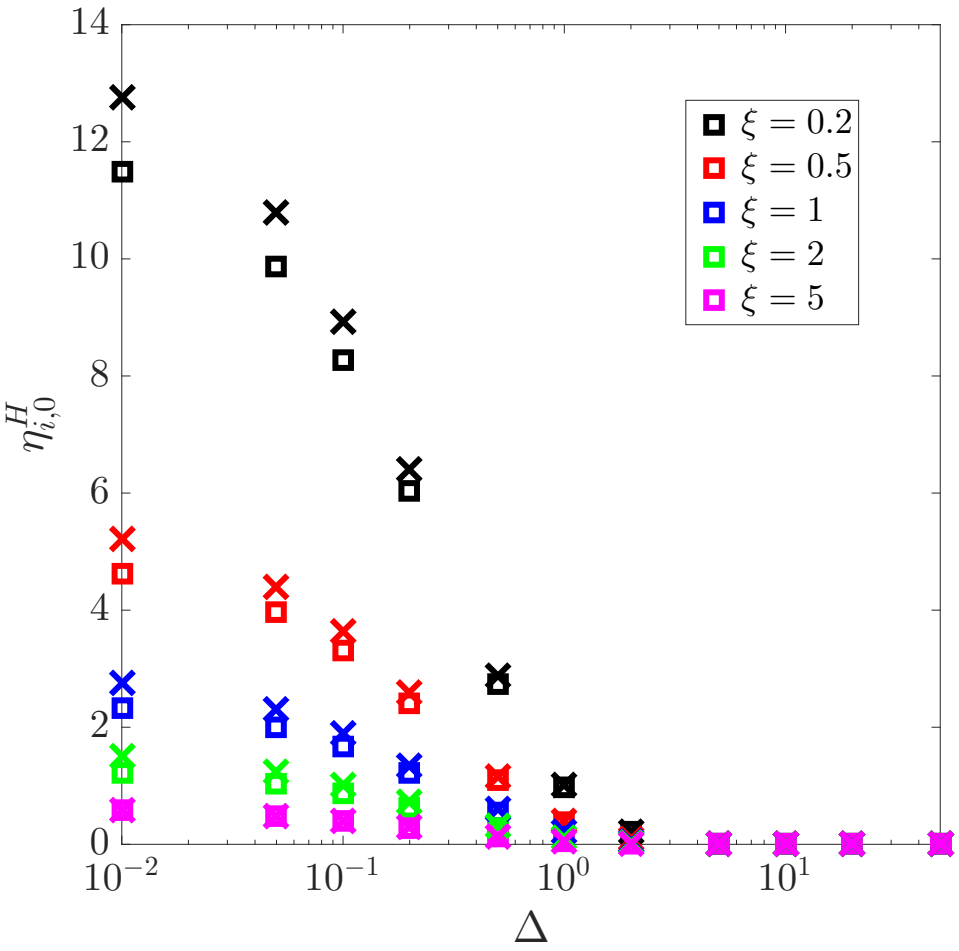

Figure 8.14: The hydrodynamic contribution to to the intrinsic microviscosity (in the absence of probe motion) scaled by the result for passive colloidal suspensions, is plotted as a function of the strength of hydrodynamic interactions Δ. Square symbols are for swimmer activity $\ell/R = U_0/D_\perp^R R = 0.1$ and crosses are for $\ell/R = 1$; U_0 is the swim speed, $D_\perp^R$ is the inverse reorientation time, and R is the size of the probe. Different colors represent different swimmer aspect ratios $\xi = L/d$.

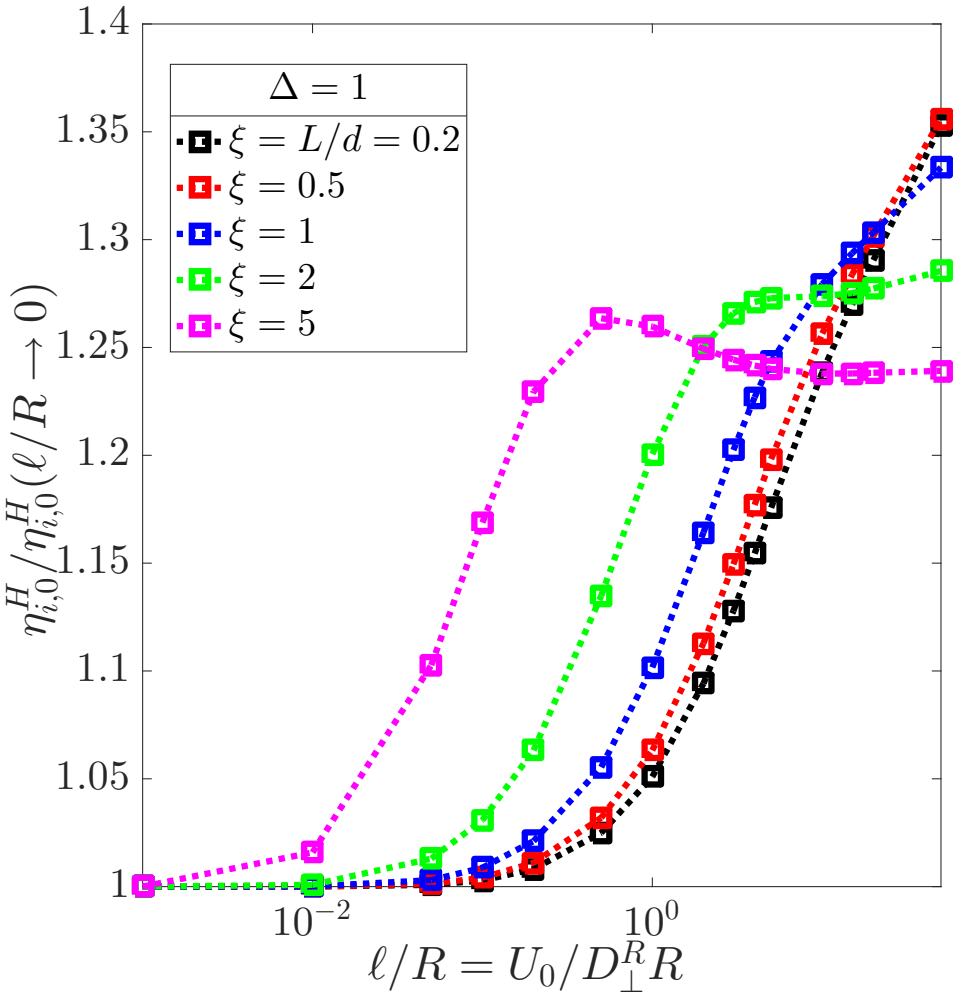

Figure 8.15: The hydrodynamic contribution to the intrinsic microviscosity, scaled by the result for passive colloidal suspensions, plotted as a function of the swimmers' activity $\ell/R = U_0/D^R_\perp R$, where U_0 is the swim speed, $D^R_\perp$ is the inverse reorientation time, and R is the size of the probe. Different colors represent different swimmer aspect ratios $\xi = L/d$. Hydrodynamic interactions are moderate: $\Delta = 1$.

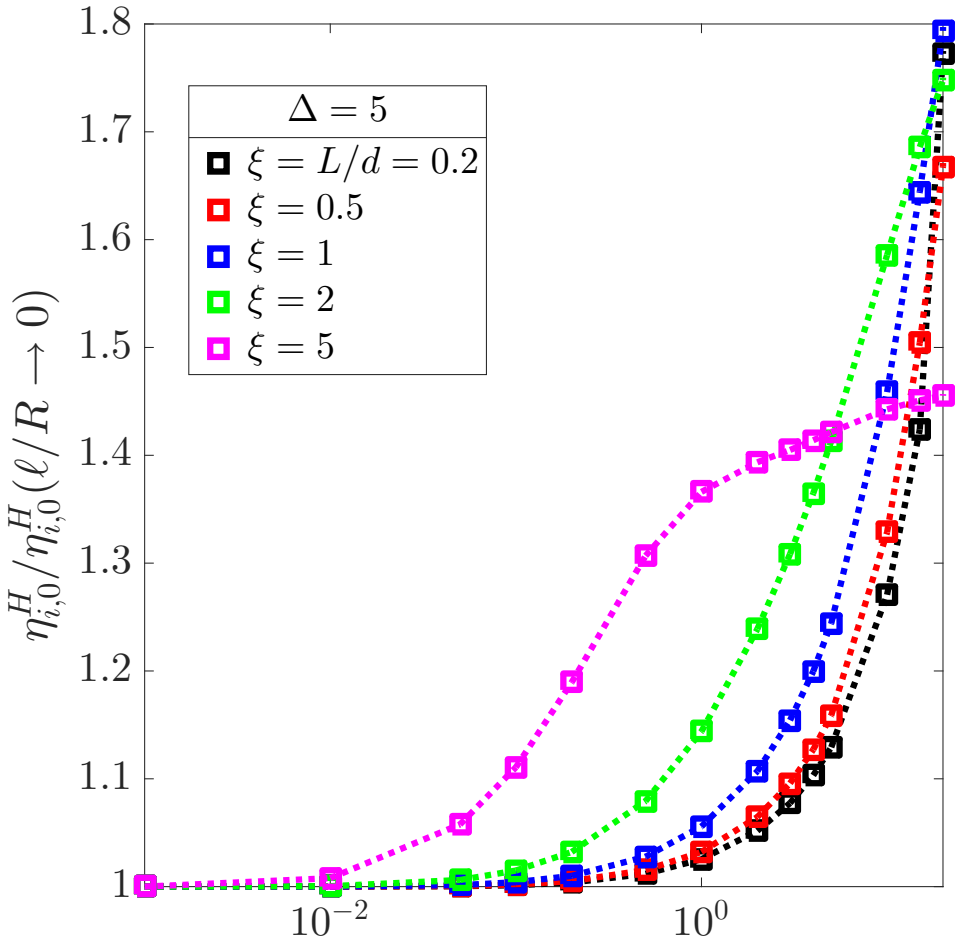

Figure 8.16: The hydrodynamic contribution to the intrinsic microviscosity, scaled by the result for passive colloidal suspensions, plotted as a function of the swimmers' activity $\ell/R = U_0/D_\perp^R R$, where U_0 is the swim speed, $D_\perp^R$ is the inverse reorientation time, and R is the size of the probe. Different colors represent different swimmer aspect ratios $\xi = L/d$. Hydrodynamic interactions are weak: $\Delta = 5$.

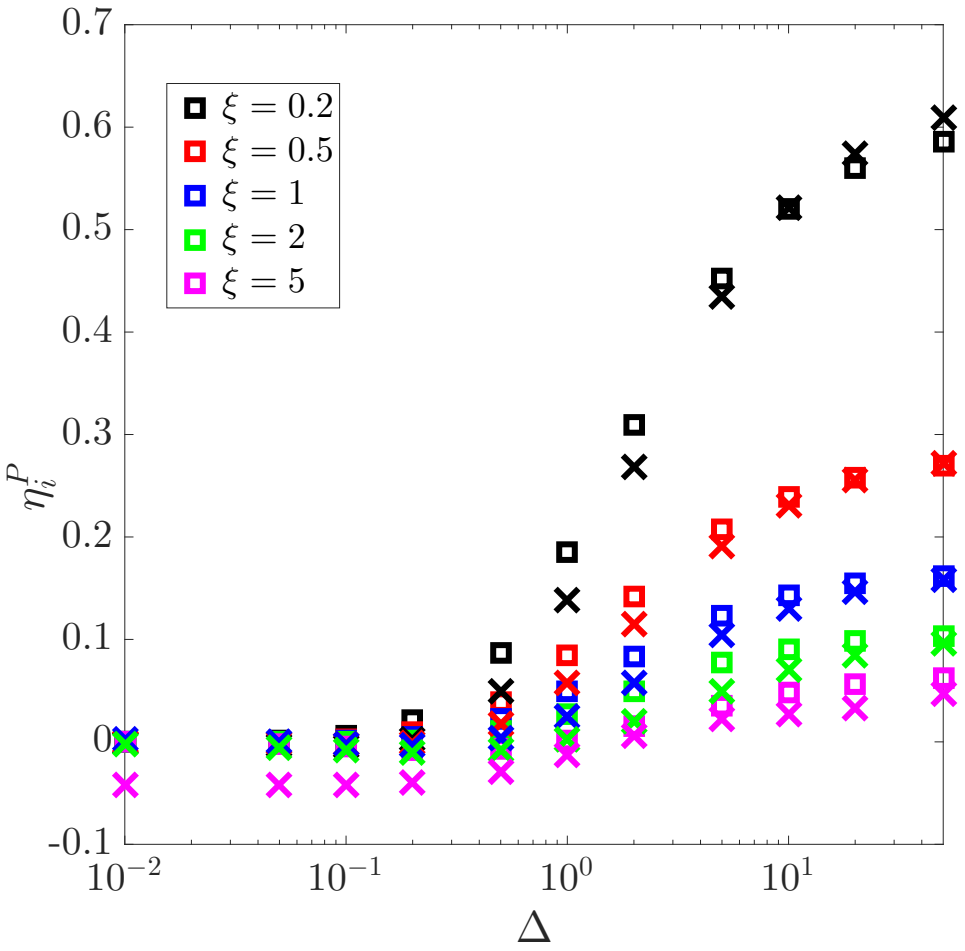

Figure 8.17: The interparticle contribution to to the intrinsic microviscosity (in the absence of probe motion) scaled by the result for passive colloidal suspensions, is plotted as a function of the strength of hydrodynamic interactions Δ. Square symbols are for swimmer activity $\ell/R = U_0/D_\perp^R R = 0.1$ and crosses are for $\ell/R = 1$; U_0 is the swim speed, $D_\perp^R$ is the inverse reorientation time, and R is the size of the probe. Different colors represent different swimmer aspect ratios $\xi = L/d$.

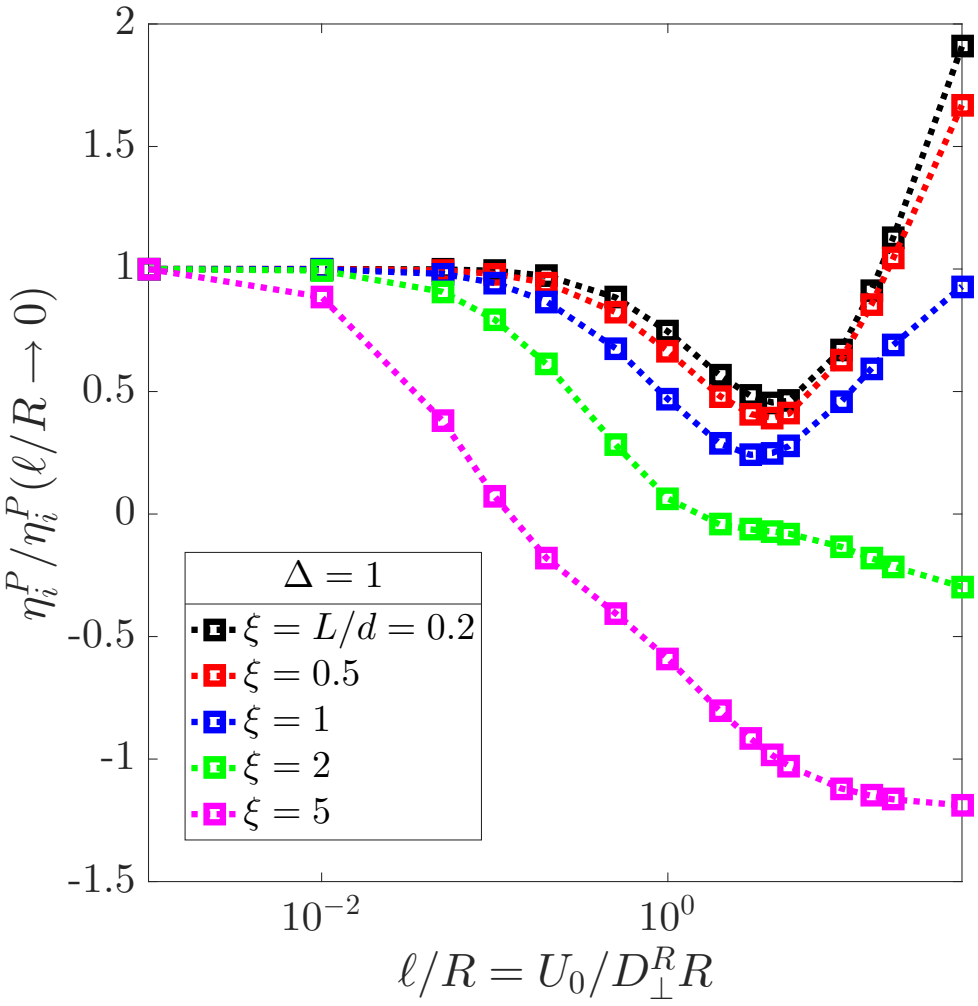

Figure 8.18: The interparticle contribution to the intrinsic microviscosity, scaled by the result for passive colloidal suspensions, plotted as a function of the swimmers' activity $\ell/R = U_0/D_\perp^R R$, where U_0 is the swim speed, $D_\perp^R$ is the inverse reorientation time, and R is the size of the probe. Different colors represent different swimmer aspect ratios $\xi = L/d$. Hydrodynamic interactions are moderate: $\Delta = 1$.

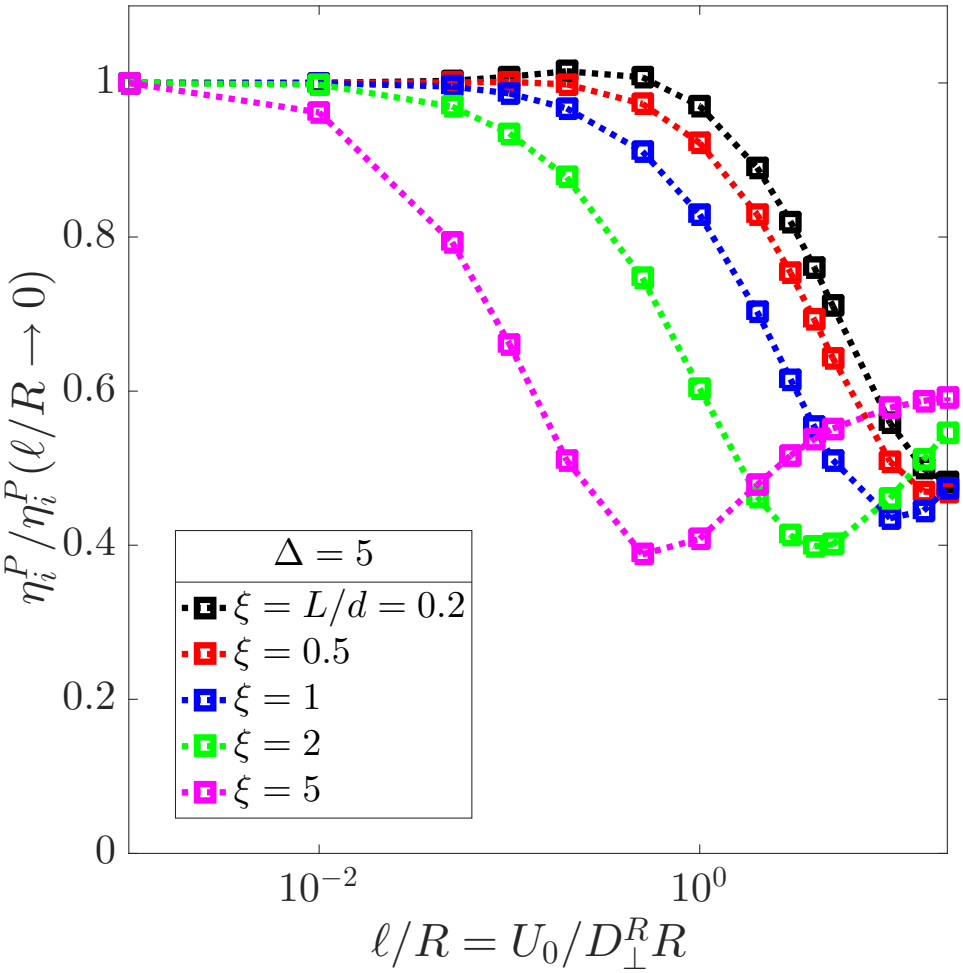

Figure 8.19: The interparticle contribution to the intrinsic microviscosity, scaled by the result for passive colloidal suspensions, plotted as a function of the swimmers' activity $\ell/R = U_0/D_\perp^R R$, where U_0 is the swim speed, $D_\perp^R$ is the inverse reorientation time, and R is the size of the probe. Different colors represent different swimmer aspect ratios $\xi = L/d$. Hydrodynamic interactions are weak: $\Delta = 5$.

BIBLIOGRAPHY

[1]A. Manela, and I. Frankel, "Generalized Taylor dispersion in suspensions of gyrotactic swimming micro-organisms", J. Fluid Mech. **490**, 99–127 (2003).

[2]G. Subramanian, and D. L. Koch, "Critical bacterial concentration for the onset of collective swimming", J. Fluid Mech. **632**, 359 (2009).

[3]A. Sokolov, and I. S. Aranson, "Physical properties of collective motion in suspensions of bacteria", Phys. Rev. Lett. **109**, 1–5 (2012).

[4]A. Sokolov, and I. S. Aranson, "Reduction of viscosity in suspension of swimming bacteria", Phys. Rev. Lett. (2009) 10.1103/PhysRevLett.103.148101.

[5]D. Saintillan, "The Dilute Rheology of Swimming Suspensions: A Simple Kinetic Model", Exp. Mech. **50**, 1275–1281 (2010).

[6]J. Bialké, "A spherical envelope approach to ciliary propulsion", J. Fluid Mech. **46**, 199 (1971).

[7]H. M. López, J. Gachelin, C. Douarche, H. Auradou, and É. Clément, "Turning Bacteria Suspensions into Superfluids", Phys. Rev. Lett. **115**, 028301 (2015).

[8]S. Nambiar, P. R. Nott, and G. Subramanian, "Stress relaxation in a dilute bacterial suspension", J. Fluid Mech. **812**, 41–64 (2017).

[9]S. C. Takatori, and J. F. Brady, "Superfluid Behavior of Active Suspensions from Diffusive Stretching", Phys. Rev. Lett. **118**, 018003 (2017).

[10]T. M. Bechtel, and A. S. Khair, "Linear viscoelasticity of a dilute active suspension", Rheol. Acta **56**, 149–160 (2017).

[11]Y. Hatwalne, S. Ramaswamy, M. Rao, and R. A. Simha, "Rheology of Active-Particle Suspensions", Phys. Rev. Lett. **92**, 1–4 (2004).

[12]B. M. Haines, A. Sokolov, I. S. Aranson, L. V. Berlyand, and D. A. Karpeev, "Three-dimensional model for the effective viscosity of bacterial suspensions", Phys. Rev. E - Stat. Nonlinear, Soft Matter Phys. (2009) 10.1103/PhysRevE.80.041922.

[13]L. Giomi, T. B. Liverpool, and M. C. Marchetti, "Sheared active fluids: Thickening, thinning, and vanishing viscosity", Phys. Rev. E - Stat. Nonlinear, Soft Matter Phys. **81** (2010).

[14]S. Heidenreich, S. Hess, and S. H. L. Klapp, "Nonlinear rheology of active particle suspensions: Insights from an analytical approach", Phys. Rev. E - Stat. Nonlinear, Soft Matter Phys. **83**, 1–8 (2011).

[15]R. Alonso-Matilla, B. Ezhilan, and D. Saintillan, "Microfluidic rheology of active particle suspensions: Kinetic theory", Biomicrofluidics **10** (2016).

[16]T. M. Squires, and J. F. Brady, "A simple paradigm for active and nonlinear microrheology", Phys. Fluids **17**, 1–21 (2005).

[17]A. S. Khair, and J. F. Brady, "Single particle motion in colloidal dispersions: a simple model for active and nonlinear microrheology", J. Fluid Mech. **557**, 73 (2006).

[18]N. J. Hoh, "Effects of Particle Size Ratio on Single Particle Motion in Colloidal Dispersions", PhD thesis (California Institute of Technology, 2013).

[19]G. Foffano, J. S. Lintuvuori, A. N. Morozov, K. Stratford, M. E. Cates, and D. Marenduzzo, "Bulk rheology and microrheology of active fluids", Eur. Phys. J. E **35** (2012) 10.1140/epje/i2012-12098-5.

[20]J. F. Brady, "Particle motion driven by solute gradients with application to autonomous motion: continuum and colloidal perspectives", J. Fluid Mech. **667**, 216–259 (2011).

[21]S. Kim, and S. J. Karilla, *Microhydrodynamics : Principles and Selected Applications* (1991).

[22]E. J. Hinch, and L. G. Leal, "The effect of Brownian motion on the rheological properties of a suspensions of non-spherical particles", J. Fluid Mech. **52**, 683–712 (1972).

[23]H. Brenner, "Transport Mechanics in Systems of Orientable Particles . IV . Convective Transport", J. Colloid Interface Sci. **47**, 199–264 (1974).

[24]R. J. Depuit, and T. M. Squires, "Micro-macro-discrepancies in nonlinear microrheology: I. Quantifying mechanisms in a suspension of Brownian ellipsoids", J. Phys. Condens. Matter **24** (2012).

[25]R. J. Depuit, and T. M. Squires, "Micro-macro discrepancies in nonlinear microrheology: II. Effect of probe shape", J. Phys. Condens. Matter **24** (2012) 10.1088/0953-8984/24/46/464107.

[26]A. S. Khair, and J. F. Brady, "Microrheology of colloidal dispersions: Shape matters", J. Rheol. (N. Y. N. Y). **52**, 165 (2008).

[27]S. Michelin, and E. Lauga, "Phoretic self-propulsion at finite P\'eclet numbers", 572–604 (2014).

[28]S. Michelin, and E. Lauga, "Geometric tuning of self-propulsion for Janus catalytic particles", Sci. Rep. **7**, 1–9 (2017).

[29]F. Jülicher, and J. Prost, "Comment on "osmotic propulsion: The osmotic motor"", Phys. Rev. Lett. **103** (2009) 10.1103/PhysRevLett.103.079801.

[30]U. M. Córdova-Figueroa, and J. F. Brady, "Osmotic propulsion: The osmotic motor", Phys. Rev. Lett. **100**, 1–4 (2008).

[31]S. Shklyaev, J. F. Brady, and U. M. Córdova-Figueroa, "Non-spherical osmotic motor: chemical sailing", J. Fluid Mech. **748**, 488–520 (2014).

[32]F. Bretherton, “The motion of rigid particles i n a shear flow at low Reynolds number”, J. Fluid Mech., 284–304 (1962).

[33]G. Jeffrey, “The motion of ellipsoidal particles immersed in a viscous fluid”, Proc. R. Soc. A Math. Phys. Eng. Sci. **102**, 161–179 (1922).

[34]D. Saintillan, and M. J. Shelley, “Theory of Active Suspensions”, in *Complex fluids biol. syst.* Edited by S. Spagnolie, (Springer, New York, 2015) Chap. 9, pp. 319–355.

[35]W. B. Russel, “The Huggins coefficient as a means for characterizing suspended particles”, J. Chem. Soc. Faraday Trans. 2 Mol. Chem. Phys. **80**, 31 (1984).

[36]W. Yan, and J. F. Brady, “The force on a body in active matter”, J. Fluid Mech. **6**, 1–11 (2015).

[37]S. Kim, “Singularity solutions for ellipsoids in low-Reynolds-number flows: With applications to the calculation of hydrodynamic interactions in suspensions of ellipsoids”, Int. J. Multiph. Flow **12**, 469–491 (1986).

[38]I. Claeys, and J. F. Brady, “Lubrication singularities of the grand resistance tensor for two arbitrary particles.”, PCH Physicochem. Hydrodyn. Hydrodyn. **11**, 261–293 (1989).

[39]A. Sokolov, L. D. Rubio, J. F. Brady, and I. S. Aranson, “Instability of expanding bacterial droplets”, Nat. Commun. **9** (2018) 10.1038/s41467-018-03758-z.

[40]K. Drescher, J. Dunkel, L. H. Cisneros, S. Ganguly, and R. E. Goldstein, “Fluid dynamics and noise in bacterial cell – cell and cell – surface scattering”, Proc. Natl. Acad. Sci. U. S. A. **108**, 10940–10945 (2011).

[41]D. J. Jeffrey, and Y. Onishi, “Calculation of the resistance and mobility functions for two unequal rigid spheres in low-Reynolds-number flow”, J. Fluid Mech. **139**, 261 (1984).

[42]Y. Almog, and H. Brenner, “Non-continuum anomalies in the apparent viscosity experienced by a test sphere moving through an otherwise quiescent suspension”, Phys. Fluids **9**, 16–22 (1997).

Chapter 9

FIXED-PROBE MICRORHEOLOGY: AN ORIENTING EXTERNAL FIELD

In suspensions of passive particles, one can measure the microviscosity of the suspension by (1) dragging the probe through the suspension using mangetic tweezers (for example) or (2) holding the probe fixed in an optical or acoustic trap and moving the bath past the probe at some velocity $\boldsymbol{U}^{\boldsymbol{bath}}$. We will refer to the latter mode as "fixed-probe" microrheology. The microviscosity in the fixed-probe problem is inferred from the force required to keep the probe fixed in the bulk flow, and—in passive suspensions—is identical to the microviscosity as measured by the force required to translate the probe at $\boldsymbol{U}^{\boldsymbol{bath}}$ through the same suspension.

With a suspension of swimmers, however, one can take a different approach to fixed probe microrheology: holding the probe fixed in an optical trap and then applying an external field that exerts a torque on the swimmers, thus biasing their average motion. For example, one could place a probe in a suspension of magnetotactic baceteria. Takatori and Brady showed that an orienting external field leads to anisotropy in the swim stress—the mechanical stress arising from the random run-and-tumble motion of the active particles— providing a novel way to control active soft materials [1]. For example, Takatori has successfully enclosed *Magnetospirillium* inside a giant unilamellar vesicle, and shown that one can apply a magnetic field to cause the vesiscle to translate and deform anisotropically.

For active materials in an external field, fixed-probe and fixed-velocity microrheology are no longer identical. The external torque $\boldsymbol{L}^{\boldsymbol{ext}}$ induces a small drift veclocity $\boldsymbol{M}^{\boldsymbol{UL}} \cdot \boldsymbol{L}^{\boldsymbol{ext}}$ in the swimmers, but the primary source of their biased motion comes from the the coupling between their change in orientation $\dot{\boldsymbol{q}} = \boldsymbol{q} \times \boldsymbol{M}^{\boldsymbol{\Omega L}} \cdot \boldsymbol{L}^{\boldsymbol{ext}}$ and their self-propulsion $U_0\boldsymbol{q}$; $\boldsymbol{M}^{\boldsymbol{\Omega L}}$ and $\boldsymbol{M}^{\boldsymbol{UL}}$ are the hydrodynamic mobilities coupling angular velocity to torque, and translational velocity to torque, respectively; $\boldsymbol{q}$ is the swimmer orientation. The mapping between moving bath particles and a moving probe is not exact in this scenario.

In this brief chapter, we formulate the general framework for determining the force on a probe in a bath of swimmers whose motion is affected by an external field. We then compare the results in the absence of hydrodynamic interactions (HI) under

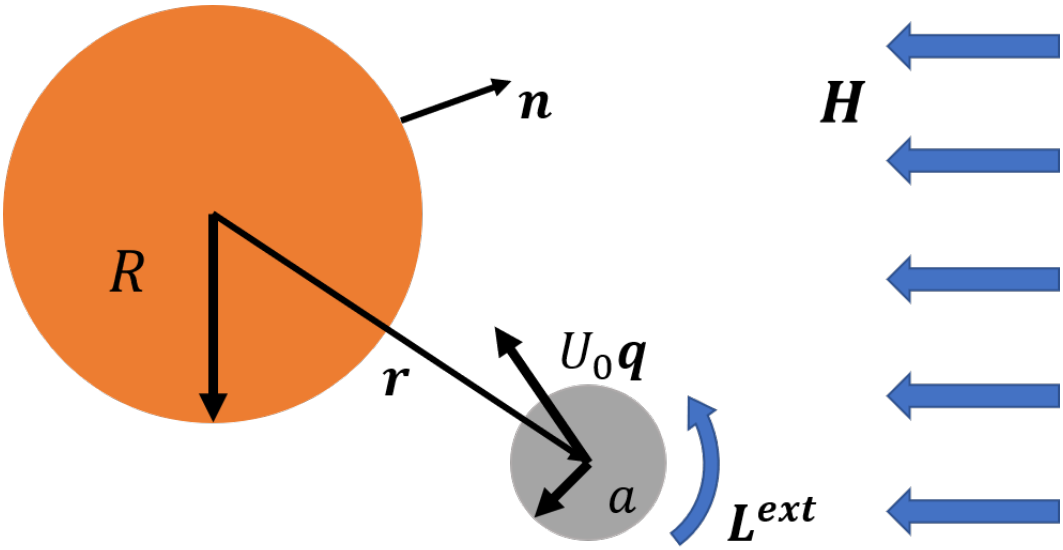

Figure 9.1: Schematic of the fixed-probe microrheology of an active suspension under the influence of an external field $\boldsymbol{H}$. The probe of size R is fixed, while swimmers of size a swim with speed U_0 and reorient their direction of motion $\boldsymbol{q}$ due to random Brownian fluctuations and a torque $\boldsymbol{L}^{ext}$ induced by the external field. The swimmer's displacement from the probe is $\boldsymbol{r}$; $\boldsymbol{n}$ is the outward-pointing unit normal of the probe (i.e. the unit vector pointing along $\boldsymbol{r}$).

the influence of a weak external field to the results found in the translating-probe microrheology problem in Chapter 3.

9.1 Model system

We consider the problem of a spherical probe of size R in a bath of ABPs being oriented by an applied field $\boldsymbol{H}$ (see Fig 9.1). The ABPs have a size a, swim velocity of constant magnitude $\boldsymbol{U_0} = U_0\boldsymbol{q}$ ($\boldsymbol{q}$ is a unit vector that points in the direction of swimming), and a reorientation time τ_R. When the suspension is sufficiently dilute, the dynamics of this system are described by a single-particle Smoluchowski for $P(\boldsymbol{r}, \boldsymbol{q}, t)$—the probability of finding a swimmer at a position $\boldsymbol{r}$ from the probe with orientation $\boldsymbol{q}$ at some instance in time t. The probe does not enter into the equations of motion, it serves only as a boundary (see Chapter 7). The general formalism for the particle fluxes from Chapter 6 applies:

$$\boldsymbol{j}^{\boldsymbol{T}} = [U_0\boldsymbol{q} + \boldsymbol{M}^{\boldsymbol{UL}} \cdot \boldsymbol{L}^{\boldsymbol{ext}} - \boldsymbol{D}^{\boldsymbol{TT}} \cdot \nabla_r \ln P - \boldsymbol{D}^{\boldsymbol{TR}} \cdot \nabla_R \ln P]P, \quad (9.1)$$

$$\boldsymbol{j}^{\boldsymbol{R}} = [\boldsymbol{M}^{\boldsymbol{\Omega L}} \cdot \boldsymbol{L}^{\boldsymbol{ext}} - \boldsymbol{D}^{\boldsymbol{RT}} \cdot \nabla_r \ln P - \boldsymbol{D}^{\boldsymbol{RR}} \cdot \nabla_R \ln P]P, \quad (9.2)$$

where $\boldsymbol{L}^{\boldsymbol{ext}} = \boldsymbol{q} \times \boldsymbol{H}$ [1, 2], the translational flux of the swimmer is $\boldsymbol{j}^T$ and the rotational flux is $\boldsymbol{j}^R$. The translational diffusivity of a swimmer is $\boldsymbol{D}^{\boldsymbol{TT}}$, its rotary diffusivity is $\boldsymbol{D}^{\boldsymbol{RR}}$ and its coupled rotation-translation diffusivity is $\boldsymbol{D}^{\boldsymbol{RT}} = (\boldsymbol{D}^{\boldsymbol{TR}})^\dagger$.

We assume that there is an external force and torque acting on the probe particle to keep it from translating or rotating upon collisions with the bath particles. This changes the mobility functions $\boldsymbol{M^{UL}}$ and $\boldsymbol{M^{\Omega L}}$ from their usual definitions to include interactions with a fixed probe, but allows us to unambiguously neglect degrees of freedom for the motion of the probe; the effective mobility functions are given in Appendix A.

Following the usual moments-averaging procedure [3], we derive the following governing equations for the suspension:

$$\frac{\partial}{\partial x_i}\left[U_0 m_i + M_{ij}^{UL}\epsilon_{jkp}m_k H_p n - D_{ij}^{TT}\frac{\partial n}{\partial x_j}\right] = 0, \tag{9.3}$$

$$n_i\left[U_0 m_i + M_{ij}^{UL}\epsilon_{jkp}m_k H_p - D_{ij}^{TT}\frac{\partial n}{\partial x_j}\right] = 0, r = R_c, \tag{9.4}$$

$$n \sim n^{\infty}, r \to \infty, \tag{9.5}$$

$$\begin{aligned}\frac{\partial}{\partial x_i}\Bigg[&U_0\left(Q_{pi} + \frac{1}{3}\delta_{pi}n\right) + M_{ij}^{UL}\epsilon_{jkr}\left(Q_{kp} + \frac{1}{3}\delta_{kp}n\right)H_r + D_{ij}^{TT}\frac{\partial m_p}{\partial x_j}\\ &+D_{ij}^{TR}\epsilon_{jkp}m_k\Bigg] + M_{ij}^{\Omega L}\epsilon_{pki}\epsilon_{jlr}H_r\left(\frac{1}{3}\delta_{kl}n + Q_{kl}\right) + D_{ij}^{RT}\epsilon_{ikp}\frac{\partial m_k}{\partial x_j}\\ &+D_{ii}^{RR}m_p - D_{ip}^{RR}m_i + \frac{2}{\tau_R}m_p = 0,\end{aligned} \tag{9.6}$$

$$\begin{aligned}n_i\Bigg[&U_0\left(Q_{pi} + \frac{1}{3}\delta_{pi}n\right) + M_{ij}^{UL}\epsilon_{jkr}\left(Q_{kp} + \frac{1}{3}\delta_{kp}n\right)H_r\\ &+D_{ij}^{TT}\frac{\partial m_p}{\partial x_j} + D_{ij}^{TR}\epsilon_{jkp}m_k\Bigg] = 0, r = R_c,\end{aligned} \tag{9.7}$$

$$m_p \sim m_p^{\infty}, r \to \infty, \tag{9.8}$$

$$\frac{\partial}{\partial x_i}\Bigg[\frac{U_0}{5}\Big(\alpha_{qpsi}-\frac{5}{3}\delta_{ps}\delta_{qi}\Big)m_q+\frac{1}{5}M^{UF}_{ij}\epsilon_{jkr}H_r\alpha_{kpsq}m_q-D^{TT}_{ij}\frac{\partial Q_{ps}}{\partial x_j} \tag{9.9}$$

$$+D^{TR}_{ij}(\epsilon_{jkp}Q_{sk}+\epsilon_{jks}Q_{pk})\Bigg]+\frac{1}{5}M^{\Omega L}_{ij}H_r\epsilon_{j\ell r}\Big(\epsilon_{pki}\alpha_{k\ell sq}m_q+\epsilon_{ski}\alpha_{k\ell pq}m_q\Big)$$

$$+D^{RT}_{ij}\frac{\partial}{\partial x_j}\Big(\epsilon_{ikp}Q_{sk}+\epsilon_{iks}Q_{pk}\Big)+\frac{6}{\tau_R}Q_{ps}$$

$$-D^{RR}_{ij}(\epsilon_{iks}\epsilon_{jmp}+\epsilon_{ikp}\epsilon_{jms})Q_{km}+D^{RR}_{ij}(2\delta_{ij}Q_{ps}-\delta_{js}Q_{ip}-\delta_{jp}Q_{is})=0,$$

$$n_i\Bigg[\frac{U_0}{5}\Big(\alpha_{qpsi}-\frac{5}{3}\delta_{ps}\delta_{qi}\Big)m_q+\frac{1}{5}M^{UF}_{ij}\epsilon_{jkr}H_r\alpha_{kpsq}m_q-D^{TT}_{ij}\frac{\partial Q_{ps}}{\partial x_j}$$

$$+D^{TR}_{ij}(\epsilon_{jkp}Q_{sk}+\epsilon_{jks}Q_{pk})\Bigg]=0, r=R_c, \tag{9.10}$$

$$Q_{ps}\sim Q^{\infty}_{ps}, r\to\infty. \tag{9.11}$$

In deriving these equations, we made the closure $\langle \boldsymbol{qqq}\rangle = \boldsymbol{\alpha}\cdot\langle \boldsymbol{q}\rangle/5$, where $\boldsymbol{\alpha}$ is the fourth-order isotropic tensor [3].

We have a condition of no-flux at particle contact: $\boldsymbol{n}\cdot\boldsymbol{j^T}=0$ at $r=R_c\equiv(R+a)$, but the far-field boundary condition has changed. Because the orienting field acts on the swimmers, the suspension will have a nonuniform (generally anisotropic) microstructure far from the probe's surface: $P^{\infty}=n^{\infty}g_0(\boldsymbol{q})$, where n^{∞} is the uniform number density of swimmers and g_0 is the orientation distribution function in the presence of the external field [1]:

$$g_0=\frac{\chi_R}{4\pi\sinh(\chi_R)}e^{\chi_R\hat{\boldsymbol{H}}\cdot\boldsymbol{q}}. \tag{9.12}$$

The parameter $\chi_R = L^{ext}\tau_R/\zeta_R$ is a relative measure of the field strength; ζ_R is the rotary (Stokes) drag on a swimmer. From this we may directly compute the orientational moments of P^{∞} in the far field:

$$\boldsymbol{m}^{\infty}=n^{\infty}\int \boldsymbol{q}g_0\,d\boldsymbol{q} \tag{9.13}$$

$$\boldsymbol{Q}^{\infty}=n^{\infty}\int (\boldsymbol{qq}-\boldsymbol{I}/3)g_0\,d\boldsymbol{q} \tag{9.14}$$

$$\boldsymbol{B}^{\infty}=n^{\infty}\int (\boldsymbol{qqq}-\boldsymbol{\alpha}\cdot\boldsymbol{q}/5)g_0\,d\boldsymbol{q} \tag{9.15}$$

$$\boldsymbol{C}^{\infty}=n^{\infty}\int (\boldsymbol{qqqq}-\boldsymbol{\kappa}:(\boldsymbol{qq}-\boldsymbol{I}/3)/14-\boldsymbol{\alpha}/15)g_0\,d\boldsymbol{q}, \tag{9.16}$$

where $\boldsymbol{\alpha}$ and $\boldsymbol{\kappa}$ are the fourth- and sixth-order isotropic tensors respectively.

When the applied external field is strong, the field variables are principally aligned with along the field's unit director $\hat{\boldsymbol{H}}$: $\boldsymbol{m}^{\infty}=\coth\chi_R\hat{\boldsymbol{H}}\sim\hat{\boldsymbol{H}}$, $\boldsymbol{Q}^{\infty}\sim\hat{\boldsymbol{H}}\hat{\boldsymbol{H}}$,

$\boldsymbol{B}^{\infty} \sim \hat{\boldsymbol{H}}\hat{\boldsymbol{H}}\hat{\boldsymbol{H}}$, $\boldsymbol{C}^{\infty} \sim \hat{\boldsymbol{H}}\hat{\boldsymbol{H}}\hat{\boldsymbol{H}}\hat{\boldsymbol{H}}$, and so on. Because the principal components of all moments are all aligned with the external field at large χ_R, including them doesn't give any more information about the structure of the number density, which is all that is required to compute the force on the probe (microviscosity). If we make the assumption that $\boldsymbol{m} = n\hat{\boldsymbol{H}}$, we can close the governing equations and still have a physically valid picture where the particles strongly align with the external field, or the external force.

When the applied external field is weak, the suspension should be nearly isotropic, and we expect the isotropic closures above to work well to leading order. That is, any deviations from a uniform suspension in the far field ($\boldsymbol{m}^{\infty}$, $\boldsymbol{Q}^{\infty}$, $\boldsymbol{B}^{\infty}$, etc.) should be very small in this limit. Indeed we find

$$\boldsymbol{m}^{\infty} = (\chi_R/3)\hat{\boldsymbol{H}} + O(\chi_R^3), \tag{9.17}$$

$$\boldsymbol{Q}^{\infty} = -\chi_R^2/45(\boldsymbol{I} - \hat{\boldsymbol{H}}\hat{\boldsymbol{H}}) + 2\chi_R^2/45\hat{\boldsymbol{H}}\hat{\boldsymbol{H}} + O(\chi_R^4), \tag{9.18}$$

$$\boldsymbol{B}^{\infty} \sim O(\chi_R^3), \qquad \boldsymbol{C}^{\infty} \sim O(\chi_R^4)...,$$

which implies that the deviations from isotropy become weaker at higher order closures. Neglecting nematic order would thus appear to be an error of $O(\chi_R^2)$, but the deviation from the far-field nematic order $\boldsymbol{Q}$ is forced by terms proportional to $\boldsymbol{m}^{\infty}$, which is $O(\chi_R)$ (see Appendix B). Though we present the framework to properly include nematic order, the results in section 8.3 only address the case where $\boldsymbol{Q}$ and all higher-order structural moments are zero, as the primary objective is a comparison with the translating probe-modes of microrheology.

9.2 Microviscosity: force on the probe

As in the fixed-velocity microrheology problem, the effective microviscosity of the suspension may be inferred from the average force on the probe:

$$\langle \boldsymbol{F}^{ext} \rangle = \int \boldsymbol{M}^{UL} \cdot \boldsymbol{L}^{ext} n dV + \zeta_P \int \boldsymbol{n} \cdot \boldsymbol{D}^{TT} n dS + \zeta_P \int (\nabla \cdot \boldsymbol{D}^{TT}) n dV, \tag{9.19}$$

where

$$\begin{aligned} \boldsymbol{M}^{UL} \;=\; & (\boldsymbol{M}_{\boldsymbol{11}}^{\boldsymbol{UF}})^{-1} \cdot \{\boldsymbol{M}_{\boldsymbol{11}}^{\boldsymbol{UL}} \cdot [\boldsymbol{M}_{\boldsymbol{11}}^{\boldsymbol{\Omega L}} - \boldsymbol{M}_{\boldsymbol{11}}^{\boldsymbol{\Omega F}} \cdot (\boldsymbol{M}_{\boldsymbol{11}}^{\boldsymbol{UF}})^{-1} \cdot \boldsymbol{M}_{\boldsymbol{11}}^{\boldsymbol{UL}}]^{-1} \\ & \cdot [\boldsymbol{M}_{\boldsymbol{12}}^{\boldsymbol{\Omega L}} - \boldsymbol{M}_{\boldsymbol{11}}^{\boldsymbol{\Omega F}} \cdot (\boldsymbol{M}_{\boldsymbol{11}}^{\boldsymbol{UF}})^{-1} \cdot \boldsymbol{M}_{\boldsymbol{12}}^{\boldsymbol{UL}}] - \boldsymbol{M}_{\boldsymbol{12}}^{\boldsymbol{UL}}\}, \end{aligned} \tag{9.20}$$

$$\begin{aligned} \zeta_P \boldsymbol{D}^{\boldsymbol{TT}} \;=\; & k_B T \boldsymbol{I} - (\boldsymbol{M}_{\boldsymbol{11}}^{\boldsymbol{UF}})^{-1} \cdot \boldsymbol{D}_{\boldsymbol{12}}^{\boldsymbol{TT}} + (\boldsymbol{M}_{\boldsymbol{11}}^{\boldsymbol{UF}})^{-1} \cdot \boldsymbol{M}_{\boldsymbol{11}}^{\boldsymbol{UL}} \cdot [\boldsymbol{M}_{\boldsymbol{11}}^{\boldsymbol{\Omega L}} - \boldsymbol{M}_{\boldsymbol{11}}^{\boldsymbol{\Omega F}} \cdot (\boldsymbol{M}_{\boldsymbol{11}}^{\boldsymbol{UF}})^{-1} \cdot \boldsymbol{M}_{\boldsymbol{11}}^{\boldsymbol{UL}}]^{-1} \\ & \cdot [\boldsymbol{D}_{\boldsymbol{12}}^{\boldsymbol{RT}} - \boldsymbol{M}_{\boldsymbol{11}}^{\boldsymbol{\Omega F}} \cdot (\boldsymbol{M}_{\boldsymbol{11}}^{\boldsymbol{UF}})^{-1} \cdot \boldsymbol{D}_{\boldsymbol{12}}^{\boldsymbol{TT}}], \end{aligned} \tag{9.21}$$

are based on the usual two-sphere mobility functions [4] and $\boldsymbol{D}^{xy}_{\alpha\beta} = k_B T \boldsymbol{M}^{xy}_{\alpha\beta}$. As the probe does not move, the appropriate quantity to which we compare the force on the probe is

$$\boldsymbol{F}^{bath} = -6\pi\eta a \boldsymbol{m}^{\infty} U_0/n^{\infty}, \tag{9.22}$$

which is the force required to keep the probe fixed in a Newtonian solvent moving at the same velocity as the average velocity of the particles. The swimmers' contribution to the effective microviscosity is thus defined as $\eta^{micro} = |\boldsymbol{F}^{ext} - \boldsymbol{F}^{bath}|/|\boldsymbol{F}^{bath}|$. If the probe were instead allowed to move—similar to the fixed-force mode of microrheology—one would compare the speed of the probe to the average velocity of the swimmers.

9.3 Linear response: no hydrodynamic interactions

In the absence of hydrodynamic interactions, $\boldsymbol{M}^{\boldsymbol{UL}} = 0$, and $\boldsymbol{M}^{\boldsymbol{\Omega L}} = \boldsymbol{I}/\zeta_R$, where $\zeta_R = 8\pi\eta a^3$ is the rotary drag on the swimmers. As in Chapter 3, one can make analytical progress in the case of $\boldsymbol{Q} = 0$ (Appendix B). The microviscosity is plotted in Fig. 9.2 as a function of ℓ/R_c—where $\ell = U_0\tau_R$ is the run-length of a swimmer—for various activity levels.

When swimming is weak, the Péclet number comparing swimming to thermal diffusion is small $Pe_s = U_0 R_c/D_T \ll 1$, where D_T is the bare Stokes-Einstein-Sutherland (SES) diffusivity of the swimmer. In this limit the microviscosity is

$$\eta^{micro} = 1 - \frac{1}{9} Pe_s^2. \tag{9.23}$$

As in Chapter 3, the onset of swim-thinning is quadratic in the perturbation away from equilibrium Pe_s, though the reduction is slightly less than in the translating probe problem. Note that in Fig. 9.2, the thermal diffusivity $D^{rel} = D_T$ for the orienting field problem, and $D^{rel} = D_P + D_T$, where D_P is the SES diffusivity of the probe for the translating probe problems.

In the continuum limit, $\ell/R_c \ll 1$, we find

$$\eta^{micro} = 1 - \frac{\sqrt{3}}{2}\frac{\ell}{R_c}, \tag{9.24}$$

This is precisely the same result found for the translating-probe microrheology problem in Chapter 3 to $O(\ell/R_c)^2$. In the continuum limit, the swimmers' behave exactly like Brownian particles with an effective diffusivity $D_T + D^{swim}$, where the swim diffusivity $D^{swim} = U_0^2\tau_R/6$ is a mechanical diffusivity arising from their

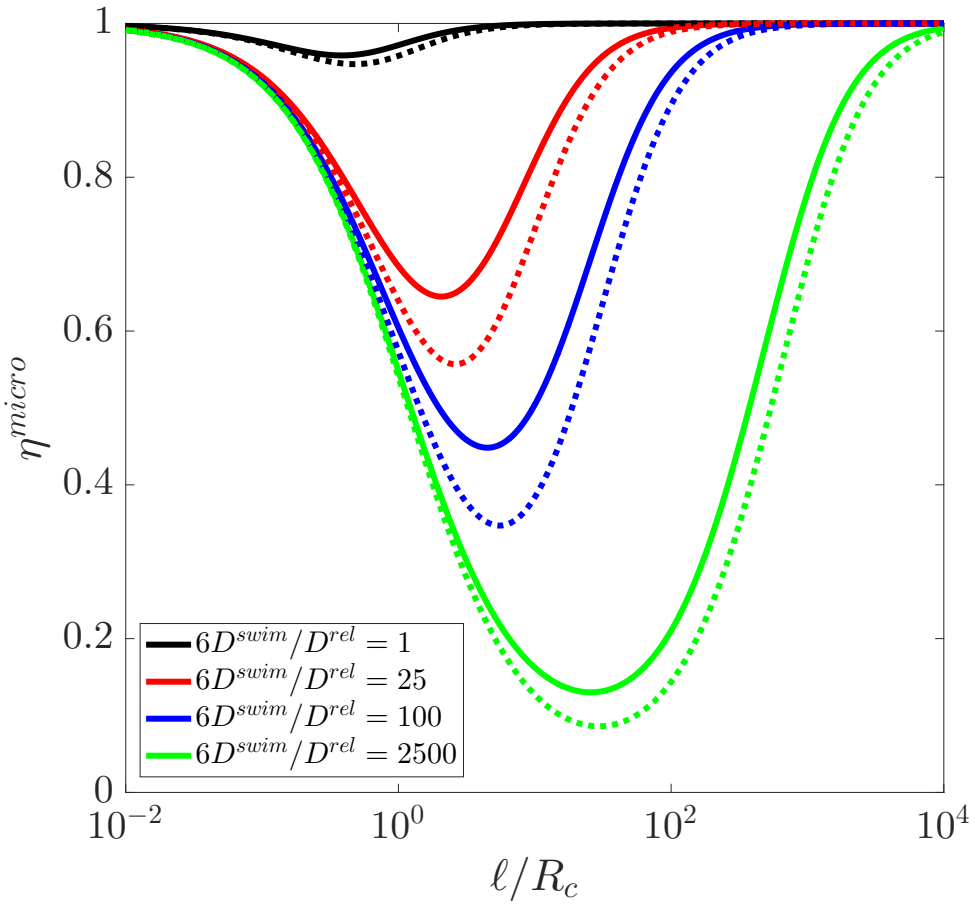

Figure 9.2: Plot of the fixed probe microviscosity for weak external fields: $\chi_R = H\tau_R/\zeta_R \ll 1$, where $\boldsymbol{H}$ is the external field moving the probe, ζ_R is the rotational Stokes drag of the swimmer, and τ_R is the reorientation time. The dashed lines are values of the microviscosity as measured by the translating probe. Different colors correspond to different activity levels: $6D^{swim}/D^{rel} = U_0^2\tau_R/D^{rel}\tau_R$, where U_0 is the swim speed and D^{rel} is the appropriate translational thermal diffusivity.

self-propulsive motion. The force required to keep the probe fixed in a bath of passive Brownian particles moving at a constant velocity is equal and opposite to the force required to move the probe at the same speed velocity through a quiescent bath. Since the swimmers are effectively Brownian in the continuum limit, we would analogously expect no difference between the fixed-probe and translating probe results.

In the limit of strong swimming ($\ell/R_c \gg 1$), $\eta^{micro} \sim Pe_s^{-1}$. We anticipate that including nematic order would change this minimum to some constant less than 1 as in the translating-probe microrheology problems. The trends are nearly indis-

tinguishable from the translating probe equivalents, though the figure reveals that there is not exact quantitative agreement. We note that the force required to hold the probe fixed will proportional to $F^{swim}\phi$ ($\boldsymbol{F}^{\boldsymbol{swim}} = \zeta U_0 \boldsymbol{q}$ and $\phi = 4\pi n^{\infty} a^3/3$) and thus may be large, even for dilute suspensions.

9.4 Future work: nonlinear response and hydrodynamic interactions

As with the linear response, we expect the nonlinear response to qualitatively, but perhaps not quantitatively match the results from the translating probe cases studied in Chapter 3. Indeed, one could even intuit that including the nematic order in the linear response field would make the minimum microviscosity finite for highly active suspensions.

Hydrodynamic interactions will play a qualitatively different role in this problem as compared to the translating probe problem. Net motion of the swimmers due to the external field requires that an equal volume of fluid be displaced in the opposite direction. Thus there is no net displacement of the volume-averaged material (fluid and particles) even when the swimmers all move in the same direction. The suspension-averaged velocity and stress are thus divergence-free. In the absence of the probe, this would result in a uniform fluid pressure and swim stress, and there can be no *material* motion. When the probe is introduced, a net external force will be required to keep the probe from moving [5], which can only be balanced by a pressure gradient in the fluid and fluid motion (the swimmers are force-free).

In the absence of hydrodynamic interactions, asking what force is required to keep the probe from translating is equivalent to asking what the phoretic velocity of the probe is when it is allowed to move. Indeed, the free-probe problem is trivial for passive bath particles in the absence of hydrodynamic interactions—the probe and bath particles would both advect with the fluid at the same speed—but under the influence of an external field it is truly the particles and not the fluid that are moving, thus the microviscosity may change. When HI are considered, the fixed-probe and free-probe problems are qualitatively different. If the probe moves, it is true force-free, phoretic motion. The suspension-averaged stress and fluid pressure can thus be uniform while still sustaining probe motion. If the probe is fixed, there is a non-zero external force in the momentum balance, which can only be balanced by a pressure gradient in the fluid.

It remains to be seen whether one could then find a negative microviscosity (or even a negative intrinsic microviscosity). A negative microviscosity in the case of a

fixed probe, implies that the structural disturbance of the probe allows the swimmers near the probe surface to reverse direction and swim against the bulk flow. In the free-probe problem, a negative microviscosity would imply that the probe is moving *faster* than the bath that is carrying it along. This result is clearly unphysical, but one would need to do the detailed calculations to find either the phoretic velocity of the probe or the force required to keep the probe fixed.

Appendix

A: Mobility functions

For an external field, the mobility functions will turn out to be exactly the same as those for the fixed spherical cavity in Chapter 6. The spherical probe of radius R is held fixed ($\boldsymbol{U}_1 = 0, \boldsymbol{\Omega}_1 = 0$) and the external force $\boldsymbol{F}^{ext}$ and torque $\boldsymbol{L}^{probe}$ necessary can be found from the force balance:

$$\boldsymbol{\mathcal{F}}_{\mathbf{1}}^{\boldsymbol{ext}} = \boldsymbol{\mathcal{R}}_{\mathbf{12}}^{\boldsymbol{\mathcal{FU}}} \cdot (\boldsymbol{\mathcal{R}}_{\mathbf{22}}^{\boldsymbol{\mathcal{FU}}})^{-1} \cdot \boldsymbol{\mathcal{F}}_{\mathbf{2}}^{\boldsymbol{other}} - \boldsymbol{\mathcal{F}}_{\mathbf{1}}^{\boldsymbol{other}}, \tag{9.25}$$

The only 'other' forces to be considered in the above equation are from thermal fluctuations; thus all the effects appear in the diffusive terms of the Smoluchowski equation. From the force balances, one can show that

$$\begin{aligned} \boldsymbol{F}^{\boldsymbol{ext}} &= (\boldsymbol{R}_{\mathbf{12}}^{\boldsymbol{FU}} \cdot (\boldsymbol{\mathcal{R}}_{\mathbf{22}})_{UF}^{-1} + \boldsymbol{R}_{\mathbf{12}}^{\boldsymbol{F\Omega}} \cdot (\boldsymbol{\mathcal{R}}_{\mathbf{22}})_{\Omega F}^{-1} - \boldsymbol{I}) \cdot \boldsymbol{F}_{\mathbf{2}}^{\boldsymbol{B}} \\ &\quad + (\boldsymbol{R}_{\mathbf{12}}^{\boldsymbol{FU}} \cdot (\boldsymbol{\mathcal{R}}_{\mathbf{22}})_{UL}^{-1} + \boldsymbol{R}_{\mathbf{12}}^{\boldsymbol{F\Omega}} \cdot (\boldsymbol{\mathcal{R}}_{\mathbf{22}})_{\Omega L}^{-1}) \cdot (\boldsymbol{L}_{\mathbf{2}}^{\boldsymbol{B}} + \boldsymbol{L}^{\boldsymbol{ext}}) \end{aligned} \tag{9.26}$$

$$\begin{aligned} \boldsymbol{L}^{\boldsymbol{probe}} &= (\boldsymbol{R}_{\mathbf{12}}^{\boldsymbol{LU}} \cdot (\boldsymbol{\mathcal{R}}_{\mathbf{22}})_{UL}^{-1} + \boldsymbol{R}_{\mathbf{12}}^{\boldsymbol{L\Omega}} \cdot (\boldsymbol{\mathcal{R}}_{\mathbf{22}})_{\Omega L}^{-1}) \cdot (\boldsymbol{L}_{\mathbf{2}}^{\boldsymbol{B}} + \boldsymbol{L}^{\boldsymbol{ext}}) \\ &\quad + (\boldsymbol{R}_{\mathbf{12}}^{\boldsymbol{LU}} \cdot (\boldsymbol{\mathcal{R}}_{\mathbf{22}})_{UF}^{-1} + \boldsymbol{R}_{\mathbf{12}}^{\boldsymbol{L\Omega}} \cdot (\boldsymbol{\mathcal{R}}_{\mathbf{22}})_{\Omega F}^{-1}) \cdot \boldsymbol{F}_{\mathbf{2}}^{\boldsymbol{B}}, \end{aligned} \tag{9.27}$$

where $\boldsymbol{F}_{\mathbf{2}}^{\boldsymbol{B}} = -k_B T \nabla \ln P$, $\boldsymbol{L}_{\mathbf{2}}^{\boldsymbol{B}} = -k_B T \nabla_R \ln P$, and $\boldsymbol{L}^{\boldsymbol{ext}} = \boldsymbol{q} \times \boldsymbol{H}$. As before, proper components of the tensor $(\boldsymbol{\mathcal{R}}_{\mathbf{22}})^{-1}$ are

$$(\boldsymbol{\mathcal{R}}_{\mathbf{22}})_{UF}^{-1} = (\boldsymbol{R}_{\mathbf{22}}^{\boldsymbol{FU}} - \boldsymbol{R}_{\mathbf{22}}^{\boldsymbol{F\Omega}} \cdot (\boldsymbol{R}_{\mathbf{22}}^{\boldsymbol{L\Omega}})^{-1} \cdot \boldsymbol{R}_{\mathbf{22}}^{\boldsymbol{LU}})^{-1} \tag{9.28}$$

$$(\boldsymbol{\mathcal{R}}_{\mathbf{22}})_{\Omega F}^{-1} = -(\boldsymbol{R}_{\mathbf{22}}^{\boldsymbol{L\Omega}})^{-1} \cdot \boldsymbol{R}_{\mathbf{22}}^{\boldsymbol{LU}} \cdot (\boldsymbol{R}_{\mathbf{22}}^{\boldsymbol{FU}} - \boldsymbol{R}_{\mathbf{22}}^{\boldsymbol{F\Omega}} \cdot (\boldsymbol{R}_{\mathbf{22}}^{\boldsymbol{L\Omega}})^{-1} \cdot \boldsymbol{R}_{\mathbf{22}}^{\boldsymbol{LU}})^{-1} \tag{9.29}$$

$$(\boldsymbol{\mathcal{R}}_{\mathbf{22}})_{\Omega L}^{-1} = (\boldsymbol{R}_{\mathbf{22}}^{\boldsymbol{L\Omega}} - \boldsymbol{R}_{\mathbf{22}}^{\boldsymbol{LU}} \cdot (\boldsymbol{R}_{\mathbf{22}}^{\boldsymbol{FU}})^{-1} \cdot \boldsymbol{R}_{\mathbf{22}}^{\boldsymbol{F\Omega}})^{-1}, \tag{9.30}$$

and $(\boldsymbol{\mathcal{R}}_{\mathbf{22}})_{\Omega F}^{-1} = -(\boldsymbol{\mathcal{R}}_{\mathbf{22}})_{UL}^{-1}$ by symmetry [4].

B: Analytical solution, $\chi_R \ll 1$

In the absence of hydrodynamic interactions the n and $\boldsymbol{m}$ governing equations simpify to

$$\nabla \cdot [Pe_s \boldsymbol{m} - \nabla n] = 0, \tag{9.31}$$

$$\nabla \cdot [\frac{1}{3} Pe_s \boldsymbol{I} n + Pe_s \boldsymbol{Q} - \nabla \boldsymbol{m}] + \gamma^2 \boldsymbol{m} - \frac{2}{3} \chi_R \gamma^2 (n \hat{\boldsymbol{H}} - 3 \boldsymbol{Q} \cdot \hat{\boldsymbol{H}}) = 0. \tag{9.32}$$

We define the total fields in terms of the equilibrium values (denoted by infinities) and their departures (denoted by primes): $n = n^\infty + n'$, $\boldsymbol{m} = \boldsymbol{m}^\infty + \boldsymbol{m}'$, $\boldsymbol{Q} = \boldsymbol{Q}^\infty + \boldsymbol{Q}'$. Using this representation and the linearity of the governing equations, this allows us to place the forcing from the orienting field at the no-flux boundaries:

$$\nabla \cdot [\nabla n' - Pe_s \boldsymbol{m}'] = 0; \tag{9.33}$$

$$\boldsymbol{n} \cdot [\nabla n' - Pe_s \boldsymbol{m}'] = Pe_s \boldsymbol{n} \cdot \boldsymbol{m}^\infty, r = 1 \tag{9.34}$$

$$n' \to 0, r \to \infty \tag{9.35}$$

$$\nabla \cdot [\nabla \boldsymbol{m}' - \frac{1}{3} Pe_s \boldsymbol{I} n' - Pe_s \boldsymbol{Q}'] - \gamma^2 \boldsymbol{m}' + \frac{2}{3} \chi_R \gamma^2 n' \hat{\boldsymbol{H}} - \chi_R \gamma^2 \boldsymbol{Q}' \cdot \hat{\boldsymbol{H}} = 0; \tag{9.36}$$

$$\boldsymbol{n} \cdot [\nabla \boldsymbol{m}' - \frac{1}{3} Pe_s \boldsymbol{I} n' - Pe_s \boldsymbol{Q}'] = Pe_s \boldsymbol{n} \cdot [\boldsymbol{Q}^\infty + \frac{1}{3} \boldsymbol{I} n^\infty], r = 1 \tag{9.37}$$

$$\boldsymbol{m}' \to 0, r \to \infty. \tag{9.38}$$

Note that we have not yet specified the magnitude of χ_R.

Because the problem is linear, we choose to further decompose the disturbance fields into three pieces: $n' = n_1 + n_2 + n_3$, $\boldsymbol{m}' = \boldsymbol{m}_1 + \boldsymbol{m}_2 + \boldsymbol{m}_3$, and $\boldsymbol{Q}'$ is taken to be zero.

The first component of the fields are defined to solve the following set of equations:

$$\nabla \cdot [\nabla n_1 - Pe_s \boldsymbol{m}_1] = 0; \tag{9.39}$$

$$\boldsymbol{n} \cdot [\nabla n_1 - Pe_s \boldsymbol{m}_1] = 0, r = 1 \tag{9.40}$$

$$n_1 \to 0, r \to \infty \tag{9.41}$$

$$\nabla \cdot [\nabla \boldsymbol{m}_1 - \frac{1}{3} Pe_s \boldsymbol{I} n_1] - \gamma^2 \boldsymbol{m}_1 = 0; \tag{9.42}$$

$$\boldsymbol{n} \cdot [\nabla \boldsymbol{m}_1 - \frac{1}{3} Pe_s \boldsymbol{I} n_1] = Pe_s \boldsymbol{n} \cdot [\boldsymbol{Q}^\infty + \frac{1}{3} \boldsymbol{I} n^\infty], r = 1 \tag{9.43}$$

$$\boldsymbol{m}_1 \to 0, r \to \infty. \tag{9.44}$$

The nematic order is small $\boldsymbol{Q}^\infty \sim O(\chi_R^2)$. To $O(\chi_R)$, this is simply the concentration profile around a stationary sphere [6] and it makes no contribution to the force on the sphere:

$$n_1 = \frac{\frac{1}{3} Pe_s^2}{2(1+\lambda) + \gamma^2} \frac{e^{-\lambda(r-1)}}{r}, \tag{9.45}$$

where $\lambda = \sqrt{\frac{1}{3} Pe_s^2 + \gamma^2}$.

The second components are defined as follows:

$$n_2 = -\frac{1}{2}\frac{Pe_s}{1+\frac{1}{3}\frac{Pe_s^2}{\gamma^2}}\frac{\boldsymbol{m}^\infty \cdot x}{r^3}, \tag{9.46}$$

$$\boldsymbol{m}_2 = -\frac{1}{3}\frac{Pe_s}{\gamma^2}\nabla n_2, \tag{9.47}$$

where $\boldsymbol{x}$ is the position of the swimmer relative to the center of the probe. Because n_2 is a dipole, it is harmonic and divergence free, thus the concentration field equations are satisfied. The polar order field must be harmonic and satisfies the polar order equation forced only by the gradient in n_2. Both fields decay at infinity and satisfy the contact condition for the concentration field:

$$\boldsymbol{n} \cdot [\nabla n_2 - Pe_s \boldsymbol{m}_2] = Pe_s \boldsymbol{n} \cdot m^\infty. \tag{9.48}$$

This term exists for all χ_R. The third components must then satisfy the following equations:

$$\nabla \cdot [\nabla n_3 - Pe_s \boldsymbol{m}_3] = 0; \tag{9.49}$$

$$\boldsymbol{n} \cdot [\nabla n_3 - Pe_s \boldsymbol{m}_3] = 0, r = 1 \tag{9.50}$$

$$n_3 \to 0, r \to \infty \tag{9.51}$$

$$\nabla \cdot [\nabla \boldsymbol{m}_3 - \frac{1}{3}Pe_s \boldsymbol{I} n_3] - \gamma^2 \boldsymbol{m}_3 + \frac{1}{3}\chi_R \gamma^2 (n_1 + n_2 + n_3)\hat{H} = 0; \tag{9.52}$$

$$\boldsymbol{n} \cdot [\nabla \boldsymbol{m}_3 - \frac{1}{3}Pe_s \boldsymbol{I} n_3] = -\boldsymbol{n} \cdot [\nabla \boldsymbol{m}_2 - \frac{1}{3}Pe_s \boldsymbol{I} n_2], r = 1 \tag{9.53}$$

$$\boldsymbol{m}_3 \to 0, r \to \infty. \tag{9.54}$$

The governing equation for $\boldsymbol{m}_3$ contains all of the effects of the external field. Because $n_1 \sim O(1)$ and $n_2 \sim O(\chi_R)$, $\boldsymbol{m}_3 \sim O(\chi_R)$ to leading order, which in turn implies that n_3 scales as χ_R to leading order as well. This means that the leading order equation for $\boldsymbol{m}_3$ is forced only by n_1 in the bulk and is forced at the boundary by the fields from Problem 2, which are both $O(\chi_R)$. Thus we can now easily decouple the concentration and polar order fields through familiar methods (see Chapter 3) and solve the problem.

If we define $n_1 = n^\infty A_1 e^{-\lambda r}/r$ for the sake of brevity, we can write n_3 in terms of two unknown coefficients:

$$n_3 = B_3\frac{\boldsymbol{m}^\infty\cdot\boldsymbol{x}}{r^3} - A_3\frac{Pe_s}{\lambda^2}\boldsymbol{m}^\infty\cdot\boldsymbol{x}\frac{e^{-\lambda r}}{r}\Big(\frac{\lambda}{r}+\frac{1}{r}^2\Big) - \frac{Pe_s}{\lambda^4}\gamma^2A_1\boldsymbol{m}^\infty\cdot\boldsymbol{x}\frac{e^{-\lambda r}}{r}\Big(\frac{\lambda}{r}+\frac{1}{r^2}\Big) - \frac{Pe_s}{\lambda^2}A_1\gamma^2\frac{\boldsymbol{m}^\infty\cdot\boldsymbol{x}}{r}e^{-\lambda r}\Big(\frac{3}{4\lambda^2r^2}+\frac{3}{4\lambda r}+\frac{1}{2}\Big). \tag{9.55}$$

The polar order $\boldsymbol{m_3}$ is

$$\begin{aligned}\boldsymbol{m_3} = {} & C_3e^{-\gamma r}\boldsymbol{m}^\infty\cdot\Big\{\frac{\boldsymbol{I}}{r}-\frac{1}{\gamma^2}\Big[\Big(3\frac{\boldsymbol{xx}}{r^5}-\frac{\boldsymbol{I}}{r^3}\Big)(\gamma r+1)+\gamma^2\frac{\boldsymbol{xx}}{r^3}\Big]\Big\}\\ & +\frac{1}{3}\frac{Pe_s}{\gamma^2}B_3\boldsymbol{m}^\infty\cdot\Big(3\frac{\boldsymbol{xx}}{r^5}-\frac{\boldsymbol{I}}{r^3}\Big)-\frac{\gamma^2}{\lambda^2-\gamma^2}A_1\boldsymbol{m}^\infty\frac{e^{-\lambda r}}{r}\\ & +A_1\gamma^2\frac{2\lambda^2-\gamma^2}{\lambda^4(\lambda^2-\gamma^2)}e^{-\lambda r}\boldsymbol{m}^\infty\cdot\Big[\Big(3\frac{\boldsymbol{xx}}{r^5}-\frac{\boldsymbol{I}}{r^3}\Big)(\lambda r+1)+\lambda^2\frac{\boldsymbol{xx}}{r^3}\Big]\\ & +\frac{A_3}{\lambda^2}e^{-\lambda r}\boldsymbol{m}^\infty\cdot\Big[\Big(3\frac{\boldsymbol{xx}}{r^5}-\frac{\boldsymbol{I}}{r^3}\Big)(\lambda r+1)+\lambda^2\frac{\boldsymbol{xx}}{r^3}\Big]\\ & +\frac{\gamma^2}{\lambda^2}A_1e^{-\lambda r}\boldsymbol{m}^\infty\cdot\Big[\frac{3}{4\lambda^2}(\lambda r+1)\Big(3\frac{\boldsymbol{xx}}{r^5}-\frac{\boldsymbol{I}}{r^3}\Big)+\frac{1}{2}\Big(\frac{\boldsymbol{xx}}{r^3}-\frac{\boldsymbol{I}}{r}\Big)+\frac{3}{4}\frac{\boldsymbol{xx}}{r^3}+\frac{\lambda}{2}\frac{\boldsymbol{xx}}{r^2}\Big],\end{aligned} \tag{9.56}$$

and the coefficients A_3, B_3, and C_3 satisfy the following algebraic equations (derived from the no-flux boundary conditions):

$$2B_3\Big(1+\frac{1}{3}\frac{Pe_s^2}{\gamma^2}\Big)-2C_3Pe_s\frac{1}{\gamma^2}e^{-\gamma}(1+\gamma)+A_1e^{-\lambda}(2+2\lambda)\frac{Pe_s\gamma^2}{\lambda^2(\lambda^2-\gamma^2)}=0 \tag{9.57}$$

$$\begin{aligned}& -C_3e^{-\gamma}\Big(\frac{3}{\gamma^2}+\frac{3}{\gamma}+2+\gamma\Big)+B_3\frac{Pe_s}{\gamma^2}+A_1\frac{\gamma^2}{\lambda^2-\gamma^2}(\lambda+1)e^{-\lambda}\\ & \quad +(3+3\lambda+\lambda^2)e^{-\lambda}\Big(\frac{A_3}{\lambda^2}+A_1\frac{\gamma^2}{\lambda^4}\Big(\frac{2\lambda^2-\gamma^2}{\lambda^2-\gamma^2}\Big)\Big)\\ & \quad +\frac{A_1}{\lambda^2}\gamma^2e^{-\lambda}\Big(\frac{5}{4}+\frac{9}{4\lambda}+\frac{\lambda}{2}+\frac{9}{4\lambda^2}\Big)=\frac{\frac{Pe_s^2}{2\gamma^2}}{1+\frac{1}{6}\beta^2}\end{aligned} \tag{9.58}$$

$$\begin{aligned}& C_3e^{-\gamma}\frac{1}{\gamma^2}(9+9\gamma+4\gamma^2+\gamma^3)-3B_3\frac{Pe_s}{\gamma^2}\\ & \quad -(9+9\lambda+4\lambda^2+\lambda^3)e^{-\lambda}\Big(\frac{A_3}{\lambda^2}+A_1\frac{\gamma^2}{\lambda^4}\Big(\frac{2\lambda^2-\gamma^2}{\lambda^2-\gamma^2}\Big)\Big)\\ & \quad -A_1\frac{\gamma^2}{\lambda^2}e^{-\lambda}\Big(\frac{14}{4}+\frac{27}{4\lambda}+\frac{27}{4\lambda^2}+\frac{5\lambda}{4}+\frac{\lambda^2}{2}\Big)\\ & \quad -\frac{1}{3}Pe_s\Big[B_3-A_3\frac{Pe_s}{\lambda^2}(\lambda+1)e^{-\lambda}-A_1\gamma^2\frac{Pe_s}{\lambda^4}(\lambda+1)e^{-\lambda}\\ & \quad -A_1\gamma^2\frac{Pe_s}{\lambda^2}e^{-\lambda}\Big(\frac{3}{4\lambda^2}+\frac{3}{4\lambda}+\frac{1}{2}\Big)\Big]=-\frac{\frac{1}{6}Pe_s^2}{1+\frac{1}{6}\beta^2}-\frac{\frac{3Pe_s^2}{2\gamma^2}}{1+\frac{1}{6}\beta^2}.\end{aligned} \tag{9.59}$$

The force required to hold the sphere fixed is

$$\boldsymbol{F} = -\boldsymbol{m}^{\infty} k_B T \frac{4\pi}{3} a^2 \left[B_3 - A_3 \frac{Pe_s}{\lambda^2}(\lambda + 1)e^{-\lambda} - A_1 \gamma^2 \frac{Pe_s}{\lambda^4}\left(\frac{5}{4} + \frac{5\lambda}{4} + \frac{\lambda^2}{2}\right)\right]. \quad (9.60)$$

BIBLIOGRAPHY

[1]S. C. Takatori, and J. F. Brady, "Swim stress, motion, and deformation of active matter: effect of an external field.", Soft Matter **10**, 9433–45 (2014).

[2]H. Brenner, "Rheology of a dilute suspension of axisymmetric Brownian particles", Int. J. Multiph. Flow **1**, 195–341 (1974).

[3]D. Saintillan, and M. J. Shelley, "Theory of Active Suspensions", in *Complex fluids biol. syst.* Edited by S. Spagnolie, (Springer, New York, 2015) Chap. 9, pp. 319–355.

[4]S. Kim, and S. J. Karilla, *Microhydrodynamics : Principles and Selected Applications* (1991).

[5]J. F. Brady, "Particle motion driven by solute gradients with application to autonomous motion: continuum and colloidal perspectives", J. Fluid Mech. **667**, 216–259 (2011).

[6]W. Yan, and J. F. Brady, "The force on a body in active matter", J. Fluid Mech. **6**, 1–11 (2015).